WHEAT STALK MICRO- AND NANOCELLULOSE BASED DEGRADABLE POLYMER COMPOSITES: MORPHOLOGICAL, MECHANICAL AND DEGRADATION BEHAVIOUR

A THESIS SUBMITTED TO THE

CENTRAL DEPARTMENT OF CHEMISTRY

INSTITUTE OF SCIENCE AND TECHNOLOGY

TRIBHUVAN UNIVERSITY, KIRTIPUR

KATHMANDU, NEPAL

FOR THE AWARD OF THE DEGREE OF

DOCTOR OF PHILOSOPHY

IN CHEMISTRY

BY

JYOTI GIRI

SEPTEMBER 2020

RECOMMENDATION

This is to recommend that **Jyoti Giri** has carried out research entitled **"Wheat Stalk Micro- and Nanocellulose Based Degradable Polymer Composites: Morphological, Mechanical and Degradation Behaviour"** for the award of Doctor of Philosophy (PhD) in **Chemistry** under our supervision. To our knowledge, this work has not been submitted for any other degree.

She has fulfilled all the requirements laid down by Institute of Science and Technology (IOST), Tribhuvan University, Kirtipur for the submission of the thesis for the award of the PhD degree.

Prof. Dr. Rameshwar Adhikari
Supervisor
Central Department of Chemistry
Tribhuvan University, Kathmandu, Nepal

Prof. Dr. Mohammad Yousuf Ali Mollah
Co-Supervisor
Department of Chemistry
Dhaka University, Dhaka, Bangladesh

त्रिभुवन विश्वविद्यालय
TRIBHUVAN UNIVERSITY
विज्ञान तथा प्रविधि अध्ययन संस्थान
Institute of Science and Technology
रसायन शास्त्र केन्द्रीय विभाग
CENTRAL DEPARTMENT OF CHEMISTRY
कीर्तिपुर, काठमाडौं, नेपाल
Kirtipur, Kathmandu, NEPAL

Central Department of Chemistry T.U.Kirtipur

पत्र संख्या:
Ref. No.:

LETTER OF APPROVAL

On the recommendation of **Prof. Dr. Rameshwar Adhikari** , this PhD thesis submitted by **Ms. Jyoti Giri** entitled **"Wheat Stalk Micro- and Nanocellulose Based Degradable Polymer Composites: Morphological, Mechanical and Degradation Behaviour"** is forwarded by Central Department Research Committee (CDRC) to the Dean, Institute of Science and Technology (IOST),T.U.

.....

Dr. Ram Chandra Basnyat
Professor,
Head,
Central Department of Chemistry
Tribhuvan University
Kirtipur, Kathmandu
Nepal

DECLARATION

Thesis entitled **"Wheat Stalk Micro- and Nanocellulose Based Degradable Polymer Composites: Morphological, Mechanical and Degradation Behaviour"** which is being submitted to the Central Department of Chemistry, Institute of Science and Technology (IOST), Tribhuvan University, Nepal for the award of the degree of Doctor of Philosophy (PhD), is a research work carried out by me under the supervision of Prof. Dr. Rameshwar Adhikari, Central Department of Chemistry, Tribhuvan University. This work is co-supervised by Prof. Dr. Mohammad Yusuf Ali Mollah, Dhaka University, Bangladesh.

This research is original and has not been submitted earlier in part or full in this or any other form to any university or institute, here or elsewhere, for the award of any degree.

Jyoti Giri

Date: 23rd September

ACKNOWLEDGEMENTS

My sincere acknowledgements to the divine strength of this nature who always blessed me with the courage to stay focus on my goal. I would like to thank GOD for offering me with enormous compassion and patients on me to accomplish this astonishing academic expedition of PhD.

I would like to express my deep honour and cordial gratitude to my supervisor Prof. Dr. Rameshwar Adhikari for his key guidance, encouragements during my ups and downs during research period, his critical analysis, constructive criticism, constant encouragement and facilitating me with his all national and international collaborations has become a great support during my entire course of study and cannot be expressed in words.

I would also like to express my sincere thanks to my co-supervisor Prof. Dr. Mohammad Yousuf Ali Mollah for his enthusiastic encouragement and collaboration for this work. I dilate my gratitude to Prof. Dr. Md. Abu Bin Hasan Susan who helped me in drafting papers for publication and always encouraged me to move forward.

I extend my sincere thanks and regards to Prof. Dr. Ram Chandra Basnyat, Head of Central Department of Chemistry and Prof. Dr. Megh Raj Pokhrel, Former Head of Central Department of Chemistry for providing the available laboratory facility. I feel heartily indebted to Prof. G. H Michler, Prof. W. G. Grellmann, Prof. H-J- Radusch, R. Lach and H. H. Le for offering the necessary facilities for preparing and characterizing the samples by Fourier transform spectroscopy (FTIR), tensile test and microhardness measurement at Martin Luther University, Halle-Wittenberg, Germany. I am grateful to Prof. Dr. Jean Marc Saiter for characterization and analysis of the results of Thermogravimetric Analysis (TGA). I am thankful to Prof. Dr. Vimal Katiyar, IIT-Guwahati, India for facilating lab facility for the preparation of nano-composites and their characterizations by GPC, DSC, contact angle, FESEM, and TEM. I am delightful to the Central Department of Biotechnology for their generous help for microbial works. My sincere thank to Dr. Sven Henning, Fraunhofer Institute for Microstructure of Materials and Systems (IMWS), Halle/Saale, Germany for microscopic investigation of the specimens.

I can no longer forget to express my thankfulness for the co-operation and affection, which I received from my seniors and friends Dr. Sharmila Pradhan, Dr. Rajesh Pandit,

Dr. Shanta Pokhrel, Dr. Netra Lal Bhandari, Dr. Shankar Khatiwada, Kedar Nath Dhakal, Komal Malla, Prakash Gautam, Bimala Dhakal, Roshan Nepal, Sagar Aryal, Sonam Tamang, Deepshikha Das, Ram Chandra Kandel, Sujindra Subedi, Achyut Nepal, Ramesh Puri, Dr. Siddhartha Mohan Bhasney, Dr. Monika Singh, Munmi Das, Chetana, Konna, Doli, Narendren Soundararajan, Dr. Purabi Bhagawati, Dr. Ngocdiep Pham, Pankaj Boruah, Dr. Prashant Bhaisya, Navajyoti Talukdar, and Kapil Khadka.

I feel pleasure to express my gratitudes to POLYCHAR (International Polymer Characterization Forum) for providing international collaboration platform to perform experiments, interpretation and publications.

I would like to express my hearty appreciation to all the teaching and non-teaching staff of Central Department of Chemistry (CDC), Tribhuvan University for their constant help and support during the entire course of study. I would like to thank Tri-Chandra Multiple Campus, Ghantaghar, Kathmandu for permitting me to complete my PhD work.

All words in the vocabulary will be worthless and meaningless if I fail to divulge my special thanks to my mother Mrs. Chinu Giri and ever loving daughter Ms. Prapti Shrestha who have always helped and supported me at the coast of their comforts and without whom this thesis would have remained an ambition. This thesis was a dream of my father late Mr. Vishnu Prasad Giri, He had a wish one day his child would become a doctor of philosophy. Therefore, I would like to give tribute to my father with this thesis.

Finally, I am grateful to Nepal Academy of Science and Technology (NAST) for providing PhD fellowship and German Research foundation (DFG), Indian National Science Academy (INSA), and University Grant Commission (UGC) for travel grants.

Jyoti Giri

September, 2020

ABSTRACT

The current scenario of rebellious nature of polymer towards degradation causes land and water pollution throughout the world and led life in critical state. The issue can be solved by using degradable polymer. This work aims to use degradable polymer instead of synthetic polymer and induce early degradation in polymer composites by incorporation of natural fibers. The objective of this work is to extract micro- (MCC) and nanocrystalline cellulose (NCC) from agricultural waste wheat stalk (WS), to prepare composites of commercially available biodegradable aliphatic-aromatic copolyester, Poly(butylenes adipate *co*-terephthalate), the PBAT with MCC and NCC extracted and to study the spectroscopic, microscopic, thermal, mechanical and degradation behaviour of the prepared composites.

MCC and NCC were extracted from WS and compounded with commercially available biodegradable aliphatic-aromatic copolyester, the PBAT, in different proportions. The resulting materials were characterized by various modern analytical techniques. The MCC and NCC obtained from WS fibers were analyzed for definite textures, the MCC being irregular bundles of the primary crystals bound together with the amorphous phase. The latter disintegrated upon acid hydrolysis yielding the rod-shaped nanocrystals possessing much larger surface area and intense hydrophilic character.

The poly(butylene adipate –*co*-terephthalate) PBAT/MCC composites were found to contain the polymer phase towards the composites surfaces whereby there was no strong bonding at polymer/filler interface. The composites showed good thermal stability with insignificant variations in their physical thermal properties. The PBAT/NCC nanocomposites showed in many respects similar behaviour as the composites with MCC.

The composites were found to visibly degrade completely within a few months under soil composting. Compared to the neat PBAT, the composites exhibited enhanced surface hydrophilicity thereby increasing their ability of degradation. In spite of seemingly remarkable decrease in mechanical stability of the polymers buried in soil for several months, no substantial lowering of the molecular weight was observed.

The future studies could be concentrated to identify precisely the mechanism of biodegradation of the polymer composites in particular with reference to contributions of inorganic substances present in the soil and in view of the presence of individual microorganism.

Keywords: *polymer composites, FTIR spectroscopy, electron microscopy, gel permeation chromatography (GPC), morphology, biodegradation*

TABLE OF CONTENTS

Page No.

LIST OF TABLES

LIST OF THE FIGURES

LIST OF THE SCHEMES

LIST OF SYMBOLS

%	Percent
°C	Degree Celsius
A	Area, Arrhenius constant, Pre-exponential factor
cm	Centimeter
cm^{-1}	Per centimeter
D	Apparent grain size
E	Tensile modulus
E_{IT}	Indentation modulus
F	Load
F_{max}	Maximum load
g	Gram
g/cm^3	Gram per centimeter cube
h	Indentation depth
HM	Marten hardness
h_{max}	Maximum Indentation depth
J	Joule
K	Kelvin
kg/mol	Kilogram per mole
kHz	Kilo Herz
kJ	Kilojoule
l	Liter
M. P.	Melting point
Mg	Milligram
mL	Milliliter
mm	Millimeter
mN	Milli Newton
MPa	Mega Pascal

mW	Milli Watt
Mw	Average molecular weight
N	Newton
nm	Nanometer
R	Universal gas constant
T	Absolute temperature
T_c	Crystallization temperature
T_m	Melting temperature
W_e	Elastic work
W_{pl}	Plastic work
wt. -%	Weight fraction in percentage
µL	Microliter
ε	Strain
θ	Diffraction angle
µm	Micrometer
σ	Stress

LIST OF ACRONYMS & ABBREVIATIONS

ATR	Attenuated total reflection
BF	Bamboo fiber
CNC	Cellulose nanocrystal
CI	Crystallinity index
CNF	Cellulose nanofiber
DCP	Dicumyl peroxide
DTG	Differential thermogravimetric (data)
EC	Electrical conductivity
EFBF	Empty fruit bunch fiber
EM	Electron microscopy
FE-SEM	Field emission scanning electron microscopy
FF	Fiber flour
FTIR	Fourier transform infrared
GPC	Gas permission chromatography
hrs	Hours
HANP	Hydroxyapatite nanoparticle
HPLC	High performance liquid chromatography
LOI	Loss on ignition
MCC	Microcrystalline cellulose
min	Minute
MWCNT	Multiwalled carbon nanotube
NCC	Nanocrystalline cellulose
OM	Optical microscopy
PBAT	Poly(butylene adipate-*co*-terephthalate) copolymer
PBS	Polybutylene succinate
PCL	Polycaprolactone
PE	Polyethylene

PET	Polyethylene terephthalate
PGA	Polyglycolic acid
PHA	Polyhydroxyalkanoate
PHB	Polyhydroxy butyrate
PHBV	Poly(3-hydroxybutyrate-*co*-3-hydroxyvalerate)
phr	Per hundred resin
PLA	Ploylactic acid
POM	Polarizing optical microscopy
PP	Polypropylene
rpm	Rotations per minute
SEM	Scanning electron microscopy
SPM	Scanning probe microscopy
TEM	Transmission electron microscopy
TEMPO	2, 2, 6, 6-tetramethylpiperidine-1-oxyl radical
TGA	Thermogravimetric analysis
UV	Ultraviolet radiation
WAXS	Wide angle X-ray scattering
WS	Wheat stalk
XPS	X-ray photoelectron spectroscopy
XRD	X-ray diffraction

CHAPTER 1

1. INTRODUCTION AND OBJECTIVES

1.1 Introduction

As most of the synthetic polymers we use today originate from raw materials based on fossil fuel, which is going to be used up quite quickly, in near future, we have no alternative sources.

Therefore, we need to think about the alternatives of synthetic polymers and at the same time, think for the lesser use of the polymers by introducing enhanced functionality and recyclability into the existing conventional polymers (Gross & Karla, 2002, Rajan *et al*., 2010).

Nowadays, polymer scientists are trying to develop renewable resources based fillers such as microcrystalline cellulose (MCC), nanocrystalline cellulose (NCC), hemicelluloses, lignin, chitosan, proteins as well as the inorganic substances like layered silicates, silica, calcium carbonate, carbon black, graphene, multiwalled carbon nanotube (MWCNT) etc. (Abraham *et al*., 2012, Malho *et al*., 2012, Cho & Park, 2010, Frone *et al*., 2011, Rajan *et al*., 2010, Lee *et al*., 2009, William *et al*., 2005, Morouco *et al*., 2016, Ozkoc *et al*., 2010, Fukusima *et al*., 2012, Rasyida *et al*.,2017, Chivrac *et al*., 2006). Depending upon the nature and compatibility of the fillers with polymers, the property of the composite materials can be modulated. Such composites find applications in aerospace engineering, medical devices, tissue engineering and in designing the smart drug delivery systems (Ozkoc *et al*., 2010, Dhar *et al*., 2014, Gopakumar *et al*., 2018, Moustafa *et al*., 2017, Cotana *et al*., 2012, Gruneberger *et al*., 2014, Leun *et al*., 2013, Lu *et al*., 2001, Sgarioto *et al*., 2014). Moreover, inorganic fillers used in polymer composites, on disposal after their utility into the open environment, usually may give hazardous impacts to livelihood. Many of them are toxic for living beings and human health as the chemicals used for compatibilization as well as for fire retardancy (such as brominated polystyrene, tetra-bromophthalic anhydride and deca-bromophenyl oxide) are proved to pose threat to the natural environment (Dasaria *et al*., 2013, Sjodin *et al*., 2001). One of the

prevalent catastrophes is depicted in Fig.1.1, as an example of plastics pollutions in Bagmati River, a river that should be serene and holy even accordingly to the region's spiritual values

Figure 1.1: Plastics debris floating on Bagmati River on Thapathali (prior to *Bagmati Cleaning Campaign*)

As an alternative, the greener methods have been introduced by using regenerated natural resources (such as cellulosic fibers) which give similar or even more advanced properties than the reinforcement effects in the conventional composites with inorganic fillers (Malho *et al*., 2012, Ozkoc *et al*., 2010). It is known that the cellulose fibers are stronger than several mineral based fibers, have a high volume to weight ratio and can be easily dispersed homogeneously into polymer matrices *via* common processing techniques (Cho *et al*., 2011, Lee *et al*., 2009). On the other hand, the renewable resources have the advantages of being inexpensive, regenerative and local availability (Abraham *et al*., 2012, Cho & Park., 2011, William *et al*., 2005). These may reduce significantly the use of fossil fuel by-products; promote green economy and smart materials development (Cotana *et al*., 2012, Saba *et al*., 2015, Su &Wu, 2011, Chauhan *et al*., 2009).

The biobased and biodegradable plastics are emerging as reliable alternatives to conventional commodity plastics (Banerjee *et al*., 2014, Leja & Lewandowicz, 2010). Several of them, however, have generally the problem of poor mechanical properties, difficulty in tuning crystallization behaviour, high manufacturing costs and reduce the ease of processing. Currently, biodegradable polyesters such as polybutylene adipate-

co-terephthalate (PBAT), polyethylene terephthalate (PET), polylactic acid (PLA), polybutylene succinate (PBS), polycaprolactone (PCL) and polyglycolic acid (PGA) are being investigated (William *et al*., 2005, Morouco *et al*., 2016, Ozkoc *et al*., 2010, Fukusima *et al*., 2012, Su & Wu, 2011). Among them completely biodegradable blends and composites based on PBAT, PCL, PLA, and PHB are becoming quite popular (Banerjee *et al*., 2014, Leja & Lewandowicz, 2010, Shah *et al*., 2007, Morouco *et al*., 2016, Gowman *et al*. 2019).

Irrespective of the materials chosen for technical applications, it is a key issue to control the morphological details of the material at different length scales to design their tailored properties profile (Ozkoc *et al*., 2010, Chivrac *et al*., 2006, Su & Wu, 2011, Banerjee *et al*., 2014). As a consequence, a comprehensive understanding of the correlation between morphology, mechanical properties and degradation behaviour of such systems is required.

Our research group has been working for several years in this direction. Bhandari (2013) studied morphology and some mechanical and thermal behaviour of the composites of synthetic polymer, the polypropylene (PP), with natural fibers comprising their ease of degradability with corresponding composites with biodegradable polymers. Similarly, Pokhrel (2016) studied chitosan based composites with a biodegradable polymer, PBAT for their mechanical properties and biodegradation behaviour. As an extension of the previous works, this research attempts to provide more precise explanations in the morphological, mechanical, deformation and degradation behaviour of PBAT based biodegradable composites fabricated with wheat stalk MCC and NCC with special emphasis on the variation of molecular properties of the polymers subjected to biodegradation.

1.2 Rationale of the Study

Nepal Government in 2011 promulgated a regulation demanding the prohibition of single use plastic bags. Kathmandu Metropolitan City announced banning of plastic in April 2013, which is a step towards utilization of sustainable and ecofriendly materials that do not degrade the natural environment. An aspect of this endeavour is to promote the development of degradable packaging materials (Rasyida *et al*. 2016).

Another challenge for materials scientists in developing countries is to use locally available, as far as possible the waste materials as resource and to modify them to make new sustainable materials opening new avenues for commercial applications.

In this respect, the evident challenge of the present work is to design novel materials from the discarded agricultural wastes. Especially, the locally available agricultural wastes are traditionally not used as high value materials but only utilized as animal feeds. Therefore, these low cost resources can be applied to make new materials. Nowadays, Nepal government has promoted the use of degradable polymer materials. Thus, the development of low cost biobased and completely degradable materials for packaging application is obviously a challenge of the present time. Therefore, current study focuses to meet the summons relevant to green practices mentioned above.

1.3 Objectives

This research aims at designing wheat stalk micro- and nanocellulose based degradable polymer composites and to study their morphological, mechanical and degradation behaviour.

The specific objectives of the research are as outlined below:

I. To extract microcrystalline cellulose (MCC) from wheat stalk (WS) flour and to further disintegrate the former into nanocrystalline cellulose (NCC) *via* acid hydrolysis and to characterize them on different length scales;

II. To prepare the composites of polybutylenes adipate-*co*-terephthalate (PBAT) with the MCC and the NCC *via* melt mixing process;

III. To study comparatively the morphological, mechanical, thermal and degradation behaviour of the micro- and nanocomposites using advanced analytical tools such as spectroscopy, microscopy, thermal and mechanical methods as well as water absorption test, contact angle measurements and soil composting; and

IV. To establish the structure-properties correlations for prepared micro- and nanocomposites.

1.4 Scope of the Study

This work targets at converting an agricultural waste, the wheat stalk, to a high value materials (MCC and NCC) in order to fabricate the completely degradable polymer materials that can be useful for general applications such as food packaging, insulation and other low load bearing applications. This study targets using locally available waste materials as resource and encompasses the essence of green practices.

The thesis is organized as follows: A brief presentation of the basic philosophy of the proposed work including objective and limitations will be the content of **Chapter 1**. Detailed review of relevant literature works with particular attention on fiber processing methodologies and structure-properties relationships of the degradable polymer composites will be illustrated in **Chapter 2. Chapter 3** gives a brief explanation on preparation of MCC and NCC from wheat stalk and then explains the preparation of PBAT/MCC and PBAT/NCC composites *via* melt mixing. The brief outline of the analytical techniques will be presented. **Chapter 4** presents and discusses the results. First, it gives insights into the structure of cellulosic fibers as a function of processing conditions. The structure-properties correlation of polymer composites will be studied using different tools including spectroscopy, electron microscopy, thermal and mechanical and chromatography. The degradation behaviour of the composites under soil burial condition will be discussed with reference to GPC results. Finally, **Chapters 5** and **6** present the conclusions and summary of the research works, respectively.

1.5 Limitations: The general limitations of this work are listed below.

This project primarily deals with naturally dried WS fibers but does not rigorously compare the properties and process parameters with that of other natural fibers.

I. The effect of various process parameters (such as effect of Na^+ ions, acid hydrolysis on structure, molar mass and crystallinity) of the fibers cannot be controlled.

II. The work is limited to laboratory scale production of MCC and NCC as well as the composites with PBAT. In general, for biodegradation analysis, individual contribution of the bacteria as well as that of minerals etc. cannot be analyzed.

1.6 Delimitations: The general delimitations of this work are as follows.

I. The materials cannot be kept beyond humidity present in the experimental environment.

II. The simultaneous dehydrating, oxidizing and charring effects of acids cannot be avoided.

III. Exact hydrolysis effect with the function of time cannot be defined.

IV. The abundance of different types of bacteria in the degrading environment (soil composting) cannot be controlled in the nature.

CHAPTER 2

2. LITERATURE REVIEW

One of the recent trends in materials science and engineering is to use polymers in different high-tech applications taking into account for their safe disposal after use. Polymers are being used extensively from the very early days of 20th century, and nowadays, we can hardly imagine any fields in everyday life where polymers are absent (Gross & Kalra, 2002, Abraham *et al*., 2012, Malho *et al*., 2012, Cho & Park, 2011, Frone *et al*., 2011, Rajan *et al*., 2009).

As most of the synthetic polymers we use today originate from raw materials based on fossil fuels, which is going to be used up quite quickly that, in near future, we wouldn't have alternative sources. Therefore, we need to think about the alternatives of synthetic polymers and at the same time, think for the lesser use of the polymers introducing enhanced functionality and recyclability into the conventional polymers (Gross & Kalra, 2002, Rajan *et al*., 2009). Nowadays, scientists are trying to develop renewable resources based fillers such as microcrystalline cellulose (MCC), nanocrystalline cellulose (NCC), hemicelluloses, lignin, chitosan, proteins as well as the inorganic fillers namely layered silicates, silica, calcium carbonate, carbon black, graphene, multiwalled carbon nanotube (MWCNT) etc. (Abraham *et al*., 2012, Malho *et al*., 2012, Cho & Park, 2011, Frone *et al*., 2011, Rajan *et al*., 2009, Lee *et al*., 2009, William *et al.,* 2005, Morouco *et al*., 2016, Ozkoc *et al*., 2010, Fukusima *et al*., 2012, Rasyida *et al*., 2017, Chivrac *et al*., 2006). Depending upon the nature and compatibility of the fillers with polymers, the property of the composite materials can be modulated. Such composites find applications in aerospace engineering, medical devices, tissue engineering and in designing the smart drug delivery systems (Ozkoc *et al*., 2010, Dhar *et al*., 2014, Gopakumar *et al*., 2018, Moustafa *et al*., 2017, Cotana *et al*., 2012, Gruneberger *et al*., 2014, Leung *et al*., 2013, Lu *et al*., 2001, Sgarioto *et al*., 2014, Sjodin *et al*., 2001).

Moreover, inorganic fillers used in polymer composites on disposal after their utility into the open environment usually may give hazardous impacts to life. Many of them

are toxic for living beings human health as the chemicals used for compatibilization as well as for fire retardancy (such as brominated polystyrene, tetra-bromophthalic anhydride and deca-bromophenyl oxide) are proved to pose threat to natural environment (Sgarioto *et al*., 2014, Sjodin *et al*., 2001).

As an alternative, the greener methods have been introduced by using regenerated natural resources (such as cellulosic fibers) which give similar or even more advanced properties than the reinforcement effects in the conventional composites with inorganic fillers (Malho *et al*., 2012, Ozkoc *et al*., 2010). It has been known that the cellulose fibers are stronger than several mineral based fibers, have a high volume to weight ratio and can be easily dispersed homogeneously into polymer matrices *via* common processing techniques (Cho & Park, 2011, Lee *et al*., 2009). On the other hand, the renewable resources have the advantages of being inexpensive, regenerative and local availability (Abraham *et al*., 2012, Cho & Park, 2011, William *et al*., 2005). These may reduce significantly the use of fossil fuel by-products; promote green economy and smart materials development (Cotana *et al*., 2012, Saba *et al*., 2015, Su & Wu, 2011, Chauhan *et al*., 2009).

Thus, the biobased and biodegradable plastics are emerging as reliable alternatives to conventional commodity plastics (Banerjee *et al*., 2014, Leja & Lewandowicz, 2011). Several of them, however, have generally the problem of poor mechanical properties, difficulty in tuning crystallization behaviour, high manufacturing costs and reduced ease of processing. Currently, biodegradable polyesters such as polybutylene adipate-*co*-terephthalate (PBAT), polyethylene terephthalate (PET), polylactic acid (PLA), polybutylene succinate (PBS), polycaprolactone (PCL) and polyglycolic acid (PGA) are being investigated (William *et al*., 2005, Morouco *et al*., 2016, Ozkoc *et al*., 2010, Fukusima *et al*., 2012, Su & Wu, 2011). Among them completely biodegradable blends and composites based on PBAT, PCL, PLA, and PHB are becoming quite popular (Banerjee *et al*., 2014, Leja & Lewandowicz, 2011, Shah *et al*., 2008, Han *et al*., 2008). Irrespective of the materials chosen for technical applications, it is a key issue to control the morphological details of the material at different length scales to design the tailored properties profile (Ozkoc *et al*., 2010, Chivrac *et al*., 2006, Su & Wu, 2011, Banerjee *et al*., 2014). As a consequence, a comprehensive understanding

of the correlation between morphology, mechanical properties and degradation behaviour of such systems is required.

This chapter aims at discussing the structure and properties of a biodegradable copolyester based composite materials with special attention to their mechanical, morphological and biodegradation behaviour. A brief introduction about the filler preparation and corresponding characterization techniques will be followed by an overview of natural fibers based polymer composites. Then, the detailed discussion on the structure-properties correlation of the copolyester/natural fibers composites will be presented. The degradation behaviour of the composites under soil burial condition will be discussed with an emphasis on molecular weight reduction and degradation mechanism. Finally, the chapter will be concluded highlighting some new trends, challenges in developing completely biodegradable and compostable composite materials.

2.1 Preparation and Characterization of Natural Fibers and Composites

The preparation of fillers for composites fabrication and the characterization of polymer interface as well as the morphology of the composite are important aspects for tailoring the properties profile of composites materials. This section addresses briefly these key issues.

2.1.1 Preparation of Micro (MCC)- and Nanocrystalline Cellulose (NCC)

The common sources of MCC and NCC are the plant-based natural fibers such as sisal (Mostafa *et al*., 2010, Palisikowski *et al*., 2017), kenaf (Han *et al*., 2008, Chan *et al*., 2013), castor oil plant (Vinayak *et al* ., 2017), bamboo (Das & Chakraborty 2008, Adhikari *et al.,* 2012, Batalha *et al.,* 2012), jute (Bledzki *et al*., 1996), pineapple leaf (Cherian, *et al.,* 2011), cotton (Teixeira *et al.,* 2010, Satyamurthy & *Vigneshwaran,* 2013) and ramie (Yu & Li, 2014) etc., There are many processes to extract MCC and NCC from the bioresources which can broadly be classified as chemical, mechanical and bacterial methods (Frone *et al*., 2011, Nagata & Inaki 2011, Giri & Adhikari, 2013, Sanjay *et al*., 2016, Siro & Plackett, 2010).

a) Chemical method

After preliminary treatments such as washing, drying, chopping, pulverizing and sieving, the raw plant fibers are generally subjected to strong alkali treatment. The process is called as *mercerization* and causes the fibers to undergo fibrillation and delignification (Vinayak *et al*., 2017, Cherian, *et al.*, 2011). Usually, alkali solutions used for this process are from caustic soda or caustic potash (Cherian, *et al.*, 2011, Pelissari *et al*., 2014) whereby the optimization of alkali concentration and processing temperature are important parameters to consider (Ibrahim *et al*., 2010). The *Mercerization* further involves the addition of Na^+ groups into the cellulosic molecular framework which can later be removed by treating with acids (Scheme 1) (Das & Chakroborty, 2008). The treatment with acids such as $(COOH)_2$, HCOOH, CH_3COOH, dilute H_2SO_4 and HCl also acts to dissolve the amorphous regions in the cellulose (Reddy & Rhim, 2014). The overall process is shown in Scheme 1 (Rajan *et al*., 2009).

$$Cellulose-OH + NaOH \rightarrow Cellulose-Na + H_2O$$
$$Cellulose-Na + H^+ \rightarrow Cellulose-OH + Na^+$$

Scheme 2.1: *Mercerization* of cellulose fiber with NaOH followed by acid treatments to microfibrillate the cellulose macrofibers (Rajan *et al*., 2009)

The raw fibers are converted to white shining crystals on bleaching with chemicals such as NaClO, NaCl, $NaClO_3$, $NaClO_2$, and H_2O_2. These usually produce nascent chlorine or oxygen to bleach the fibers and at the same time also dissolve hemicelluloses and amorphous regions exposing neat cellulose crystallites (Rajan *et al*., 2009, Cherian, *et al.*, 2011, Pelissari *et al*., 2014, Dai & Fan, 2010, Rosli *et al*., 2013, Cesar *et al*., 2015, Yan *et al*., 2009). Scheme 2, for instance, shows the bleaching action of NaClO on natural fibers (Rajan *et al*., 2009).

$$NaClO \rightarrow Na^+ + \quad OCl^-$$
$$OCl^- + 2e^- + HOH \rightarrow Cl^- + 2OH^-$$

Scheme 2.2: Oxidative bleaching of cellulose microfibers by sodium hypochlorite solution for synthesis of white crystalline MCC (Rajan *et al*., 2009)

Cellulose fibers after above procedure easily give rise the MCC. Further disintegration into the nano-sized crystals can be achieved by controlled hydrolysis with strong acids

under constant and vigorous stirring or sonication. The chemical disintegration is quite challenging in term of purification of the cellulosic fiber as a great deal of mass loss may occur. Acid treatments leading to the formation of the NCC have been reported by several authors (Liu *et al*., 2010, Shaheen & Emam, 2018, Chen *et al*., 2013, Ponce-Reyes *et al*., 2014) by variation of acid concentration, time of treatment, temperature, and freeze-drying procedures. As a result, the NCC crystals aggregate, several tens of nanometers width and up to several hundred nanometer lengths, can be obtained.

b) Mechanical method

I. Compression and roller mechanical technique

In compression mechanical method, cellulosic fibers are placed between beds of two metal plates at high force of 10 tons for 10 seconds whereas in roller mechanical technique fibers are passed between two rollers in which one is mobile while other is fixed. These techniques were used to fibrillate wood dust and corn stover into nanofibers (Shaheen & Emam, 2018, Chen *et al*., 2013).

II. Homogenization

In this technique, cellulose fibers are passed through a narrow valve at very high pressure and released suddenly to normal pressure which acts as the shear force to explode the inner fibers. The basic concept of this technique is to release all binding forces initially applied to the nanofibers while forming macroscopic fibers. Usually raw and mercerized fibers are employed for homogenization. The technique was used for nanofibrillation of hard and softwood pulps, banana peels and sugar cane baggage (Siro & Plackett, 2010, Pelissari *et al*., 2014, Stelte & Sanadi, 2009, Li *et al*., 2012, Sofla *et al*., 2016).

III. Ultrasonication

Ultrasonication is an electro-mechanical process of disintegrating of MCC into the NCC. Sound energy of more than 20 kHz is used to agitate particles present in the aqueous cellulose suspension which leads nanofibrillation to the followed by breakage of intermolecular bonds (Dai & Fan, 2010, Oksman *et al*., 2011). In addition to the energy of the ultrasound, the treatment time, temperature and presence of impurities can signify the morphology and hence the properties of the NCC.

c) Bacterial synthesis

One of the most important features of bacterial cellulose is its chemical purity, which distinguishes it from cellulose extracted from higher plants, usually associated with hemicelluloses and lignin, removal of which involves several steps. Due to their unique properties ultra-fine, uniform reticulated structure, the bacterial nanocellulose find multiple applications in paper, textile industries, food, and cosmetics as well as in tissue engineering and medicine (Czaja *et al*., 2006).

Bacteria such as Acetobacter xylinus, Rhizobium, Agrobacterium, Escherichia coli, and Sarcina have been found to biosynthesize cellulose nanofibers with high crystalline texture (Bielecki *et al*., 2005, Iguchi, 2000). Further, NCC and MCC fibrils can be synthesized by bacteria in presence of glucose, oxygen, nitrogen, and micronutrients. In this process, various carbon compounds in the nutrition media are utilized by the microorganisms to polymerize their molecules into a single, linear β-1, 4-glucan chains and secrete outside the bacterial cell. First, nascent β-1,4- glucan chains are produced. Then a number of such chains combine to form microfibrils which are interwoven with each other to give a thick gelatinized network of the fibers (Czaja *et al*., 2006). The amount and nature of bacterial cellulose production vary, besides the nature of the microorganisms with the type of carbon sources (such as glucose, mannitol, glycerol, fructose, sucrose, and galactose) (Mikkelsen *et al*., 2009).

2.1.2 Preparation of Polymer Composites

There are a vast number of references available for fabrication of polymer composites involving biodegradable polymers and natural fibers. In brief, the common processing rout involves the physical mixing of the components in a drum, followed by agitation inside an internal mixture under inert atmosphere and palletization. The samples fabricated during melt compounding of the pellets are then subjected to molding by various means such as compression, blowing casting, injection and spinning, calendaring, blowing and printing (Cho & Park, 2011, Rajan *et al.*, 2009, Frone *et al.*, 2011, Lee *et al*., 2009, William *et al*., 2005, Morouco *et al*., 2016, Fukusima *et al*., 2012, Chivrac *et al*., 2006, Dhar *et al*., 2014, Su & Wu, 2011, Das & Chakraborty, 2008, Adhikari *et al.*, 2012, Yu & Li, 2014).

2.1.3 Characterization Techniques

There are several techniques that characterize the specific properties of the polymeric materials. The choice of the techniques depends primarily on the nature of the properties that are relevant for the particular application. For the degradable materials intended for packaging, insulation and other low load bearing fabrications, the stability against thermal and mechanical stress as well as the structural details linked to those properties are of particular interest. In this section, we briefly highlight the techniques used for such characterizations. The detailed information on those issues are available in specific monographs and reviews (Michler, 2008, Thomas, 2013, Thomas & Stephen, 2010, Sawyer *et al*., 2008, Guo, 2016 and Grellmann & Seidler, 2011).

a) Structural characterization by microscopy

Morphological characterization of the materials is generally determined by microscopic (optical as well as electron microscopy) and X-ray diffraction techniques. These methods provide a wide range of information on different length scales. The structural details of fibers and polymer composites ranging from a few Angstroms up to over 100 mm can be evaluated by these tools (Lee *et al*., 2009). An overview of different microscopic technique in view of their resolution power is presented in Fig 2.1 (Adhikari & Michler 2009)

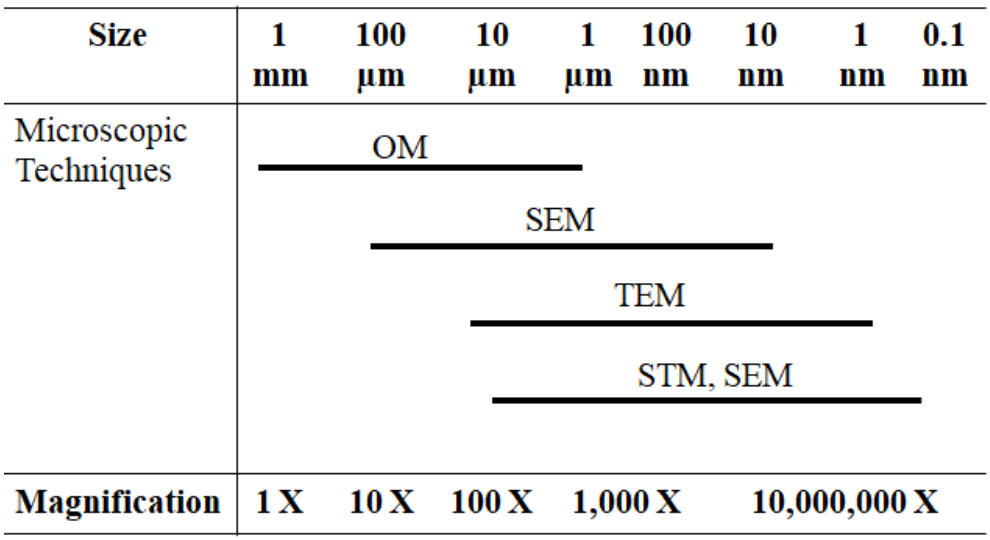

Figure 2.1: Resolution ability of different microscopic tools (Adhikari & Michler, 2009)

The optical microscopy (OM) offers the overview imaging of the microscopic structures which are a few microns up to a few millimeters. Polarizing optical microscopy (POM) gives, in most cases, the clear idea about the microscopic dimension as well as information about the structural heterogeneity of the materials including macroscopic crystalline textures (Sawyer *et al*., 2008, Adhikari & Michler 2009).

Scanning electron microscopy (SEM) (Rajan *et al*., 2009, He *et al.*, 2007, Okubo *et al*., 2004, Bozzolz *et al*., 1992) and transmission electron microscopy (TEM) (Stelte & Sanadi, 2009, Bozzolz *et al*., 1992, Yang & Ye, 2012, Rosa *et al*., 2010) offer the resolution of up to individual nanofibers illuminating the insight into the polymer/fiber interface.

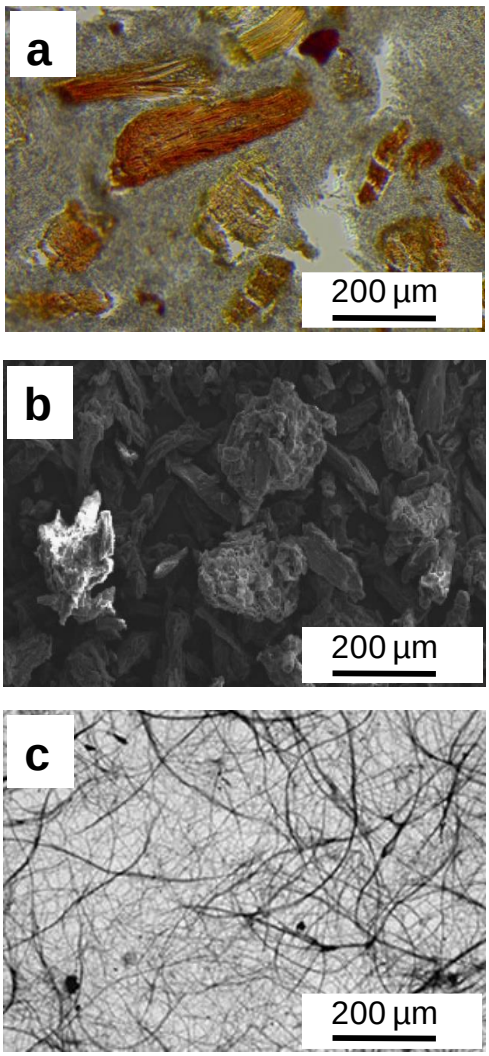

Figure 2.2: Micrographs showing morphology of natural fibers at different length scales: a) optical photograph of the fibers embedded in a polymer matrix, b) microcrystalline cellulose (Avicel) (Abraham *et al*., 2012), and c) cellulose nanofibers obtained from the banana peel (Pelissari *et al*, 2014)

The scanning probe microscopy (SPM) including scanning tunneling microscopy (STM) and scanning force microscopy (SFM) can easily go into atomic resolution domain of materials characterizations (Mikkelsen *et al*., 2009, Michler, 2008, Thomas *et al*., 2013, Thomas & Stephen, 2010, Sawyer *et al*., 2008, Guo, 2016, Grellmann & Seidler 2011). Thus, it can be easily followed that the scanning probe techniques and electron microscopy (EM) possess the central position among the modern nanoscale characterization techniques for detailed characterization of the polymeric materials.

As illustration, Fig. 2.2 shows the morphology of cellulosic fibers on different length scales as observed by POM, SEM and TEM. The overview of natural fibers along the longitudinal axis is presented in Fig. 2.2a in which the gray scale of birefringence in fiber surface represents the crystalline texture of the fibers. The field emission SEM imaging of the chemically processed MCC fibers illustrated in Fig 2.2b depicts crystalline nature of cellulosic fibers while the micrograph in Fig. 2c shows the structure of individual nanofiber obtained from the banana peel fibers on 7 times passes in homogenizer (Pelissari *et al*., 2014). It should be, nevertheless, admitted that the information obtained by microscopic tools is limited to very local structural details. For more integral structural details of the materials, diffraction and spectroscopic techniques and required.

b) X-ray diffraction and spectroscopic characterization

Many polymeric materials, including natural polymers and fibers, are semicrystalline in nature and their crystalline behaviour can be well revealed by X-ray diffraction (XRD). In this method, the intensity of the peaks along with the 2θ values precisely signifies the crystalline behaviour. The diffractogram can be used to calculate the crystallinity index (CI), determine the nature of crystals as well as quantify the d-spacing (practically the distance between two crystalline layers) (Sawyer *et al*., 2008, Mathew *et al*., 2012, Herrera *et al*., 2012, Guo, 2016). The crystallinity index can be calculated by Segal equation (Segal, 1959):

$$Crystallinity\ index\,(\%) = \frac{I_{200} - I_{am}}{I_{200}} \times 100\,\% \qquad (2.1)$$

where, I_{200} = 2θ Intensity value for crystalline cellulose, and

I_{am} = 2θ intensity value for amorphous cellulose.

On the basis of many studies, it can be concluded that the cellulosic fibers depict the crystalline peaks at the 2θ values between 12 ° to 25 ° (at 16°, 17°, 19° and 22°)of the diffractogram (Adhikari *et al*., 2012, Pelissari *et al*., 2014, Mathew *et al*., 2005, Maiti *et al*., 2011). For instance, the XRD patterns of banana peel fibers obtained by a series of mechano-chemical processing steps on banana peels are presented in Fig. 2.3. The size of the nanocrystals was manipulated by allowing the cellulosic nanomaterial to pass through the homogenizer for 3, 5 and 7 times which resulted in the decrease of the particle size in the same order (which have been designated as N3, N5, N7, respectively in Fig. 2.3 (Pelissari *et al*., 2014). The figure shows an increasing trend of the crystallinity on decreasing the particle size of NCC.

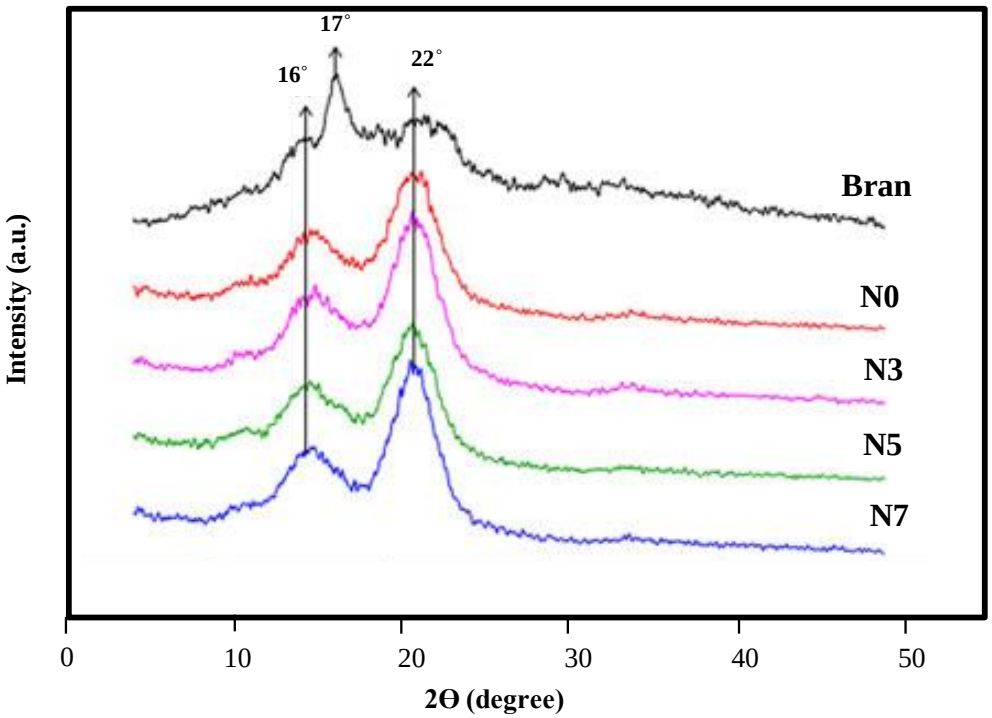

Figure 2.3: XRD patterns for banana peel (Bran), NCC (N0) and the NCC passing through homogenizer for 3 (N3), 5 (N5) 7 (N7) times (Pelissari *et al*., 2014)

In the similar manner, the crystallization behaviour of polymers and composites with natural fibers can be determined by XRD (Nam *et al*., 2003, Mandal & Charabarty, 2014). The method allows the observation of filler influence on nucleation of crystalline phases of the polymer matrix.

The spectroscopic techniques such as Fourier transform infrared (FTIR), Raman, and X-ray photoelectron spectroscopy (XPS) can be utilized in order to access molecular level information on the interaction between different phases, nature of the interface etc. by analyzing the position and intensity of the spectral peaks. In particular, in FTIR spectra, the spectral positions are directly linked to different functional groups and thus may signify the interaction at the interfacial region. The information can be thus later linked with the resulting mechanical and other physicochemical properties of the materials (Adhikari *et al*., 2012, Pokhrel *et al*., 2016a).

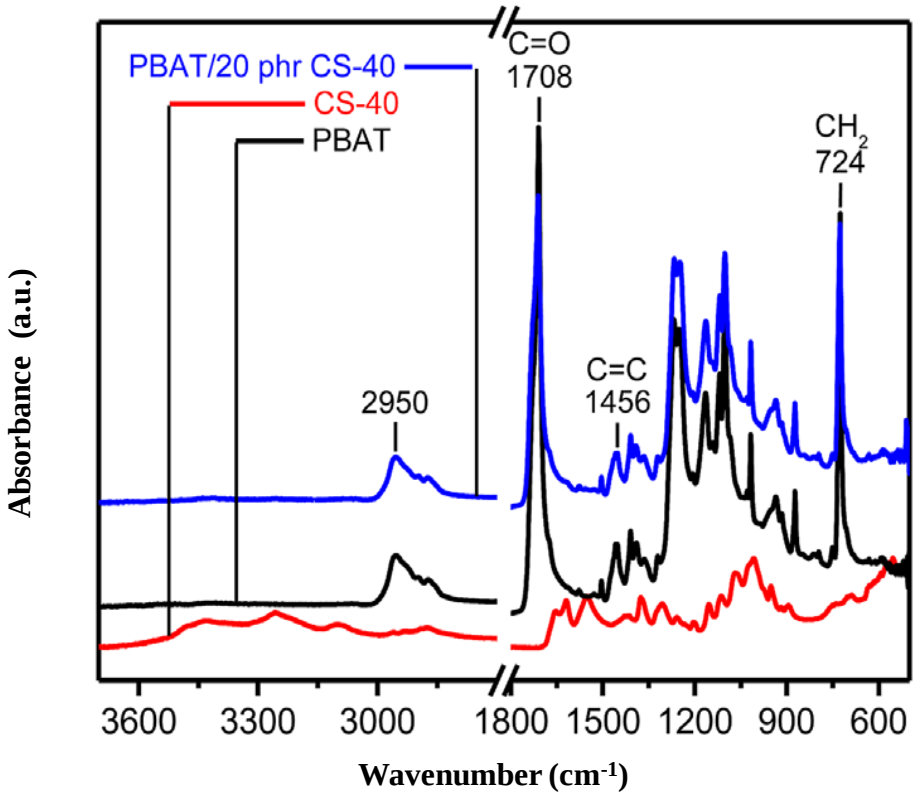

Figure 2.4: FTIR absorption spectra of the PBAT compared to that of chitosan prepared by deacteylation with 40 % NaOH (CS-40) and PBAT/20 phr CS-40 composites (Pokhrel *et al*., 2016a)

Pokhrel *et al*. (2016) illustrated the application of spectroscopy in characterization of polymer composites comprising biodegradable copolyester, the PBAT, chitosan from prawn shell origin deacetylated with 40 % NaOH (CS-40) and 20 % by wt. of chitosan PBAT composite, (see Fig. 2.4) Let us first examine the peaks corresponding to the copolyester. The small peaks located at 1456 cm^{-1} (Pokhrel *et al*., 2016a) give IR absorption for vibrational stretching of C-H bond in the CH_3 group of PBAT.

Moreover, the peak at 1099 cm^{-1} indicates the presence of C-O-C stretching vibration of the ester bond of the PBAT. Similarly, the peak centered at 724 cm^{-1} represents the aromatic ring present in the polymer (Kramer *et al*., 2006).

In the spectra of the composites surfaces, there are no peaks corresponding to the chitosan. The presence of the only peaks corresponding to the PBAT in both the composites indicates the dominance of the PBAT towards the surface of the composite films. The FTIR spectra further illustrate that in spite of good compatibility between chitosan with the PBAT, there is no significant bonding of chemical nature, also supporting the notion of microscopic results (Pokhrel, 2016b). In brief, the spectroscopic data act as a signature for chemical identity of the materials also illustrating, if there is the presence of any chemical interaction in the interfacial region and preference of any components towards the surface.

c) Mechanical, thermal and degradation behaviour

Mechanical properties of polymeric materials and fibers can be determined by different methods such as tensile as well as compression, impact and dynamic mechanical testing (Grellmann & Seidler, 2011). On the other hand, thermal and degradation behaviour can be measured by various methods as well (Guo, 2016). These measurements not only provide the materials specific properties profile of the substances but also record the signature of various chemical treatments and interfacial modifications.

Here, we present an example of the effect of variation in NaOH treatments for deacetylation to prepare chitosan and its thermostability in comparison to commercial chitosan (Pokhrel *et al*., 2016a). The tensile mechanical and degradation behaviour will be discussed in the next sections.

The plot in Fig. 2.5 illustrates of thermogravimetric analysis of PBAT, CS-40, PBAT/20 phr CS-40 and 60 phr CS-40 (Pokhrel *et al*., 2016a). PBAT and chitosan show single step degradation process where as composites show two-steps degradation processes. The chitosan shows weight loss of up to 72 % at around 414 °C although it starts to degrade at 258 °C, the major degradation occurring at T_{max} is 425 °C (Pokhrel *et al*., 2016a).

The complete degradation of the PBAT, CS-40, PBAT/20 phr CS-40 and PBAT/60 phr CS-40 at 425 °C leaving the residual mass of 4 %, 8 %, 13 % and 18 % in the form of char after combustion at 600 °C. Thus, on comparing thermal behaviour, one can observe that the chitosan induce thermal stability into the composites (Pokhrel *et al*., 2016a).

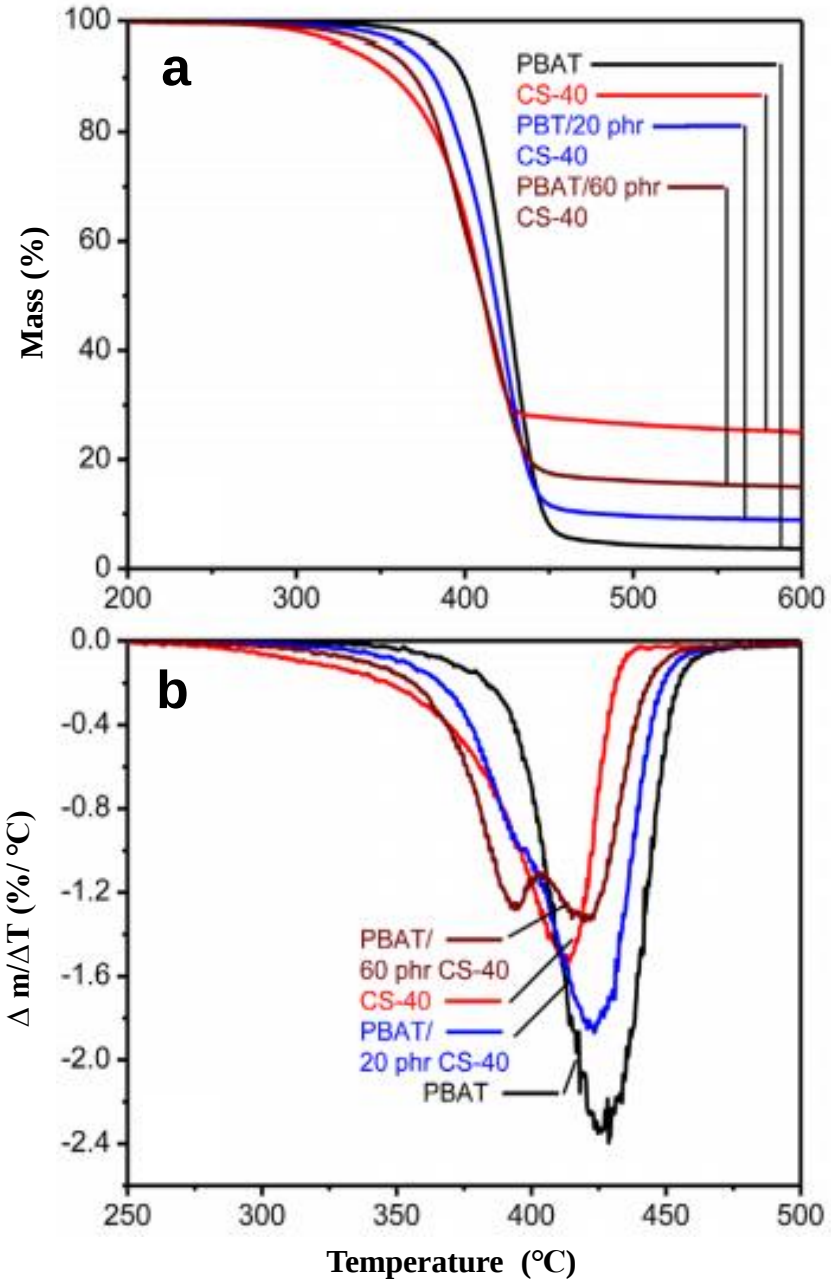

Figure 2.5 Comparative TGA thermograms of PBAT, chitosan, PBAT/20 % wt. of chitosan and PBAT/60 % wt. of chitosan (Pokhrel *et al*., 2016a)

Thus, the thermogravimetric measurements allow the comparison of the thermostability of the materials at hand, irrespective of whether the material is the fibers or the blends or the composites with natural fibers.

2.2. Natural Fibers and Degradable *Green* Composites

2.2.1 Natural Fiber Composites

It has been already pointed out that the common fillers of both scientific and economic interest have been the flours or fibers derived from wood flour (Demir *et al*., 2006, Beg & Pickering, 2008a, Beg & Pickering, 2008b, Sanadi., 1995, Rana *et al*., 1998, Nachtigall *et al*., 2007), rice husks (Marti-Ferrer *et al*., 2005), and other natural fibers such as flax, sisal, kenaf, kraft, jute etc. (Bledzki *et al*., 1996, Marti-Ferrer *et al*., 2005, Yang *et al*., 2006, Yang *et al*., 2004). Particular attention has been paid in many studies on the use of agricultural and carpentry wastes (such as rice husks, cotton rests, saw dusts etc. (Demir *et al*., 2006, Beg & Pickering, 2008a, Beg & Pickering, 2008b, Ichazo *et al*., 2001) as filler to prepare novel composite materials.

A large volume of scientific data concerning the processing, properties and morphological aspects of natural fillers in polyolefins (Beg & Pickering, 2008a, Ichazo *et al*., 2001), polyesters (Sreekumar *et al*., 2007) and thermosetting resins (Biswas & Satapathy, 2010) can be found in the literature. Aiming at the study of the thermal, mechanical and morphological properties of the composites of commodity plastics such as polypropylene (PP) and polyethylene (PE), the former was blended with carpentry waste of the wood *Shorea robusta* and investigated for morphological, mechanical and thermal properties of the composites (Adhikari *et al*., 2012). The morphological results are presented in Fig. 2.6.

Fig. 2.6a is the SEM image of fracture surface PP/60 wt. % wood flour composite comprising no compatibilizer. There are sharp ridges at the interfacial region; formed by incompatibility between the components (Adhikari *et al*., 2012). Fig. 2.6b presents the SEM micrograph of the corresponding sample containing 5 wt.-% maleic anhydride grafted PP (PP-g-MA) as a compatibilizer in the polypropylene matrix. The fracture surface morphology of the composite presented is quite similar to that

presented in Fig. 2.6a with typical structures of the wood fibers and the surrounding polypropylene matrix. The wood structures in Fig. 6b are rougher and have no cracks at the boundaries with the matrix. The filler particles further keep their basic morphology, but exhibit rougher surface textures implying the presence of good bonding between the particles and matrix (Adhikari *et al*., 2012).

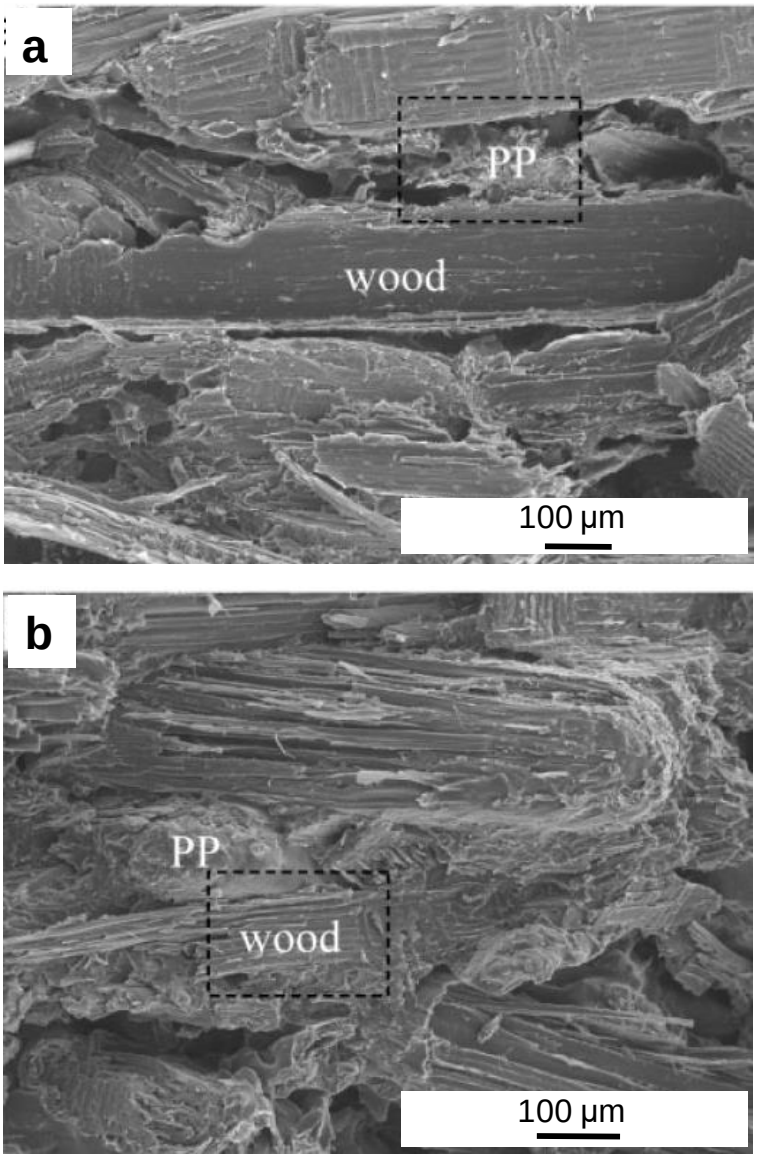

Figure 2.6: SEM images of composites containing 60 wt.-% wood flour in PP matrix; a) no compatibilizer and b) with compatibilizer (Adhikari *et al*., 2012)

Such morphological behaviour is typical of hydrophobic polymers with hydrophilic natural fibers. There is generally a clear indication of role of compatibilizers in the

morphological properties of the composites (Ozkoc *et al*., 2010).

The micrographs in Fig. 2.6 are presented to illustrate the basic morphology of natural fibers composites and the effect of compatibilizer on the morphology and thus on resulting properties of the materials (Adhikari *et al*., 2012). The presence of natural fibers in contact with petrochemical based commodity plastics may facilitate the weathering process of the polymer. However, it should be kept in mind that these composites are able to biodegrade. In the next section, the structure and properties of the completely degradable composite materials will be illustrated.

2.2.2 Degradable Polymer Composites

Biodegradable polyesters and copolyesters (Pal & Katiyar, 2017, Palisikowski *et al*., 2017, Kitagawa *et al*., 2005, Lee *et al*., 2004) have been recently used as a matrix to prepare new materials. Among the biodegradable polymers, PLA and polybutylene succinate (PBS), aliphatic-aromatic copolyesters etc. have got particular commercial attention due mainly to their biodegradability and sustainability (Leja & Lewandowicz, 2010, Shah *et al*., 2007, Adhikari *et al*., 2012, Yan *et al*., 2009).

Thus, aiming at the development of completely biodegradable composite materials based on locally available low cost bamboo flour (BF) as filler, structure-properties correlations in the composites of the aliphatic-aromatic copolyester (a commercial product, the PBAT, called as Ecoflex) and bamboo flour (BF) were studied. For instance, the SEM micrographs of the fracture surfaces of two different composites (having 20 and 60 wt.-% of alkali treated bamboo flour) are presented in Fig. 2.7 (Adhikari *et al*., 2012).

In the composites with 20 wt.-% BF (Fig. 2.7a), both the matrix and filler can be easily recognized. At several locations, BF fibers which have been pulled-out from the matrix can be observed. Also, the holes formed by the pulled-out fibers are visible on the micrographs (Adhikari *et al*., 2012).

At high BF content, the matrix fraction practically disappears on the micrographs as it functions only as binding materials for the BF. In the composite with 60 wt.-% BF (Fig. 2.7b), the fibers are as randomly and uniformly distributed as in the case of low

filler content composite. The fibers have no preferential orientation. It is indeed very interesting to note that a very large amount of BFs can be dispersed into the polymer matrix without using any compatibilizer (Adhikari *et al*., 2012).

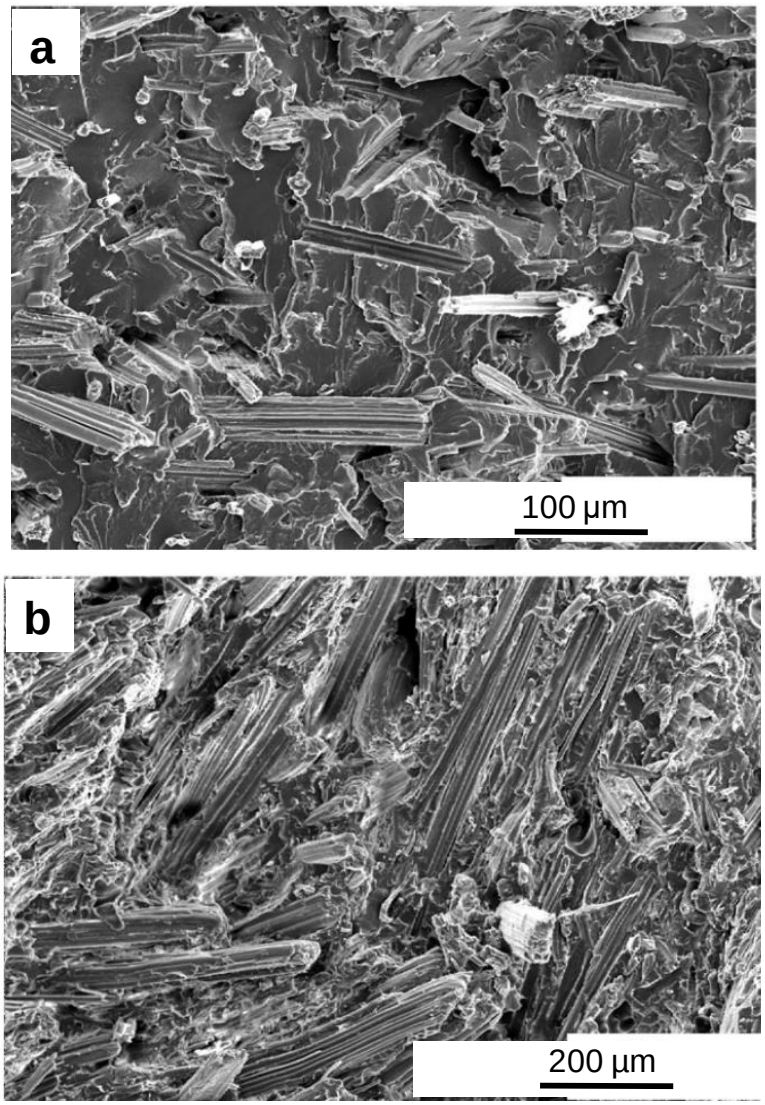

Figure 2.7: Scanning electron micrographs of the Ecoflex/BF composites: (a) 20 wt.-% BF and (b) 60 wt.-% BF; cryo-fractured surface of the specimens (Adhikari *et al*., 2012)

For gaining closer insight into the morphology of the Ecoflex/BF composites, the compression molded samples were studied by wide-angle X-ray scattering (WAXS) using reflection modes which provided the information on the structure of materials on the surface as well as bulk of the specimens. The results are presented in Fig. 2.8 (Adhikari *et al*., 2012). In the pure Ecoflex, several peaks corresponding to the semi-crystalline framework of the matrix could be ascertained. The Ecoflex crystalline

reflections of the composites observed at values of 2θ 17.3°, 20.2° and 23° progressively disappeared, implying that the structure of the matrix was gradually destroyed by the presence of BFs. As a result, in the composites with 40 % BF or more, the structure of the BFs predominated, and the diffractogram of cellulose appeared (Adhikari *et al*., 2012).

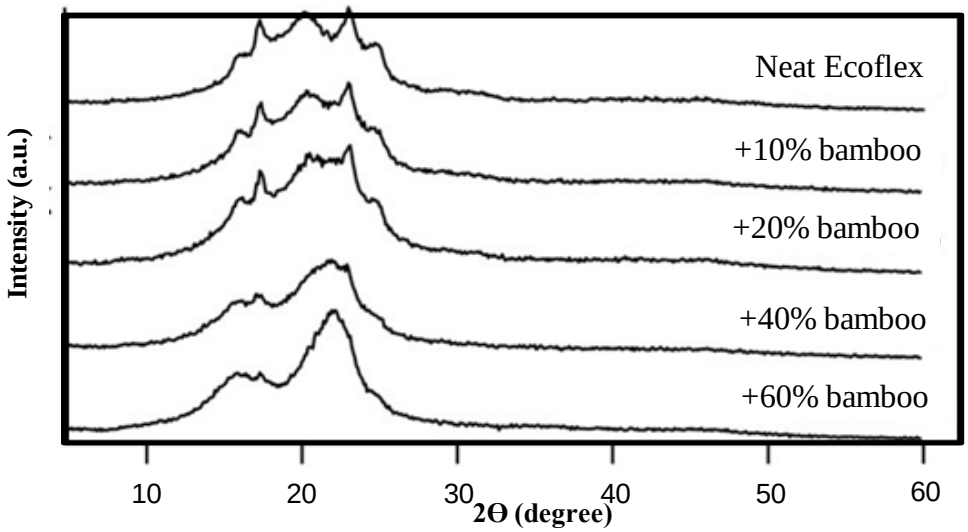

Figure 2.8: WAXS patterns of Ecoflex/BF composites containing various amount of BFs recorded in reflection mode (Adhikari *et al*., 2012)

It was demonstrated that the BF could be rather easily incorporated quite homogeneously into the biodegradable polymeric matrix up to high content. The filler weakly adhered to the matrix as demonstrated by the pulling-out of BFs on the electron micrographs, which was further attested by thermogravimetric analysis (Adhikari *et al*., 2012).

The tensile mechanical properties of Ecoflex/BF composites are presented in Fig. 2.9 (Adhikari *et al*., 2012). The results illustrate that the pristine polymer exhibits large plastic deformation, accompanied by yielding, cold drawing, and strong strain-hardening phenomenon showing elongation at break of 800 % and tensile strength of over 30 MPa. The addition of 20 wt.-% of the filler BF shows a drastic reduction in both breaking strains as well as tensile strength. Nevertheless, the yield strength of the composites increases with filler content. The composites are thus suitable for low load bearing applications (Adhikari *et al*., 2012).

The mechanical properties of the composites are suited only for low load bearing applications. The matrix/filler compatibility should be improved in order to enhance the mechanical properties of the composites (Adhikari *et al*., 2012).

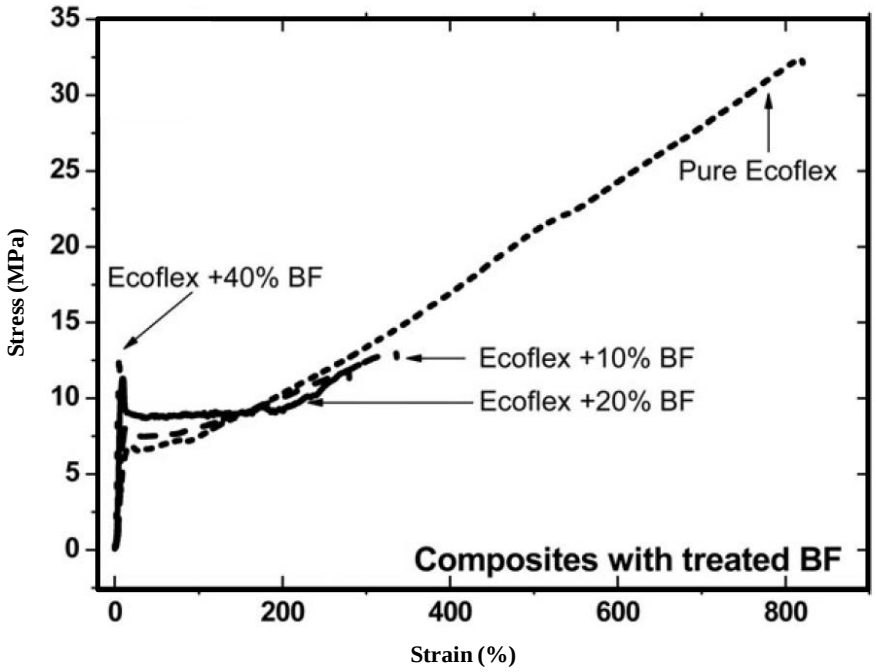

Figure 2.9: Tensile stress–strain curves of Ecoflex/BF composites with various BF contents (Adhikari *et al*., 2012)

In spite of the matrix being degradable, such materials (as the composites based on PLA, PHB, and Ecoflex etc.) may not be termed as completely degradable as the filler and matrix remain intact due to the presence of compatibilizers at the filler/matrix interface (Adhikari *et al*., 2012, Sreekumar *et al*., 2007, Palisikowski *et al*., 2017). In the next section, we will deal with the composite materials using micro- and nanocrystalline celluloses derived from agricultural wastes and also shed light on the degradation behaviour of such materials.

2.2.3 Completely Degradable Green Polymer Composites

The completely degradable *green* composites are those in which the polymers are derived from green sources. Besides, all, the constituents of the composites must undergo degradation under soil composting conditions. Such composites are indeed

the need of the present situation. Degradable polymers with aromatic ring usually do not go biodegradation or composting process as breakage of such ring needs high energy and in the soil there are no microbes which can enzymatically deteriorate the aromatic rings to convert the polymers into simpler forms (Dhar *et al*., 2014). Polymers containing simple hydrolysable chemical bonds (such as ester, ether bonds) get easily decomposed under soil burial conditions and attached by bacteria and minerals (Palisikowski *et al*., 2017, Novotny *et al*., 2015). Thus, Polylactic acid (PLA), Polyhydroxyalkanoates (PHA), Poly(3-hydroxybutyrate-*co*-3-hydroxyvalerate) (PHBV) and their composites with bio-fillers such as MCC, NCC, starch, hydroxyapatite, lignin, chitin, and chitosan are used to prepare completely green composites (Adhikari *et al*., 2012, Pokhrel *et al*., 2016a). These composites even due to the presence of the biogenic fillers undergo early degradation. There are many types of researches on evaluating the effect of filler nature and duration in biodegradation of polymeric materials (Abraham *et al*., 2012, Pokhrel *et al*., 2016b, Pereda *et al*., 2011, Ochi, 2008, Kabir *et al*., 2012).

a) Introduction to biodegradation

Polymers comprise giant molecules which undergo degradation when their bonds break. The later process can be induced by exposure to light (such as UV radiation), environmental weathering, and soil composting or microbial incubation (Shah *et al*., 2007, Nagata *et al*., 2011). Here, the special interest lies in the discussion of biodegradation of polymers, blends, and composites caused by the action of microbes or fungi or under soil burial condition.

I. Microbial degradation

The degradation of the polymeric materials can be done by incubating with the specific bacteria which can feed on those materials and break the macromolecules during metabolic activity. The bacteria produce primary and secondary metabolites or some specific enzymes which have the capacity to break the stereospecific and stereoselective bonds. *Bacillus subtilies, Aspergillus niger, Streptococcus aureus candida, Escheria coli are* some of the organisms which are been proved as potential agents for degradation of polymeric materials (Moustafa *et al*., 2017, Nam *et al*., 2003, Giri *et al*., 2013, Novotny *et al*., 2015, Sharma *et al*., 2003). Besides the nature

of microbes, the nature, dimension of biogenic fillers and the surrounding environment in terms of pH, temperature, presence of different ions and minerals also affect the degradation process (Mikkelsen *et al*., 2009, Bandera *et al*., 2014, Kramer *et al*., 2006., Demir *et al*., 2006, Rana *et al*., 1998, Pereda *et al*., 2011, Novotny *et al*., 2015, Esmaeli *et al*., 2013, Carrasco *et al*., 2011).

II. Soil composting

The soil on upper level of earth crust offers habitat for different organisms such as bacteria, virus, fungi, insect, small rodents, reptile and mammals all live together adapting along with wide varieties of flora. Usually, the good degradation process is expected when the soil contains a higher amount of micro-organisms, acidity and the corrosive minerals contents (Banerjee *et al*., 2014, Leja *et al*., 2010, Shah *et al*., 2007).

Turning towards the renewable flora-based resources of the nature, either from agriculture or from the forest products, it can be observed that major part of the plant bodies is made up of macromolecular cellulosic materials (Rajan *et al*., 2009, Chan *et al*., 2013, Cherian *et al*., 2011, Yu & Li, 2014, Giri & Adhikari, 2013, Sanjay *et al*., 2016, Pelissari *et al*., 2014, Ibrahim *et al*., 2010, Reddy & Rhim, 2014). After end use of the products, a large part of the agricultural and forest residues become wastes. Thus, these waste parts of the plants can be one of the renewable resources to prepare MCC and NCC, which is in line with major principles of the green chemistry signifying the conversion of waste to value-added products (Leja & Lewandowicz, 2010, Carrasco *et al*., 2011, Saxena *et al*., 2008, Cho, 2012, Wu, 2012, Faguaga *et al*., 2012).

b) Morphological variation

In this section, among different kinds of biodegradable polymer composites, we focus on the structural characterization of some PLA/PBAT blends and their composite with ramie fibers.

First the Ramie/PLA (20/80 by wt./wt. ratio) was prepared by melt mixing. The stiffness of the composites was increased and the samples acted quite brittle. Fig. 2.10 compares for mechanical properties such as loss in toughness with addition of PBAT *via* impact test (Yu & Li, 2014).

A closer look at Fig. 2.10b reveals further that there is a physical interaction between the polymer matrix and filler although there is no specific chemical bonding (Yu & Li, 2014). PBAT in the composites act for the phase segregation and stress transferring which ultimately facilitates the failure in fiber pull out and fiber breakage (Yu & Li, 2014).

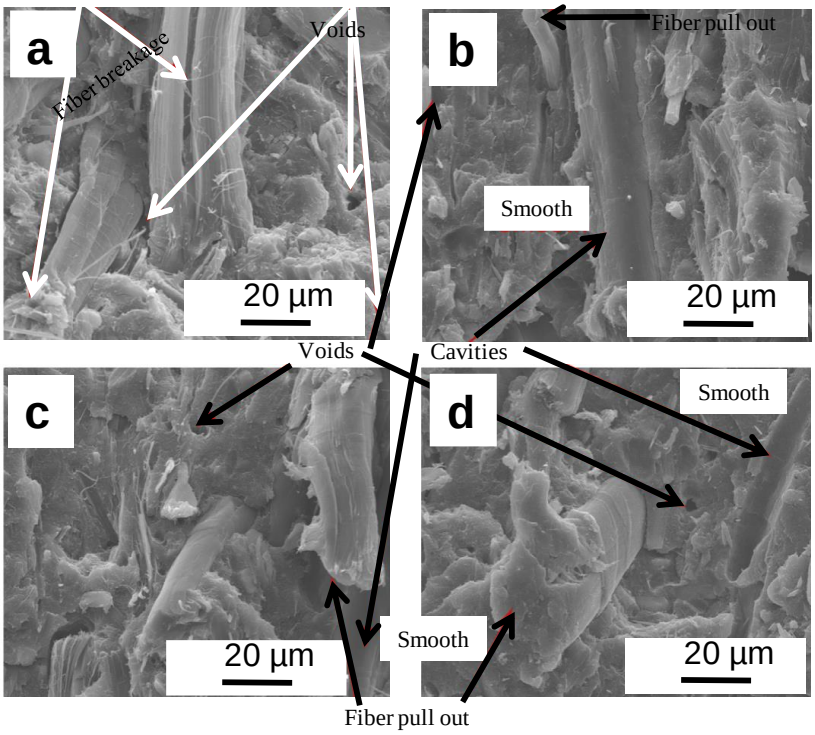

Figure 2.10: SEM micrograph of fractured surface of notched izod specimens of ramie/PLA/PBAT blend composites with various PBAT % ; (a) ramie/PLA, (b) ramie/PLA/5% PBAT blend, (c) ramie/PLA/10% PBAT blend and (d) ramie/PLA/15 % PBAT (Yu & Li, 2014)

The other properties of the composites were evaluated *via* soil composting tests, contact angle as well as water absorption measurements, scanning electron microscopy (SEM) and gel permeation chromatography (GPC) (Morouco *et al.*, 2016, Pokhrel *et al.*, 2016a). Compared to the neat PCL, the composites showed enhanced surface hydrophilicity with cellulose nanofibers (CNF) thereby increasing the ability for biocompatibility. Even more the hydroxyapatite nanoparticles enhance biocompatibility in PCL/CNF composites (Morouco *et al.*, 2016).

These results are in consistence with the conclusions drawn in similar works reported in the literature including blends and composites with chitosan (Li *et al*., 2003), starch (Shi *et al*., 2011), clay (Chieng *et al*., 2010), and other systems comprising polylactides and other degradable systems (Siro & Plackett, 2010, Liu *et al*., 2010, Panaitescu *et al*., 2011).

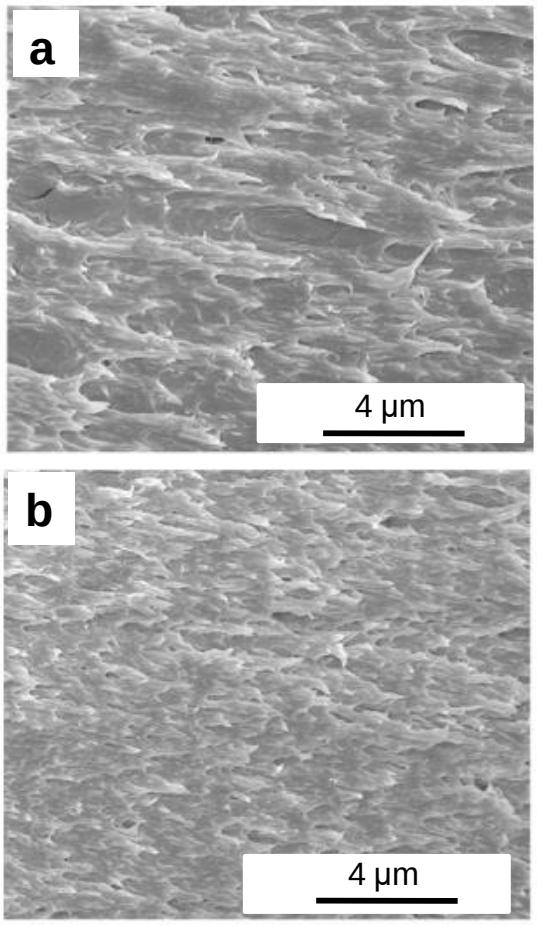

Figure 2.11: SEM micrographs of PVA/acid hydrolyzed NCC (a) and PVA/TEMPO mediated NCC (b) Nanocomposites. SEM micrographs of PBAT composite comprising 2 wt.-% of NCC (Zhou *et al*., 2012)

For the sake of comparison, in Fig. 2.11, the morphology of a nanocomposite of the PVA comprising 2 wt.-% of the NCC prepared by 2, 2, 6, 6-tetramethylpiperidine-1-oxyl radical (TEMPO) mediated oxidation can be observed (Zhou *et al*., 2012). Indeed, the nanofiller content brings the significant effect of large surface areas on the properties of the nanocomposites lies in the range of 1-5 wt.- % (Cho *et al*., 2006, Yang, 2006, Paul & Robeson, 2008). Thus, it makes sense to present the results comprising a lower amount of the nanofiller.

The agglomeration tendency of the nanofiller into the polymer is a sign of the incompatibility of the filler with the adhering matrix (Birinchi *et al*., 2013). The uniform dispersion of the NCC in the polymer matrix is clearly exhibited in Fig. 2.11, without agglomeration of the filler. The micrographs presented in Fig. 2.11 depict a reasonable PVA/NCC compatibility, which is also supported by the presence of cylindrical shaped fillers with the thickness in the range of 40-80 nm (Zhou *et al*., 2012).

Looking at the thickness of individual nanocrystals from acid hydrolysis or TEMPO-mediated oxidation or ultrasonicated and corresponding microcrystals, the average number of the nanocrystals per microcrystal bundle was estimated to be approximately 100. Thus, it can be concluded that the nano-fibrillation could bring in case of cellulosic materials by increasing the surface area by about 100 times. Hence, the nanocomposites can be considered to be much more effective than the conventional ones (Zhou *et al*., 2012).

c) Surface properties

The surface property of the composites, particularly the hydrophilicity, also correlates with their susceptibility towards biodegradation. The nature of the surface determines how the material responds with highly polar substances such as water. During contact angle measurements, generally, the water droplets form the angles with interacting surfaces whose dimension depends upon hydrophilicity or hydrophobicity of the substrate. Higher contact angle represents hydrophobicity whereas the lower contact angle represents hydrophilicity (Dhakal *et al*., 2012, Spiridon *et al*., 2016).

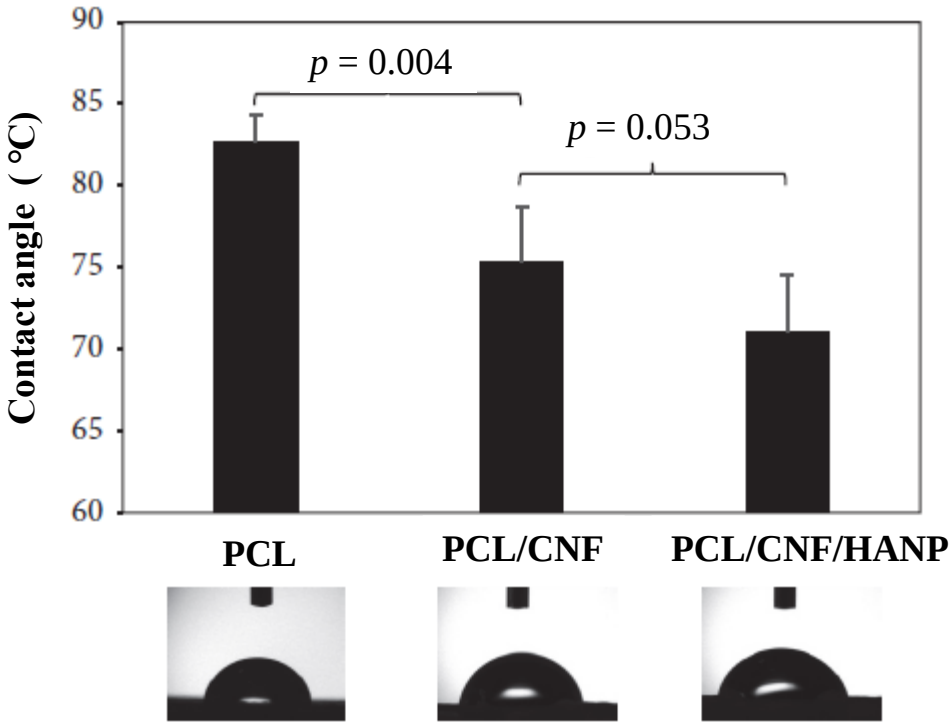

F**igure 2.12:** Photographs showing spontaneous contact angles of water droplets on surfaces of pure PCL (a), and composites comprising 1 % of CNF (b) and 1 % of CNF plus 5 % of HANP (c) (Morouco *et al.*, 2016)

Fig. 2.12 shows spontaneous decrease in contact angles formed by water droplets on the surfaces of pure PCL and PCL/CNF binary and PCL/CNF/Hydroxyapatite nanoparticle (HANP) trinery composites (Morouco *et al.*, 2016). At first glance, the contact angle on the PCL surface looks larger i.e. 82.7° (implying slightly higher hydrophobicity) than on that of the composites (75.3° for PCL/CNF and 71.1° for the PCL/CNF/HANP composites). The decreased hydrophobicity of the composites surfaces compared to the pure PCL can be attributed to the presence of the hydrophilic fibers fractions towards the surface (Dai *et al.*, 2011). Similarly, it illustrates that the hydrophobicity of the specimens primarily depends on the chemical nature of the fillers. The results imply that the hydrophilic OH groups in CNF are distributed on the surface of the composite which ultimately lowers the contact angle value for the water droplets. Moreover HANP adds more hydrophilicity in the PCL/CNF/HANP composites (Morouco *et al.*, 2016). Higher the hydrophilic fillers the higher would be the ease of filler dispersion in composites and thus higher would be the interaction with water, the result is consistent with literature work (Spiridon *et al.*, 2016).

In summary, the wetting behaviour can be correlated with the degradation susceptibility of the composites at hand, the nanocomposites being more susceptible to water absorption and thereby providing higher ease of degradation under soil burial conditions (Morouco *et al.*, 2016, Hassan *et al.*, 2011, Wan *et al.*, 2009). The composites dealt with in Fig. 2.12 have been found to possess excellent water absorption behaviour, thereby increasing the ease of hydrolysis and bond cleavage under microbial attack.

2.2.4 Degradation under Soil Burial Conditions

Morphological studies of the materials subjected to degradation under soil burial conditions were carried out. Thus, the information on the physical states upon various stress conditions was obtained. The morphological features of the samples after the experiments are presented in Fig. 2.13 (Pokhrel *et al*., 2016a).

The photographs in Fig. 2.13 show that highly ductile PBAT and PBAT/Chitosan composites on soil composting become brittle (Pokhrel *et al*., 2016a). The surface of the composites was found to be attacked by the microbes. After 1 month of composting, the samples turned very brittle which ultimately induced fragility to the specimens containing chitosan produced by deacetylation with 70 % NaOH for chitin (Pokhrel *et al*., 2016a).

The morphological feature of samples in Fig. 2.13, were further studied in detail by SEM (Pokhrel *et al*., 2016a). In the beginning of the soil composting, the voids of various diameters appeared on the samples surfaces, as a result of consumption of the filler particles as nutrients, by the microbes which increases with soil burial period, the fillers content vanish completely after 4 months.

Many researchers are working to address this environmental issue. Bhandari, 2013, prepared PBAT/natural fiber composites to study its susceptibility for degradation. Similarly, Pokhrel, 2016 studied degradation in soil environment. These works try to explain the degradation process of the composites materials on soil composting, which finally would lead to embrittlement of the polymeric materials. Similarly, surface property and deformation behaviour during tensile test would also explained. (Tesfaye *et al*., 2017, Singh *et al*., 2008, Liu *et al*., 2014).

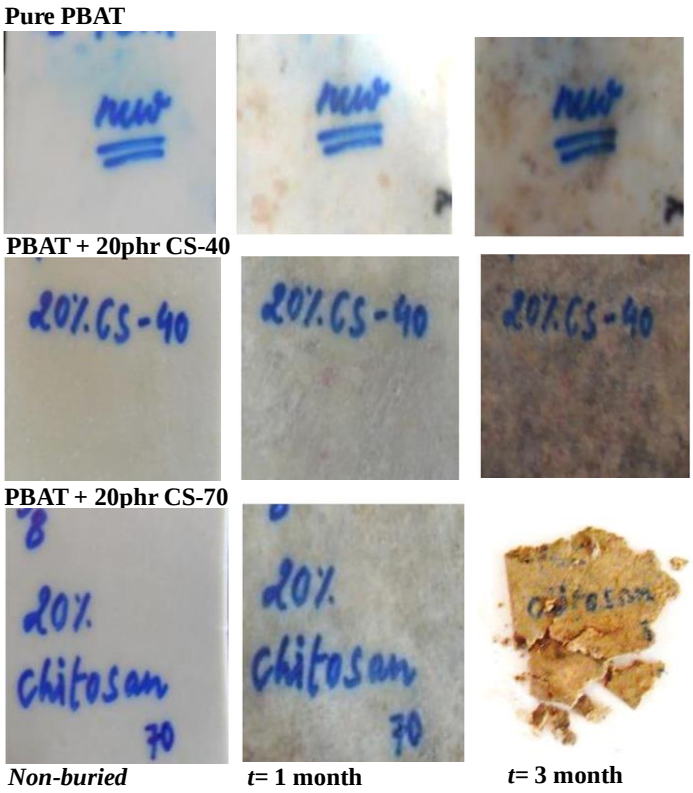

Figure 2.13: Photographs of different PBAT/chitosan composites subjected to soil burial for different periods of time as indicated (Pokhrel *et al*., 2016a)

2.3. Biodegradation Mechanisms

Usually, any kind of degradation starts from the points of weak bonding in the heterogeneous materials. It is known that the chemical linkages, such as ester, ether, amide and hydrogen bonds are susceptible to hydrolysis and can be easily attacked by chemicals and microbes (Itry *et al*., 2012).

The degradation process may proceed with the action of some kinds of acids or enzymes on those weak active sites thereby fragmenting the giant molecules into smaller entities including the liberation of some gases. The polymeric materials can even undergo photolytic degradation on long exposure to sunlight, microwaves or ultra-violet radiations and generate free radicals (Nagata *et al*., 2011).

The biodegradation is a complex process which has been considered to take places in three basic stages (Itry *et al*., 2012): biodeterioration, biofragmentation, and

assimilation, in which the influence of the abiotic factors cannot be undermined. The biodiversity of the microorganisms and their efficacy towards the formation of complex bio-film and their catalytic abilities transform the degraded substances to the nutrients represent highly sophisticated natural phenomena (Mikkelsen *et al*., 2008, Sharma *et al*., 2003).

The biodeterioration stage can be pretty well accessed by thermal and microscopic methods while the fragmentation stage can be monitored by evaluating the changes in the molecular characteristics. The production of carbon dioxide gas is a simple signature of the bioassimilation process which, of course, involves the formation of various kinds of metabolites and microbial biomass (Bielecki *et al*., 2005, Iguchi, 2000, Czaja *et al*., 2006, Mikkelsen *et al*., 2009, Sharma *et al*., 2003, Esmaeli *et al*., 2013). The terminal groups and gaseous substances, as well as the biofilms produced during the degradation processes, can be analyzed by different spectroscopic techniques (Palisikowski *et al*., 2017, Siotto *et al*., 2013, Novotny *et al*., 2015, Itry *et al*., 2012).

In case of polyesters and copolyesters, which have been primarily dealt in the work where two important biodegradation mechanisms are represented in Schemes 3 and 4 (Itry *et al*., 2012).

I. Hydrolytic mechanism

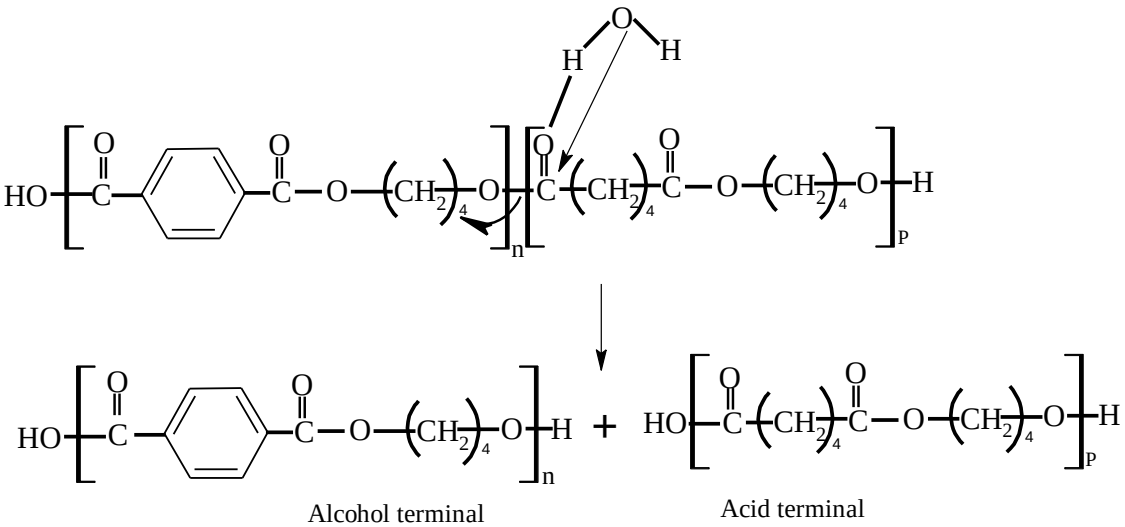

Scheme 2.3: PBAT degradation via hydrolytic attack on carbonyl group of ester to liberate free -COOH and -OH groups; the letters "p" and "n" refer to the degree of polymerization of respective segments ((Itry *et al*., 2012)

II. Main chain scission

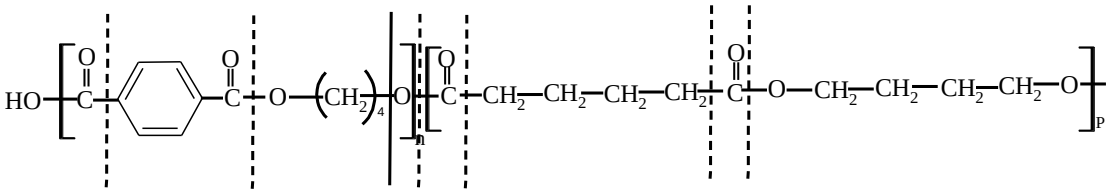

Scheme 2.4: PBAT degradation by chain scission at different positions of macromolecular skeleton under the influence of different factors such as soil burial and the actions of heat as well as pressure (Itry *et al*., 2012)

SUMMARY, TRENDS AND NEW OPPORTUNITIES

In this chapter, attempts have been made to offer an overview, with recent research outputs and applications, the structure-properties correlations of different polymer composites. The results can be summarized as follows.

1. The lignocelluloses-based micro-and nano-fillers can be synthesized by various chemical, mechanical and bioinspired (or biosynthetic) methods and be evaluated in terms of their structural and molecular characteristics *via* spectroscopic, microscopic, scattering and chromatographic techniques.
2. The micro- and nanocrystalline cellulosic fillers can be incorporated to a pretty high weight fraction easily into the biodegradable copolyester matrix even without the use of compatibilizer. However, their uses are limited to prepare composites for a low load bearing application.
3. The copolyester based composite materials undergo rapid fragmentation process under soil burial conditions leading to highly brittle materials within a few months duration. The molecular weight degradation has been, however, not been quantitatively determined that significant. Also the detailed degradation mechanisms should be explored.

There is a trend of utilizing the copolyesters and their composites for biomedical applications (Moraoco *et al*., 2016, Ozkoc *et al*., 2010, Sgarioto *et al*., 2014), for smart packaging films (Dhar *et al*., 2014, Moustafa *et al*., 2017, Pal & Katiyar, 2017),

functional coatings and for flexible conducting materials (Gopakumar *et al.*, 2018). These strategies are achieved by introducing different functional groups *via* grafting onto the natural polymer chains and then making graft and block copolymers with synthetic polymers. The challenge will be then to find suitable routes for biodegradation as the latter is a complex process and a single microbial strain would not be sufficient. In this case, microbial communities can be employed.

There are several biodegradation pathways suggested for various polymeric materials including degradable copolyesters which have been successfully employed. However, the routes for controlled degradation processes leading to the solution to the fundamental environmental problems are yet to evolve. In our Nepalese context, due to the presence of large microbial biodiversity in the region, and proven opportunities to design the desired microbial communities *via* uncomplicated genetic manipulation, there are unparalleled opportunities. The thermophilic and cold-loving bacteria might offer great potential in terms of degradation of the polymers, in general, which still need to be explored.

CHAPTER 3

3. MATERIALS AND METHODS

3.1 Materials

3.1.1 Polymer Matrix

Completely biodegradable thermoplastic aliphatic aromatic-copolyester poly(butylene adipate-co-terephthalate), PBAT (Ecoflex®FBX 7011, a commercial product of BASF SE, Ludwigshafen, Germany) was used as the polymer matrix. The chemical structure of the PBAT is depicted in Fig. 3.1. It has density of 1.26 g/cm^3 and polydispersity index of 2.40. The GPC analysis showed the average molecular weight (M_w) of the PBAT is 161373 g/mol. The glass transition temperature (T_g) and melting point (M. P.) of PBAT have been found to be -30 ℃ and of 115 ℃, respectively.

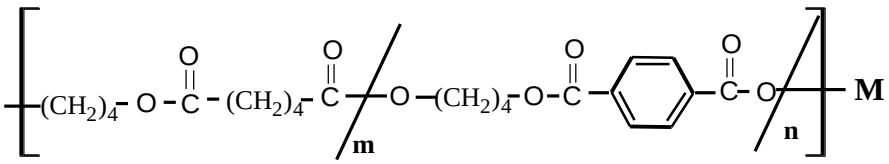

Figure 3.1: Chemical structure of poly(butylene adipate-co-terephthalate) (PBAT); m, n and M stand for degree of polymerization of polyester of adipic acid, polyester of dimethyl terephthalate and degree of polymerization of PBAT, respectively (Itry *et al*., 2012)

3.1.2 Reference Microcrystalline Cellulose

In this work, as a reference material, a commercial microcrystalline cellulose (MCC), the Jelucel HM400X, a trademark of Dow Chemicals, Germany, was used. The material was supplied by Prof. A. K. Bledzki, University of Kassel, Germany. This MCC has been named as *MCC-R*.

3.1.3 Natural Fibers

The main glory of this work is using filler source from the natural agricultural waste, the stalks of wheat (*Triticum aestivum*), which was used to extract the novel materials MCC and NCC. The wheat stalks were collected from the nearby village of Kritipur Municipality, Taudaha. Fig. 3.2 shows the bundles of wheat stalks, which were

chopped into 1 cm long pieces and washed properly. The sun-dried stalks pieces were then subjected to grinding to fine powders with the help of laboratory grinder. The fiber flour (FF) was filtered through sieves to obtain the particles with diameter ≤ 200 μm.

Figure 3.2: Photograph showing bundles of wheat straw collected from agricultural farm

3.1.4 Chemicals

The laboratory grade chemicals (such as NaOH, NaOCl, $NaHSO_3$, conc. H_2SO_4, absolute alcohol and acetone) were purchased from Qualigen Fisher Scientific, Mumbai, India; and were used without further purification.

3.2 Sample Preparation

3.2.1 Preparation of Micro (MCC)- and Nanocrystalline Cellulose (NCC)

Wheat stalk FF was subjected to different chemical and thermomechanical treatment to convert them to MCC and NCC. The processes are schematically illustrated in Fig. 3.3.

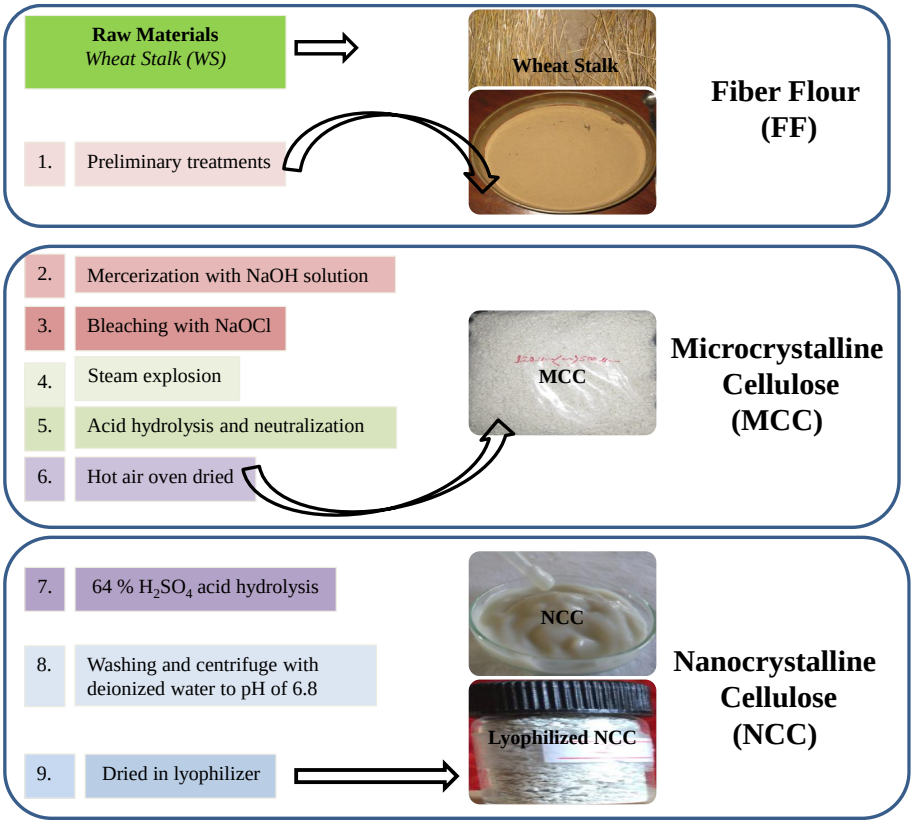

Figure 3.3: Schematic representation of different disintegration steps (left side) and photographs (right side) showing different stages of conversion of wheat FF to MCC and NCC

a) Preparation of MCC

The wheat stalk FF was mercerized with 5 % NaOH solution with fiber to solution weight/volume ratio of 1:50 while heating at 60 °C with constant stirring for 3 hr (Cherian *et al*., 2011, Liu *et al*., 2010). The mixture was neutralized to pH of 7 with 5 % H_2SO_4 solution and finally washed with triple deionized water. The powder was steam exploded in laboratory autoclave at 0.1379 MPa pressure for 30 minutes followed by bleaching with 4 % NaClO solution with constant stirring for 2 hours. Finally, the mixture was treated with 1 % $NaHSO_3$ solution in 1:50 weight/volume ratio to remove excess of NaClO and washed properly with deionized water (Paula et al., 2008, Siro & Plackett, 2010, Rosli *et al*., 2013)

The fiber flour was treated with 20 % H_2SO_4 with stirring in an ice bath for microfibrillation with flour to acid weight/volume ratio of 1:3) for 20 min and washed properly with triple deionized water and finally with absolute alcohol. The shining white cellulose powder, microcrystalline cellulose (MCC), thus obtained was dried in vacuum oven at 80 °C (Chan *et al*., 2013, Rajan *et al*., 2009, Rosli *et al*., 2013).

b) Preparation of NCC

The MCC extracted from wheat stalk was nano-fibrillated by treating with 64 % H_2SO_4 in drop wise fashion from the burette, with MCC fiber to solution weight volume ratio of 1:10 with constant stirring using magnetic stirrer for half an hour, followed by sonication for an hour. The hydrolysis process of MCC in 64 % H_2SO_4 was quenched by addition of triple deionized water in excess. The white suspension of the MCC in water thus obtained was nanocrystalline cellulose (NCC). The NCC was made acid free by washing with deionized water followed by centrifuging at 8000 rpm (Cherian *et al*., 2011, Rosli *et al*., 2013). The NCC produced was white gel-like on observation which was washed with deionized water and acetone in order to remove water. Then dried in lyophilizer (Telstar, Lyo Quest, Spain). The NCC obtained was grinded properly so that very fine white amorphous powder was obtained which is homogeneously dispersed in water to form turbid solution. Thus the powder of NCC was obtained. Fig. 3.3 explains all the experimental protocols. Table 3.1 collects the type of fibers and abbreviations of the fibers used in this work.

Table 3.1: List of natural fibers used in this work

S.No.	Sample Code	Remarks
1.	WS	Wheat stalk, Fiber Flour (FF)
2.	MCC	Microcrystalline cellulose from WS
3.	NCC	Nanocrystalline cellulose from MCC, WS source
4.	MCC-R	Commercial microcrystalline cellulose

3.2.2 Preparation of Polymer Composites

The composites of PBAT were prepared with MCC, NCC, WS and MCC-R by melt mixing and extrusion processes, respectively.

a) PBAT/MCC microcomposites

The MCC and PBAT were dried in hot air oven at 80 ℃ for 8 hrs. Both of them were mixed in an internal melt mixture (Model:Brabender Plasticorder 2100, The Netherlands) maintained at 120 ℃ and 70 rpm for 15 min. First of all, the polymer was melted for 2 min. Then the MCC was added and subsequently mixed for 13 min.

These mixtures were then fetched into the roll mills to make sheets of the composites. Each composite was compression molded into 1 mm thick sheets (using molding apparatus of model COLLIN P200P/M) at 160 °C and 100 MPa pressure for 4 min using standard protocols (Rajan *et al.*, 2009, Siyamak *et al.*, 2012a, Siyamak *et al.*, 2012b, Pokhrel, 2016b). The samples prepared are listed in Table 3.2.

Table 3.2: List of PBAT/MCC microcomposites prepared by melt mixing in internal mixture

S.No.	Sample code	PBAT weight fraction	MCC weight fraction
1	PBAT	100	0
2	M-10	100	10
3	M-20	100	20
4	M-40	100	40
5	M-60	100	60

Other reference samples were also prepared with raw wheat stalk FF and commercial MCC, the Jelucel (i.e., MCC-R.), which are listed in Tables 3.3 and 3.4. These experiments were performed in Hochschule, Merseburg (HoMe), Germany.

Table 3.3: List of reference polymer composites prepared by melt mixing PBAT with WS fiber flour

S.No.	Sample code	PBAT weight fraction	FF weight fraction
1	W-10	100	10
2	W-20	100	20
3	W-40	100	40

Table 3.4: List of M′-composites prepared by melt mixing PBAT with Jelucel, the commercial reference, MCC-R

S.No.	Sample code	PBAT weight fraction	MCC weight fraction
1	PBAT	100	0
2	M′-10	100	10
3	M′-20	100	20
4	M′-40	100	40
5	M′-60	100	60

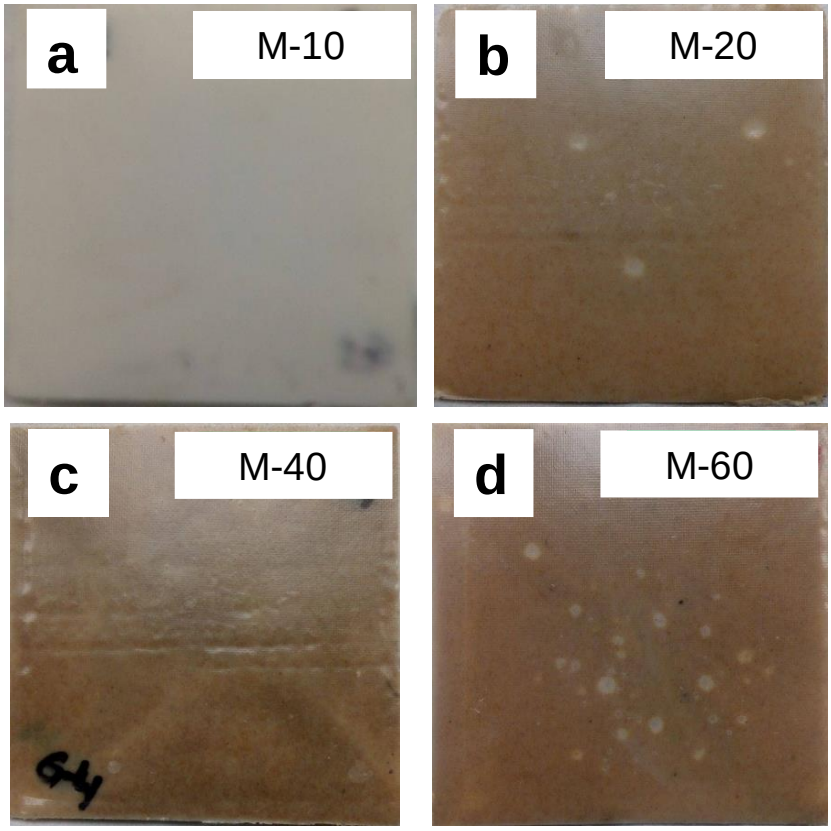

Figure 3.4: Photographs showing PBAT/MCC composites after compression molding (a) pure PBAT, (b) PBAT+10 wt. fraction of MCC, (c) PBAT+20wt. fraction of MCC, and (d) PBAT+40wt. fraction of MCC

b) PBAT/NCC Nanocomposites

NCC was dried in oven for 8 hrs. Dried NCC powder was mixed with dry PBAT in corotating twin screw extruder (Thermoscientific, HAAKE Minilab II). The specific amount of NCC and PBAT was mixed at 135 ℃ for 5mins at 100 rpm (Rajan *et al*., 2009, Siyamak *et al*., 2012a, Siyamak *et al*., 2012b). NCC was mixed upto 10 parts by weight of Polymer. A dias with approximately 0.5 mm thickness and 5 mm diameter was used to take out the composites. Long white stripes of NCC/PBAT composites came out from the machine. The compounding process resulted only 7 g of the composites which is very less, so it was not feasible to prepare sheets in compression molding. The nanoparticles usually have very high dispersion in comparison to microparticles. So the lesser amount of NCC is enough to give the significant effect. Therefore here the nanocomposites are prepared from 1-10 weight fractions of filler. Table 3.5 presents the list of nanocomposites prepared.

Table 3.5: List of PBAT/NCC nanocomposites prepared using twin extruder by melt mixing

S.No.	Sample code	PBAT weight fraction	NCC weight fraction
1	N-1	100	1
2	N-2	100	2
3	N-3	100	3
4	N-5	100	5
5	N-10	100	10

3.3 Characterization Techniques

The samples were studied for their structural, mechanical, thermal as well as degradation behaviour using wide range of analytical techniques.

3.3.1 Spectroscopy, Microscopy and X-Ray Scattering

Structural analysis was carried out by Fourier Transform Infrared (FTIR) Spectroscopy while the morphologies were investigated by Scanning Electron Microscopy (SEM), Transmission Electron Microscopy (TEM) and X-ray diffraction (XRD).

a) Fourier transform infrared (FTIR) spectroscopy

This technique is used to determine the chemical bonding, functional groups and chemical interactions present in the materials under investigation.

In this work, Fourier transform infrared (FTIR) spectroscopy (Perkin Elmer FTIR-2000 with attenuated total reflectance (ATR) mode) was used for analyzing the FTIR spectra recorded in absorbance mode within the wavenumber range of 500–4000 cm^{-1} with the resolution of 10 cm^{-1}. The spectroscopic characterizations were mainly carried out, in the Martin Luther University, Halle-Wittenberg, Germany and IIT, Guwahati, India.

b) Scanning electron microscopy (SEM)

Scanning electron microscopy is one of the most widely used surface characterization techniques employed to interpret the topography, morphology, composition and interacting phases, and also provides crystallographic information of the surfaces.

In this work, SEM micrographs were captured by JSM 6300 (JOEL). Cryo-fractured surfaces and tensile deformed specimens for the SEM were sputter-coated with thin film of gold (Au) and attached to conductive adhesive tape.

b) Transmission electron microscopy (TEM)

The shapes and sizes of the NCC particles with higher resolution were observed by JEOL (JEM-2100F) Transmission Electron Microscope (TEM). The NCC suspension (0.001 g/mL) was prepared by sonicating the mixture for 5 hr. Then, 0.05 µl of suspension was dropped onto a carbon coated copper grid with a micropipette and dried at 40 °C in vacuum oven for 24 hr.

c) X-Ray diffraction (XRD)

The grain size (D) and d-spacing between the crystal layers were studied for the fibers extracted and composites prepared by X-ray diffractometer (Rigaku, TTRAX III 18KW, Japan and Bruker, Germany) on Cu-Kα radiation (λ = 1.5406 Å) at scan rate of 0.05° per 0.5s for 2θ range 5-50°.

The apparent grain size (D), was calculated by Sherrer equation (3.1) and d-spacing was measured by Bragg's Law (Guo, 2016, Arruda *et al.* 2015).

$$Apparent\ grain\ size\ (D) = \frac{K \times \lambda}{\beta\ Cos\theta} \qquad (3.1)$$

where, β = Full width half maxima (FWHM), and

D = Apparent grain size of cellulose crystallite.

K = Constant (0.9), dimensionless shape factor

Bragg's Law gives relation to calculate d-spacing as follows;

$$2d\ Sin\ \theta = n\ \lambda \qquad (3.2)$$

where, θ = Angle of diffraction

n= 1 (for 1st order diffraction)

Similarly, Crystallanity index (CI) is calculated by deconvolution method of calculating area under the peak. According to this method area under the crystalline peak and area under broad amorphous band is calculated by origin 8.0 software and crystalline area

and amorphous area are subjected in equation (3.3) to get crystllinity index (Rambo & Ferreira, 2015).

$$CI(\%) = \frac{I_c}{I_c + I_{am}} \times 100 \qquad (3.3)$$

where, I_c= Area of under crystalline adjusted peak

I_{am}= Area of amorphous broad band

3.3.2 Deformation Behaviour

Mechanical deformation properties of the polymer composites were analyzed by three different methods: microindentation, tensile testing and fracture surface analyses.

a) Microindentation

Microhardness measurements of the composites were performed on Fischerscope® (Helmut Fischer, Germany) microhardness tester equipped with pyramidal Vickers diamond indenter at ambient temperature. The samples films approximately 1 mm thick, 1 cm wide and 1 cm long, were penetrated by the indenter with the loading rate of 1000 mN/20 seconds. The maximum load was 1 N.

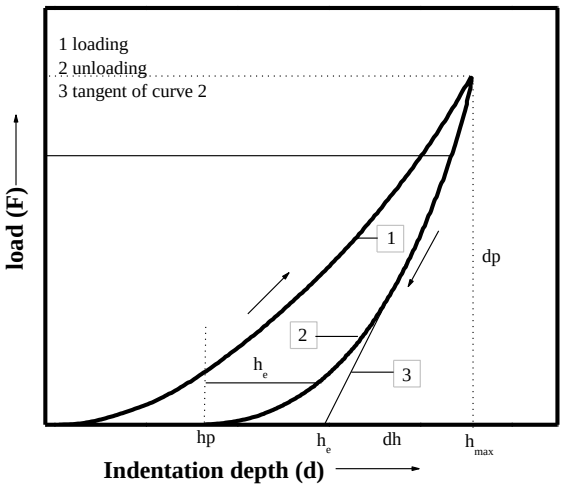

Figure 3.5: Load (*F*) *versus* indentation depth (*h*) curves obtained from microindentation test carried out at room temperature showing elastic and plastic work of deformation (w_e and w_{pl}), maximum load (F_{max}) and maximum indentation depth (h_{max})

The principle of indentation measurements typical based on loading–unloading curve obtained from the instrumental indentation illustrated in Fig. 3.5. The evaluation of

force (F) *versus* indentation depth (h) curves gives for both plastic and elastic works of deformation (Michler & Grellmann, 2010).

Marten's hardness was calculated using equation (3.4) (Lach *et al*., 2010).

$$HM = F/A = F/26.43h^2 \quad (3.4)$$

where, F = testing load in mN, h = penetration depth in mm and A = is the surface area of indenter in mm^2.

Indentation modulus is calculated by equation (3.5) (Lach *et al*., 2013)

$$E_{IT} = \frac{1-\upsilon^2}{0.5\sqrt{\frac{24.5}{\pi}}\left(\frac{dh}{dF}\right)_{F_{max}}\left(4h_{max} - 3F_{max}\left(\frac{dh}{dF}\right)_{F_{max}}\right) - 8.73\times10^{-13}\ Pa^{-1}} \quad (3.5)$$

where, F_{max} = maximum load applied on the test specimens, h_{max} = maximum penetration depth

b) Tensile testing

The mechanical deformation behaviour was further characterized by uniaxial tensile testing using universal tensile machine (Zwick/Roel/Z005, Germany). Tensile stress applied to the polymer and elongation (strain) can be defined as follows (Adhikari *et al*., 2012):

$$stress\,(\sigma) = \frac{Force\,(F)}{Cross\,\text{sec}tional\ area\ of\ specimens\,(A)} \quad (3.6)$$

$$Strain\,(\varepsilon) = \frac{L - L_o}{L_0} \times 100 \quad (3.7)$$

where, L_0 = initial measured length

L = Length after elongation

Dog-bone-shaped tensile specimens, 75 mm long and approximately 1mm thick (see Fig. 3.6), were punched out of the compression molded plaques. The tensile load was applied at the constant crosshead speed of 50 mm/min. at 23 °C. Tensile strength and

Young's modulus were evaluated from resulting stress- strain curves. The average data of five experiments were taken for the statistics.

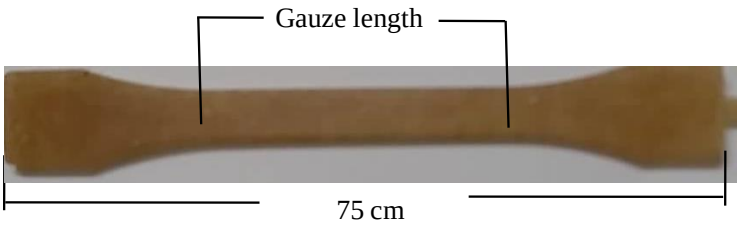

Figure 3.6: Schematic showing the dog bone shaped specimen for tensile test

Additionally, for the PBAT/NCC composites, tensile properties were measured using extruded strips of dimensions 50 mm length, 1 mm thickness and 5 mm width using universal testing machine (KIC-2-050-C, Kalpak Instruments and Controls, India) equipped with 500 N load cell at a constant cross-head speed of 100 $mm \cdot min^{-1}$. Three replicates of each sample were tested and the mean of the obtained results was reported along with standard deviation.

The tensile experiments were performed at Martin Luther University Halle-Wittenberg, Germany and IIT Guwahati, India.

c) Fracture surface analysis

To understand how the fracture processes have proceeded tensile testing of the specimens and how it can be correlated to mechanical behaviour tensile fracture during surface analysis is one of the fruitful observations. The morphology of tensile fracture surfaces of the deformed sample gives information about the deformation pattern of the composites on the application of tensile load. Therefore, the fracture surfaces of the deformed tensile bar, as shown in Fig. 3.7, were kept for SEM analysis.

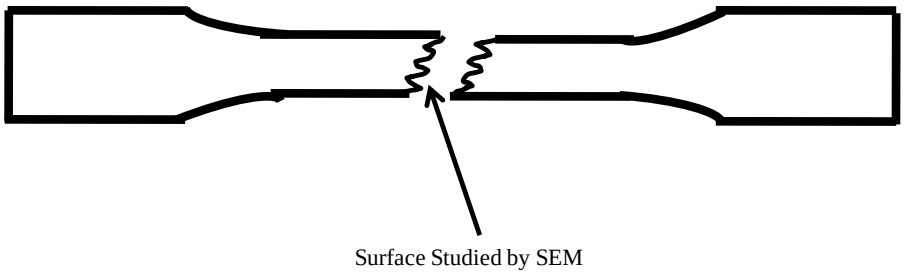

Figure 3.7: Tensile deformed specimen for fracture surface analysis by SEM

3.3.3 Thermogravimetric Analysis (TGA)

Thermogravimetric analyses were using Mettler-Toledo, TGA/SDTA 851 equipment, under the inert atmosphere of dry nitrogen from 30 ^{o}C to 600 ^{o}C with the heating rate of 20 ^{o}C/min. These observations were carried out in Martin Luther University, Halle-Wittenberg, Germany and IIT, Guwahati using standard methods (Pal & Katiyar, 2016, Pradhan *et al.*, 2012, Pokhrel, 2016b). Approximately 6-7 mg of samples was used for each experiment.

The TGA data obtained was also used to calculate activation energy for thermal degradation (E_a, kJ/mol) by using Arrhenius equation (3.8) for pure MCC, PBAT and composites.

$$\frac{d\alpha}{dt} = F(\alpha)KT = A.e^{(\frac{-E_a}{RT})}.F(\alpha) \qquad (3.8)$$

where $\alpha = (m_i\text{-}m)/(m_i\text{-}m_f)$, degraded mass fraction of the substrate (with m_i= initial mass of the substrate, m_f = final mass of the substrate and m = mass of the substrate at the specific temperature, A is a the pre-exponential factor (1/min), E the apparent activation energy (J/mol), T the absolute temperature (K) and R the gas constant (8.3136 J/mol K). The equation gives the rate of degradation of the materials in term of mol/min.

The data ln(dm/dt) *versus* 1/T of every sample plotted kept for the linear fit. From the slope of the curve, the value of E was calculated (Pokhrel *et al.*, 2016a, Pokhrel, 2016b, Pandit 2015).The calculations give two types of activation energies for each composite specimen. Each of the E values can be correlated with the degradation of each component (the MCC and the PBAT).

3.3.4 Surface Property Analysis

a) Wetting property

Wetting property indicates the affinity of the fibers to get attached to the polymer chains. In this test about 1 g of each PBAT/MCC composite dipped into toluene, left over night and stirred well with magnetic stirrer for 2 hrs till the sample fully dissolved in the solvent. The mixture is then filtered with *Whatman-40* filter paper.

The residue obtained was the MCC and which were washed properly with toluene. The MCC fibers were then dried well in hot air oven for 2 hrs at 60 ℃. The MCC fibers were analyzed by FTIR and SEM.

b) Contact angle measurements

The wettability test was carried out using contact angle analyzer (GmbH DSA25, KRUSS, Germany) with ~4 µl drop volume of millipore water at 23 ± 1 ℃ by sessile drop method. A flat specimen was dried overnight at 60 ℃ in vacuum oven. The deionized water was then dropped onto on the flat surface of the sample using a syringe (fitted above the sample holder). During analysis, the droplet geometry was captured with the help of a camera, placed in front of the sample holder. The measurement was replicated for four times by selecting a new spot on the sample surface. The average values are reported elsewhere (Pal & Katiyar, 2016).

c) Water absorption

Each sample was dried in hot air oven for 8 hr at 80 ℃ before experiments. Each specimen was kept in the environment chamber at 23 ℃ in presence of demineralized water for a week and every day the amount of water absorbed by composites were measured and data were normalized to plot against the time in per day for each sample by equation (3.9):

$$water\ absorbed \quad (\%) = \frac{w_f - w_i}{w_i} \times 100\ \% \qquad (3.9)$$

where, w_f is final dry weight of the composites in environment chamber and w_i is the initial dry weight of the composite.

3.3.5 Degradability Analysis

The preliminary degradation behaviour of the samples was inspected by water absorption analysis. The details of the degradation behaviour were investigated by conducting soil burial experiments, fracture surface analyses and gel permeation chromatography (GPC).

a) Soil burial experiment

MCC/PBAT composites were cut in square sized 8 cm x 8 cm with approximately 1 mm thickness, for this experiment. Composites were buried flat 40 cm down into the soil at different places for 6 months, 15 cm apart from each other. After the burial, samples were watered and capsicums were planted on the top of the soil. Water was sprinkled regularly in the morning and evening to keep the soil moist (Kijchavengkul *et al*., 2010, Pokhrel *et al*., 2016b, Mostafa *et al*., 2010, Su & Wu, 2011).

Soil composting biodegradation test was carried out in National Agricultural Research Council (NARC), Khumaltar, Lalitpur. The depth of 40 cm under the soil surface is found to be ideal for the soil burial tests (Pokhrel *et al*., 2016b). Fig. 3.8 shows the soil burial site used for the composting. The soil was observed for its mineral constituents as well as for micronutrients. Biochemical tests for microbes and fungi were also performed. The chemical constituents, texture and microbial environment of soil is well tabulated in Table 3.6 and Table 3.7 after standard analytical methods. Specimens were observed in 2 months of interval.

Figure 3.8: Greenhouse site of National Agricultural Research Council (NARC) for composites burial experiment

Table 3.6: Micronutrient constituents of the bed soil at NARC site where composting experiments were performed for the PBAT/MCC composites

LOI (%)	Insoluble (%)	R_2O_3 (%)	K_2O (%)	PO_4 (mg/Kg)	N (%)	pH	EC (µmho/cm)	Calcium	Magnesium	Moisture (%)
1.1	1.5	27.5	5	5	0.09	7.8	477	trace	0.5	0.5

Table 3.7: Texture and bacterial content of the soil in compositing site

Soil composition (wt. %)			Bacterial nature
Clay	*Sand*	*Slit*	Bacillus spp., rod shaped; Gram positive
29.1	31.8	39.1	

b) *Morphological analysis by SEM*

Degraded samples were studied by scanning electron microscopy to observe the morphological deformation in the composites. Properly washed and dried degraded samples were sputter-coated with gold (Au) in a carbon tape and observed. In this work, SEM micrographs were captured for degraded specimens by JSM 6300 (JOEL) and Zeiss-Sigma 300.

c) Molecular characterization by GPC

GPC analysis was carried out using Shimadzu LC Solution Chromatograph with refractive index detector (RID-10A), at 1 mL/min eluent flow rate and 40 µL sample injection volume. In a typical experiment (40 mg) of specimens were dissolved in 20 mL of high performance liquid chromatography (HPLC) grade chloroform for 2 days and filtered using 0.25 µm membrane filters. The instrument was calibrated with polystyrene standards. These tests were carried out in IIT-Guwahati, India.

CONCLUDING REMARKS

The overview of the sample preparation, nomenclature of the series and different techniques used in the experimental work along with the kind of information obtained are summarized in Fig. 3.9 and Table 3.8.

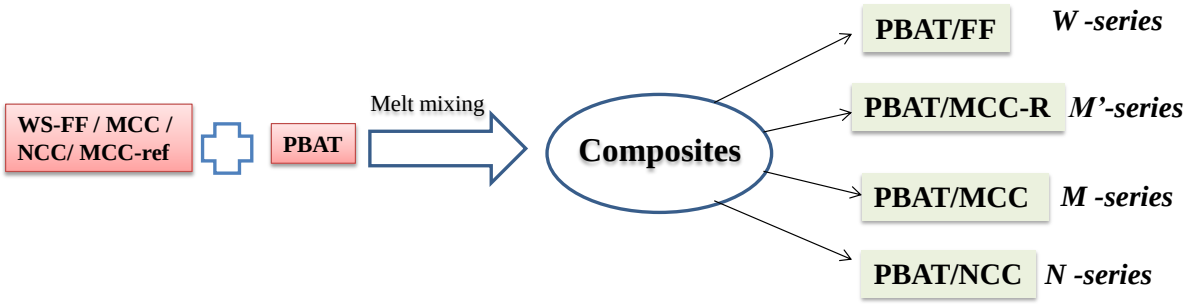

Figure 3.9: Diagrammatic representation of preparing biodegradable polymer composites of different series (W, M', M and N series) of PBAT with WS-FF, MCC-R, MCC and NCC

Table 3.8: Summary of characterization techniques and specimen preparation for the study of various properties

Techniques	Properties studied	Specimen preparation
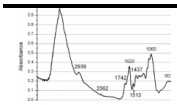 *Fourier Transform Infrared (FTIR) spectroscopy*	Molecular structure, bonding information, chemical or physical interaction	As prepared sheet, clean surface, decontaminated; ATR mode, analysis in solid state
 *Electron microscopy (SEM/TEM)*	Microscopic structure, morphology, interfacial structure, microphase separation	Cryo-fracturing and gold sputtering for SEM; a drop of NCC suspension put into Cu grid,vacuum dried for TEM
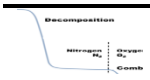 *Thermogravimetric analysis(TGA)*	Thermostability, degradation kinetics	~0.6 g specimen in TGA pan, experiment under different environmental condition
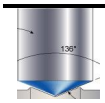 *Mechanical testing (indentation, tensile)*	Deformation behaviour, strength, stiffness, ductility, toughness	Clean and flat sample surface as processed for indentation; Dog bone shaped specimens for tensile testing
 *Water absorption*	Hydrophilicity	Samples are dried in vacuum oven for 24 hr at 60 ℃ to prepare moisture free samples for test
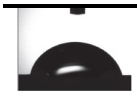 *Contact angle*	Hydrophilicity, ease of biodegradation	Clean smooth surface ~ 0.5 cm glued onto glass plates and vacuum dried
 *Soil burial*	Mass loss due to (bio)degradation, surface deterioration	8 cm x 8 cm specimen, vacuum dried
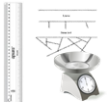 *Gel permission chromatography (GPC)*	Molar mass reduction, fracture mechanism	~40 mg of sample dissolved in 20 mL of $CHCl_3$, filtered with 2 μm pore size paper.

CHAPTER 4

4. RESULTS AND DISCUSSION

This chapter discusses the results of the experimental works performed in the course of the doctoral project. The results are expressed for in 4 different sections: 1) structural and thermal characterization of cellulosic fibers and polymers; 2) structure-properties correlation of polymer composites; 3) structure-properties correlation of nanocomposites, and 4) investigation of surface properties and degradation behaviour.

4.1 Structural and Thermal Characterization of Fibers and Polymers

The MCC and the NCC obtained from natural fibers as well as the pure PBAT used in this work have structural variations by virtue of their inherent chemical and physical properties that can be differentiated by spectroscopic, microscopic and thermal methods. This section describes the fundamental properties of the starting materials in general and of the fibers as a function of processing conditions in particular.

4.1.1 Structural and Thermal Properties of Fibers

a) Spectroscopic characterization

Fig. 4.1a presents the FTIR spectra of commercial MCC (Jelucel HM400X; named as MCC-R) and the wheat stalk (WS) powder. The spectra found in both the substances are similar; only a few peaks of the MCC being sharper and more distinct than the WS. The spectra have broad absorption bands between 3600 cm^{-1} to 3000 cm^{-1} representing the O-H stretching vibration and the strong intra- and intermolecular hydrogen bonds present in cellulose (Gemci, 2010, Ibrahim, 2010, Manimaran *et al*., 2018, Pang *et al*., 2014). The FTIR peak located at 1593 cm^{-1} stands for the small bending vibration of OH bond. The axial C-H stretching of cellulose can be seen at 2894 cm^{-1} which is more intense and sharper in MCC-R than in the WS due to exposed fiber surface. The C-H stretching and CH_2 wagging vibrations of cellulose are signatured by the peaks located at 1369 cm^{-1} and 1315 cm^{-1}, respectively (Gemci, 2010). Likewise, the characteristic anti-symmetric bridge stretching of C-O and C-O-C pyranose ring vibration of cellulose are represented by the peak located at 1157 cm^{-1} (Gemci, 2010, Paula *et al*., 2008). Similar types of C-O stretching and C-O-C

glycosidic bond stretching are attested by strong band at 1023 cm^{-1} (Guerrero *et al.*, 2016, Sakhawy *et al.*, 2018).

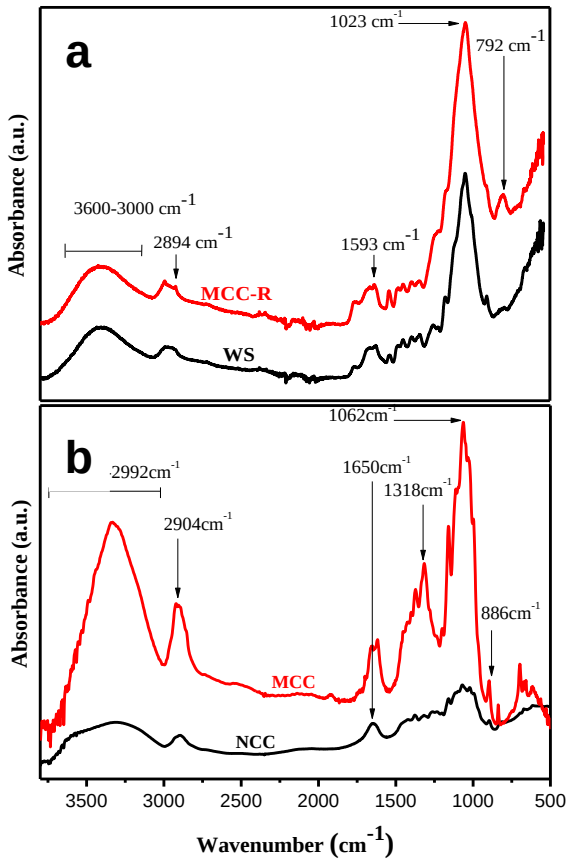

Figure 4.1: FTIR spectra of different forms of natural fibers studied in this work: (a) pure wheat stalk (WS) powder compared to MCC-R, and (b) the MCC and the NCC extracted from the WS powder

The absorption peak at 890 cm^{-1} represents the typical structure of cellulose showing C–O–C stretching vibration for β, 1,4-glycosidic linkages (Manimaran *et al.*, 2018, Wu, 2012, Giri *et al.*, 2019a). In WS fibers, a few peaks (such as around 1300 cm^{-1}) are quite different than commercial MCC (MCC-R), such as phenolic C–O stretching which signifies the presence of lignin and similar natural polymers in the neat WS. WS fibers further bear quite sharp peak corresponding to aromatic rings centered at 1604 cm^{-1} for lignin in comparison to MCC-R (Gwon et al., 2010, Pan *et al.*, 2013).

Fig. 4.1b compares the FTIR spectra of MCC with that of NCC obtained from the WS fibers. Both of them have almost identical spectra as also reported elsewhere (Satyamurthy & Vigneshwaran, 2013). The FTIR peaks of the NCC are less intense than the MCC due to the reduction in crystallinity value and break down of numerous intra- and intermolecular H-bonds (Manimaran *et al.*, 2018, Pan *et al.*, 2013). The

prominent cellulose peaks appear more intense in the MCC at their respective positions as compared to the WS due to the exposure of the MCC crystallites by dissolution of lignin and hemicellulose during chemical treatments. Few more cellulosic peaks are observed in MCC and NCC, such as one at 1642 cm^{-1} representing carbonyl C=O stretching of a saturated hydrocarbon. Similar observations were made by other authors (Rosli *et al.*, 2013).

It can be summarized that similar to the commercial one, the MCC extracted from the WS possessed intense peaks centered at 3330 cm^{-1}, whereas these peaks became broad and diffuse in the NCC of the same origin, which can be attributed to possible breakdown of inter- and intramolecular H-bonding due to strong acid treatment.

b) Morphological characterization

The microscopic techniques provide direct morphological details of the materials at different length scales. The electron micrographs depict fiber surface morphology, including their size and dimensionality as well as overall surface texture.

The SEM images of the MCC derived from the WS fiber are shown in Fig. 4.2. The MCC fibers are semicrystalline in nature with length of approximately 25 μm and width of 5 μm. In nature, the MCC has amorphous cellulose residing in between the microcrystallites forming a long cylindrical structure (with aspect ratio of approximately 5:1). The higher magnification SEM image in Fig. 4.2b shows partial fibrillation of the MCC bundle with smooth texture on its surface. The presence of smooth texture can be attributed to the dissolution of amorphous region of the WS fibers by the chemicals such as NaOH, NaOCl and H_2SO_4.

The micrograph of commercial MCC reported by Patnaitescu *et al.* (2011) is also quite similar in shape and size compared to the MCC synthesized in this work. Likewise Rajan *et al.* (2009) reported similar microfibrils obtained from bamboo shoots after chemical treatments (Rajan *et al.*, 2009, Krishnprasad *et al.*, 2009). The effects of chemical treatments leading to fibrillation and smoothing of the fibers are well presented by different authors. (Das & Chakraborty, 2009, Cadena-Chamoro *et al.*, 2017, Vinayak *et al.*, 2017).

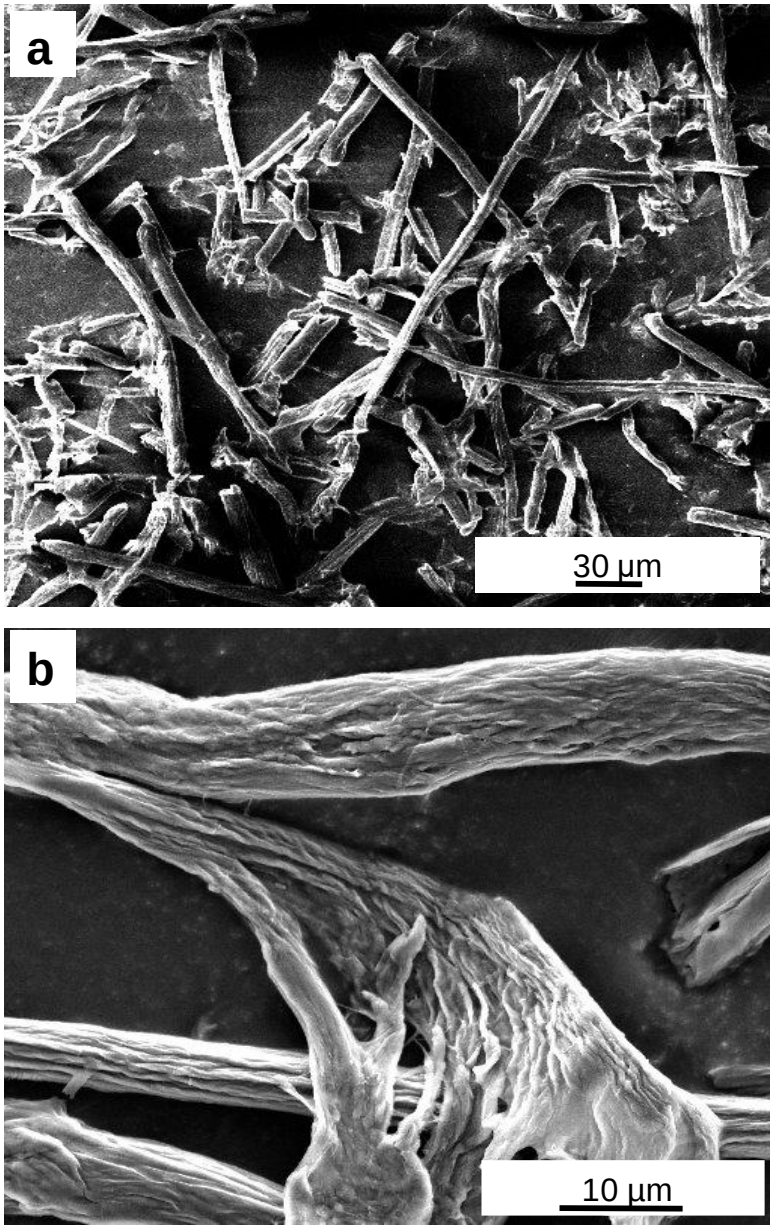

Figure 4.2: Lower (a) and higher (b) magnifications of the SEM images of the MCC extracted from WS

SEM technique using field emission cathode (i. e., FESEM) is very useful for morphological studies of MCC and NCC under almost environmental condition (Vinayak *et al*., 2017, Carrasco *et al*., 2011). The FESEM has an advantage of high resolution capability combined with the ability to study the surface texture of the materials. The sample was prepared by air drying of the material in hot air oven. The results obtain on NCC powder by means of FESEM methods are presented in Fig. 4.3.

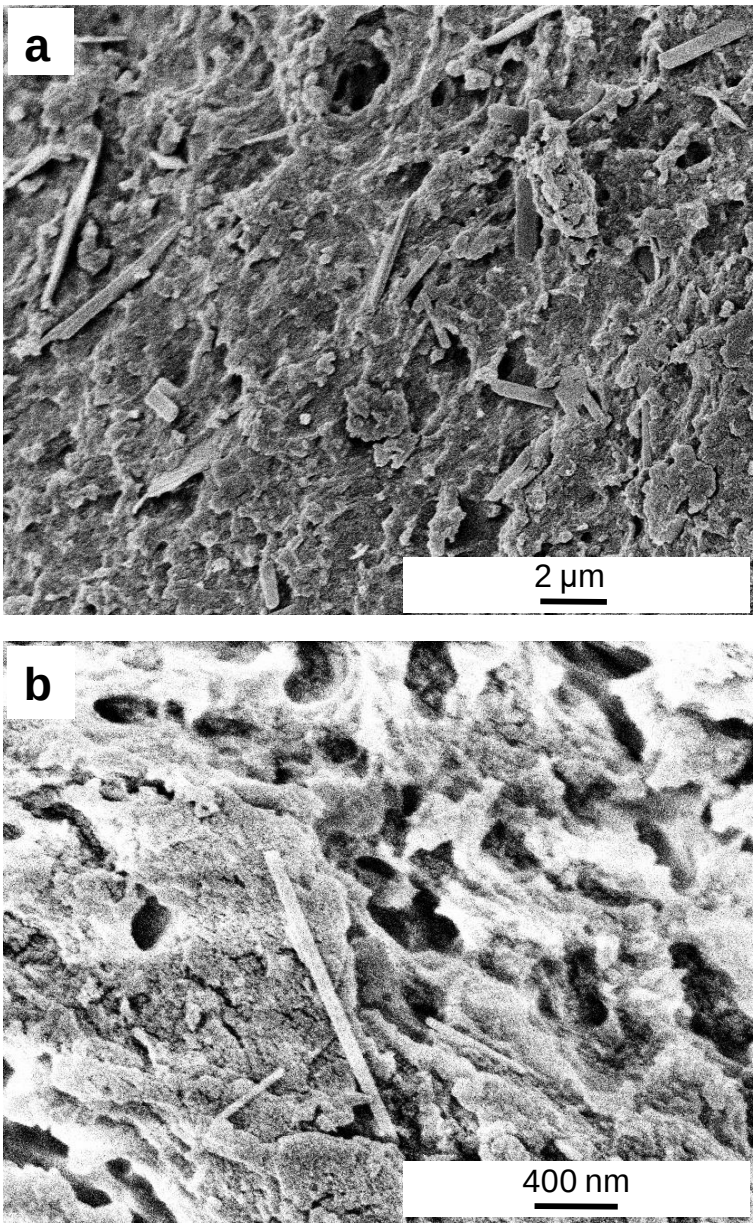

Figure 4.3: Lower (a) and higher (b) magnifications of FESEM images showing nanosized cellulose particles extracted from WS: Note: NCC agglomerates with crystallites projecting outwards

The strong acid hydrolysis performed on the MCC produced the NCC. In Fig. 4.3a, the synthesized NCC powder seems to have coarse surface structure with large agglomeration of the particles. Only few NCC crystallites are projecting outside from the agglomerate. The surface has some pores of different sizes which facilitate the absorbing and releasing capacity of the NCC for different materials such as drugs, filtration devices and purification units. The agglomeration of the nanocrystals is caused by the storage of the nano-fibrillated cellulose.

The shape of the NCC is more distinct in Fig. 4.3b, showing its rod shaped texture. The largest NCC aggregates observed has the dimension approximately 1000 nm long

and 80 nm wide, whereas the smallest one is about 200 nm long and 50 nm wide. A review paper by Gacitua *et al.* is coherent to show rod-like cotton NCC (Gauitua *et al*., 2010), similar to the NCC extracted from WS, whereas bacterial cellulose on hydrolysis gives nano-whisker (Kramer *et al*., 2006).

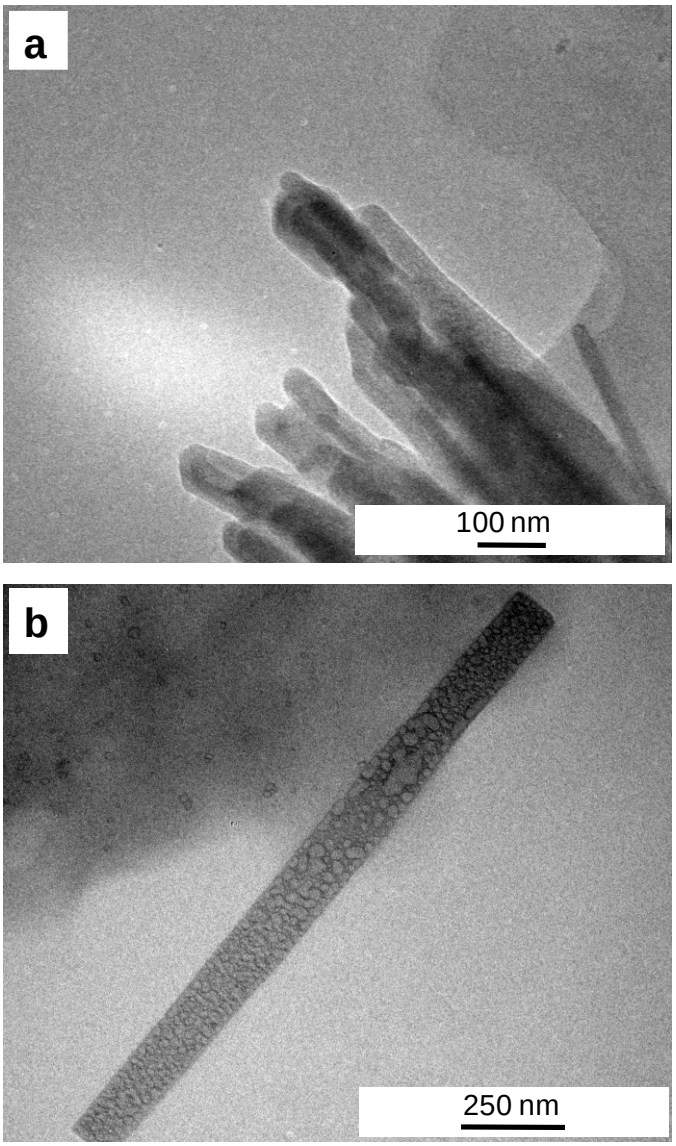

Figure 4.4: TEM images of NCC extracted from MCC; (a) bundle showing NCC fibers in MCC, and (b) a single NCC crystallite dispersed from MCC

The microscopic investigation is more luminous with the results from transmission electron microscopy (Fig. 4.4) on the specimens prepared by sonication of nanocellulose dispersed in water followed by deposition on TEM grids. Fig. 4.4a manifests that NCC fibers are in a bundle before nano-fibrillation, which are then exposed out on acid hydrolysis followed by the dissolution of amorphous region and binders present between the NCC fibrils. These NCC get dispersed into rod-like

crystals, which is shown in Fig. 4.4b. These NCC, being very hydrophilic in nature due to the presence of free -OH groups on its surface, can easily absorb water droplets or moisture which is clearly visible in Fig. 4.4b.

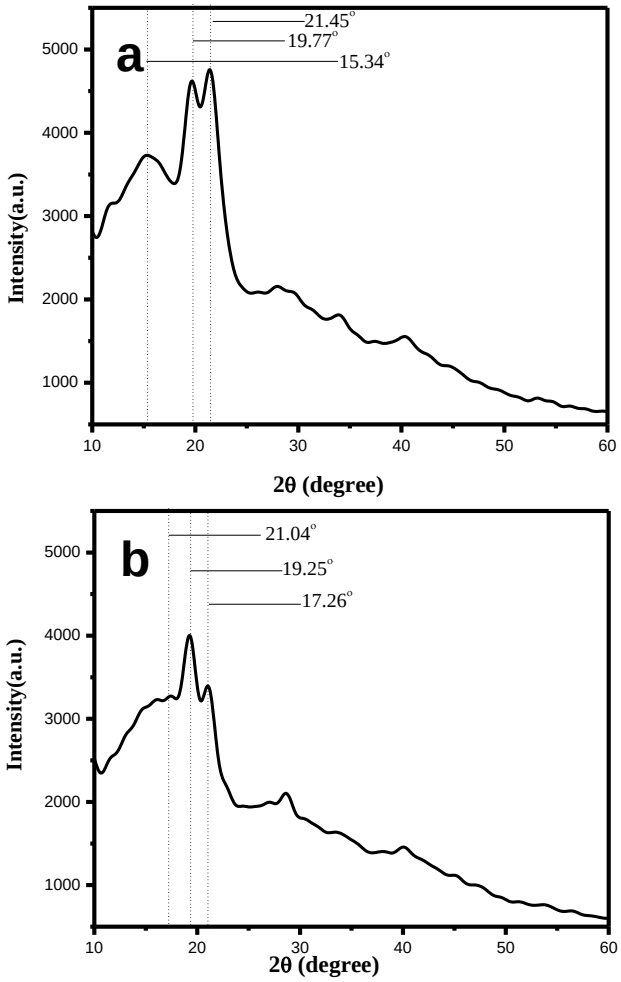

Figure 4.5: XRD patterns of MCC and NCC extracted from WS fibers.

The NCC crystallite has many water droplets absorbed on its surface showing its water loving nature. The NCC crystal is found to be approximately 25-50 nm wide and 300 nm long. The results are in agreement with the NCC produced from flax *via* acid hydrolysis (Cho *et al*., 2011, Liu *et al.*, 2010), whereas the MCC-R, (the Avicel®, PH-101, Fluka, USA) gives NCC with lower dimensions 6.96±0.87 nm width and 178±55nm long (Cho *et al*., 2011). Mueller *et al.*, (2011) varied acid hydrolysis time from 30 mins to 240 mins to observe the variation in size of the nano-crystallites from pseudo-stem of banana and found length of the crystallites are ranging from 465 nm to 320 nm. Similarly, width is ranging from 20 nm to 15 nm (Mueller *et al.*, 2011). Other

sources such as *agave augustifolia* gives needle shape NCC approximately of similar dimension as that produced in this work (Rosli *et al.,* 2013) and sugar cane bagasse on high homogenization gives circular shaped NCC crystals (Krishnaprasad *et al*., 2009).

Overall, from the microscopic results, it can be concluded that the MCC and NCC obtained from the WS fibers possess characteristic textures, the MCC being irregular bundles of the primary crystals bound together by the amorphous phase. The latter disintegrates upon acid hydrolysis giving rise to the elongated rod-shaped sharp nanocrystals having much larger surface area and thus intense hydrophilic character.
The fibers were further studied using XRD whereby the diffractograms were utilized to calculate the d-spacing, apparent grain size (D) and crystallinity index (CI) of the crystallites. The diffraction patterns of the MCC are shown in Fig. 4.5a. The XRD plot of the MCC shows 2θ peaks at 15.34°, 19.77° and 21.45°. These peaks have been assigned to the cellulose I (Guerrero *et al*., 2016 and Sonia & Dasan, 2013). The higher diffraction intensity at 2θ values at 21.45° indicates the crystalline nature of the MCC as shown also by Teixeira *et al.,* (2010) in cotton fiber. Likewise, the 2θ value around 12° - 17° indicates shouldering of cellulose I and amorphous nature as mentioned earlier by Sonia and Dasan, (2013). The peaks observed in the MCC correspond to crystallographic plane of cellulose I (Adsul *et al*., 2012, Mandal *et al*., 2011).

Table 4.1:XRD data showing Crystallinity index, d-spacing and apparaent grain size (D) calculated for NCC, MCC extracted from WS origin and polymer PBAT

S.No.	Sample Code	CI (%)	d-spacing(nm)	D-grain size (nm)
1	NCC	51.28	0.448	0.191
2	MCC	43.28	0.408	2.542
3	PBAT	79.78	0.382	0.874

The d-spacing and D was determined by Sherrer equation (Guo, 2016, Bhattarai, 2006). The comparative data for CI shows the higher value of the crystallinity index (51.23) for NCC compared to much lower value of the MCC (43.28) (Rambo & Ferreira, 2015). The acid hydrolysis dissolves all amorphous zone around 12° - 17° exposing the clear crystals of the NCC (Sonia & Dasan, 2013). The d-spacing (from 0.408 for MCC to 0.448 for NCC) value is also indicates more ordered arrangement due to chemical

interactions as reported in literature (Cherian *et al*., 2010, Dai & Fan, 2010, Krishnaprasad *et al*., 2009).

c) Thermal behaviour

The raw materials used in this work are stable towards thermal parameters under normal environment. The plot in Fig. 4.6 illustrates of thermogravimetric analysis of MCC and NCC from WS origin and shows two steps degradation. Early degradation of MCC starts at 225 ℃ and complete degradation occurs at 402 ℃. The major degradation occurs at T_{max} of 373 ℃, which can be observed from the accompanying differential curve dotted line. The MCC shows initial mass loss up to 7 % at around 120 ℃ which corresponds to the removal of water and other volatile substances. The complete thermal degradation of MCC occurred at around 400 ℃ with the char yield of 1.33 % at 600 ℃ which is consistent with the values reported for cellulosic materials of different origins (Wu, 2012).

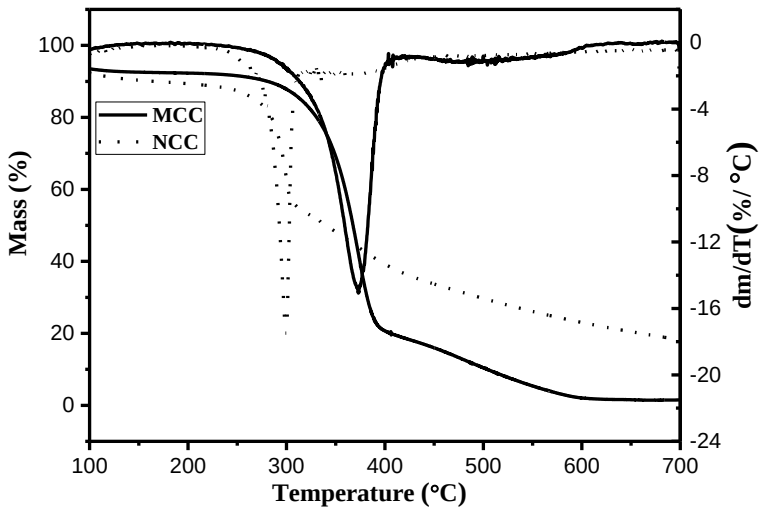

Figure 4.6: TGA thermograms of MCC and NCC extracted from WS; dotted line represents the differential curve of mass vs. temperature data

Similarly, NCC also losses its weight by 10 % due to removal of water and volatiles at around 120 ℃ while its degradation starts at 231℃. NCC being more crystalline has sharp degradation T_{max} at 299 ℃ in comparison to MCC (372 ℃). The complete degradation of the NCC occurs at 408 ℃ leaving the residual mass of 22.16 % in the form of char after combustion at 600 ℃. The char left are oxidized at higher temperature which is found to limit the production of combustible gases and can even

decrease the exothermic pyrolytic reaction inhibiting the thermal conductivity of the burning materials. Thus, on comparing thermal behaviour, one can observe that the MCC is found to be more thermally stable than the NCC as NCC has larger interacting thermal exposure.

4.1.2 Structural and Thermal Characterization of PBAT

a) Structural characterization of PBAT

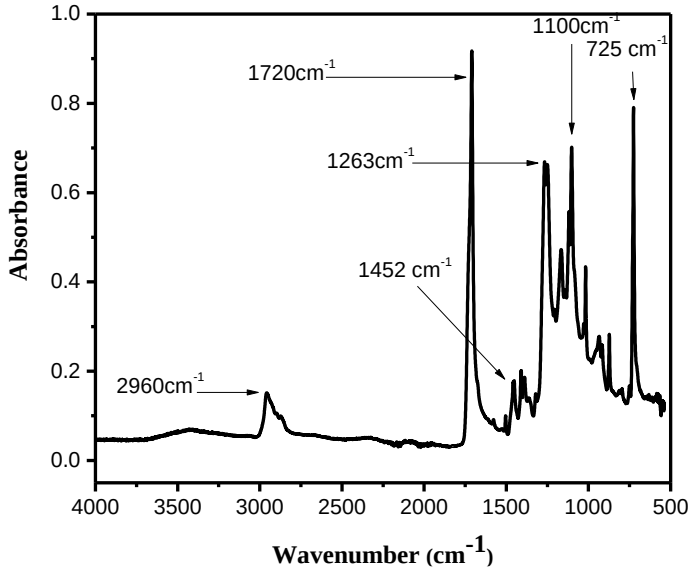

Figure 4.7: FTIR spectra of the polymer PBAT used in this work

The spectrum of the polymer PBAT, is shown in Fig. 4.7. The spectrum has an intense absorption peak at 1720 cm^{-1} which represent C=O stretching of the ester group in carbonyl compound (Das & Chakraborty, 2008, Chang & Chen, 2016). Absorption bands at 1499 cm^{-1}, 1452 cm^{-1}, 1400 cm^{-1}, 1386 cm^{-1}, 1362 cm^{-1}, and 1323 cm^{-1} correlate the C-H vibration of CH_3 group of PBAT (Al-Itry, 2012). Similarly, absorption bands at 1263 cm^{-1} and 1169 cm^{-1} represent C-O stretching of carbonyl group conjugated with phenyl group (Nayak, 2010). Likewise, the absorption band at 1118 cm^{-1} and 1100 cm^{-1} correspond to C-O-C stretching vibration of ester (Pang *et al*., 2014). The prominent band between 2957 cm^{-1} to 2869 cm^{-1} gives symmetrical stretching vibration of the axial C-H group in saturated hydrocarbon (Wu, 2012, Nayak, 2010). Another intense peak at 725 cm^{-1} represents aromatic stretching of the benzene ring (Castro *et al*., 2016, Nayak *et al*., 2102).

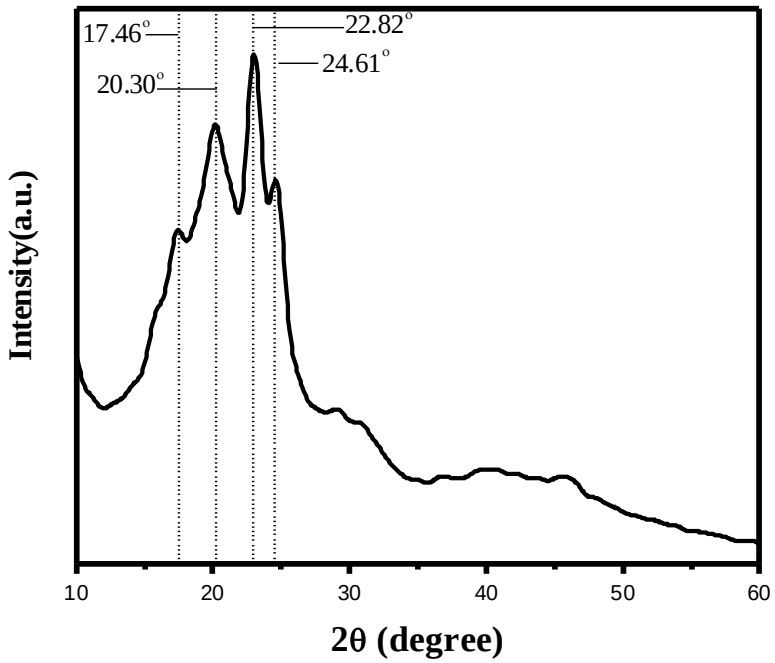

Figure 4.8: X-ray diffractogram of the polymer PBAT used in this work

The justification for the PBAT being biodegradable is FTIR spectra in Fig. 4.7, where the carbonyl and ester bonds are present, at 1720 cm^{-1} (for C=O), 1263 cm^{-1}, 1169 cm^{-1}, 1118 cm^{-1} and 1100 cm^{-1} (for antisymmetrical stretching of C-O and C-O-C ring vibration) which could be the site for H-bonding for water or moisture and mild acid hydrolysis. The FTIR spectra evidenced the biodegradability of PBAT due to presence of carbonyl group (absorbance FTIR peak at 1720 cm^{-1}) and easily hydrolysable ester bond. Siyamak *et al.*, Al-Itry *et al.*, and Wu *et al.* also reported similar FTIR spectra for PBAT.

The X-ray diffractogram of the PBAT shown in the Fig. 4.8 has four diffraction 2θ peaks at 17.46°, 20.30°, 22.82° and 24.61° which indicates crystalline nature of PBAT and are in agreement with the data of XRD given in Arruda *et al.* (2015), Rasyida *et al.* (2017), Wu, 2012 and Chivrac *et al.* (2006), which attests the crystalline nature of the polymer.

The semicrystalline morphology of the PBAT was also presented in an earlier work (Adhikari *et al.*, 2013). It was found that the PBAT comprised of small spherulites, a few microns in diameter. The lamellar texture if the sample was found to be

characterized by worm-like short crystalline textures. The crystalline texture of the PBAT was also recently authenticated *via* the AFM by Tavares *et al*. (2018). Similarly, the CI value 79.78 % shown in Table 4.1 clearly shows semi-crystalline behaviour of the PBAT. Pak *et al*. (2013), mentioned orthorhombic crystalline structure for such type of diffraction pattern observed in his work.

b) Thermal characterization of PBAT

Fig. 4.9 further shows that PBAT has single step thermal degradation, starting at around T_{1st} = 333 ℃ and maximum degradation occurs at 424 ℃. The polymer degrades almost completely with char yield of 3.3 % at 600 ℃ under the inert atmosphere. In presence of air, residual char also degrades completely after 600 ℃ which is consistent with the literature data (Ibrahim *et al*., 2010, Sakhawy *et al*., 2018). Beyond 600 ℃ under air environment, the system has the oxidizing environment where the char left completely burns to volatile gases (Cesar *et al*., 2015). Fukusima *et al*, (2012) also presented the similar thermal behaviour for oxidizing char, which was also mentioned in earlier on biomaterials (Fukusima *et al*., 2012).

Unlike MCC and NCC which degrade in various steps and at lower temperatures (Fig. 4.6).The PBAT has single step of sharp degradation temperature at 424 ℃, which is very high compared to MCC and NCC. Therefore, it is clear that the PBAT can be utilized for high temperature processing.

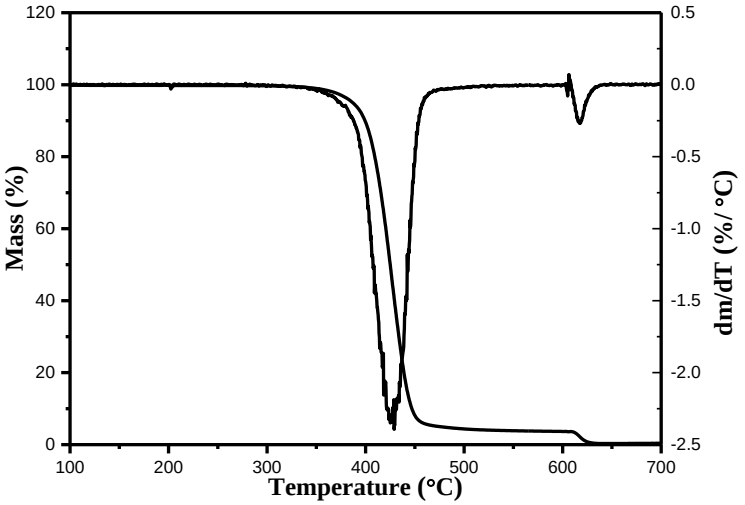

Figure 4.9: TGA thermogram of the polymer PBAT used in this work

CONCLUDING REMARKS

The results presented in this section can be concluded as follows and summarized in Table 4.2:

- The **spectroscopic analyses** conclude that the virgin WS fibers are structurally quite similar to the commercial MCC. Similar to the commercial one, the MCC extracted from the WS posses intense IR peak centered around 3330 cm^{-1}, whereas this peak becomes broad and diffuse in the NCC, which can be attributed to possible breakdown of inter- and intramolecular H-bonding caused by strong acid treatment.
- From the **microscopic results** obtained from SEM and TEM, it has been concluded that the MCC and NCC obtained from WS fibers are characterized by definite textures, the MCC being irregular bundles of the primary crystals bound together with the amorphous phase. The latter is found to disintegrate upon acid hydrolysis giving rise to rod-shaped sharp nanocrystals which have much larger surface area and thus intense hydrophilic character.
- The **XRD data** reveals that the natural fibers extracted from the WS predominantly contains Cellulose I (Sharp XRD peaks located at 2θ values of 20.34° and 22.02°) form of the crystals whereby the nanofibrillation increased the degree of crystallinity by about two folds.
- As per **thermogravimetric results**, the MCC and NCC are found to be generally thermally stable while the NCC slightly less stable. The higher thermal stability of the MCC can be attributed to the protective coating provided by the amorphous part of the cellulose which gets eliminated due to the strong acid treatment.
- The **semicrystalline nature of the PBAT** is well postulated by the XRD peaks that can be correlated to morphology described by other methods. The PBAT's biodegradability can be linked with the presence of its hydrolysable ester and carbonyl groups. It is found to be quite stable towards thermal treatment completely degrading at 424 ℃.

Table 4.2: Summary of structure and properties of natural fibers and PBAT determined by various methods

Methods	**MCC**	**NCC**	**PBAT**
FTIR	Sharp -OH band between 3600 cm^{-1} - 3000 cm^{-1} and other signature related cellulose peaks	Reduced cellulose peak with broad H-bonding of OH group between 3732 cm^{-1} - 2992 cm^{-1}	Aromatic, aliphatic C-H stretching at 2957 cm^{-1} and 2869 cm^{-1}, C=O group 1720 cm^{-1}
SEM	Fibrillar semicrystalline structure with amorphous zone embedding the crystallites	Agglomerated coarse surface with projections of few single NCC crystallites on the surface.	Morphology comprising 2-4 μm diameter spherulites (as per literatures)
TEM	not applicable in this work	200 nm long and 50 nm wide rod shaped crystallites	Short worm-like lamellar structure as per literatures.
XRD	Semicrystalline texture CI = 43.28%	Low crystallinity, CI =51.28%	Semicrystalline in nature; CI = 79.78%
TGA	Two steps degradation. Thermally stable, upto = 225 ^{o}C and T_{max} =372 ℃	Two steps degradation, Thermally stable up to = 225 ℃, and T_{max}= 299 ℃.	Single step degradation. Thermally stable up to=333 ℃ and T_{max}= 424 ℃

4.2 Structure-Properties Correlation of Polymer Composites

In this section, polymer composites prepared from PBAT with WS and MCC are characterized to establish their structure - properties correlation using different spectroscopic and microscopic techniques. Further, the thermogravimetric data are utilized to clarify their thermal stability. Mechanical and morphological properties are particularly addressed.

4.2.1 Structure and Morphology of Polymer Composites

Molecular structure of the polymers and the nature of interactions in polymers composites can be well explained by the FTIR data, the latter being responsible for determining most of their physical properties. The interaction phenomena describe how fibers and PBAT adhere to each other which manifest in the mechanical strength of composites during various applications.

a) Spectroscopic investigations of composites

The Fig. 4.10a compares FTIR spectra of PBAT, WS flour and three different composites with WS (called as W-composites). The W-composites have identical spectra as PBAT (see FTIR spectrum PBAT in Fig. 4.7). Therefore, in all the W-composites, the major cellulosic peaks explained in Fig. 4.1, have been masked by the PBAT. Further, the spectra given in Fig 4.10b exhibit the evolution of small absorption bands in W-composites at 2918 cm^{-1} and 2849 cm^{-1} with the increasing WS loading. This indicates the interaction between PBAT and WS by axial symmetrical C-H stretching in saturated hydrocarbon of PBAT with that of C-H stretching vibration of the cellulose.

Similar result was observed when palm fruit bunch fiber was compounded with PBAT without modification (Nagata & Inaki, 2011). However, when this system was modified with succinic anhydride (SAH) and dicumyl peroxide (DCP), there was the formation of new ester bond (Siyamak *et al*., 2012a, Balaji *et al*., 2017). The interacting bond eventually increased the mechanical strength of the composites (Siyamak *et al*., 2012a). Such interaction was also observed in nanocomposites of

poly(butylene succinate) and PBAT containing organically modified montmorillonite (OMMT) (Chieng *et al*., 2010, Plaza & Quizada, 2016).

The peaks observed at 2915 cm^{-1} and 2850 cm^{-1} in the W-composites implies that there is a sort of the physical interaction between the PBAT and the WS. Similarly, combined peak of carbonyl C=O group present in PBAT and cellulose is found at 1712 cm^{-1}. The lower shift in the value of the absorption frequency is due to the presence of WS in the PBAT (Pokhrel *et al*., 2016a). There is no specific new bond of chemical nature formed in the composite.

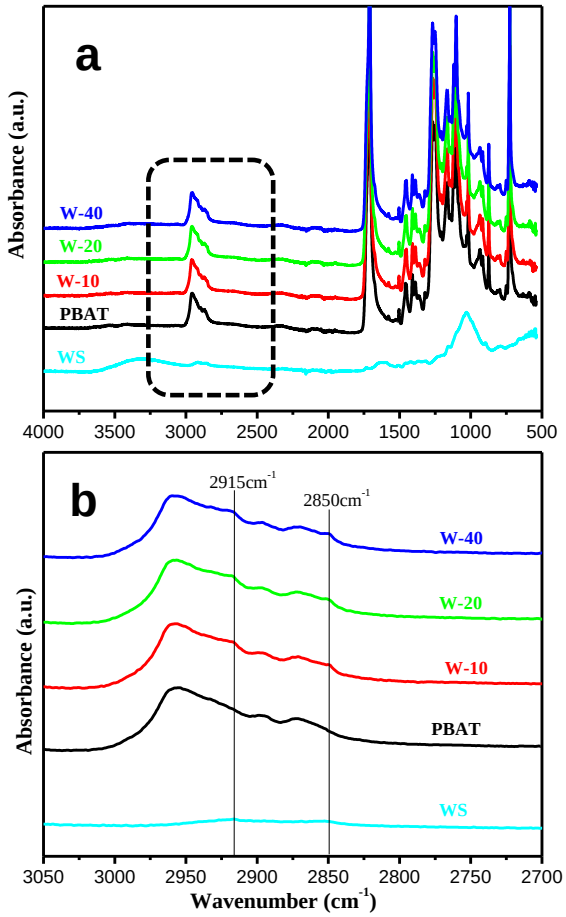

Figure 4.10: Comparison of FTIR spectra of WS fiber, PBAT and W-composites with variation of WS content; a part of (a) is magnified in (b)

The lack of chemical interaction between WS and PBAT implies that the W-composites have only physical interaction.

It can be observed that the FTIR spectra of composites with microcrystalline cellulose (called as M-composites) presented in Fig.4.11 are identical and are very much similar

to the PBAT spectra as in the core of W-composites (shown in Fig. 4.10). Therefore in all composites, the major peaks of MCC have been masked by the PBAT. A part of the spectra in between the range of 3000 cm^{-1} and 2800 cm^{-1} has been magnified in the Fig. 4.11b.

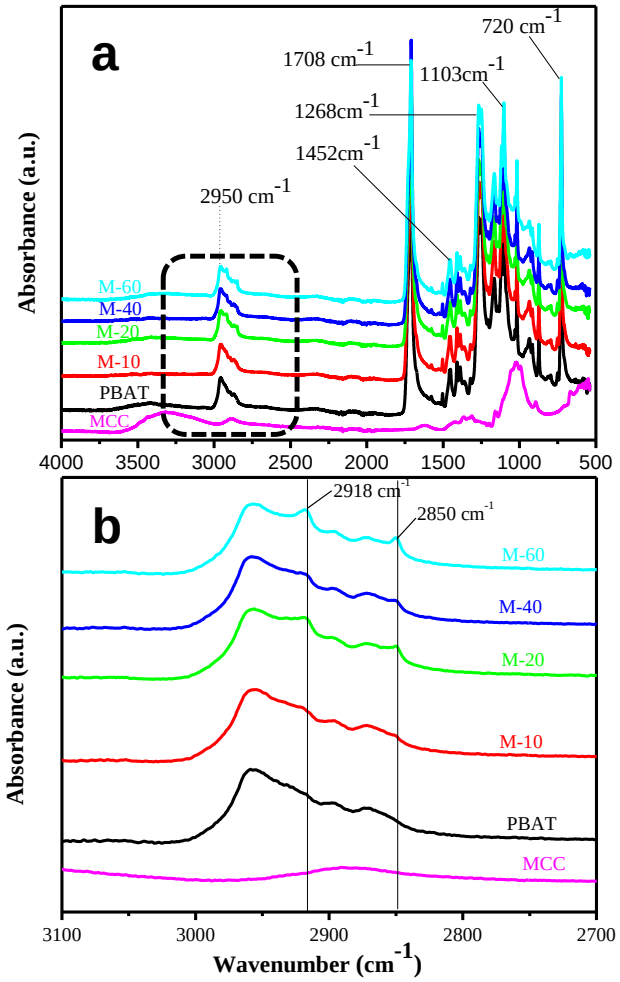

Figure 4.11: FTIR spectra of MCC, PBAT and their composites; a part of spectra of (a) is magnified in (b)

The close observation of the spectra given in Fig. 4.11b makes it clear that there is a growing trend of physical interaction of the PBAT with the MCC in the composites, as in the previous case with W-composites (compare with Fig. 4.10). Further, PBAT phase has been found to dominate in the spectra of the composites. A clear indication of strong physical interaction at the polymer/filler interfaces has been observed (Giri *et al*., 2020). To shed closer light into this behaviour wetting experiments were carried out (next section).

b) Wetting at PBAT/MCC interface

In order to cross-check the physical interaction present at the PBAT/MCC interface, wetting of biofiller by polymer chains have been analyzed by FTIR spectroscopy and SEM. First, a small piece of a composite was dissolved in toluene followed by discarding the solution for thorough washing of the fibers and drying at elevated temperature. The SEM micrographs of the fibers thus obtained are presented in Fig.4.12.

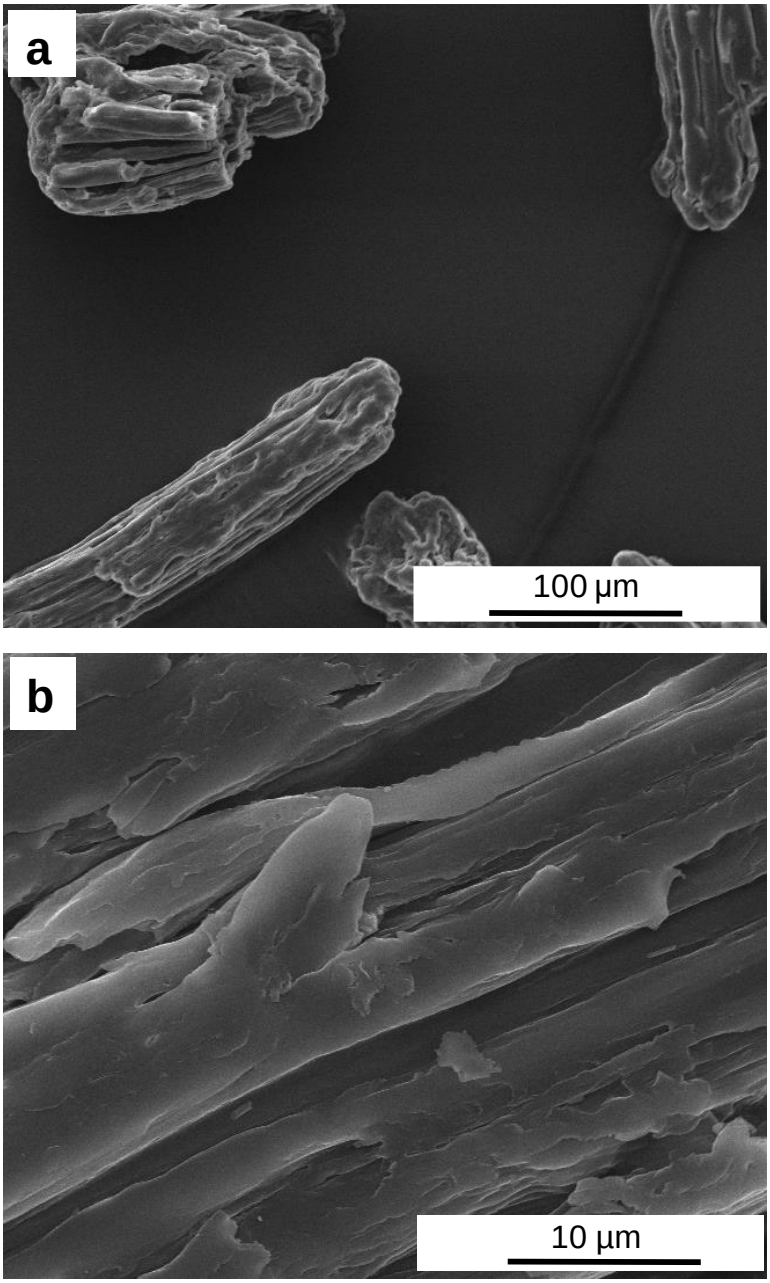

Figure 4.12: SEM images of wetted MCC with PBAT; a part of (a) is magnified in (b)

The images show that the MCC after removal of embedded PBAT matrix is still wrapped with PBAT molecules. The micrograph gives an impression of polymer sheaths covering the fibers. Thus, the physical interaction, as indicated by FTIR spectroscopy, has been found to result in a sort of compatibilizer case formation around the natural fibers.

The extracted fiber surface, whose morphology has been presented in Fig. 4.12, was subjected to FTIR analysis using ATR mode. The typical result is presented in Fig. 4.13, comparing the extracted fiber with the neat MCC.

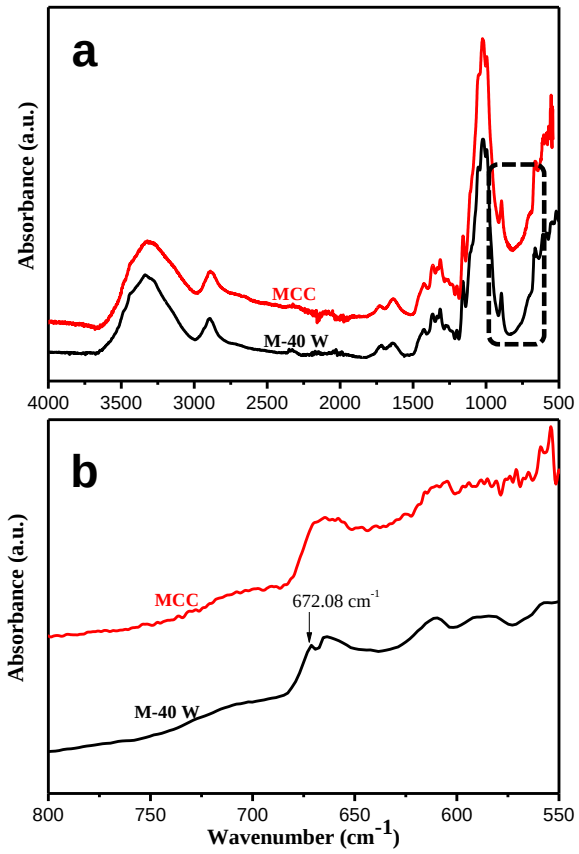

Figure 4.13: FTIR plot of pure MCC and the MCC extracted from M-40. A part of (a) is magnified in (b) for closer observation

The FTIR plot in Fig. 4.13 shows that the MCC obtained after dissolving the polymer shows similar absorbance as that for the neat MCC. However, on close observation of the FTIR plot (Fig. 4.13b), a peak at 672 cm^{-1} appears which represents absorbance

due to formation of H-bonding between OH-groups of MCC and C=O group of polyester. Similar type of absorption peak was also indicated a recent works performed on the composites of the bamboo fiber with polyesters (Das & Chakraborty, 2009). The plot of FTIR clearly illustrates the H-bonding between MCC and PBAT in M-40, although it is a simple weak H-bonding, is enough to show good compatibility between MCC and PBAT in the composites.

c) Microscopic characterization

The internal morphology of the composites can be well described by microscopic observations. The information regarding the orientation of fillers, distribution and their compatibility with the polymer matrix provide evidences for their mechanical strength, degradation phenomena and many more. In this section, SEM micrographs of W-40 and M-40 are presented as examples for showing internal morphology of the composites.

The SEM image of cryofractured W-40 is shown in Fig. 4.14 where more or less uniform dispersion of WS fibers in PBAT can be seen. WS fibers are randomly arranged in the composites. The raw WS were approximately 25 μm wide and 300 μm long. Fibers have very coarse serrated outer surface.

Due to difference in polarity of hydrophobic PBAT and hydrophilic WS fibers, they are incompatible to each other so the mixing of PBAT and WS is only due to physical forces. Nevertheless, the fibers seem to be quite compatible with the matrix; the fiber matrix separation (i.e. debonding) is observed only occasionally.

Such type of debonding of fiber is also seen in composite of ramie fiber with and poly(lactic acid) (Yu & Li, 2014). The incompatibility of raw fibers such as cassava starch, starch and even inorganic fiber OMMT was observed with PBAT (Brandelero *et al*., 2010, Shi *et al*., 2011, Ozkoc *et al*., 2010). Saiter *et al*. also reported incompatibility of starch with glycerol (Saiter *et al*., 2010). There are many signs of fibers pull out and void formation in the composites (Siyamak *et al*., 2012a, Siyamak *et al*., 2012b). It was reported that on surface modification of PBAT with 4 % SAH and using DCP the voids formation phenomena can be significantly suppressed (Siyamak *et al*., 2012b).

In Fig. 4.15, the cryofractured surface of the composite, M-40 shows uniform dispersion of MCC in PBAT during melt mixing process, similar to the W-composites. In addition, there is no void or crack at the interfacial region attesting the presence of some compatibility between the polymer and filler although the FTIR spectrum indicates only physical mixing between two components.

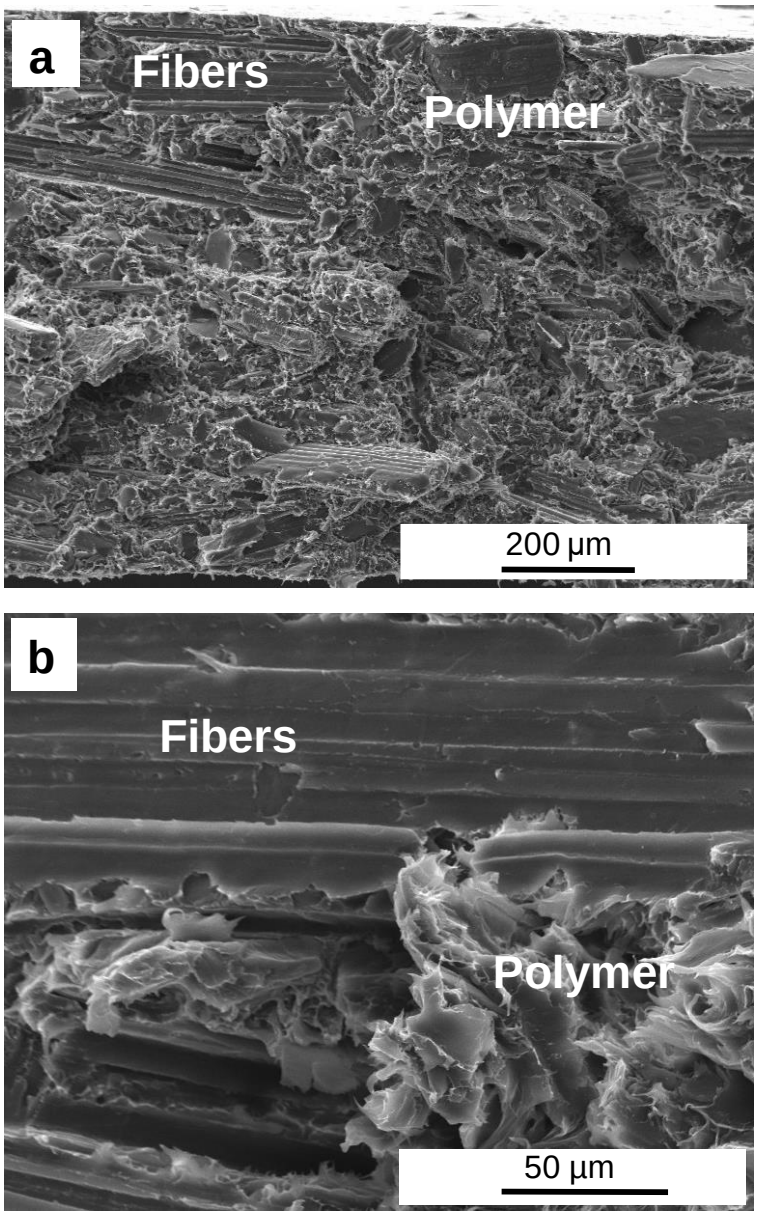

Figure 4.14: Lower (a) and higher (b) magnification SEM images of the cryofractured surface of the composite W-40; apart of (a) is magnified in (b)

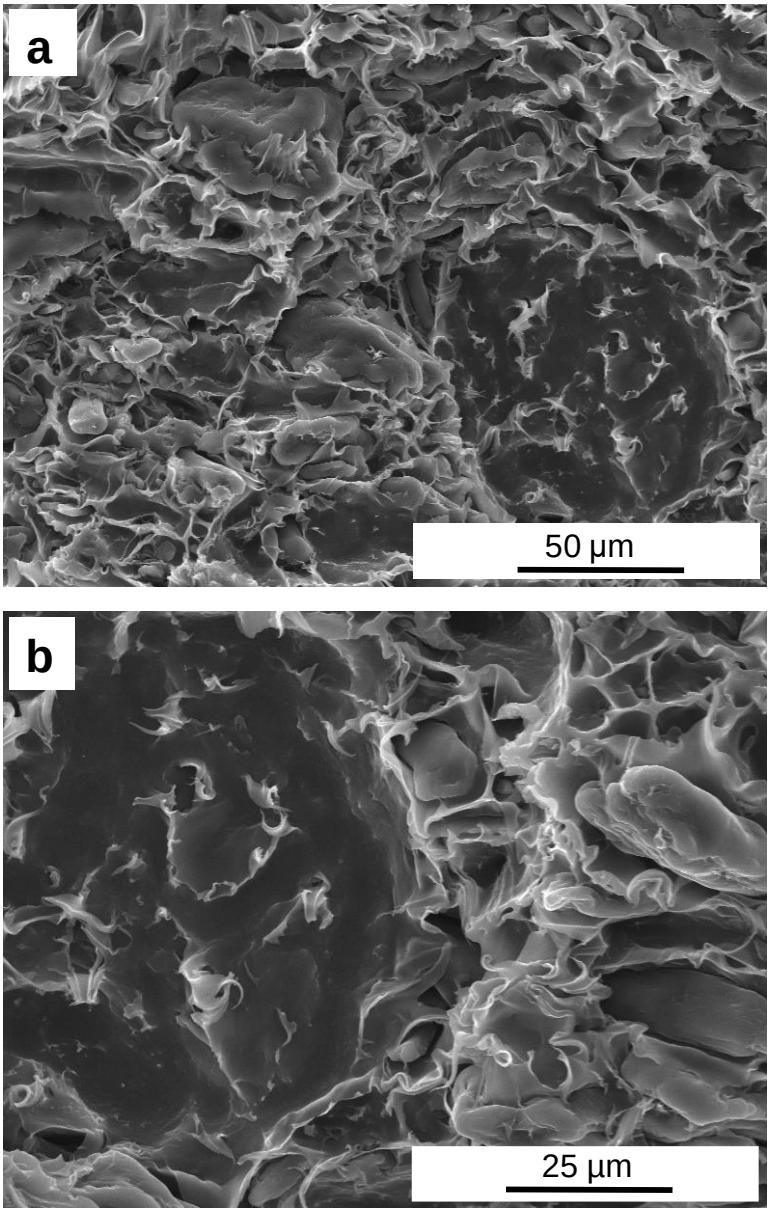

Figure 4.15: Lower (a) and higher (b) magnification SEM images of the cryofractured surface of the composite M-40; a part of (a) is magnified in (b).

Moreover, the exposure of -OH groups of cellulose after mercerization of fibers, form H-bonding with the matrix (Tian *et al.*, 2018). The cryofractured surface has many MCC fibers that are projecting out from the surface. Similarly, many MCC are pulled out forming pores on the surface. The size of the MCC seems to vary in the composites still most of them have 5-6 µm in diameter and the length also around 20-25 µm. (see Section 4.1.1). Agglomeration of MCC can be seen in some places which was also observed in the composite of cellulose acetate and PBAT/PBAT g-AA and explained as H-bonding of cellulose acetate with PBAT (Wu, 2012). However,

anisotropic micro-pores were observed in composites comprising cellulose and PLA (Gauitua, Ballerini & Zhang, 2005, Kramer *et al*., 2006).

Microscopic observation thus demonstrated the quite uniform dispersion of WS and MCC in PBAT matrix with compatibility of physical nature. MCC seems to have good interaction with PBAT in comparison to WS, as mercerization exfoliates OH-groups of cellulose which interact with carbonyl group of PBAT *via* H-bonding.

d) X-ray diffraction analysis

X-ray diffraction (XRD) data give information about the crystalline structure of the materials on microscopic scale. The crystallinity index (CI) and diffraction patterns observed in different miller indices explore the relative amount and type of crystals of different components. The variation in crystallinity of the polymer due to interaction with foreign substances such as fiber can be well explained by this technique. Fig 4.16 shows that the CI, degree of crystallinity of the polymer is not affected upon MCC loading into polymer matrix. The results are also presented in Table 4.3.

In Fig. 4.16 five diffraction peaks corresponding to the PBAT are clearly seen in M-5 and M-10 which is in agreement with the literature (such as Chivrac *et al*., 2006, Mukherjee *et al*., 2014, Wu, 2012). The diffraction peaks located at 2θ values at 17.34 ^{o}, 20.9 ^{o}, 23.30 ^{o} and 24.92 ^{o} are the signatures of PBAT and are found to be at same 2θ values for M-5 and M-10. Among these few peaks have quite less intensity than former. This can be implied that there is not such significant contribution in trans-crystallinity in the system interface (Mukherjee *et al*., 2014). The Scherrer equation (Equation 3.1) and Bragg's Law (Equation 3.2) are used to measure crystallite size and d-spacing (Pradhan, 2015, Cho, Park & Kadla, 2012, Bhattarai, 2006, Guo, 2016).

The CI value of PBAT is slightly increased by addition of 5 wt. fraction of MCC, due to increase in surface area for crystallization growth and decreased on further addition of MCC due to the MCC agglomeration as shown in Table 4.3. Likewise, d-spacing is also decreasing which can be attributed to the attractive interaction between MCC and PBAT as also supported by FTIR spectra shown in Fig. 4.11.

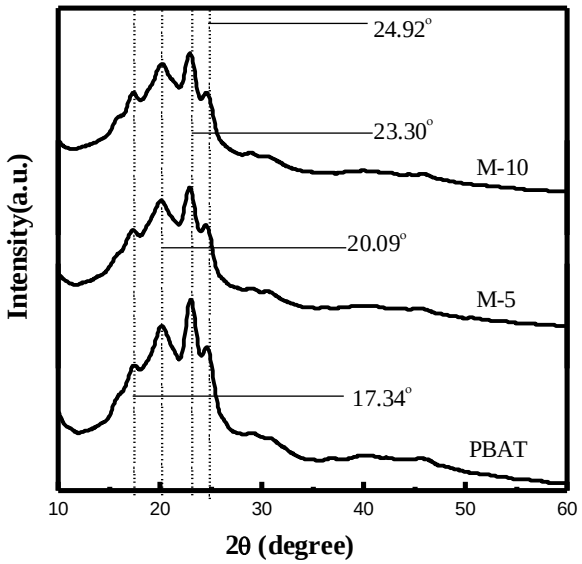

Figure 4.16: X-ray diffractogram showing comparative plot of M-5, PBAT and MCC

Table 4.3: XRD data showing Crystallinity index (CI), d- spacing and apparent grain size (D) in different microcomposites M-5, M-10 and PBAT

S. No.	Sample code	CI (%)	d-spacing (nm)	D-Grain size(nm)
1	PBAT	79.78	0.382	0.874
2	M-5	82.05	0.378	0.88
3	M-10	71.38	0.382	0.889

The minute observations of apparent grain size (D) and d-spacing value (see Table 4.3) of M-composites increases with increasing MCC content in comparison to the PBAT. Although D values remains almost constant in M-5 and M-10 which manifest that MCC in the PBAT does not affect morphological parameters. Similar type of result was also observed for unplasticized coffee ground filler with PBAT composite (Moustafa *et al*., 2016).

4.2.2 Thermal Behaviour of Composites

Thermal behaviour explains the thermal stability of the materials under analysis. Thermal stability is a criterion to distinguish the material for its application. At the same moment it also clarifies its temperature dependent properties such as

crystallinity, melting point, etc., which are the major determining factor to select the materials for its application.

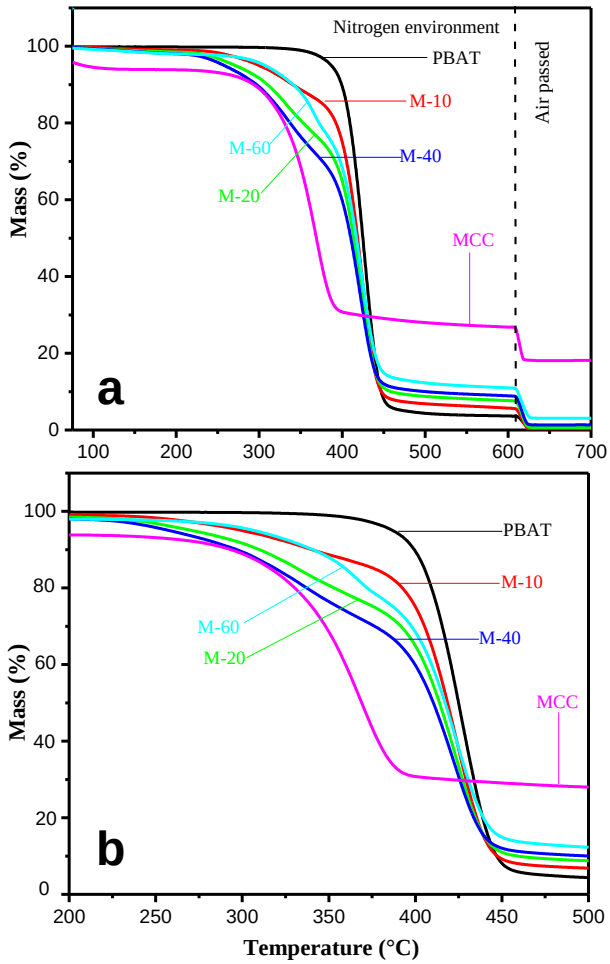

Figure 4.17: TGA curves of pure PBAT and pure MCC compared with that of the some M-composites; a part of (a) is magnified in (b)

Fig. 4.17a presents the plot of thermogravimetric analysis of PBAT, MCC and four different composites (i.e. M-10, M-20, M-40 and M-60). Some of the major degradation zones have been magnified in Fig. 4.17b. The thermal behaviour of MCC and PBAT has been already discussed in Chapter 4, section 4.1 (sub-section 4.1.1c and 4.1.2b) by explaining TGA and DTG plots.

The cumulative thermal effect of MCC and PBAT is distinctly explored under nitrogen environment and clearly shown in Fig. 4.17. It can be observed that the thermal behaviours of the composites are expected, intermediate between the starting components (i.e. MCC and PBAT).

The increasing concentration of MCC in the composites increases higher affinity for degradation.

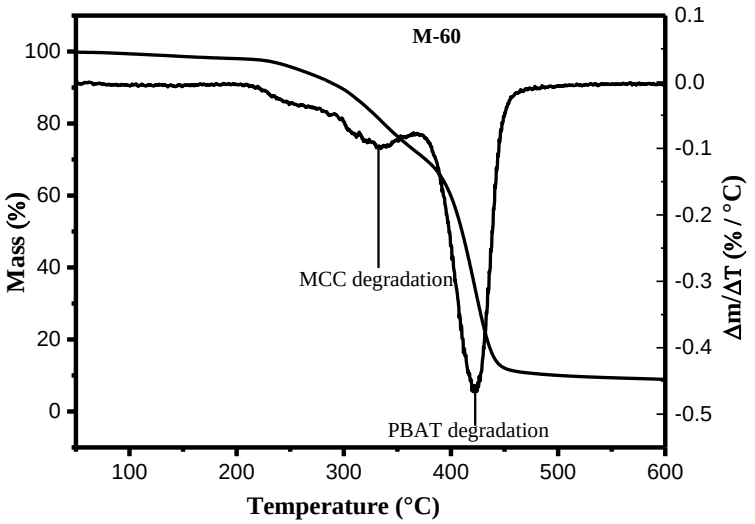

Figure 4.18: TG and DTG curves of M-60 to show two stages of degradation for MCC and PBAT as a function of temperature

The degradation behaviour is clearly marked by two regimes for examples see Fig. 4.18 for M-60; first at around 230 ℃ corresponding to MCC and another at around 420 ℃ corresponding to PBAT. On the progress of thermal degradation composites yield char with the increase in MCC content in composites, which is tabulated in Table 4.4. For all the materials beyond 600 ℃, there is a definite amount of residual mass (for M-60=11.23% mass) corresponding to char.

One of the interesting property that can be observed in TGA curves is related to the residual mass of the materials at high temperature (Cesar *et al*., 2015). The residual mass is actually the amount of materials left after thermal degradation in inert environment some of these are even withstand in oxidizing environment as well. The amount of char can be well correlated with fire retardancy properties (Cesar *et al*., 2015, Cho *et al*., 2011).

The fire retardancy of the material can be explained on the basis of amount of char yield by the MCC (Wang *et al*., 2008). The char limits the production of combustible gases and even decreases exothermic pyrolytic reaction inhibiting the thermal conductivity of the burning materials (Wang *et al*., 2008, Cesar *et al*., 2015). Therefore, char yield indicates the flame retardancy of the materials (Wang *et al*.,

2008). Beyond 600 ℃ under oxygen, the system has oxidizing environment where the char left in the composites completely burns to volatile gases. However, even under presence of air, the MCC has 18.42 % residual mass, due to the formation of stable char.

Now, let us have a closer look in Table 4.4. It can be seen that the char of PBAT at 600 ℃ is 3.3 % while that of MCC 27.26 %, it means that PBAT is much combustible significantly than that of MCC (Fukusima *et al*., 2012, Cesar *et al*., 2015).

The amount of residual mass (the char content) increases in the composites compared to pure PBAT (see Table 4.4). Now for composites, the amount of char for M-10, M-20, M-40 and M-60 progressively increases from 5.92 to 11.23 %. The increasing char yield in composites is well supported by fire retardant property of PBAT as mentioned in literatures (Mandal & Chakrabarty, 2014, Wang *et al*., 2008, Wu, 2012, Trovatti, 2012, Abraham, 2012).

Thus, from the Table 4.4, it can be summarized that increase of MCC content in composites increases the residual mass reflecting fire retardancy property.

Table 4.4: char yield of the- composites for different MCC contents at 600 ℃ under inert environment

Sample No.	**MCC**	**PBAT**	**M-10**	**M-20**	**M-40**	**M-60**
Char yield (%)	27.26	3.30	5.92	7.63	9.26	11.23

Using the TGA data, activation energy of thermal degradation (E_a) of materials can be calculated through using Arrhenius equation (Equation 4.2).

$$\frac{d\alpha}{dt} = F(\alpha)KT = A.e^{(\frac{-E_a}{RT})}.F(\alpha) \qquad (4.2)$$

where $\alpha = (m_i\text{-}m)/(m_i\text{-}m_f)$, degraded mass fraction of the substrate (with m_i = initial mass of the substrate, m_f = final mass of the substrate; and m = mass of the subatrate at the specific temperature (T), A = the pre-exponential factor (1/min), E = the

apparent activation energy (J/mol), T = the absolute temperature (K) and R the gas constant (8.3136 J/mol K).

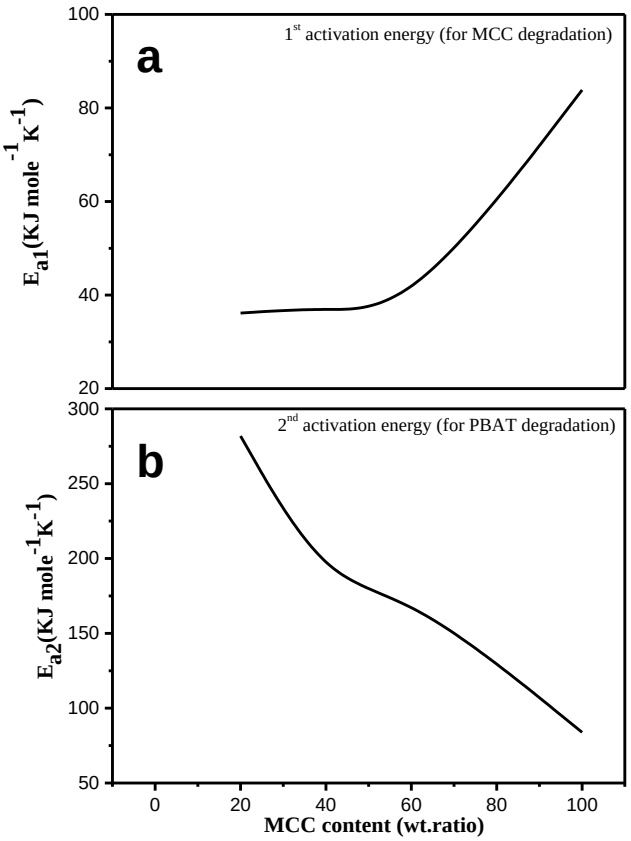

Figure 4.19: (a) Plot of 1st activation energy; (b) plot of 2nd activation energy, as a function of pure MCC content

The data ln(dm/dt) *versus* 1/T of every sample plotted keeps a straight line for linear fit. From the slope of the curve, the value of E_a can be calculated (Pokhrel, 2016a, Pandit, 2015, Pradhan, 2015). The calculations give two types of activation energies for each composite material. Each of the E_a values can be correlated later with the degradation behaviour of each component i.e. MCC and PBAT of the composite.

Fig. 4.19a stands for the 1st activation energy corresponding to pure MCC and the MCC fraction in the composites. The plot shows that the 1st activation energy increases sharply from 30 $KJmole^{-1}K^{-1}$ (in the composite, M-10) to nearly 83 $KJmole^{-1}K^{-1}$ (for MCC). This can be attributed for the formation of larger interfacial area, and

thus facilitates embedded MCC phase to degrade in composites to form voids in the place of MCC. The larger agglomeration in MCC have less interfacial surface and requires higher energy leading to high value of E_{a1}. Similarly, Fig. 4.19b presents the 2nd activation energy corresponding to the degradation of PBAT in the composites. Here, the plot shows that with increase in MCC content in the composites, the degradation becomes easier eventually to the formation of interfacial voids that might have been created by MCC degradation in 1st degradation stage and consequently, the PBAT might have fully exposed to the high temperature during TGA.

The thermogravimetric analyses show composites prepared have two distinct zone of degradation with improving fire retardancy with respect to the MCC content in the composites. Such behaviour was also distinctly shown by water bamboo husk- PLA composites (Wang *et al*., 2008), Empty fruit bunch fiber-PBAT (Siyamak *et al*., 2012) and PP/Kenaf fibers composites as well (Han *et al*., 2008).

4.2.3 Mechanical Deformation Behaviour

Application of mechanical force on the composites brings about plastic deformation of structures tearing finally to the failure of the materials. In this section the composites prepared are investigated for their deformation behaviour on application of tensile strength and indentation forces.

a) Tensile properties

The stress-stain curves of the samples are given in Fig. 4.20a. The values of elongation at break (ε_b) and tensile strength (σ_{max}) of the samples as a function of MCC content are presented in Fig. 4.20b.

In Fig. 4.20a the pristine PBAT shows highly ductile property, with its elongation at break (ε_b) of 730 % and holds stress more than 30.0 MPa similar to the values mentioned in the literatures (Teamsinsungvon *et al*., 2010). Although, PBAT shows highly ductile behaviour while the composites with low amount of MCC (such as M-10 and M-20) still show ductile nature (ε_b value of > 250 %).

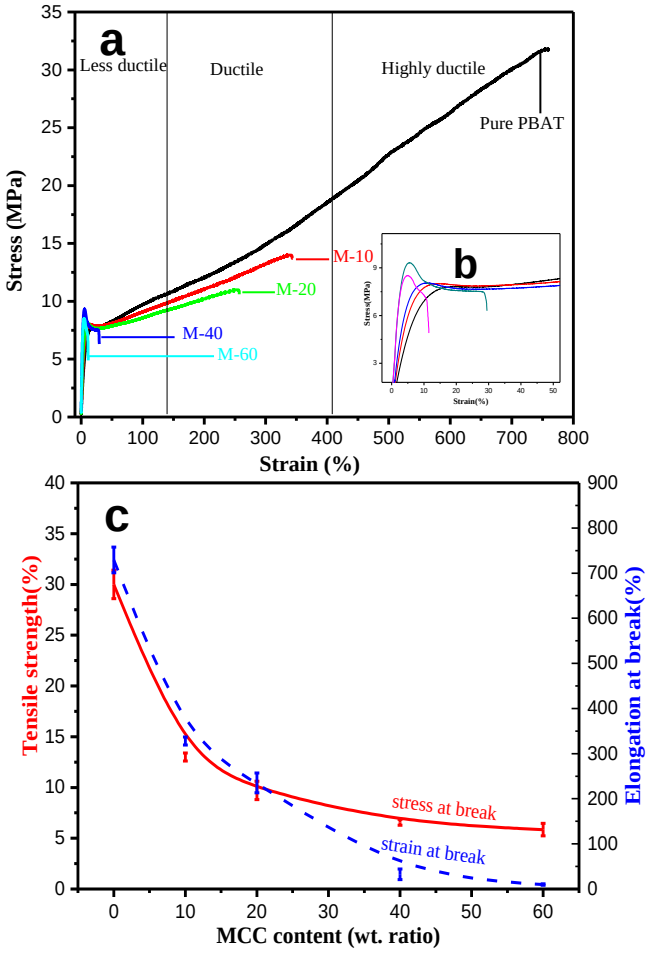

Figure 4.20: (a)The stress-strain plots for pure PBAT and composites of MCC ; (b); closure view of (a) at the deformation point (c) tensile strength (σ_{max}) and elongation at break (ε_b) values of the samples in the MCC content in the composites

The composites show, however, drastic reduction in tensile strength (from > 30 MPa to~15 MPa). At higher MCC content (such as M-40 and M-60), both values of ε_b and σ_{max} decrease drastically indicating the premature failure of the samples, as MCC might create voids at interfacial region, form cracks and propagated on further application of load. The justifications for such deformation in stress holding capacity are also reported in literatures (Siyamak *et al.*, 2012b). Therefore, MCC incorporation in PBAT induces deterioration in tensile properties with respect to tensile strength and elongation at break.

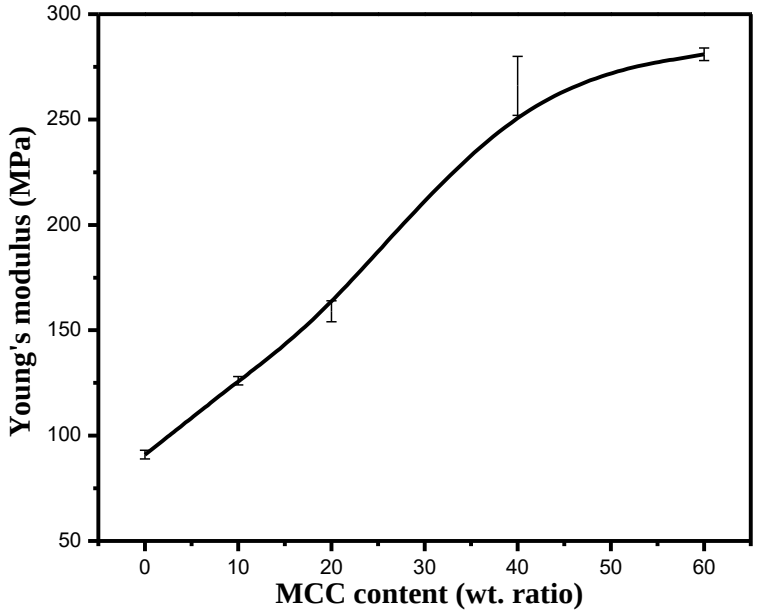

Figure 4.21: Variation of Young's modulus with the increasing concentration of MCC in M-composites

Thus three regions of mechanical behaviour can be ascertained for the composites: I) highly ductile II) ductile and III) less ductile (see Fig. 4.20a). Similarly, ratio of stress and strain for the composites at point of stress-strain curve gives Young's modulus (E_Y) value of which directly correlates with the stiffness or hardness in the materials with increasing loading of MCC in composites. The closer look on Fig. 4.20b indicates reinforcement in stiffness of the composites with addition of MCC and yield stress is also increasing in similar way. The Fig. 4.20c also supports premature failure of the composites by deteriorating tensile strength and ε_b with higher loading of MCC. Similar property was also observed in cellulose acetate/PBAT composites (Wu, 2012).

Although MCC deteriorates the tensile property of the composites, it reinforces hardness which can be easily explained by increasing E_Y as shown in Fig. 4.21 for MCC composites. Here, the value for E_Y for PBAT 90.64 MPa is enhanced to 125.46 MPa (for M-10) and 280.45 MPa (for M-60) by addition of MCC. Similar, behaviour was obtained for empty fruit bunch fiber (EFBF)-PBAT composites (Siyamak *et al*., 2012). Tensile modulus of the PBAT and composites enhance due to the increased stiffness and brittleness by the addition of MCC which is reported by many literatures (Lee *et al*., 2009, Liu *et al*., 2010)

b) Microhardness measurement

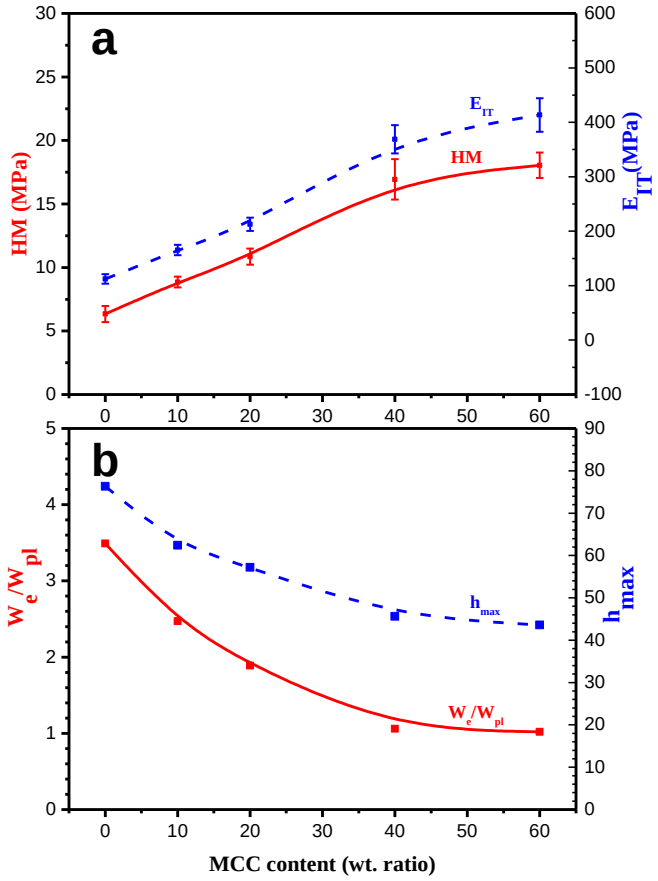

Figure 4.22: (a) Martens hardness (HM) and indentation modulus (E_{IT}) (b) ratio of elastic and plastic work (W_e/W_{pl}) and indentation depth (E_{IT}) as a function of MCC content for PBAT and MCC composites

Mechanical properties of the material are further studied by microindentation measurements. The 5 replicate samples are allowed to examine by pyramidal diamond indenter at predefined load 1000 mN, to obtain statistical reasonable data. Martens hardness, indentation modulus, and indentation depth provides information of viscoelastic and viscoplastic behaviour of the polymer and its composites.

The mathematical relation explained in experimental section equation 3.3 and 3.4 are used to measure the martens hardness (HM) and indentation modulus (E_{IT}) for PBAT and MCC composites to present in Fig. 4.22a. The HM and E_{IT} are increasing in Fig. 4.22 due to the increase in stiffness and toughness with MCC loading in composites. Here HM and E_{IT} values 6.30 MPa, 112.4 MPa for PBAT increases to 8.81MPa, 164.17 MPa for M-10 and 18.07 MPa, 412.88 MPa for M-60 respectively. Increase in plastic phase (MCC) correlates the increasing indentation modulus of the composites

as described by the literature (Rajesh, 2015, Balta-Calleja & Fakirov, 2000). Such effect is also called as skin-core effect and applicable for polymer composites with fillers (Schone *et al*., 2014).

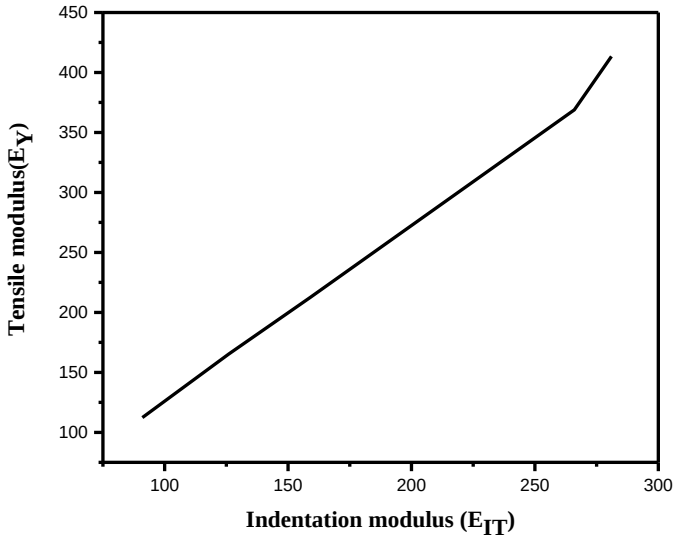

Figure 4.23: The plot showing relation between Young's modulus (E_Y) and indentation modulus (E_{IT}) for PBAT and M-composites with the increasing concentration of MCC

The hardness can also be correlated to measure viscoelastic properties using indentation depth (h_{max}), the ratio of energies and plastic deformation (W_e/W_{pl}) (see in Fig. 4.22b). The ratio W_e/W_{pl} for pure PBAT is quit high about 3.5 % which means that it show a large part of elastic deformation. The value of W_e/W_{pl} decreases progressively in the composites.

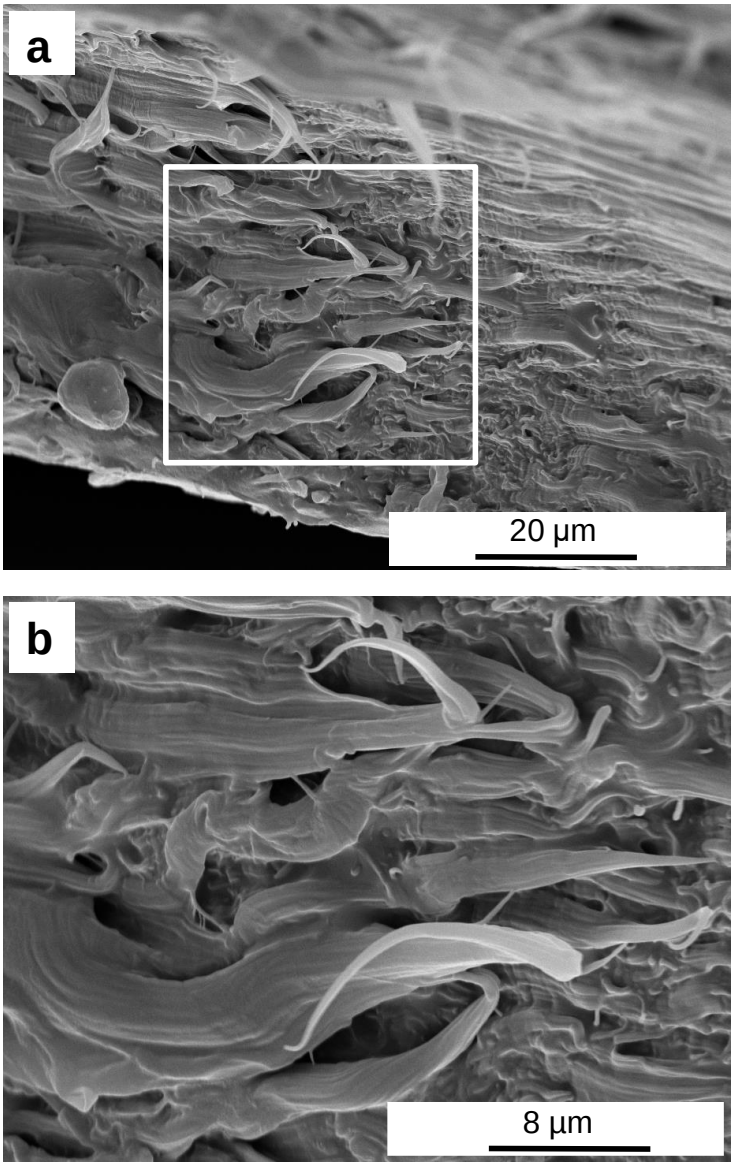

Figure 4.24: SEM images of different magnifications showing tensile fracture surface morphology of PBAT; a part of (a) is magnified in (b)

In the composites the decrease in elastic energy (or increase in plastic energy) is correlated with pronounced stress holding capacity during tensile test, the notion of formation of macro voids in the samples (Okubo *et al*., 2005). In the similar manner, the values of h_{max} also found to decrease from 76 µm (for PBAT) to 43.5 µm (for MCC), which implies resistance to elastic deformation (Balta- Calleja & Fakirov, 2000). The comparative study of mechanical characterizations (tensile and indentation tests) of the PBAT and MCC composites come to conclude that both E_Y and E_{IT} both increase linearly with loading of MCC in PBAT (Fig. 4.23).

c) Fracture surface analysis

The mechanical deformation in polymer and composites is induced by crazing and shear yielding mechanism due to application of external forces (Adhikari & Michler, 2009). These phenomena result in many micromechanical deformation process or failure of the specimen structural changes which on critical extent leads to fracture (Balta-Calleja & Fakirov, 2000). Thus the tensile properties of the materials can be correlated with the ways the materials deform on microscopic scales (Adhikari & Michler, 2009).

The Fig. 4.24 shows the SEM images of different magnification of tensile fracture surfaces of the PBAT. The fracture surface depicts very long needle like fibrillar structures which have been formed by stretching (or large plastic like flow) of the matrix material. The coil like appearance is formed by relaxation of highly stretched fibrils upon the release of the tensile load. Such deformation in structure cause the pointed tipped fibrils which attest the large plastic deformability (Huy *et al*., 2003) of the polymer absorbing a large amount of applied energy and account for the high ductility of the polymer. This kind of behaviour is representative of ductile polymers like iPP, HDPE etc. (Lezak *et al*., 2006, Dusunceli & Colak, 2008). Such a deformation phenomena leads ultimately to high ductility and high strength caused by strain hardening. The polymers finally under category I (highly ductile) in Fig. 4.20a show predominantly this deformation phenomenon. On the other hand, the higher elasticity in polymers makes it difficult to break easily (Siyamak *et al*., 2012a, Wu 2012). In Fig. 4.24b the compact polymer surface with long smooth fibrils of polymer clearly notifies the ductile nature of PBAT and needs higher strength to get deformed.

Such types of deformation are also observed in W-40 composite of WS in PBAT (see Fig 4.25).

The filler WS here act as toughening agent, which absorbs energy and form micro-voids indicating the defected sites to start premature cracks initiator. The critical limits for the growth of these crack leads to fracture. The higher concentration of the WS in the polymer matrix induces many plastic deformations in different directions which ultimately produce many short polymer fibrils during shear yielding. During

elongation on tensile pull, the fibrils enlarge as shown in Fig. 4.25a. The fibrils are not smooth due to the presence of WS in the composites.

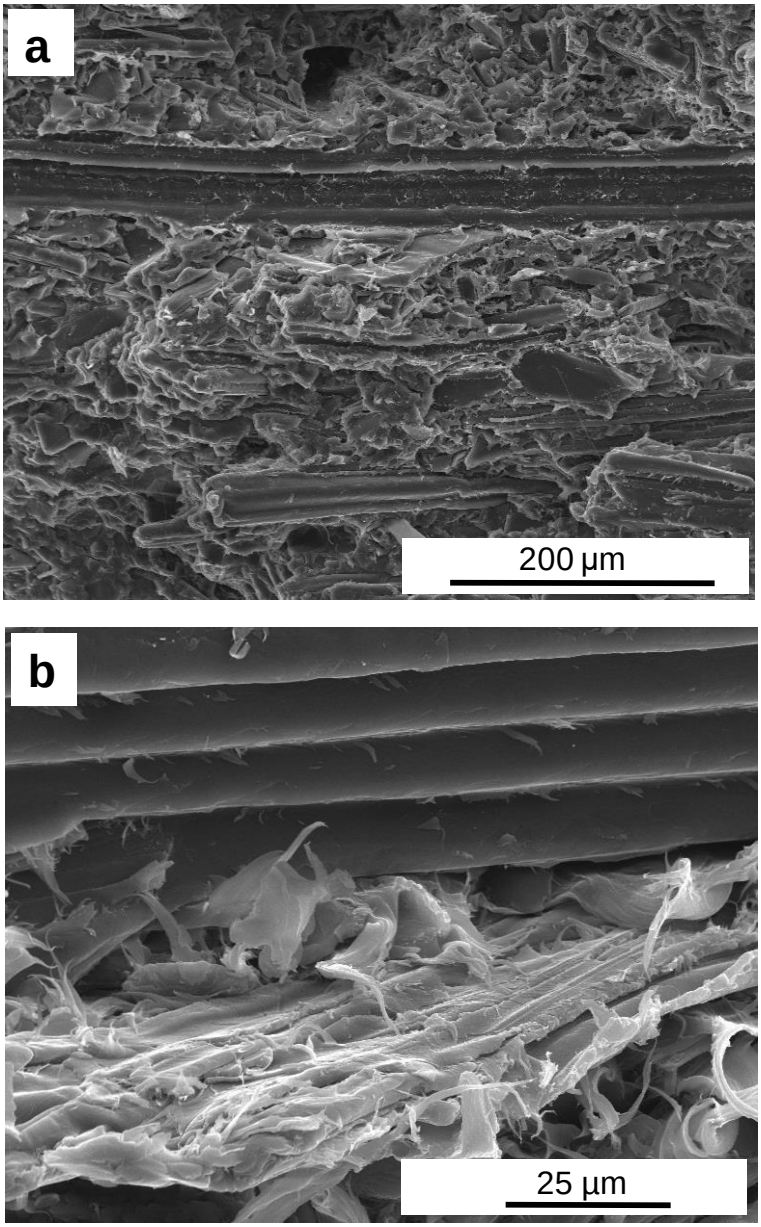

Figure 4.25: SEM images of different magnification, showing tensile fracture surface morphology of W-40; a part of (a) is magnified in (b)

The closer look into the tensile fracture Fig. 4.25b shows many fibrillar PBAT on the fracture surface due to homogeneous dispersion of WS interrupting smooth microfibrils growth. The micrograph shows the composite might have reach to early fracture due to incompatibility between WS and PBAT. There is a good slip of WS in PBAT matrix during shear yielding which ultimately reach to early fracture (Siotto *et*

al., 2013). Let us now examine the fracture surface morphology of the composite at low MCC content (such as M-10), which shows quite ductile behaviour during tensile testing (see Fig. 4.20a).

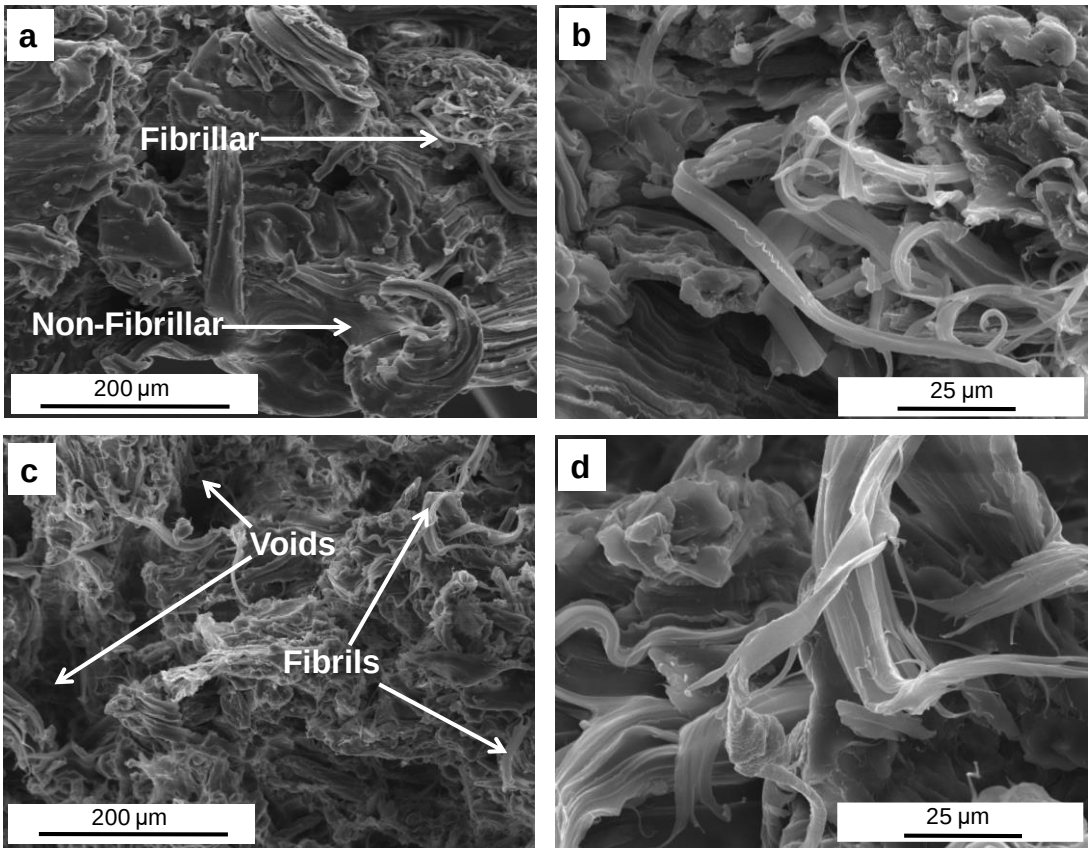

Figure 4.26: SEM images of different magnification, showing tensile fracture surface morphology of M-10; a part of (a) is magnified in (b) and M-40; a part of (c) is magnified in (d)

The tensile fracture surface of the M-10 is depicted by SEM images presented in Fig. 4.26 a, b. The fibrillar origin of PBAT was observed for the M-10 as in pure PBAT indicating highly plastic form of deformation during tensile testing. At the same moment there are few voids formed by the slipping MCC fibers from the matrix. The slip out of polymer filler interface leading to the formation of void is made possible by the presence of only weak attractive interaction of the components. Nevertheless, the large part of fracture surface is covered by highly deformed, strain hardened and pointed tipped, ribbon like features of the PBAT phase. This kind of behaviour account for the ductile and strong nature of the composite corresponds to Regime II in Fig. 4.20a. It can be expected that the composite M-20 would show similar phenomenon on the tensile fracture surface.

The analysis of tensile fracture surfaces of the sample M-40 exhibits entirely different kind of structure. It has to be noted that this sample shows predominantly brittle behaviour (Regime III in Fig. 4.20a). In addition, the morphology of near fracture surface of the sample specimen is presented in Fig. 4.26 c and d.

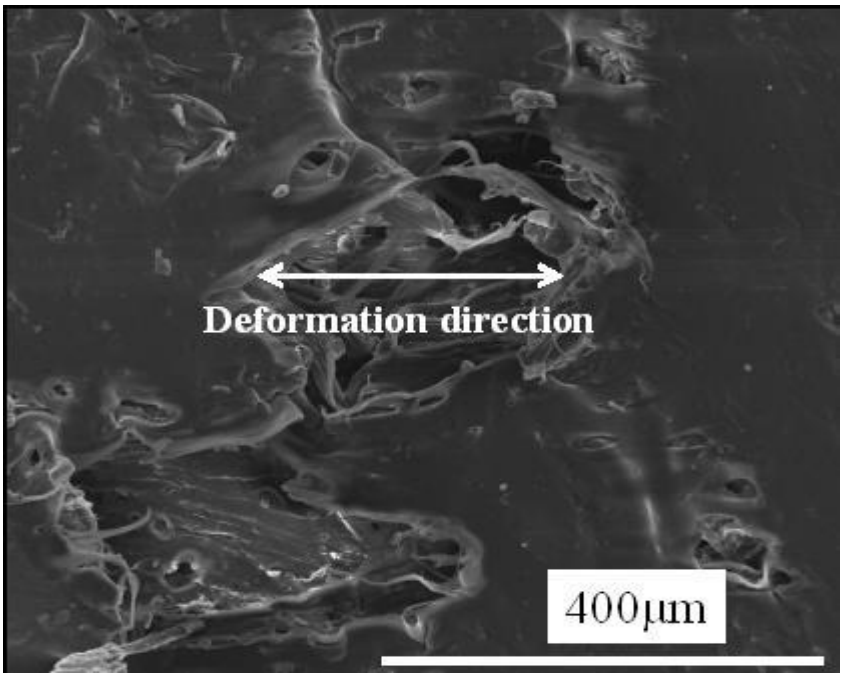

Figure 4.27: Micrographs of tensile fracture surface side view of M-40 showing deformation on the surface at lower magnification of 400µm

In the first glance, the fracture surface shows intact MCC frame work which eventually donot get dislodge or pulled out due to deformation but allow the embedded surrounding PBAT matrix to cause limited plastic deformation.

The matrix polymer deform and form fibrillar structure as in PBAT (see Fig. 4.26d and compare with Fig. 4.20b) but the deformation is limited to a quite high volume which eventually lead to premature failure with the consequence of low ductility as shown by Region III in Fig. 4.20a.

The comparative studies for mechanical deformation in the composites are found to be increasing with MCC content in the composites. The deformation pattern is followed with shear yielding of the fibrillar PBAT accompanied with void formation due to MCC in the composites. The effect of shear yielding is not only observed in the tensile fracture surface but can be seen on the top surface of tensile fracture specimens. The

phenomena of shear yielding and micro-voids are clearly seen in Fig. 4.26 for M-40 composite.

In this case, the filler particles act as stress concentration which even permit the tearing of the specimens from the surface (Fig. 4.24c and d) restricting the large plastic deformation and strain hardening. The surface tearing of specimen exposing the weak filler polymer interface towards void formation could be the reason for premature failure of the specimens and brittle behaviour.

Based on the microscopic examination of fracture behaviour, the mechanical behaviour of the composite can be summarized by Scheme 4.1. Different regimes can be identified.

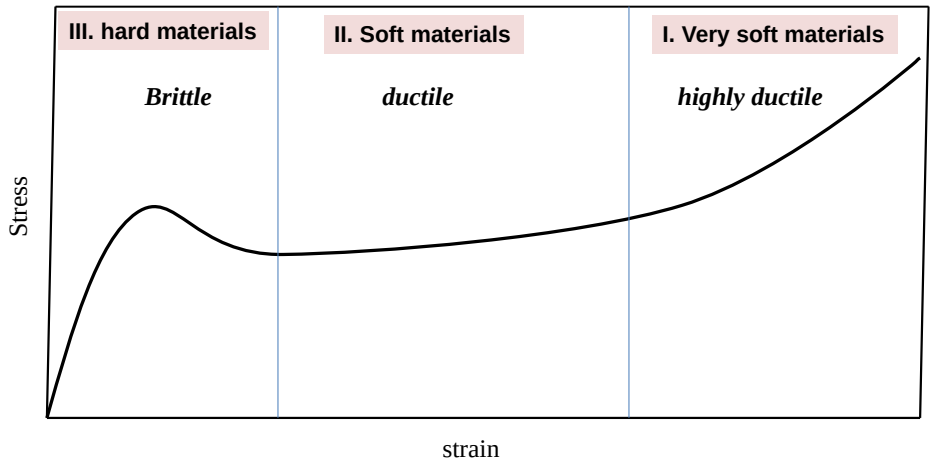

Scheme 4.1: Schematic diagram showing the deformation behaviour of the polymer composites

Regime I

This regime illustrates the properties of the pure PBAT and the composites with low filler content. Also the nanocomposites (section 4.3) fall under this category. These materials are highly ductile and show large plastic deformation and strong strain hardening leading to the formation of highly extended needle-like structure at fracture surface upon fracture.

Regime II

This regime illustrates the properties of the composites with intermediate filler content. These materials are quite ductile and show large plastic deformation and no strong or low degree of strain hardening. Cold drawing is the main feature of the materials. As a result, only localized plastically deformed regions are formed at fracture surface upon fracture.

Regime III

This regime illustrates the properties of the composites with high filler content. These materials are quite hard and brittle and show very low plastic deformation and break right beyond the yield point. As a result, the localized plastically deformed zones are rarely observed.

CONCLUDING REMARKS

The results for structure-properties correlation of polymer composites presented in this section are concluded as follows and tabulated in Table 4.5.

- The FTIR spectroscopy illustrates that the PBAT phase dominates in the spectra of the composites implying that the MCC phase preferentially gets localized towards the bulk of the samples. Furthermore, there is a sufficient physical interaction between the components to get quite uniform distribution of the fillers.
- Owing to the segregation of the components held together by purely physical forces into two separate phases, there are two distinct thermally activated degradation regimes characterized by separate activation processes. The large PBAT/MCC interfacial areas might have provoked more rapid thermal degradation of the composites compared to the pure components.
- The PBAT is highly ductile material in terms of tensile properties. The composites maintain their high ductility up to 20 % by weight of the MCC in the composite. The drastic reduction in the ductility for higher filler loading is due to premature failure that might have been caused by void formation and initiation at the interfacial region.
- Three regimes of deformation processes are identified: very ductile, ductile and brittle. Those have been correlated with corresponding deformations processes *via* fracture surface analysis.

Table 4.5: Summary of structural, thermal and mechanical properties of PBAT/WS and PBAT/MCC-composites

Methods	**PBAT/MCC**
FTIR	No significant covalent bond between MCC and PBAT; Only distinct physical interaction at interface preferential PBAT localization towards surface
Wetting analysis	MCC in M-composites are wetted or bound by PBAT due to H-bonding between OH group of MCC with C=O group of polyester
Morphology	Good dispersion of MCC in PBAT; MCC quite good compatible with PBAT
XRD	crystallinity not significantly affected by MCC addition
TGA	Thermally stable, two steps degradation; 1st for MCC and the 2nd one for PBAT; MCC induces early degradation of composite, E increases with increasing MCC content
Mechanical (Tensile test)	Ductility, σ_{max} and ε_b decreased at MCC loading. E_Y increases with MCC loading; 3 regimes of deformation observed
Mechanical (Indentation test)	Martens hardness and indentation modulus increases and indentation depth decreases with increase in MCC content in PBAT
Fracture surface analysis	All composites seem to be elastic but MCC content increase voids and entanglements in fibrillar deformation, leading to brittleness Different regions show unique deformation behaviour high ductile, ductile and brittle; correlated with fracture surface morphologies

4.3 Structure-Properties Correlation in Nanocomposites

In section 4.2, the microcomposites materials formed by PBAT and MCC have been discussed. It has been concluded that PBAT/MCC composites are quite good in terms of their mechanical and thermal properties and suit for light weight applications. The objective of this section is to investigate the structure and properties of corresponding nanocomposites.

4.3.1 Structural Properties

The molecular characteristics of the PBAT/NCC composites can be adequately explained by FTIR spectra which give straight forward information on the functional groups and types of bonding present in the system. Similarly, the X-ray and electron microscopy data provide close insight into crystallinity and internal morphology of the composites, respectively.

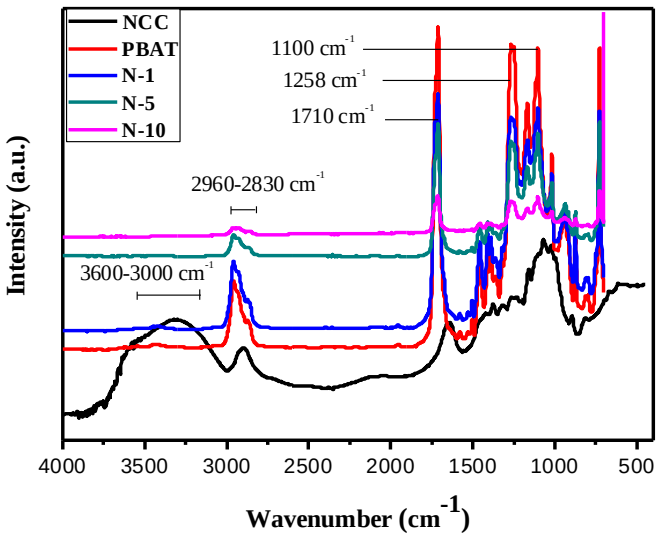

Figure 4.28: FTIR spectra of the PBAT and NCC compared with some PBAT/NCC nanocomposites of various compositions (i.e. N-1, N-5 and N-10)

Fig. 4.28 shows the FTIR spectra of the PBAT, NCC and some of the nanocomposites (such as N-1, N-5 and N-10). The spectra do not show specific features for the NCC in any of the nanocomposites, which may be partly due to the very low quantity of the NCC present in the composite. It further suggests the absence of NCC towards the sample surfaces. Thus, the composites show absorbance dominated for the PBAT

indicating that the NCC doesnot localize on the surfaces of the nanocomposites as also discussed in the literature (Zhou *et al*., 2012).

The composites lack broad absorption band at 3600 -3000 cm^{-1} (characteristic of the O-H stretching vibration) and at 2960-2830 cm^{-1} (characteristic of the C-H stretching vibration) that would otherwise signify the presence of H-bonding and C-H stretching between the NCC and the PBAT on the sample surfaces. The sharp IR peak located at 1710 cm^{-1} corresponds to C=O group present in PBAT which is slightly shifted towards higher wavenumber (i.e. 1720 cm^{-1}) in the composites. The intense peaks at 1263 cm^{-1} and 1100 cm^{-1} corresponds C-O stretching of the carbonyl and C-O-C stretching of ester in the nanocomposites respectively (Yang & Ye, 2012, Pereda *et al*., 2011, Anirudhan & Rajeena, 2013). Indeed, the FTIR spectra of PBAT/NCC composites are very much similar to that of the PBAT/MCC microcomposites (compare Fig. 4.10 and 4.28).

As in microcomposites, the PBAT/NCC nanocomposites surfaces have dominating phase of PBAT and there is no specific chemical interaction between PBAT and NCC. Thus these also represent merely the compounds formed by physical mixing.

The internal morphology of the nanocomposites is observed by performing scanning electron microscopy on the cryofractured surfaces of the samples. Fig. 4.29 provides the SEM micrographs of two different nanocomposites (N-1 and N-5) as indicated. The surface texture shows smooth continuous matrix phase of PBAT while the NCC forms the dispersed phase. The smooth surface of nanocomposites is also attested by the Ma *et al*., (2011), in their composites up to 5 % wt. ratio of NCC. Similar results were reported earlier in many literatures (Khan *et al*., 2013). Thus, the NCC is found to be quite compatible with the polymer matrix as attested by the absence of cracks at the NCC/PBAT interfacial region.

There are certain areas occupied by short fiber-like NCC structures (observed as needle-like spikes in Fig. 4.29) indicated by white arrows. The NCC fibrils are about 0.5 μm long and few tens to few hundred nanometers wide and are found to protrude out of the fracture surfaces. Such type of cryofractured surfaces of nanocomposites are also reported in many literatures (Rahimi *et al*., 2017, Jonoobi *et al*., 2014). The

cellulosic filler was found to primary materials performing to localize towards the bulk materials although retain the crystalline behaviour of polymer.

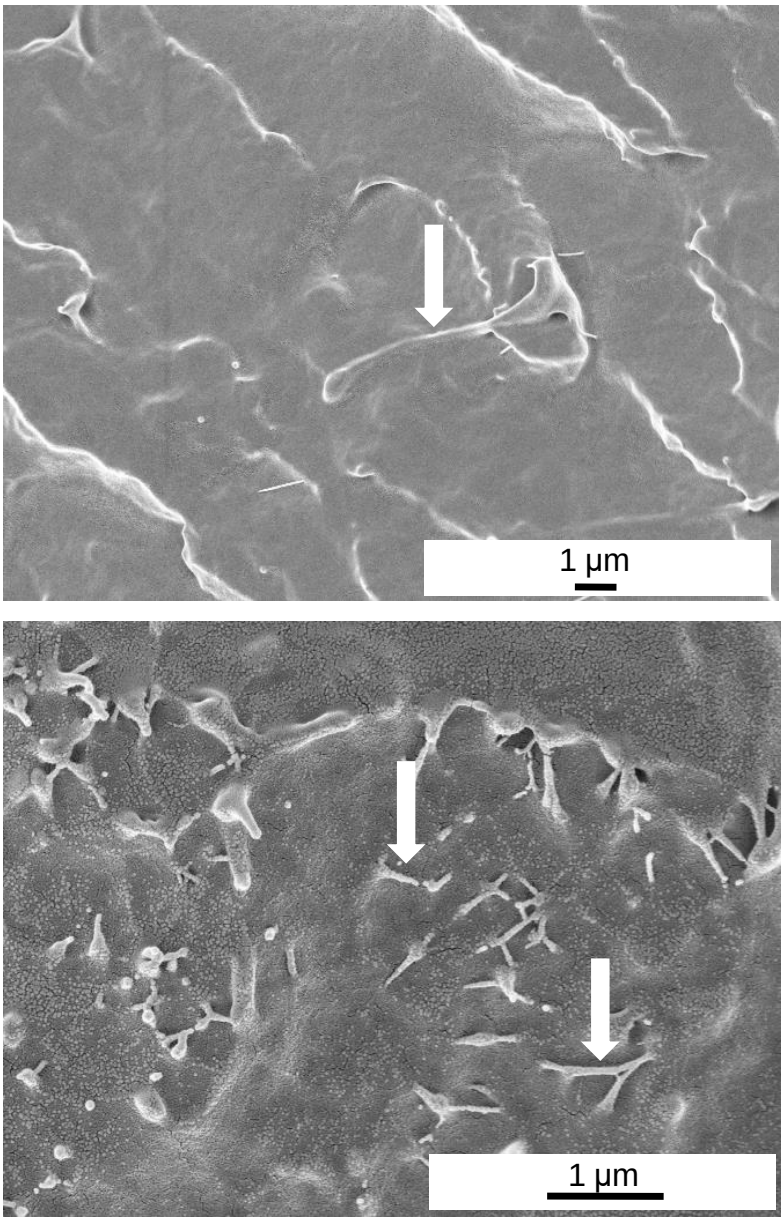

Figure 4.29: SEM images of fracture surfaces of PBAT/NCC nanocomposites N-1 (a) and N-5 (b)

XRD patterns of some of the nanocomposites are presented in Fig. 4.30. At first glance, the patterns of the nanocomposites are found to be similar to that of neat PBAT and microcomposites (see Fig 4.8 and Fig 4.16). The peak positions has shifted towards lower 2θ values for nanocomposites due to the closely packed agglomerated NCC, shown in Fig 4.30 which is in agreement with literature (Abraham *et al*., 2012). The shifting of peak is due to the change in crystal lattice parameter of the unit cell.

The diffraction patterns of the nanocomposites are dominated by the PBAT phase. Thus, the crystalline nature of the PBAT is retained in all the nanocomposites. The NCC does not influence the crystallization behaviour of the PBAT as also suggested in the literature (Ma *et al*., 2011, Wu, 2012, Huq *et al*., 2012).

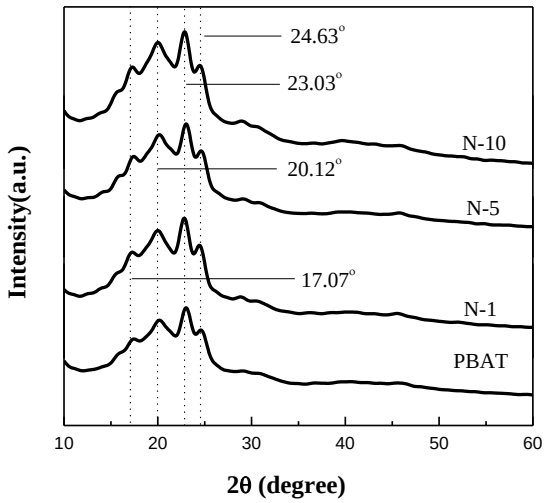

Figure 4.30: X-ray diffractograms of PBAT, NCC, and two PBAT/NCC nanocomposites N-1and N-5

Fig 4.30 can be used to calculate CI, d-spacing and apparent grain size (D) by Sherrer's equation and Bragg's law (Rambo & Ferreira, 2015, Bhattarai, 2006, Cho, Park & Kadle, 2012, Pradhan, 2015). The data observed are presented in Table 4.6. The results indicate increasing CI value with increasing NCC content upto 5 wt.% which is due to the increasing surface area for crystallization growth on NCC. In N-10 CI value decrease due to agglomeration of NCC inducing hindrance in crystallization by NCC fibers possibly due to formation of many H-bonds (Maity *et al*., 2011, Adhikari & Bhandari *et al*., 2012, Dhar *et al*., 2017, Wu *et al*., 2012).

The d-spacing (distance between two molecular layers) and D values for crystal lattice in the nanocomposites are not significantly influenced by NCC. Still d-spacing value found quite small variation from 0.378 nm to 0.381 nm and 0.377 nm on increasing the NCC loading from 1 and 10 weight fractions, respectively.

Table 4.6: XRD data showing Crystallinity index (CI), d-spacing between layers of the PBAT crystals and apparent grain size (D) in different nanocomposites N-1, N-5 and N-10

S. No.	Sample Code	CI (%)	d-spacing (nm)	D-Grain size (nm)
1	PBAT	79.78	0.382	0.874
2	N-1	80.75	0.378	0.888
3	N-5	81.21	0.381	0.845
4	N-10	74.66	0.377	0.878

The structural characterization of the nanocomposites by spectroscopic, microscopic and diffraction means reveal, in summary, that the nanocomposites comprise the compatible constituents which keep their identity in the composite materials. The morphology of the fillers and matrix remain unchanged.

4.3.2 Thermal and Mechanical Behaviour

a) Thermostability of nanocomposites

In Fig. 4.31, it can be observed that the nanocomposites undergo thermal degradation (with the mass loss) as a function of temperature. The thermal degradation behaviour of PBAT/NCC nanocomposites is similar with pure PBAT matrix. The pure PBAT degrades at only one zone at around 430 ℃ whereas the nanocomposites show two steps degradation process that can be better explained by Fig. 4.32b. The early onset of the degradation process in NCC is at around 70 ℃ which can be correlated with the loss of volatile substances and moisture.

The cellulosic entities thermally degrade at 250 ℃ with 22 % of residual mass of char left at 700 ℃ under oxidative environment. Thus, in the nanocomposites with lower NCC contents such as for N-1, N-3 and N-5, there is negligible contribution for the degradation at lower temperature while the contribution becomes significantly high for higher concentration of the NCC (such as for N-10). In N-10, the clear early NCC degradation at 250 ℃ is observed in accordance with literature (Pienhiro *et al*., 2017, Voronova *et al*., 2012).

The two step degradation processes can be more precisely observed in the differential curves some of the examples as illustrated in Fig. 4.32. It should be stressed that all the nanocomposites are found to thermally degrade completely to almost zero residual mass upon release to the oxidative environment (Siyamak *et al*., 2012a, Wang *et al*., 2008). Similar behaviour was also observed for the microcomposites. The PBAT/NCC nanocomposites have been found to be thermally stable up to temperature of around 287 ℃.

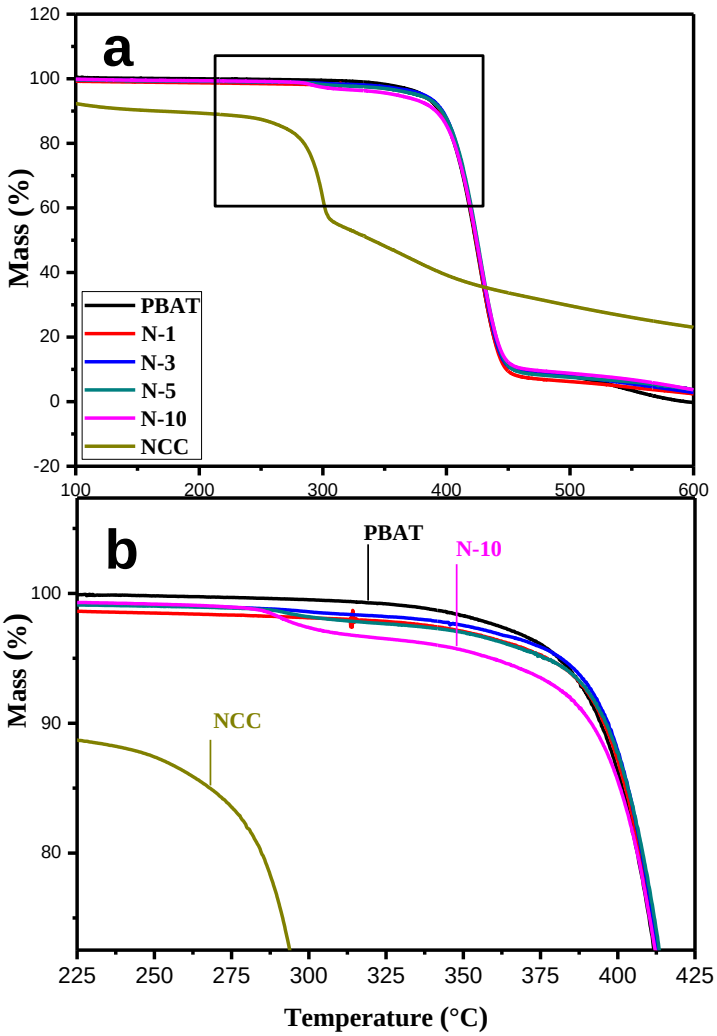

Figure 4.31: TGA thermograms of PBAT, NCC and some PBAT/NCC nanocomposites, a part of thermograph presented in (a) is magnified in (b)

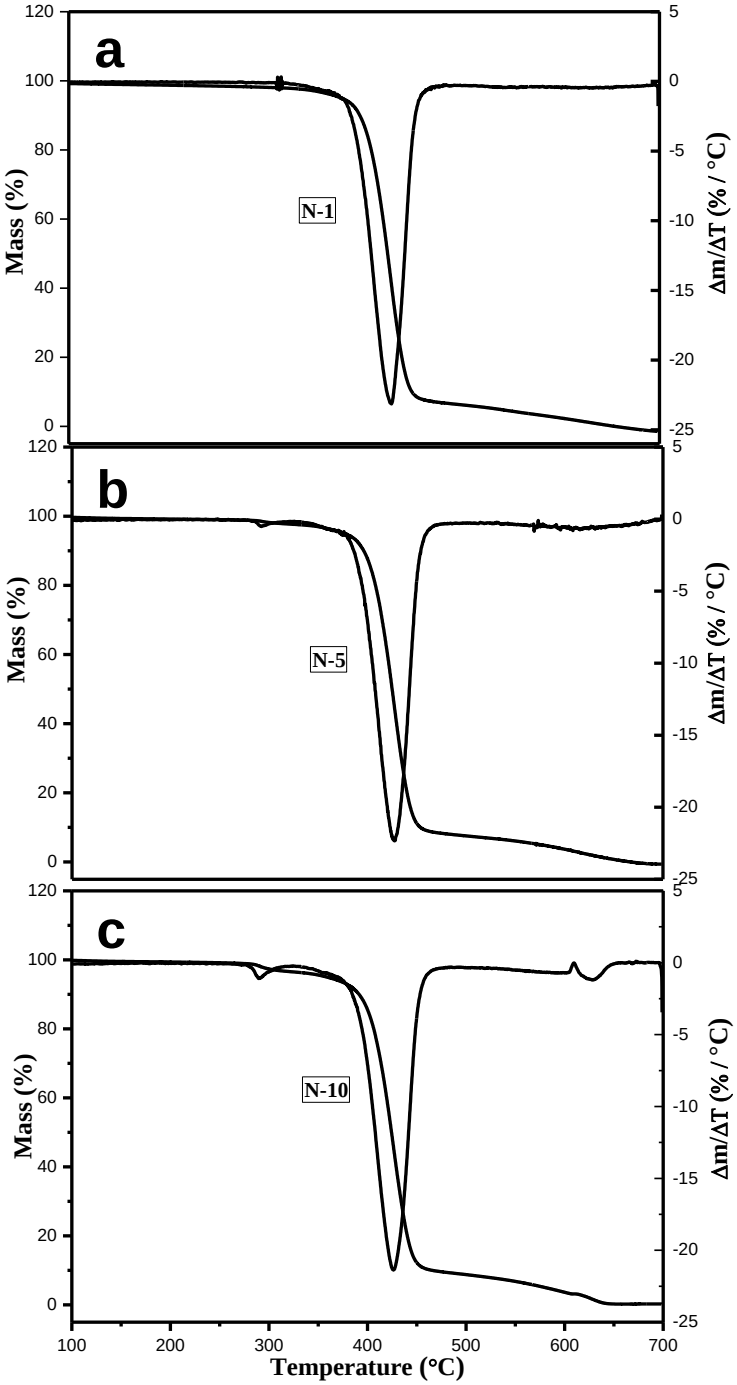

Figure. 4.32: TGA plots of some of the nanocomposites presented in Fig. 4.3with their differential curves

b) Tensile properties

The tensile stress-strain curves of some of the nanocomposites compared to PBAT are shown in Fig. 4.33. The properties like tensile strength yield stress as well as the

elongation at break show decreasing trend with the NCC content. There is seemingly no reinforcement effect up to some extent. Nevertheless, the composites are tough materials showing significant elastomeric behaviour as shown by high elongation at break of several hundred percent. Also the slopes of the initial part of curves are found to decrease in the nanocomposites implying that there is rather a negative impact on the stiffness of the material due to addition of the soft nanofiller. There is rather a sort of softening effect (or become elastic) in low amount of NCC loading (up to 5 % weight ratio in N-5). On higher loading of NCC, the composites become harder and more brittle.

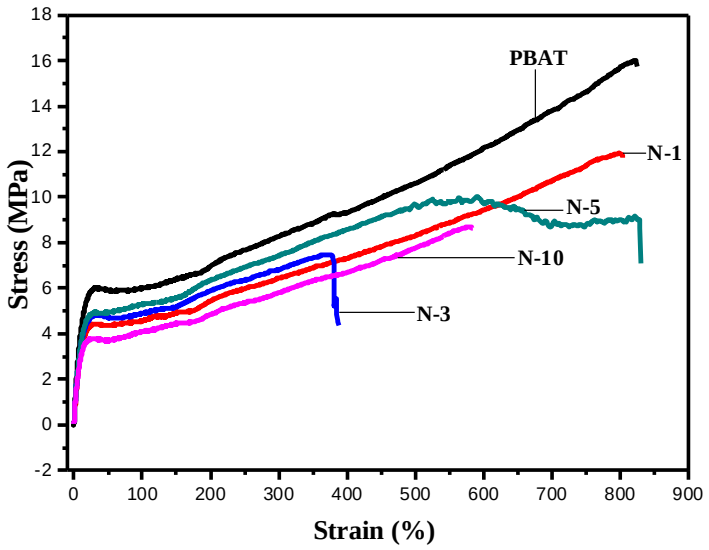

Figure 4.33: Stress-strain curves for PBAT and PBAT/NCC nanocomposites

The nanocomposites were found to deteriorate their elongation at break with increasing NCC (up to N-5). The result indicates that the NCC does not affect significantly the mechanical property of the nanocomposites and is agreement with the literatures (Rahimi *et al.*, 2017, Pinheiro *et al.*, 2017). The NCC here acts as plasticizer. The lesser amount of NCC dispersed homogeneously interact with polymer, matrix to enhance the stress-bearing capacity whereas higher loading of NCC (i.e. above 5 % wt. ratio), the NCC starts to agglomerate and hence lowering the interaction surface area. Hence, microscopic voids and cracks might form as in the microcomposites to result in early failure of the materials (Pirani *et al.*, 2013, Chen *et*

al., 2019). The deterioration in tensile properties may be attributed to the agglomeration of the particles and thus significantly reduced interfacial area between filler and matrix. The results obtained are supported by other literatures as well (Lu *et al*., 2019, Sabaruddin, Tahir *et al*., 2018, Kan *et al*., 2013). It should be mentioned that the results obtained for the nanocomposites are surprising as the nanofiller in general should bring reinforcing effect, and hence requires more investigations in future.

c) Hardness properties

The nanocomposites were further investigated in terms of their hardness related properties *via* microindentation methods. The results on universal hardness (or Martens hardness, HM) and indentation modulus (E_{IT}) are plotted in Fig. 4.34.

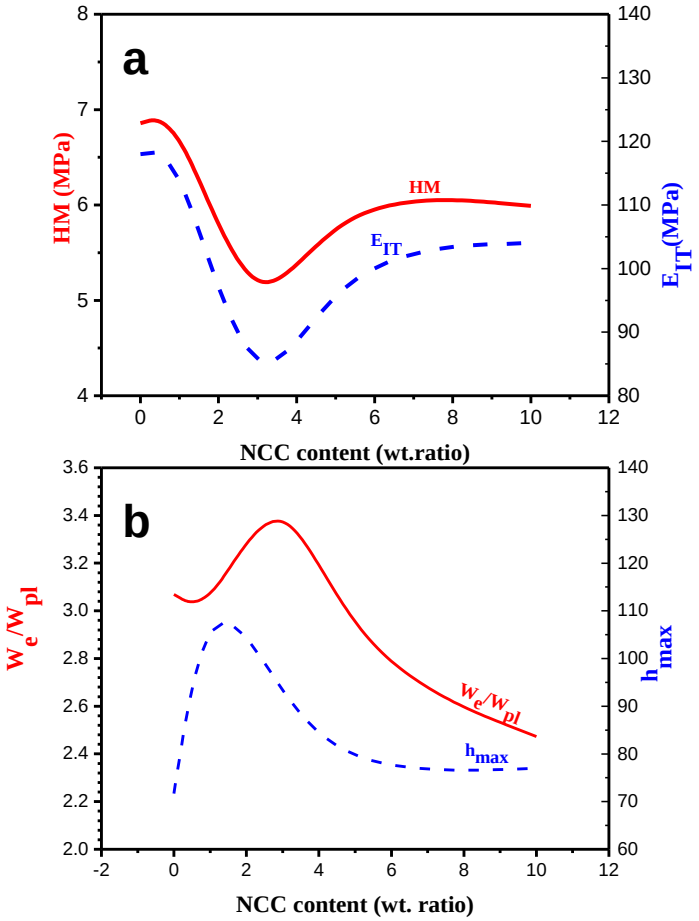

Figure 4.34: The ratio of elastic and plastic work performed (W_e/ W_{pl}) on and the maximum indentation depth (h_{max}) of the pure PBAT and PBAT/NCC nanocomposites

The value of HM and E_{IT} of the composites are found to first decrease (up to 3 % by weight of NCC) and then increase beyond 5 % by weight of the filler. The observation can be explained by the concept of plasticization by the nanofiller at low filler content leading to softening of the materials and hence causing a decrease in hardness and modulus values. At higher filler content, the reinforcing effect increases which manifests in the increased hardness related parameters.

The elastomeric parameters (W_e/W_{pl} and h_{max}), quantifying the extent of elastomeric properties relative to plastic deformation can be calculated using the microhardness F-h curves. The results are presented in Fig. 4.34b. The ratio W_e/W_{pl} gives the ratio of elastic to plastic deformation energy which increases first up to 3 % by weight of NCC and then again decreases. In the similar manner, the maximum indentation depth (h_{max}) varies in the nanocomposites.

The ratio of W_e/W_{pl} gives the extent of elastomeric nature. The higher value of W_e/W_{pl} indicates more elastic nature of the composites and *vice versa*. The initial increase in the elastic work relative to plastic deformation energy correlates well with the decrease in the HM values, attributable to plasticization effect. At higher filler content, the plasticization effect decreases and the reinforcing effect dominates leading to increase in hardness and decrease in the elastic deformation energy. In the similar trend, the values of h_{max} vary.

CONCLUDING REMARKS

The results presented in this section for structure-properties correlation in nanocomposites are concluded as follows and tabulated in the Table 4.7.

- The structural characterization of the nanocomposites by spectroscopic, microscopic and diffraction means reveal that the nanocomposites comprise the compatible constituents which keep their identity in the composite materials. The morphology of the fillers and matrix remain unchanged.
- **FTIR analysis** showed that the nanocomposites show the NCC phase homogeneously dispersed in PBAT matrix and are held together by physical

interactions. The **SEM analysis** also manifested the homogeneously dispersed NCC in PBAT matrix.

- The nanocomposites are thermally stable up to their application ranges showing two stages of degradations separately for NCC at 250 ℃ and for PBAT at 430 ℃; similar behaviour as for microcomposites.
- The tensile properties of the nanocomposites are found to degrade in terms of elongation at break, tensile strength and Young's modulus. The initial increase in the elastic work relative to plastic deformation during indentation tests correlates well with the decrease in the HM values, attributable to plasticization effect. At higher filler content, the plasticization effect decreases. Consequently, the reinforcing effect dominates leading to an increase in hardness and decrease in the elastic deformation energy.

Table 4.7: Summary of properties of PBAT/NCC nanocomposites

Methods	**PBAT/NCC**
FTIR	No chemical bonding; dominance of the PBAT phase on the surface
SEM	Uniform dispersion of NCC in PBAT; no significant gap between PBAT and NCC, indication of partial compatibility.
XRD	Crystallinity index increases with NCC incorporation into PBAT
Tensile Test	No reinforcement effect observed; might be due to plasticizing effect of the NCC
Microindentation	Decrease in properties at low filler content (plasticization) and increase at higher filler content (reinforcement)
TGA	Stable, two steps degradation of composites, NCC induces early degradation; still the composites are stable to 230 ℃

4.4 Investigation of Surface Properties and Biodegradation Behaviour

In this section, the surface properties, susceptibility toward biodegradation and degradation behaviour of the composites will be discussed. In fact, the presence of moisture and water on the surface of material becomes the sites for the microbial attack. Therefore, this section describes comparatively wettability of the composite surfaces, water holding capacity and degradation under soil burial condition as a function of filler contents and treatment time.

4.4.1 Surface Properties Correlation

The surface property of the composites, particularly the hydrophilicity, also correlates with their susceptibility towards degradation. The nature of the surface determines how the material responds with highly polar substances such as water. During contact angle measurements, generally, the water droplets form the angles with interacting surfaces whose dimension depends upon hydrophilicity or hydrophobicity of the substrate. Higher contact angle represents hydrophobicity whereas lower contact angle represents hydrophilicity (Conciecao *et al*., 2019 and Pereda *et al*., 2011).

Fig. 4.35 shows photographs of spontaneous contact angles formed by water droplets on the surfaces of pure PBAT and two different composites (M-5 and N-5). At the first glance, the contact angle on the PBAT surface looks slightly larger (implying slightly higher hydrophobicity) than on that of the composites. Indeed, the contact angles θ measured for the surfaces of PBAT, M-5 and N-5 composites are 83.3°, 77.1° and 70.1°, respectively. The decreased hydrophobicity of the composites surfaces compared to pure PBAT can be attributed to the presence of hydrophilic cellulosic fractions (Dai *et al*., 2017). The fact that the spontaneous contact angles of both the composites M-5 and N-5 are smaller, further illustrates that the hydrophobicity of specimens primarily depends not only on the chemical nature but also on the dimensional nature (micro- or nanoscale) of the biofiller. Similarly, the length-scale effect is also observed for M-5 (θ = 77.1°) and N-5 (θ = 70.1°), respectively (see Fig. 4.35). The lower the particle size of the hydrophilic fillers, the higher will be the ease of filler dispersion in composites and thus higher will be the interaction with water. This result is consistent with literature work (Pereda *et al*., 2011).

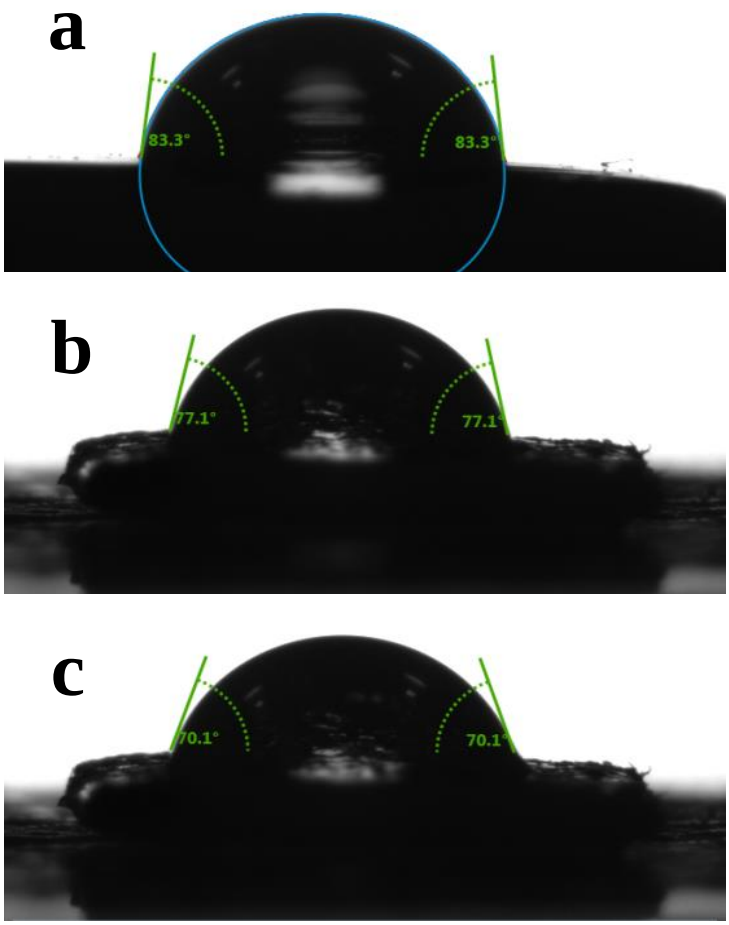

F**igure 4.35:** Photographs showing spontaneous contact angles of water droplets on the surfaces of (a) pure PBAT, (b) composite M-5, and (c) composite N-5

The results from surface contact angle measurement, however, suggests that there is some segregation of the cellulose towards the sample surface that attracts water onto it although there was no clear evidence of surface segregation of the filler as per electron microscopic data. It should be kept in mind that the microscopic results provide local structural details of the materials, as a matter of fact, that do not necessarily correlate completely with the macroscopic properties (Michler & Balta Calleja, 2012).

To analyze the wetting behaviour of samples in more details, the contact angles formed by the composites were investigated at various time intervals. The results are summarized in Fig. 4.36.

It can be observed that the contact angle is decreasing with progress of time and increase in NCC contents in the nano composites, indicating their enhanced

hydrophilic character. For instance, N-10 composite has the contact angle value of 77.1° which decreases to 68.8° after 60 s of water-substrate interaction which is well described in Giri *et al*., 2019b.

Fig. 4.36 shows decreasing contact angle values with decreasing filler particle size which manifest the increasing hydrophilic character of nanocomposites than that of microcomposites due to the wider and more homogeneous dispersion of NCC in the PBAT matrix. NCC being smaller in size, the dispersion is 100 times more than that of MCC as indicated by the morphological explanation. In sections 4.1 and 4.3, similar results are reported in literature where the nanocellulose interacts with water showing lower contact angle value (Pereda *et al*., 2011). Other hydrophilic nanoparticles such as calcium phosphate in polystyrene also increase hydrophilicity (Thomas *et al*., 2008) whereas hydrophobic glass fiber in epoxy resin showed decrease in hydrophilic character (Hameed *et al*., 2007).

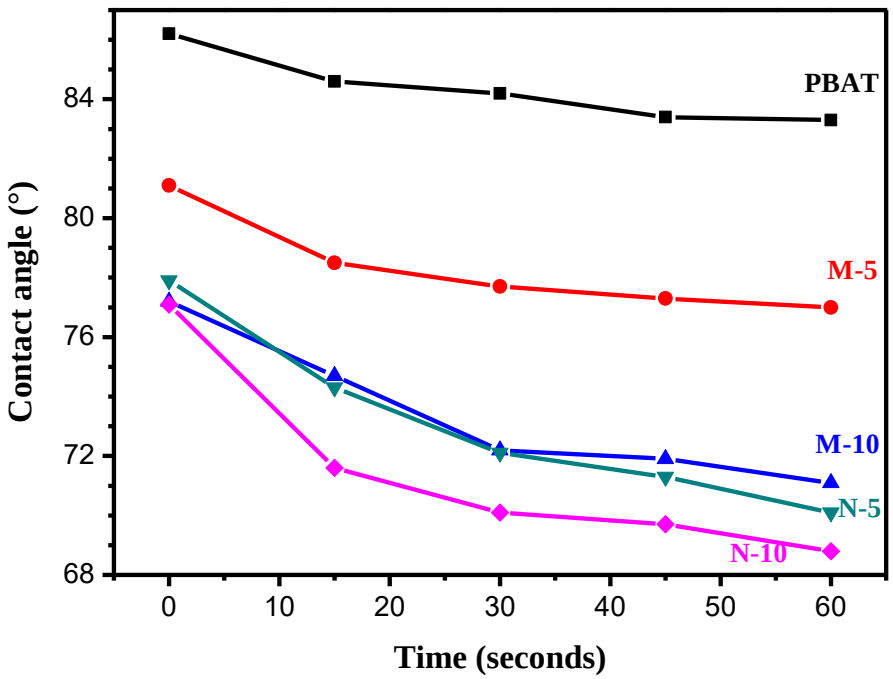

Figure 4.36: Contact angles of water droplets placed on different samples surfaces as a function of treatment time

Thus, the nature of filler in composite changes the wettability of the composite. This directly proves that MCC and NCC being hydrophilic in nature increases hydrophilicity in their composites with PBAT. Moreover wider dispersion of NCC in PBAT matrix further increases hydrophilic character.

In conclusion, the wettability behaviour can be correlated with the degradation susceptibility of the composites at hand, the nanocomposites being more susceptible to water absorption and thereby may provide higher ease of degradation under soil burial conditions (to be discussed later in another section). Thus, in order to gain additional insight into the water absorption behaviour of composites, the materials were studied in details using environmental chamber (Section 4.4.2).

4.4.2. Water Absorption Behaviour

As already mentioned in earlier section, the water absorption property of the composites can be regarded as an important hint for their biodegradability. Fig. 4.37 shows the percentage water uptake capacity of different PBAT/MCC composites as a function of MCC content at 23 °C. It can be observed that the pure PBAT absorbs about 1 wt % of water with respect to total weight of the polymer after 24 hours. This practically insignificant amount of water absorption can be attributed to the partial polarity in the C=O bond present in the PBAT (Morokuma *et al*., 1971). This notion is also supported by the relatively low contact angle of the pure PBAT θ=83.3 (see Fig. 4.36) compared to purely hydrophobic polymers such as polypropylene PP (θ = 170°) and polystyrene PS (θ = 140° - 150°) (Liu *et al*., 2010, Zhang *et al*., 2006).

Figs. 4.37 and 4.38 depict the amount of water uptake as a function of the time of treatment of the samples inside the environmental chamber recorded up to 7-8 days for the composites with different amount of MCC and NCC, respectively. The nature of the shape of the curves is found to be identical for both MCC and NCC composites independent of the amount of the filler content. A steady-state plateau is reached for each sample after about 6 days.

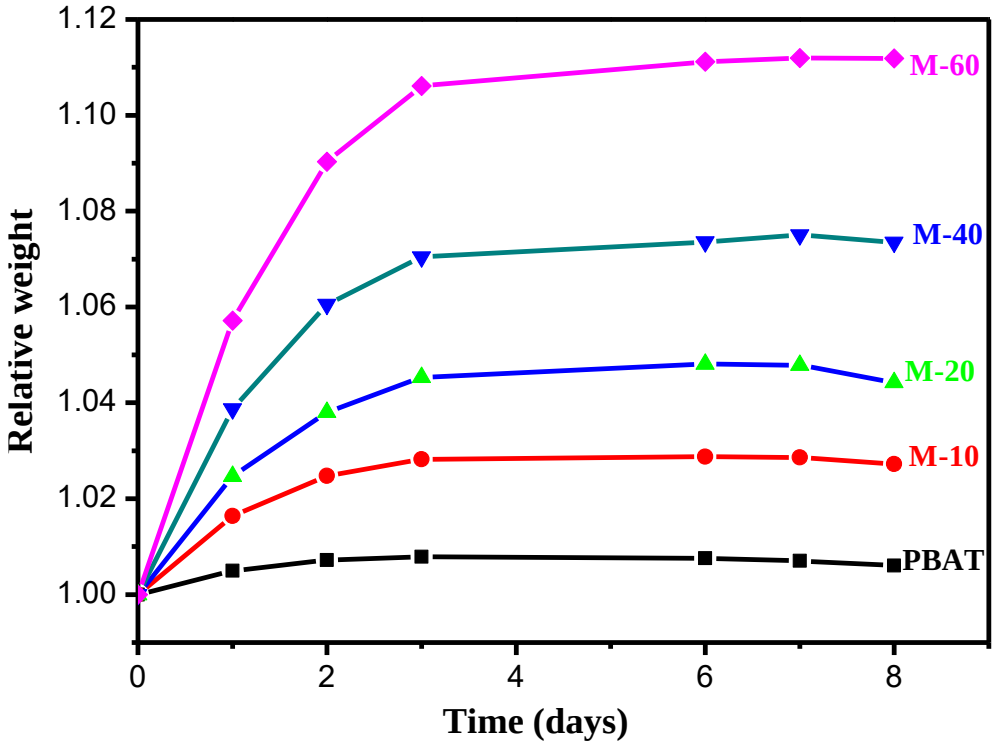

Figure 4.37: Variation of water uptake amount by PBAT based composites comprising different amounts of MCC

The composite M-10 absorb quite little amount of water (2 % of its dry weight after 6 days) whereas pure PBAT absorbed even smaller amount of water (only 1 % of its dry weight). The water absorption was found to be further increase with the increase of the exposure time and content of MCC. For instance, the sample M-60 saturates with water, about 12 % of the sample weight on exposure to water vapor in the environmental chamber (Wu, 2012).

Similar phenomena were seen in PBAT/NCC composites at laboratory at 23 °C for water uptake behaviour with increasing concentration of NCC and with the function of time (see Fig. 4.38). The comparison of Figs.4.37 and 4.38 shows that the amount of water absorbed is independent of particle size as N-10 and M-10 absorb practically equal amount of water.

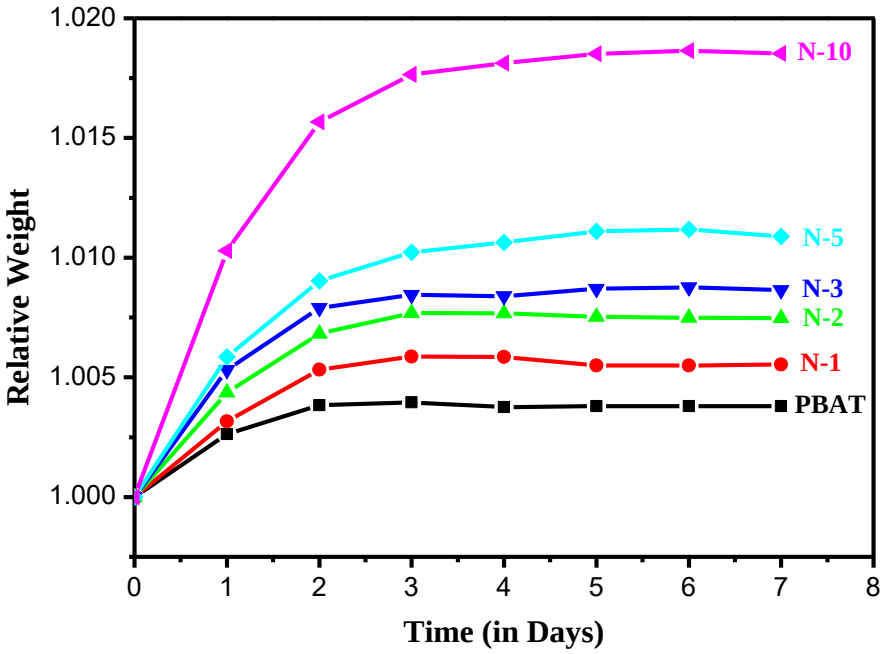

Figure 4.38: Variation of water uptake amount by PBAT based composites comprising different amounts of NCC

The increasing trend of water absorption shown in Figs. 4.37 and 4.38 can be correlated to state the increasing concentration of MCC and NCC enhances water holding capacity in the composites, respectively (Pal & Katiyar, 2017). The notion that the water absorption occurs due to the increasing concentration of MCC and NCC in PBAT matrix is supported by literature works (Wu, 2012, Pokhrel *et al*., 2016b, Samarasekara *et al*., 2018, Liu *et al*., 2017, Kramer *et al*., 2006). Biomaterial chitosan also increases water absorption in PBAT/chitosan composite with its increasing concentration (Pokhrel *et al*., 2016b). PLA/NCC absorbs higher amount of water compared to PLA/MCC (Samarasekara *et al*., 2018). Moreover, higher water interaction is observed for higher content of NCC in PLA (Liu *et al*., 2017).

In conclusion, the hydrophilic M-series and N-series composites both show increasing water holding capacity with the increase in MCC and NCC loading into it. The property correlates with the degradability of the composites which can be studied by soil composting (Section 4.4.3).

4.4.3 Effect of Soil Burial on Composites Degradation

Morphological studies of the samples subjected to degradation under soil burial conditions have been carried out using optical and electron microscopy which offer

reliable information on the physical state of the composites under various stress conditions. Different stages of the surface morphological features of the samples subjected to different periods of soil burial are studied.

The photographs of the samples are presented in Figs. 4.39.

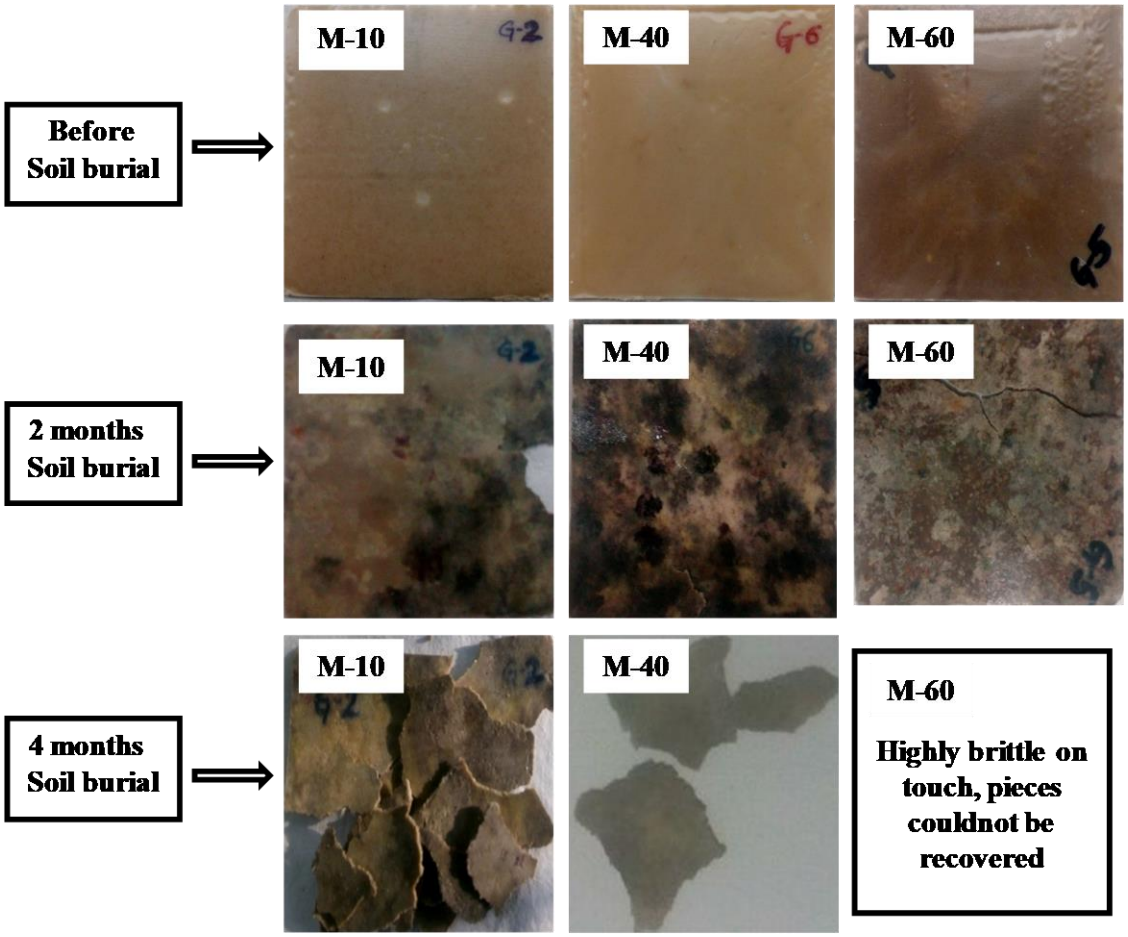

Figure 4.39: Photographs of different PBAT/MCC composites subjected to soil burial for different periods of time as indicated

The photographs in Fig. 4.39 shows that compared to the highly ductile nature of the virgin PBAT, on soil composting, both the PBAT and its composites became quite brittle. The surfaces of the composites were found to be attacked by the microbes with some noticeable residual microbial pigments and the fungal growth on the sample surfaces. After 4 months of composting, the samples turned very brittle, the fragility of the specimens being more pronounced for the composites having higher amount of the MCC, also in consistence with the soil burial of PBAT/chitosan composites

(Pokhrel *et al*., 2016b). In 6 months of soil burial specimens were indistinguishable from soil.

a) Morphological analysis

Among the samples presented in Fig 4.39, neat PBAT and composites M-20 have been studied after soil burial experiments. The fracture surface morphology of PBAT, composite M-20 and M-40 after 4 months of soil burial are presented in Fig. 4.40, 4.41 and 4.42.

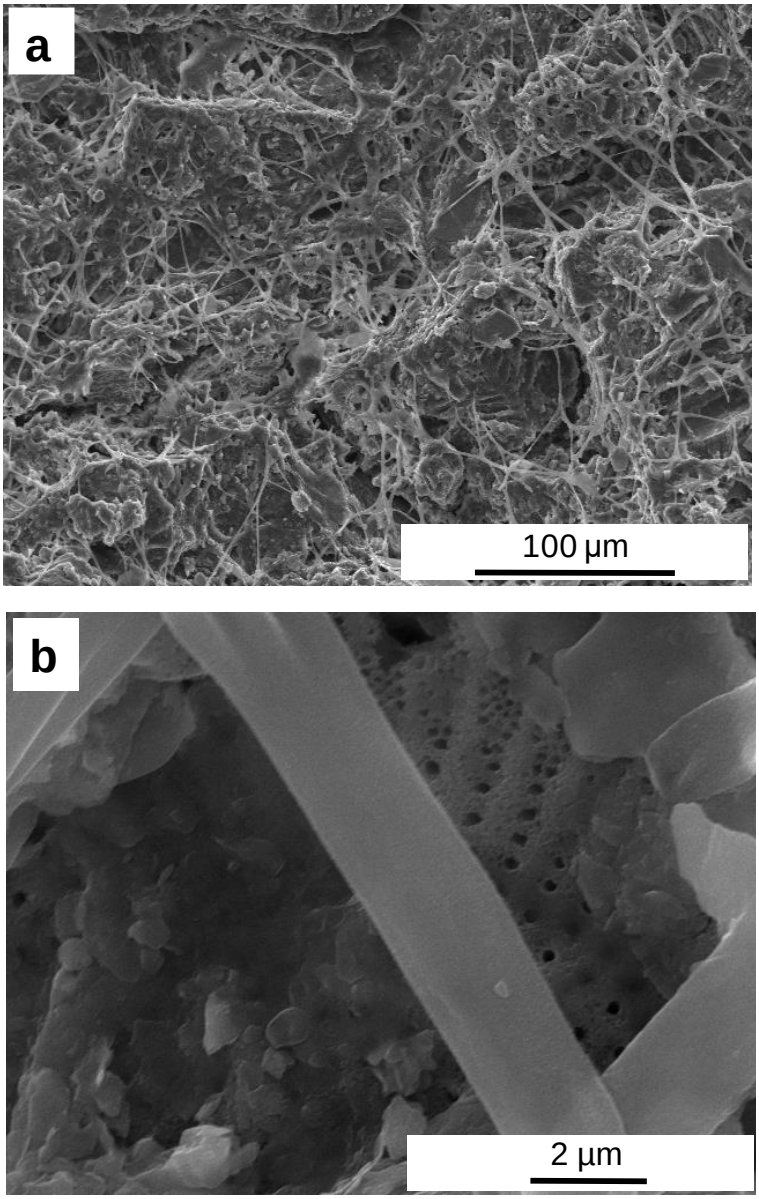

Figure 4.40. Lower (a) and higher (b) magnifications of SEM images showing fracture surface morphology of pure PBAT subjected to 4 months of soil burial experiment

The specimens for fracture surface morphological studies are prepared by simple breaking with hand. The sample buried under the soil for 4 months. The fracture surfaces are sputter coated with gold and inspected by SEM in secondary electrons mode.

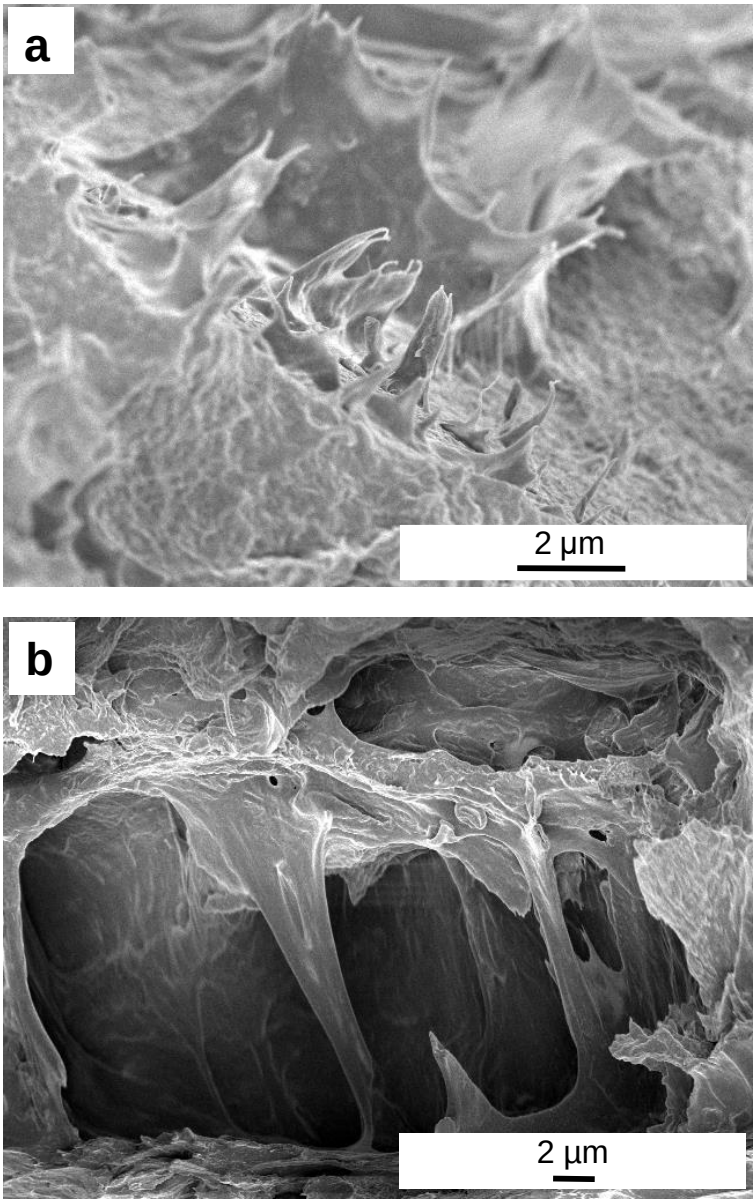

Figure 4.41. Lower (a) and higher (b) magnifications of SEM images showing fracture surface morphology of M-20 subjected to 4 months of soil burial experiment

The neat PBAT develops a sort of porous internal morphology after 4 months of soil burial, (see 4.40a). The porous structure frame work formation may be attributed to

the dissolution and disintegration of a part of degraded material. After 4 months the spongy nature is formed with numerous micro-voids.

The composite M-20 degrades in similar manner (see Fig. 4.41) while the fracture surface morphology of the M-20 were drastically affected by soil burial for 4 months. Numerous voids are formed at the place of MCC. During soil burial MCC being organic matter degrades first and form large voids with numerous cracks initiated from the surface as shown in Fig 4.41.

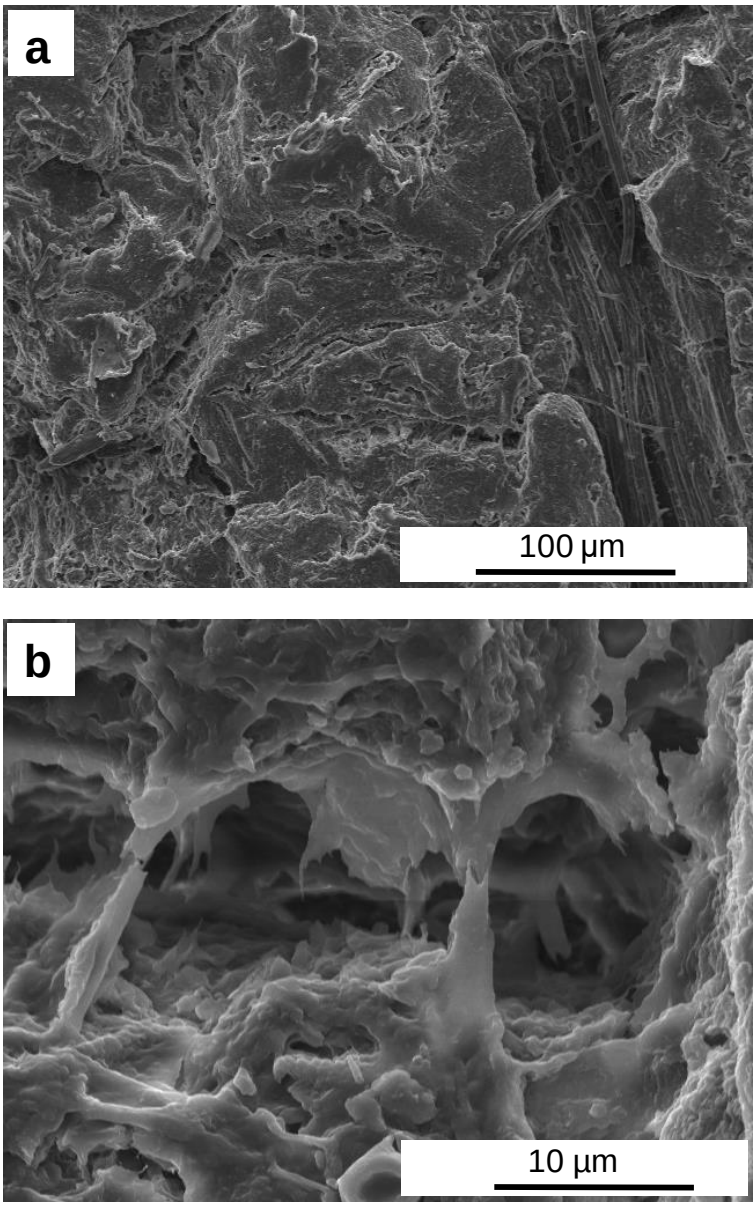

Figure 4.42: Lower (a) and higher (b) magnifications of SEM images showing fracture surface morphology with microbial colony growth at cracks and voids of M-40 subjected to 4 months of soil burial experiment

In Fig. 4.41, the void-like structures of various sizes appear in the samples, which might have been formed by consumption of the filler particles as nutrients by the microbes. With increase in the soil burial period, the amount of the fillers decrease which completely vanish after 4 months of soil burial (see Fig. 4.41). At the same time, the PBAT matrix also deteriorates in random way further implying that the cellulosic filler augments the degradation of the PBAT. The wetting test result is a testimony; the PBAT sheath wrapped around MCC also degrades with PBAT on its intimate contact (Tesfaye *et al*., 2017, Kramer *et al*., 2006, Singh & Sharma, 2008).

The samples became mechanically deteriorated and brittle upon soil burial for 4 months. Thus, even the sample collection after more than 4 months of degradation was not possible. The samples on precise close observation on its crack surface found to grow some microbial colonies growth (Giri *et al*., 2019b). At the same time, the PBAT matrix gets teared off in random way further implying that the cellulosic filler boost the degradation of the PBAT (Tesfaye *et al*., 2017, Singh & Sharma *et al*., 2008, Liu *et al*., 2014).

In Fig.4.42, M-40 composite has observed the clear growth of the microbial colony. The colonies formed are very specific in its flower-bud like morphology. These microbial colonies are grown on the composites surface and might have feed on the composite as carbon source for energy, which bring degradation in the composite. MCC completely vanished; polymer PBAT chain in intimate contact with MCC is also degrading to smaller fragments during soil burial. The PBAT became a good host for the microbes, showing its good biocompatibility by providing suitable environment for microbes.

This phenomenon is exemplified by the morphology of the composite M-40 buried into the soil for 4 months. As in the previous case of fracture surface is characterized by brittle plastics factures; roughness and large voids in addition to the microbial colonies. On the basis of microscopic results, nothing can be declared concerning the molecular mechanism of degradation. Thus GPC studies were carried out (discussed in next section).

b) GPC molecular weight analysis

The variations of the molecular properties of the PBAT in neat form and in the form of related composites materials are investigated by gel permeation chromatography (GPC) using PS standard. The results are summarized in Table 4.8.

GPC delivers quite reliably the comparative data for molecular size and their polydispersity index (D) (as denoted by the M_w/M_n values, where M_w and M_n stand for weight and number average molecular weights, respectively) of the polymer. For the sake of simplicity in comparison, we limit our discussion on the value of M_w.

The PBAT shows a complex chromatogram (details not presented here) with several peaks implying a wide distribution of molecular weights and distributions. We concentrate on the major peak values.

Table 4.8: Molecular weight variation of PBAT in pure form and in different composites with MCC at different intervals of soil burial tests

Sample Code	Neat Sample		2 months		4 months	
	M_w(kg/mol)	D	M_w(kg/mol)	D	M_w(kg/mol)	D
PBAT	48.62	2.01	**	**	21.60	2.04
M-20	37.27	1.90	32.61	2.03	23.32	2.66
M-40	**	**	**	**	18.64	2.36

[#] soil burial period for composting experiment; ** not measured

From Table 4.8, it is apparent that, under soil burial conditions, the M_w values of the pure PBAT decreases from 48.62 kg/mol to 21.60 kg/mol in 4 months. The value of D remains, however, constant. In case of M-20 composite, the M_w values decrease much sharply while for the M-40 composite the decrease is only from 37.27 kg/mol (for near PBAT) to 32.61 kg/mol (for 2 months degradation) and then to 23.32 kg/mol (for 4 months of degradation). Thus, the M_w value variation for the composite M-40 appears much more drastic.

The results imply that cellulosic filler enhances the degradability of the polymer which is consistent also with the results from the microscopic studies; the higher amount of filler being more favorable for the molecular weight reduction. Similar type

of molecular weight lowering was observed on soil composting of poly(butylene sebacate) (Siotto *et al*., 2013).

It can be concluded that the PBAT shows significant ease of degradation in molecular weights under soil burial conditions which is further enhanced by the presence of the cellulosic filler. However, it should be stressed that the polymer chains are not completely degraded but are rather turned into smaller fragments that may be present for longer times as microscopic particles in the soil forming a sort of microplastics aggregates. The PBAT might be prone to further microbial degradation but based on the current results the duration of the PBAT in the soil and even in water flowing through the soil, as microscopic particles cannot be ascertained (Arslan *et al*., 2016, Fukusima *et al*., 2012, Pinheiri, 2017, Wang *et al*., 2015). In the similar manner, also the degradation in molecular parameters might have been affected. However, based on the current study, no particular inferences can be drawn.

CONCLUDING REMARKS

The result presented in this section to explain surface property and biodegradation behaviour of composites of M and N series are concluded as follows and also summarized in Table 4.9.

- The wettability behaviour measured by **contact angle measurements** can be correlated with the degradation susceptibility of the composites. The nanocomposites have been found to be more susceptible to water absorption and thereby provide higher ease of degradation under soil burial conditions.
- The composites show enhanced **water holding capacity** with the increase in MCC and NCC loading. The property correlates well with the degradability of the composites.
- The **microbial colonies** are grown on the composites surface that might have fed on the composite as nutrient, which brings degradation in the composite. During soil burial experiment, the MCC completely vanished; the PBAT chain in intimate contact with MCC and NCC were also found degrading to smaller fragments during soil burial. The PBAT became a good host for the microbes, showing its good biocompatibility by providing survival environment for microbes.

- ❖ The **microscopic results** confirm degradability of the composites with increase in filler content on one hand, and with the period of soil burial experiment on the other. PBAT and composites show significant ease of degradation in molecular weights upon soil burial which is further enhanced by the presence of cellulosic filler.
- ❖ The **GPC results** confirm the degradation of molecular weight of polymer under soil burial conditions. However, the polymer chains are not completely degraded but are rather turned into smaller fragments that may be present for longer times as microscopic particles in the soil might form microplastics aggregates.

Table 4.9: Comparative summary for the surface properties and degradation behaviour for the composites materials

Methods	**PBAT/MCC composites**	**PBAT/NCC composites**
Contact Angle	Decreases with increasing MCC content i.e. hydrophilicity increases implying measurement of water droplet and composite surface degree of interaction. Pure PBAT has contact angle 83.3° and M-60 has 71°	Decrease as in the PBAT/MCC surfaces. The effect found to be higher; more hydrophilic than PBAT/MCC composites. N-10 has 68.8°
Water absorption	Water holding capacity increases with MCC content	Similar behaviour as PBAT/MCC system. The effect is higher
Soil Composting	• Surface deteriorated on soil burial. • Early degradation of composites than PBAT • Composites become brittle on soil burial; could not be recovered after 6 months • M_w values of PBAT (48 kg/mol), in composites (M-40) decreased to 18.64 kg/mol on 4 months of soil burial. • The composites even became host for bacterial colony promoting more biodegradation	This is not completed; results are expected to be similar with PBAT/MCC; faster degradation expected due to larger surface areas offered by nanofibers

CHAPTER 5

5. CONCLUSIONS AND RECOMMENDATIONS

5. 1 Conclusions

- The spectroscopic analyses conclude that the virgin WS fibers are structurally quite similar to the commercial MCC. Similar to the commercial one, the MCC extracted from the WS possess intense IR peak centered around 3330 cm^{-1}, whereas this peak becomes broad and diffuse in the NCC, which can be attributed to possible breakdown of inter- and intramolecular H-bonding caused by strong acid treatment.

- The MCC and NCC were successfully extracted from WS which were structurally equivalent to commercial samples. Those were found to be characterized by definite textures, the MCC being irregular bundles of the primary crystals bound together with the amorphous phase.

- The semicrystalline nature of the PBAT was well postulated by the XRD peaks that can be correlated to the morphology described by other methods. The PBAT's biodegradability can be linked with the presence of its hydrolysable ester and carbonyl groups. It is found to be quite stable towards thermal treatment.

- The PBAT phase was found to dominate in the spectra of the composites implying that the MCC phase preferentially gets localized towards the bulk of the composites. Owing to the segregation of the components held together by purely physical forces into two separate phases, there are two distinct thermally activated degradation regimes characterized by separate activation processes. Large PBAT/MCC interfacial areas might have provoked more rapid thermal degradation of the composites compared to the pure components.

- The PBAT is highly ductile material. Three regimes of deformation processes are identified: very ductile, ductile and brittle. Those have been correlated with corresponding deformations processes via fracture surface analysis.

- The structural characterization of the nanocomposites by spectroscopic, microscopic and diffraction means reveal that the nanocomposites comprise the compatible constituents which keep their identity in the composite materials. The morphology of the fillers and matrix remain unchanged.
- The nanocomposites are thermally stable up to their application ranges showing two stages of degradations separately for NCC at 250 ℃ and for PBAT at 430 ℃; similar behaviour as for microcomposites.
- The tensile properties of the nanocomposites are found to degrade in terms of elongation at break, tensile strength and Young's modulus. The wettability behaviour measured by contact angle measurements can be correlated with the degradation susceptibility of the composites. The composites show enhanced water holding capacity with the increase in MCC and NCC loading. The property correlates well with the degradability of the composites.
- The GPC results confirmed the degradation of molecular weight of polymer under soil burial conditions while the macromolecular chains were not completely destroyed. However, the polymer chains are not completely degraded but are rather into microplastics aggregates.

5.2 Recommendations

- The structure properties correlations in the nanocomposites have not been understood correctly which shall be followed in future works.
- The complete biodegradation mechanism in consideration of temperature, time, minerals effect and complete molar mass degradation is also left for future studies.
- The future study should also concentrate on the development of prototypes of the composites products targeted to some specific packaging applications.

CHAPTER 6

6. SUMMARY

In line of the notion of green chemistry and need for utilizing locally available wastes for developing new materials, there is an global action to promote the development of degradable packaging materials. There is a challenge for using locally available and as far as possible the waste materials as resource and to modify them to make new sustainable materials opening new avenues for commercial applications. Therefore, these low cost resources can be applied to make new materials (**Chapter 1**). Hence, this work aims at designing wheat stalk micro- and nanocellulose based degradable polymer composites and to study their morphological, mechanical and degradation behaviour.

To begin with, in **Chapter 2**, extensive literature survey has been carried out attempting to make an overview, with recent research outputs, applications, and the structure-properties correlations of different polymer composites. Following conclusions can be drawn.

1. The lignocelluloses-based micro-and nano-fillers can be synthesized by various chemical, mechanical and bioinspired (or biosynthetic) methods and be evaluated in terms of their structural and molecular characteristics.
2. The micro- and nanocrystalline cellulosic fillers can be incorporated to a pretty high weight fraction easily into the biodegradable copolyester matrix even without the use of compatibilizer. The copolyester based composite materials undergo rapid fragmentation process under soil burial conditions leading to highly brittle materials within a few months duration.
3. There is a trend of utilizing the copolyesters and their composites for biomedical applications, for smart packaging films, functional coatings and for flexible conducting materials. These strategies are achieved by introducing different functional groups *via* grafting onto the natural polymer chains and then making graft and block copolymers with synthetic polymers

4. Several biodegradation pathways have been suggested for various polymeric materials including degradable copolyesters which have been successfully employed.

The overview of the sample preparation, nomenclature of the series and different techniques used in experimental work along with the kind of information obtained are illustrated in **Chapter 3**.

Completely biodegradable thermoplastic aliphatic aromatic-copolyester poly(butylene adipate-co-terephthalate), PBAT (Ecoflex® FBX 7011, a commercial product of BASF SE, Ludwigshafen, Germany) was used as the polymer matrix. HM400X, a trademark of Dow Chemicals, Germany, was used as reference MCC. The main source of filler source was the natural agricultural waste, the stalks of wheat (*Triticum aestivum*), which was used to extract the novel materials MCC- and nanocrystalline cellulose (NCC). The composites of PBAT were prepared with MCC, NCC, WS, MCC-R by melt mixing and extrusion processes. Structural analysis was carried out by Fourier Transform Infrared (FTIR) spectroscopy while the morphologies were investigated by Scanning Electron Microscopy (SEM), Transmission Electron Microscopy (TEM) and X-ray diffraction (XRD). Thermal and mechanical stability of the composites were measured by Thermogravimetric analysis (TGA), tensile test and microindentation test respectively. Similarly, molecular weight distribution of PBAT at different stages of soil composting for the composites were optimized by Gel Permission Chromatography (GPC).

Chapter 4 discusses the results of the experimental works as summarized below.

Chapter 4.1 structural and thermal characterization of cellulosic fibers and polymers

- The **spectroscopic analyses** conclude that the virgin WS fibers are structurally quite similar to the commercial MCC. Similar to the commercial one, the MCC extracted from the WS possess intense IR peak centered around 3330 cm^{-1}, whereas this peak becomes broad and diffuse in the NCC, which can be attributed to possible breakdown of inter- and intramolecular H-bonding caused by strong acid treatment.

- From the **microscopic results**, it has been concluded that the MCC and NCC obtained from WS fibers are characterized by definite textures, the MCC being irregular bundles of the primary crystals bound together with the amorphous phase.

- The **XRD data** reveals that the natural fibers extracted from the WS predominantly contains Cellulose I (Sharp XRD peaks located at 2θ values of 20.34° and 22.02°) form of the crystals whereby the nanofibrillation increased the degree of crystallinity.

- As per **thermogravimetric results**, the MCC and NCC are found to be generally thermally stable while the NCC slightly less stable. The higher thermal stability of the MCC can be attributed to the protective coating provided by the amorphous part of the cellulose which gets eliminated due to the strong acid treatment.

- The **semicrystalline nature of the PBAT** is well postulated by the XRD peaks that can be correlated to the morphology described by other methods. The PBAT's biodegradability can be linked with the presence of its hydrolysable ester and carbonyl groups. It is found to be quite stable towards thermal treatment.

Chapter 4.2: structure-properties correlation of polymer composites

- The **FTIR spectroscopy** illustrates that the PBAT phase dominates in the spectra of the composites implying that the MCC phase preferentially gets localized towards the bulk of the samples. There is a sufficient physical interaction between the components.

- Owing to the segregation of the components held together by purely physical forces into two separate phases, there are two distinct thermally activated degradation regimes characterized by separate activation processes. Large PBAT/MCC interfacial areas might have provoked more rapid **thermal degradation** of the composites compared to the pure components.

- The PBAT is highly ductile material in terms of **tensile properties**. The composites maintain then high ductility up to 20 % by weight of the MCC in the composite. The drastic reduction in the ductility for higher filler loading is

due to premature failure that might have been caused by void formation and initiation at the interfacial region.

- Three regimes of deformation processes are identified: very ductile, ductile and brittle. Those have been correlated with corresponding deformations processes *via* fracture surface analysis.

Chapter 4.3: structure-properties correlation of nanocomposites

- The structural characterization of the nanocomposites by spectroscopic, microscopic and diffraction means reveal that the nanocomposites comprise the compatible constituents which keep their identity in the composite materials. The morphology of the fillers and matrix remain unchanged.
- **FTIR analysis** showed that the nanocomposites show the NCC phase homogeneously dispersed in PBAT matrix and are held together by physical interactions. The **SEM analysis** also manifested the homogeneously dispersed NCC in PBAT matrix.
- The nanocomposites are thermally stable up to their application ranges showing two stages of degradations separately for NCC at 250 ℃ and for PBAT at 430 ℃; similar behaviour as for microcomposites.
- The **tensile properties** of the nanocomposites are found to degrade in terms of elongation at break, tensile strength and Young's modulus. The initial increase in the elastic work relative to plastic deformation during **indentation tests** correlates well with the decrease in the HM values, attributable to plasticization effect.

Chapter 4.4: investigation of surface properties and degradation behaviour

- The wettability behaviour measured by **contact angle measurements** can be correlated with the degradation susceptibility of the composites. The nanocomposites have been found to be more susceptible to water absorption and degradation under soil burial.
- The composites show enhanced **water holding capacity** with the increase in MCC and NCC loading. The property correlates well with the degradability of the composites.

- The **microbial colonies** are grown on the composites surface that might have fed on the composite as nutrient, which brings degradation in the composite. During soil burial experiment, the MCC completely vanished. The **microscopic results** confirmed degradability of the composites with increase in filler content on one hand, and with the period of soil burial experiment on the other.
- The **GPC results** confirmed the degradation of molecular weight of polymer under soil burial conditions while the macromolecular chains were not completely destroyed. However, the polymer chains are not completely degraded but are rather into microplastics aggregates.

REFERENCES

Abraham, E., Elbi, P.A., Deepa, B., Jyotish Kumar, P., Pothen, L.A., Narine, S.S. & Thomas, S. (2012). X-ray diffraction and biodegradation analysis of green composites of natural rubber/nanocellulose. *Polym. Degrad. Stab*. **97**, 2378-2387. doi: org/10.1016/j.polymdegradstab

Adhikari, R. & Michler, G.H. (2009). Polymer Nanocomposites characterization by microscopy. *Polym. Rev.* **49**, 141–180. doi: 10.1080/15583720903048094

Adhikari, R., Bhandari, N.L., Causin, V., Le, H.H., Radusch, H.J., Michler, G.H. & Saiter, J.M. (2012). Study of morphology, mechanical properties, and thermal behavior of green aliphatic-aromatic copolyester/bamboo flour composites. *Polym. Eng. Sci.* **52**, 2296-2303. doi: org/10.1002/pen.23335

Adhikari, R., Bhandari, N.L., Le, H.H., Henning, S., Radusch, H.J., Michler, G.H., Garda, M.R. & Saiter, J.M. (2012). Thermal, mechanical and morphological behavior of poly(propylene)/wood flour composites. *Macromol. Symp*. **315**, 24–29.

Adsul, M., Soni, S.K., Bhargava, S.K., & Bansal, V. (2012). Facile approach for the dispersion of regenerated cellulose in aqueous system in the form of nanoparticles, *Biomacromolecules* **13,** 2890–2895. doi.org/10.1021/bm3009022

Anirudhan, T.S. & Rejeena, S.R. (2013). Selective adsorption of hemoglobin using-grafted- magnetite nanocellulose composite. *Carbohydr. Polym.* **93**, 518-527. doi.org/10.1016/j.carbpol.2012.11.104

Arruda, L.C., Magaton, M., Bretas, R.E.S., & Ueki, M.M. (2015). Influence of chain extender on mechanical, thermal and morphological properties of blown films of PLA/PBAT blends. *Polym. Test*. **43**, 27–37. doi:10.1016/j.polymertesting.2015.02.005

Arslan, A., Cakmak, S. & Cengiz A. & Gumusderelioglu M. (2016). Polybutylene adipate -co-terephthalate) scaffolds: processing, structural characteristics and cellular responses. *J. Biomater. Sci. Polym. Edition*. **27**, 1841-1859.

Banerjee, A., Chatterjee, K., & Madras, G. (2014). Enzymatic degradation of polymer: a brief review. *Mater. Sci. Technol.* **30**, 567-573. doi: org/10.1179/1743284713Y.0000000503

Batalha, L.A.R., Colodette, J.L., Gomide, J.L., Barbosa, L.C.A., Maltha, C.R.A., & Gomes, F.J.B. (2012). Dissolving pulp producing from bamboo. *Bioresources* **7**, 640-651.

Beg, M.D.H., & Pickering, K.L. (2008a). Mechanical performance of Kraft fibre reinforced polypropylene composites: Influence of fibre length, fibre beating and hygrothermal ageing. *Composites Part A*. **39**, 1748–1755. doi: 10.1016/j.compositesa.2008.08.003

Beg, M.D.H., & Pickering, K.L. (2008b). Reprocessing of wood fibre reinforced polypropylene composites. Part II: Hygrothermal ageing and its effects. *Composites Part A*. **39**, 1565–1571. doi: 10.1016/j.compositesa.2008.06.002

Bhandari N.L. (2013). *Morphology and deformation behavior of natural-fibers-thermoplastics composites.* Central Department of Chemistry. Institute of Science and Technology, Tribhuvan University, Kathmandu, Nepal.

Bhattarai, J. (2006). Structure and corrosion behavior of sputter-deposited W-Mo alloys. *J. Nepal Chem. Soc*. **21**, 19-25.

Bielecki, S., Krystynowicz, A., Turkiewicz, M., & Kalinowska, H. (2002). *Bacterial cellulose; Biopolymers*: Polysaccharides, Munster, Germany, Wiley-VCH, Verlag GmbH.

Birinchi, L., Cotana, F., Fortunati, E., & Kenny, J.M. (2013). Production of nanocrystalline cellulose from lignocellulosic biomass: Technology and applications. *Carbohydr. Polym.* **94**, 154-169. doi: org/10.1016/j.carbpol.2013.01.033

Biswas, S., & Satapathy, A. (2010). A comparative study on erosion characteristics of red mud filled bamboo–epoxy and glass–epoxy composites. *Mater. Desig.* **31**, 1752–1767. doi:10.1016/j.matdes.2009.11.021

Bozzolz, J.J., Lonnie, D., & Jones, R. (1992). *Electron Microscopy, Principals and Techniques for Biologists.* Johns & Bartlett Pub.

Bledzki, A.K., Reihmane, S., and Gassan, J. (1996). Properties and modification methods for vegetable fibers for natural fiber composites. *J. Appl. Polym. Sci.* **59**, 1329-1336.

Brandelero, R.P.H., Yamashita, F., & Grossmann, M.V.E. (2010). The effect of surfactant Tween 80 on the hydrophilicity, water vapor permeation, and the mechanical properties of cassava starch and poly(butylene adipate-co-terephthalate) (PBAT) blend films. *Carbohydr. Polym.* **82**, 1102–1109. doi:10.1016/j.carbpol.2010.06.034

Cadena Ch., E.M., Vélez R., J.M., Santa, J.F., & Otálvaro G., V. (2017). Natural fibers from plantain pseudostem (Musa Paradisiaca) for use in fiber-reinforced composites, *J. Nat. Fib.* **14,** 678–690. doi.org/10.1080/15440478.2016.1266295

Carrasco, G.C., Miettinen A., C. Hendriks, C.L.L., Gamstedt, E.K., & Kataja, M. (2011). *Structural characterization of Kraft pulp fibres and their nanofibrillated materials for biodegradable composite applications, Nanocomposites and Polymers with Analytical Methods.* **Chapter 10**, Crotia, Intechopen. DOI: 10.5772/2/1580

Cesar, N.R., Marcelo, A., da-Silva, P., Botaro, V.R., & Menezes, A.J.d. (2015). Cellulose nanocrystals from natural fiber of the macrophyte Typha domingensis: extraction and characterization. *Cellulose*. **22**, 449-460. doi.org/10.1007/s1057

Chan, C.H., Chia, C.H., Zakaria, S., Ahmad, I., & Dufresne, A. (2013). *Production and characterization of cellulose and nano-crystalline cellulose from kenaf core wood.* Bioresources **8**, 785-794.

Chauhan, Y.P., Sapkal, R.S., Sapkal, V.S., & Zamre, G.S. (2009). *Microcystalline cellulose from cotton rags (waste from garment and hosiery industries).* Int. J. Chem. Sci. **7,** 681-688.

Chen, X., Kuhn, E., Wang, W., Park, S., Flanegan, K., Trass, O., Tenlep, L., Tao, L. & Tucker, M. (2013). Comparison of different mechanical refining technologies on the enzymatic digestibility of low severity acid pretreated corn stover. *Bioresour. Technol*. **147**, 401-408. doi: org/10.1016/j.biortech.2013.07.109

Cherian, B.M., Leao, A.L., de Souza, S.F., Coata, L.M.M., Olyveira, G.M.d., Kottaisamy. M., Nagarajan, E.R., & Thomas, S. (2011). Cellulose nanocomposites with fibres nanofibrs isolated from pineapple leaf fibers for medical applications. *Carbohydr. Polym*. **86**, 1790-1798. doi: org/10.1016/j.carbpol.2011.07.009

Chieng, B.W., Ibrahim, N. A. & Yunus, W. M. Z. W. (2010). Effect of organo-modified montmorillonite on poly(butylenes succinate)/poly(butylenes adipate-co-terepthalate) nanocomposites. *eXPRESS Polym. Lett.* **4**, 404-414. doi: 10.3144/expresspolymlett.2010.51

Chivrac, F., Kadlecová, Z., Pollet, E. & Avérous, L. (2006). Aromatic copolyester-based nano-biocomposites: Elaboration, structural characterization and properties. *J. Polym. Env.***14**, 393–401. doi:10.1007/s10924-006-0033-4

Cho, J., Joshi, M.S. & Sun, C.T. (2006). Effect of inclusion size on mechanical properties of polymeric composites with micro and nano particles. *Compos. Sci. Technol*. **66**, 1941-1952. doi: org/10.1016/j.compscitech.2005.12.028

Cho, M.J. & Park, B.D. (2011). Tensile and properties of nanocellulose-reinforced poly(vinyl alcohol) nanocomposites, *J. Ind. Eng. Chem.* **17,** 36–40. doi.org/10.1016/j.jiec.2010.10.006

Cho, M.J., Park, B.D. & Kadla, J.F. (2012). Characterization of electrospun nanofibers of cellulose nanowhisker/polyvinyl alcohol composites. *Mokchae Konghak*. **40**, 71-77. doi: org/10.5658/WOOD.2012.40.2.71

Cotana, F., Brinchi, L., Gelosia, M., Coccia, V., & Petrozzi, A. (2012). Nanocrystalline cellulose from lignocelluloses biomass: applications and future prospects. *20th European Biomass Conference and Exhibition, Italy*. 1182-1194. doi:10.1016/j.carbpol.2013.01.03

Conceição, I. D. da, Silva, L. R. C. da, Alves, T. S., Silva, H. de S. e, Barbosa, R., & Sousa, R. R. M. de. (2019). Investigation of the Wettability Using Contact Angle Measurements of Green Polyethylene Flat Films and Expanded Vermiculite Clay Treated by Plasma. *Mater. Res.* **22,** 1-7. doi:10.1590/1980-5373-mr-2018-0918

Czaja, W., Krystynowicz, A., Bielecki, S., & Brownjr, R. (2006). Microbial cellulose—the natural power to heal wounds. *Biomaterials* **27**, 145–151. doi:10.1016/j.biomaterials.2005.07.035

Dai, D., & Fan, M. (2010). Characteristic and performance of elementary hemp fibre. *Mater. Sci. Applications.* **1,** 336-342. doi:10.4236/msa.2010.16049

Dai, X., Xiong, Z., Na H, & Zhu, J. (2017). How does epoxidized soybean oil improve the toughness of microcrystalline cellulose filled polylactide acid composites? *Compos. Sci. Technol.* **90**, 9-15.

Das, M. & Chakraborty, D. (2008). The effect of Alkalization and fiber loading on the mechanical properties of bamboo fiber composites, part 1: - polyester resin matrix. *J. Appl. Polym. Sci.* **112**, 489-495. doi: org/10.1002/app.29342

Dasaria, A., Yub, Z.Z., Caic, G.P., & Maic, Y.W. (2013). Recent developments in the fire retardancy of polymeric materials. *Prog. Polym. Sci.* **38**, 1357–1387. doi:10.1016/j.progpolymsci.2013.06.006

Demir, H., Atikler, U., Balkose, D. & Tihminlioglu, F. (2006). The effect of fiber surface treatments on the tensile and water sorption properties of polypropylene–luffa fiber composites. *Composites A.* **37**, 447-456. doi: org/10.1016/j.compositesa.2005.05.036

Dhar P., Gaur S.S., Soundararajan N., Gupta A., Bhasney S.M., Milli M., Kumar A. & Katiyar V. (2017). Reactive extrusion of polylactic acid/ cellulose

nanocrystal films for food packaging applications: Influence of filler type on thermomechanical, rheological, and barrier properties. *Indus. Eng. Chemistr. Res.* **56**, 4718-4735.

Dhar, P., Bhardwaj, U., Kumar, A., & Katiyar, V. (2014). Cellulose Nanocrystals: A potential nanofiller for food packaging applications. food additives and packaging; *ACS Symposium Series*; **Chapter 17**. pp. 197-239 American Chemical Society: Washington, DC. doi: 10.1021/bk-2014-1162.ch017

Dhar, P., Tarafder, D., Kumar, A. & Katiyar, V. (2016). Thermally Recyclable polylactide acid/cellulose nanocrystal films through reactive extrusion process. *Polymer*. **87**, 268-282.

Dusunceli, N. & Colak, O.U. (2008). The effects of manufacturing techniques on viscoelastic and viscoplastic behavior of high density polyethylene (HDPE*). Mater. Desig.* **29**, 1117–1124. doi:10.1016/j.matdes.2007.06.003

Esmaeli, A., Pourbabaee, A.A., Alikhani, H.A., Shabani, F. & Esmaeili, E. (2013). Biodegradation of low-density polyethylene (LDPE) by mixed culture of Lysinibacillus xylanilyticus and Aspergillus niger in soil. *PLOS One.* **8**, 1-10. doi: org/10.1371/journal.pone.0071720

Faguaga, E., Perez, C.J., Villarreal, N., Rodriguez, E.S. & Alvarez, V. (2012). Effect of water absorption on the dynamic mechanical properties of composites used for windmill blades. *Mater. Des.* **36**, 609-616. doi: org/10.1016/j.matdes.2011.11.059

Frone, A.N., Panaitescu, D.M. & Donescu, D. (2011). Some aspects concerning the isolation of cellulose micro-and nano fibers. *Sci. Bull.* **73,** 133-152. https://www.scientificbulletin.upb.ro/rev_docs_arhiva/full20599.pdf

Fukushima, K., Wu, M.H., Bocchini, S., Rasyida, A., & Yang, M.C. (2012). PBAT based nanocomposites for medical and industrial applications. *Mater.Sci. Eng.C* **32**, 1331-1351. doi: org/10.1016/j.msec.2012.04.005

Gasperi, J., Dris, R., Bonin, T., Rocher, V., & Tassin, B. (2014). Assessment of floating plastic debris in surface water along the Seine River. *Environ. Pollut.* **195**, 163–166. doi:10.1016/j.envpol.2014.09.001

Gauitua, W., Ballerini, A. & Zhang, J. (2005). Polymer nanocomposites: synthetic and natural fillers a review. *Maderas Clencia y Technologia*. **7,** 159–178. doi.org/10.4067/S0718-221X2005000300002

Gemci R. (2010). Examining the effects of mercerization process applied under different conditions to dimensional stability. *Sci. Res. Essays*. **5**, 560-571.

Giri, J. & Adhikari, R. (2013). A brief review on extraction of nanocellulose and its application. *BIBECHANA* **9**, 81-87. doi: org/10.3126/bibechana.v9i0.7179

Giri, J., Lach R., Grellmann, W., Susan, M.A.B.H., Saiter, J.M., Henning, S., Katiyar, V., & Adhikari, R. (2019b). Compostable composites of wheat stalk microcrystalline cellulose and Poly(butylene adipate-co-terephthalate): Surface properties and degradation behaviour. *J. Appl. Polym. Sci. **48149***, 1-10. DOI: 10.1002/app.48149

Giri, J., Lach, R., Le, H.H., Grellmann, W., Radusch, H-J, Saiter, J.M. & Adhikari, R. (2020). Structural, thermal and mechanical properties of composites of poly(butylenes adipate-co-terephathalate) with wheat straw microcrystalline cellulose. *Polym. Bull.1-17.* DOI: https://doi.org/10.1007/s00289-020-03339-5

Giri, J., Lach, R., Sapkota, J., Susan, M.A.B.H., Saiter, J.M., Henning, S., Katiyar, V. & Adhikari, R. (2019a). Structural and thermal characterization of different types of cellulosic fibers. *BIBECHANA* **16**: 177-186. doi: org/10.3126/bibechana.v16i0.21650

Giri, J., Le, H.H., Radusch, H.J., Lach, R., Grellmann, W., Lebek, W. & Adhikari, R. (2013). Effect of Ketuki Fiber on Morphology and Mechanical Properties of Thermoplastics Composites. *Nep. J. Sci. Technol.* **13,** 73-79.

Gopakumar, D.A., Pai, A.R., Pottathara, Y.B., Pasquini, D., Carlos de Morais, L., Luke, M., Kalarikkal, N.K., Grohens Y., & Thomas, S. (2018). Cellulose nanofiber-based polyaniline flexible papers as sustainable microwave

absorbers in the x-band. *ACS Appl. Mater. Interfaces*.**10,** 20032−20043. doi: 10.1021/acsami.8b04549

Gowman, A., Picard, M., Lim, L., Misra, M., & Mohanty, A. (2019). Fruit Waste Valorization for Biodegradable Biocomposite Applications: A Review. *BioResources*, **14**, 10047-10092.

Grellmann, W. & Seidler, S. (2011). *Deformation and Fracture Behaviour of Polymers (Engineering Materials)*. Springer. doi: 10.1115/1.1523359

Gross, R.A. & Kalra, B. (2002). Biodegradable polymers for the environment. *Science* **297**, 803-807. doi:10.1126/science.297.5582.803

Gruneberger, F., Kunniger, T., Zimmermann, T. & Arnold, M. (2014). Nanofibrillated cellulose in wood coatings: mechanical properties of free composite films. *J. Mater. Sci.* **49**, 6437-6448.

Guerrero, M.B., Maqueda, L.A.P., Artiaga, R., Jiménez, P.E.S. & Cosp, J.P. (2016). Structural and chemical characteristics of sisal fiber and its components: effect of washing and grinding, *J. Nat. Fib.* **14,** 26–39. doi.org/10.1080/15440478.2015.1137529

Guo. Q. (2016). *Polymer Morphology-Principles- Characterization-Processing*. WILEY.ISBN-13: 978-1118452158

Gwon, J.G., Lee, S.Y., Doh, G.H. & Kim, J.H. (2010). Characterization of chemically modified wood fibers using FTIR spectroscopy for biocomposites. *J. Appl. Polym. Sci.* **116,** 3212–3219. doi.org/10.1002/app.31746

Hameed, N., Thomas, S.P., Abraham, R. & Thomas, S. (2007). Morphology and contact angle studies of poly(styrene-co-acrylonitrile) modified epoxy resin blends and their glass fibre reinforced composites. *eXPRESS Polym. Lett.* **1**, 345-355.

Han, Y.H., Han, S.O., Cho, D. & Kim, H. I. (2008). Dynamic mechanical properties of natural fiber/polymer biocomposites: The effect of fiber treatment with electron beam. *Macromol. Res*. **16**, 253-260. doi: org/10.1007/BF03218861

He, J., Tang, Y. & Wang, S.Y. (2007). Differences in morphological characteristics of bamboo fibres and other natural cellulose fibres: studies on X-ray diffraction, solid state 13C-CP/MAS NMR, and second derivative FTIR spectroscopy data. *Iran Polym. J.* **16**, 807–818.

Herrera, M.A., Mathew, A.P. & Oksman, K. (2012). Comparison of cellulose nanowhiskers extracted from industrial bio-residue and commercial microcrystalline cellulose. *Mater. Lett.* **71**, 28-31. doi: org/10.1016/j.matlet.2011.12.011

Huq, T., Salmieri, S., Khan, A., Khan, R. A., Le Tien, C., Riedl, B., Fraschini C., Bouchardc J., Uribe-Calderond J., Kamal M. R. & Lacroixa M. (2012). Nanocrystalline cellulose (NCC) reinforced alginate based biodegradable nanocomposite film. *Carbohydr. Polym.* **90**, 1757–1763. doi:10.1016/j.carbpol.2012.07.065

Huy, T.A., Adhikari, R., & Michler, G.H. (2003). Deformation behavior of styrene-block-butadiene-block-styrene triblock copolymers having different morphologies. *Polymer*. **44**, 1247–1257. doi:10.1016/s0032-3861(02)00548-7

Ibrahim, N.A., Hadithon, K.A., & Abdan, K. (2010). Effect of fiber treatment on mechanical properties of kenaf-fiber-ecoflex composites. *J. Reinf. Plast. Compos*. **29**, 2192-2198. doi: org/10.1177/0731684409347592

Ichazo, M., Albano, C., González, J., Perera, R. & Candal, M. (2001). Polypropylene/wood flour composites: treatments and properties. *Compos. Struct*. **54,** 207–214.

Iguchi, M., Yamanaka, S., & Budhiono, A. (2000). Review Bacterial cellulose—a masterpiece of nature's arts. *J. Mater. Sci.* **35,** 261–270. doi.org/10.1023/A:1004775229149

Itry, R.A., Lamnawar, K., & Maazouz, A. (2012). Improvement of thermal stability, rheological and mechanical properties of PLA, PBAT and their blends by

reactive extrusion with fuctionalized epoxy. *Polym. Degrad. Stab.* **97,** 1898-1914. doi: org/10.1016/j.polymdegradstab.2012.06.028

Jonoobi, M., Mathew, A.P., & Oksman, K. (2014). Natural Resources and Residues for Production of Bionanomaterials. *Materials and Energy*. 19–33. doi:10.1142/9789814566469_0003

Kabir, M. M., Wang, H., Lau, K. T., & Cardona, F. (2012). Chemical treatments on plant-based natural fibre reinforced polymer composites: An overview. *Composites Part B: Eng.* **43**, 2883–2892. doi:10.1016/j.compositesb.2012.04.053

Khan, R.A., Beck, S., Dussault, D., Salmieri, S., Bouchard, J. & Lacroix, M. (2013). Mechanical and barrier properties of nanocrystalline cellulose reinforced poly(caprolactone) composites: Effect of gamma radiation. *J. Appl. Polym. Sci.*, **129**, *3038–3046.* doi:10.1002/app.38896

Kijchavengkul, T., Auras, R., Rubino, M., & Selke, S. (2010). Biodegradation and hydrolysis rate of aliphatic aromatic polyester. *Polym. Degrad. Stab.* **95**, 2641-2647.

Kitagawa, K., Ishiaku, U.S., Mizoguchi, M. & Hamada, H. (2005). Bamboo-based ecocomposites and their potential applications. In: Natural Fibers, Biopolymers, and Biocomposites. **Chapter 11**. CRC Press, Boca Raton, USA.

Kramer, F., Klemm, D., Schumann, D., Heßler N., Wesarg, F., Fried, W. & Stadermann, D. (2006). Nanocellulose polymer composites as innovative pool for biomaterial development. *Macromol. Symp.* **244**, 136-148. doi: org/10.1002/masy.200651213

Lach, R., Kim, G.M., Adhikari, R., Michler, G.H. & Grellmann, W. (2013). Indentation Methods for Characterising the Mechanical and Fracture Behaviour of Polymer Nanocomposites. *Nep. J. Sci. Technol.* **13**, 115–122. doi:10.3126/njst.v13i2.7723

Lach, R., Michler, G.H. & Grellmann, W., (2010). Microstructure and indentation behaviour of polyhedral oligomeric silsesquioxanes-modified thermoplastic polyurethane nanocomposites. *Macromol. Mater. Eng. NA-NA*. doi: 10.1002/mame.200900393

Lee, S.H., Ohkita, T. & Kitagawa, K. (2004). Eco-composite from poly(lactic acid) and bamboo fiber. *Holzforschung*. **58,** 529-536. doi: 10.1515/hf.2004.080

Lee, S.Y., Mohan, D.J., Kang, I.A., Doh, G.H., Lee, S. & Han, S.O. (2009). Nanocellulose reinforced PVA composite films: Effect of acid treatment and filler loading. *Fibers Polym*. **10**, 77-82. https://springer.com/article/10.1007/s12221-009-0077-x

Leja, K. & Lewandowicz, G. (2010). Polymer biodegradation and biodegradable polymers - a review. *Polish J. Environ. Studies.* **19**, 255-266. http://yunus.hacettepe.edu.tr/~damlacetin/kmu407/index_dosyalar/2.%20makale.pdf

Leung, A.C.W., Lam, E., Chong, J., Hrapovic, S. & Luong, J.H.T. (2013). Reinforced plastics and aerogels by nanocrystalline cellulose. *J. Nanoparticles Res.* **15**, 1-24.

Lezak, E., Bartczak, Z. & Galeski, A. (2006). Plastic deformation behavior of β-phase isotactic polypropylene in plane-strain compression at room temperature. *Polymer*, **47**, 8562–8574. doi:10.1016/j.polymer.2006.10.016

Li, J., Wei, X., Wang, Q., Chen, J., Chang, G., Kong, L., Su, J. & Liu, Y. (2012). Homogeneous isolation of nanocellulose from sugarcane bagasse by high pressure homogenization. *Carbohydr.Polym*. **90,** 1609–1613. doi.org/10.1016/j.carbpol.2012.07.038

Li, L., Ding, S. & Zhou, C. (2003). Preparation and degradation of PLA/chitosan composite materials. *J. Appl. Polym. Sci*. **91**, 274–277. doi: 10.1002/app.12954

Liu, D.Y., Yuan, X.W., Bhattacharyya, D. & Easteal, A.J. (2010). Characterisation of solution cast cellulose nanofibre-reinforced poly(lactic acid). *eXPRESS Polym. Lett.* **4,** 26–31. doi.org/10.3144/expresspolymlett.2010.5

Liu, J., Zhuo, Y., Du, S. & Li, Q. (2017). Integrated ferroelectrics-an international journal preparation and characterization of PLA/NCC nanofibers. *Integr. Ferroelectr.* **179,** 31-37.

Liu, M., Jia, Z., Liu, F., Jia, D. & Guo, B. (2010). Tailoring the wettability of polypropylene surfaces with halloysite nanotubes. *J. Colloid Interface Sci.* **350**, 186-193.

Liu, Y., Li, Y., Chen, H., Yang, G., Zheng, X. & Zhou, S. (2014). Water-induced shape-memory poly(d,l-lactide)/microcrystalline cellulose composites. *Carbohydr. Polym.* **104**, 101–108. doi: org/10.1016/j.carbpol.2014.01.031

Lu, J., Sun, C., Yang, K., Wang, K., Jiang, Y., Tusiime, R., Yang, Y., Fan, F., Sun, Z., Liu, Y., Zhang, H., Han, K. & Yu, M. (2019). Properties of Polylactic Acid Reinforced by Hydroxyapatite Modified Nanocellulose. *Polymers*, **11**, 1-13. doi:10.3390/polym11061009

Lu, Y., Tekinalp, H.L., Eberle, C.C., Peter, W., Naskar, A.M., & Ozcan, S. (2001). Nanocellulose in polymer composites and biomedical applications. *Nanocellulose*. **13**, 47-54.

Ma, H., Zhou, B., Li, H.-S., Li, Y.-Q. & Ou, S.-Y. (2011). Green composite films composed of nanocrystalline cellulose and a cellulose matrix regenerated from functionalized ionic liquid solution. *Carbohydr. Polym.* **84**, 383–389.doi:10.1016/j.carbpol.2010.11.050

Maiti, S., Ray, D., Mitra, D., Sengupta, S. & Kar, T. (2011). Structural changes of starch/polyvinyl alcohol biocomposite films reinforced with microcrystalline cellulose due to biodegradation in simulated aerobic compost environment. *J. Appl. Polym. Sci*. **122**, 2503-2511. doi: org/10.1002/app.34377

Malho, J.M., Laaksonen, P., Walther, A., Ikkala, O. & Linder, M.B. (2012). Facile method for stiff, tough and strong nanocomposites by direct exfoliation of

multilayered graphene into native nanocellulose matrix. *Biomacromol.* **13**, 1093-1099. doi: 10.1021/bm2018189

Mandal, A. & Chakrabarty D. (2011). Isolation of nanocellulose from waste sugarcane bagasse (SCB) and its characterization, *Carbohydr. Polym*. **86,** 1291–1299. doi.org/10.1016/j.carbpol.2011.06.030

Mandal, A. & Chakrabarty, D. (2014). Studies on the mechanical, thermal, morphological and barrier properties of nanocomposites based on poly(vinyl alcohol) and nanocellulose from sugarcane bagasse. *J. Ind. Eng. Chem.* **20**, 462-473. doi: org/10.1016/j.jiec.2013.05.003

Manimaran, P., Senthamaraikanna, P.,Sanjay, M. R., Marichelvam, M. K. & Jawaid, M. (2018). Study on characterization of *Furcraeafoetida* new natural fiber as composite reinforcement for lightweight applications. *Carbohydr. Polym.* **181,** 650–658. doi.org/10.1016/j.carbpol.2017.11.099

Mathew, A.P., Oksman, K. & Pierron, D. (2012). Harmand, M.F. Fibrous cellulose nanocomposite scaffolds prepared by partial dissolution for potential use as ligament or tendon substitutes. *Carbohydr. Polym.* **87**, 2291-2298. doi: org/10.1016/j.carbpol.2011.10.063

Mathew, A.P., Oksman, K. & Sain, M. (2005). Mechanical properties of biodegradable composites from poly lactic acid (PLA) and microcrystalline cellulose (MCC). *J. Appl. Polym. Sci*. **97,** 2014–2025. doi: 10.1002/app.21779

Michler, G.H.(eds.) (2008). *Electron Microscopy of polymers*. Springer. Lipzig, Germany. doi: 10.1007/978-3-540-36352-1

Michler, G.H., & Baltá-Calleja, F.J. (2012). *Nano- and Micromechanics of Polymers: Structure Modification and Improvement of Properties*. Hanser Verlag Munich.

Mikkelsen, D., Flanagan, B.M., Dykes, G.A. & Gidley, M.J. (2009). Influence of different carbon sources on bacterial cellulose production by

Gluconacetobacter xylinus strain ATCC 53524. *J. Appl. Microbio*. **107,** 576–583 (2009). doi:10.1111/j.1365-2672.2009.04226.x

Morokuma, K. (1971). Molecular orbital studies of hydrogen bonds. III.C=O...H-O hydrogen bond in $H_2CO...H_2O$ and $H_2CO...2H_2O$. *J. Chem. Phys.* **55**, 1236-1244.

Morouco, P., Biscaia, S., Viana, T., Franco, M., Malca, C., Mateus, A., Moura, C., Ferreira, F.C., Mitchell, G. & Alves, N.M. (2016). Fabrication of poly(ε-caprolactone) scaffolds reinforced with cellulose nanofibers, with and without the addition of hydroxyapatite nanoparticles. *BioMed. Res. Int. vol.* **2016**:10pages. doi: org/10.1155/2016/1596157

Mostafa, H.M., Sourell, H. & Blockisch, F.J. (2010). The mechanical properties of some bioplastics under different soil type for use as a biodegradable drip tubes. *Agric. Eng. Int.* **12**, 12-21. http://cigrjournal.org/index.php/Ejounral/article/view/1497/1270

Moustafa, H., Guizani, C., & Dufresne, A. (2016). Sustainable biodegradable coffee grounds filler and its effect on the hydrophobicity, mechanical and thermal properties of biodegradable PBAT composites. *J. Appl. Polym. Sci.* **134**, 1-11. doi:10.1002/app.44498

Moustafa, H., Kissi, N.E., Abou-Kandil, A.I., Abdel-Aziz, M.S. & Dufresne, A. (2017). PLA/PBAT bionanocomposites with antimicrobial natural rosin for green packaging. *ACS Appl. Mater. Interfaces.* **9**, 20132–20141. doi:10.1021/acsami.7b0555

Mueller, S., Weder, C. & Foster, E.J. (2014). Isolation of cellulose nanocrystals from pseudostems of banana plants. *RSC Adv.* **4,** 907–915. doi.org/10.1039/C3RA46390G

Mukherjee, T., Czaka, M., Kao, N., Gupta, R.K., Choi, H.J., & Bhattacharya, S. (2014). Dispersion study of nanofibrillated cellulose based poly(butylene adipate-co-terephthalate) composites. *Carbohydr. Polym.* **102**, 537–542. doi:10.1016/j.carbpol.2013.11.047

Nagata, M. & Inaki, K. (2011). Biodegradable and photocurable multiblock copolymers with shape-memory properties from poly(ε-caprolactone) diol, poly(ethylene glycol) and 5-cinnamoyloxyisophthalic acid. *J. Appl. Polym. Sci.* **120**, 3556-3564. doi: org/10.1002/app.33531

Nam, J.Y., Ray, S.S. & Okamoto, M. (2003). Crystallization behavior and morphology of biodegradable polylactide/layered silicate nanocomposite. *Macromolecules.* **36**, 7126–7131. doi: 10.1021/ma034623j

Novotny, C., Erbanova, P., Sezimova, H., Malchova, K., Rybkova, Z., Malinova, L., Prokopova, I. & Brozek, J. (2015). Biodegradation of aromatic-aliphatic copolyesters and polyesteramides by esterase activity-producing microorganisms. Int. Biodeter. Biodegrad. **97**, 25-30.

Ochi, S. (2008). Mechanical properties of kenaf fibers and kenaf/PLA composites. *Mech. Mater.* **40**, 446–452. doi:10.1016/j.mechmat.2007.10.006

Oksman, K., Etang, J. A., Mathew, A., & Jonoobi, M. (2011). Cellulose nanowhiskers separated from a bio-residue from wood bioethanol production. *Biomass Bioenergy*. **35**, 146-152.

Okubo, K., Fujii, T., & Yamamoto, Y. (2004). Development of bamboo-based polymer composites and their mechanical properties. *Composites: Part: A.* **35**, 377–383. doi: org/10.1016/j.compositesa.2003.09.017

Ozkoc, G., Kemaloglu, S., & Quaedflieg, M. (2010). Production of poly(lactic acid)/organoclay nanocomposites scaffolds by microcompounding and polymer/particle leaching. *Polym. Compos*. **31**, 674-683. doi:org/10.1002/pc.20846

Pak, Y.L., Bin Ahmad, M., Shameli, K., Yunus, W.M.Z.W., Ibrahim, N.A., & Zainuddin, N. (2013). Mechanical and Morphological Properties of Poly-3-hydroxybutyrate/Poly(butyleneadipate-co-terephthalate)/Layered Double Hydroxide Nanocomposites. *J. Nanomater.* **2013,** 1–8. doi:10.1155/2013/621097

Pal, A.K., & Katiyar, V. (2016). Thermal degradation behaviour of nanoamphiphilic chitosan dispersed poly (lactic acid) bionanocomposite. *Int J Biol Macromol.* **95,** 1267-1279. dx.doi.org/10.1016/j.ijbiomac.2016.11.024

Palisikowski, P.A., Kuchnier, C.N., Pinheiro, I.F. & Morales, A.R. (2017). Biodegradion in soil of PLA/PBAT Blends compatibilized with chain Extender. *J. Polym. Environ.* **26**, 330-341. doi: 10.1007/s10924-017-0951-3

Pan, M., Zhou, X. & Chen, M. (2013). Cellulose nanowhiskers isolation and properties from acid hydrolysis combined with high pressure homogenization. *BioResources.* **8,** 933–943.

Panaitescu, D.M., Frone, A.N., Ghiurea, M., Spataru, C.I., Radovici, C. & Iorga, M.D. (2011). *Advances in Composites Materials-Ecodesign and Analysis: Properties of polymer composites with cellulose microfibrils.* Intechopen, Croatia.

Pandit, R. (2015). *Templating Nanostructures In Epoxy Resin Using Styrenic Block Copolymers*. Central Department of Chemistry. Institute of Science and Technology, Tribhuvan University, Kathmandu, Nepal.

Pang, J.H., Liu, X., Wu, M., Wu, Y.Y., Zhang, X.M. & Sun, R.C. (2014). Fabrication and characterization of regenerated cellulose films using different liquids, *J. Spectr.* 1-8. doi.org/10.1155/2014/214057

Park, H.Y., Kim, S.S., Kim, S.G. & Seo, K.H. (2012). Modification of physical properties of PBAT by using TPS. *3rd International conference on Biology, Environment and Chemistry*. **46**, 67-71.

Paul, D.R. & Robeson, L.M. (2014). Polymer nanotechnology: *nanocomposites polymer*. **49**, 3187-3204 (2008). doi: org/10.1016/j.polymer.2008.04.017

Paula, M.P.d., Larcerda, T. M. & Frollini, E. (2008). Sisal cellulose acetates obtained from heterogeneous reaction. *eXPRESS Polym. Lett.* **2**, 423-428.

Pelissari, F.M., Sobral, P.J.d.M. & Menegalli, F.C. (2014). Isolation and characterization of cellulose nanofibers from banana peels. *Cellulose* **21,** 417-432. doi:org/10.1007/s10570-013-0138-6

Pereda, M., Amica, G., Racz, I. & Marcovich, N.E. (2011). Structure and properties of nanocellulose films based on sodium caseinate and nanocellulose fibers. *J. Food. Eng.* **3**, 76-83.

Pinheiro, I.F., Ferreira, F.V., Souza, D.H.S., Gouveia, R.F., Lona, L.M.F., Morales, A.R. & Mei, L.H.I. (2017). Mechanical, rheological and degradation properties of PBAT nanocomposites reinforced by functionalized cellulose nanocrystals. *Euro. Polym. J.* **97,** 356-365. doi.org/10.1016/j.eurpolymj.2017.10.026

Pirani, S., Abushammala, H. M. N. & Hashaikeh, R. (2013). Preparation and characterization of electrospun PLA/nanocrystalline cellulose-based composites. *J. Appl. Polym. Sci.* **130,** 3345–3354. doi:10.1002/app.39576

Pokhrel, S., Lach, R., Le, H.H., Wutzler, A., Grellmann, W., Radusch, H.J., Dhakal, R.P., Esposito, A., Henning, S., Yadav, P.N., Saiter, J.M., Heinrich, G. & Adhikari, R. (2016a). *Fabrication and characterization of completely biodegradable copolyester–chitosan blends: I. spectroscopic and thermal characterization.* Macromol. Symp. **366**, 23–34.

Pokharel, S. (2016b). *Chitosan based polymer blends: preparation, mechanical properties and biodegradability*. Central Department of Chemistry. Institute of Science and Technology, Tribhuvan University, Kathmandu, Nepal.

Ponce-Reyes, C.E., Chanona-Perez, J.J., Garibay-Febles, V., Palacios-Gonzalez, E., Karamath, J., Terres-Rojas, E. & Calderon-Dominguez, G. (2014). Preparation of cellulose nanoparticles from agave waste and its morphological and structural characterization. *Revista Mexicana de Ingenieria Quimica*. **13**, 897-906.

Pradhan, S., Lach, R., Grellmann, W. & Adhikari, R. (2012). Nanofiller reinforced polyolefin elastomer: effect on morphology and mechanical properties of composites. *Nep. J. Sci. Technol.* **13**, 103-108.

Rahimi-Nasrabadi, M., Khoshroo, A., & Mazloum-Ardakani, M. (2017). Electrochemical determination of diazepam in real samples based on fullerene-functionalized carbon nanotubes/ionic liquid nanocomposite. *Sensors and Actuators B: Chemical*. **240**, 125–131. doi:10.1016/j.snb.2016.08.144

Rajan, K.P., Veena, N.R., Maria, H.J., Rajan, R., Skrifvars, M. & Joseph, K. (2010). Extraction of bamboo microfibrils and development of biocomposites based on polyhydroxybutyrate and bamboo microfibrils. *J. Comp. Mater.* **45**, 1325-1329. doi.org/10.1177/0021998310381543

Rajan, K.P., Veena, N R., Maria, H.J., Rajan, R., Skrifvars, M., Joseph, K. (2009). Mechanical and thermal properties of bamboo microfibril reinforced polyhydroxybutyrate biocomposites, *J. Polym. Env.* **17,** 109–114. doi.org/10.1007/s10924-009-0127-x

Rambo, M.K.D. & Ferreira M.M.C. (2015). Determination of cellulose crystallinity of banana residues using near infrareded spectroscopy and multivariate analysis. *J. Braz. Chem. Soc.* **26**, 1491-1499. dx.doi.org/10.5935/0103-5053.20150118

Rana, A.K., Mandal, A., Mitra, B.C., Jacobson, R., Rowell, R. & Banerjee, A.N. (1998). Short jute fiber-reinforced polypropylene composites: Effect of compatibilizer. *J. Appl. Polym. Sci.* **69**, 329–338.

Rasyida, A., Fukushima, K., & Yang, M.C. (2017). Structure and properties of organically modified poly(butylene adipate-co-terephthalate) based nanocomposites. IOP Conference Series: *Mater. Sci. Eng.* **223**, 012-023. doi:10.1088/1757-899x/223/1/012023

Reddy, J.P. & Rhim, J.W. (2014). Isolation and characterization of cellulose nanocrystals from garlic skin. *Mater. Lett.* **129**, 20-23. doi: 10.1016/j.matlet.2014.05.019

Rosa, M.F., Medeiros, E.S., Malmonge, J.A., Gregorski, K.S., Wood, D.F., Mattoso, L.H.C., Glenn, G., Orts, W.J. & Imam, S.H. (2010). Cellulose nanowhiskers from coconut fibers: effect of preparation conditions on their thermal and morphological behavior. *Carbohydr. Polym*. **81**, 83-92. doi. 10.1016/j.carbpol.2010.01.059

Rosli, N.A., Ahmad, I. & Abdullah, I. (2013). Isolation and characterization of cellulose nanocrystals from Agave angustifoliafibre. *Bioresources.* **8,** 1893-1908.

Saba, N., Jawaid, M., Othman, Y.A. & Paridah, M.T. (2015). A review on dynamic mechanical properties of natural fibre reinforced polymer composites. *Construc. Build. Mater.* **106**, 149-159. doi: org/10.1016/j.conbuildmat.2015.12.075

Sabaruddin, F.A., Md Tahir, P. & Lee, S.H. (2018). Mechanical properties of PP/kenaf core nanocomposites made from nanocrystalline cellulose as an additive. *J. Reinforced Plastic. compos.* doi:10.1177/0731684418804882

Saiter, J.M., Dobircau, L., Saiah R., Sreekumar, P.A., Galandon, A., Gattin, R., Leblanc, N. & Adhikari, R. (2010). Relaxation map of a green thermoplastic film. Glass transition and fragility. *Physica B*, **45**, 900-905.

Sakhawy, M.E., Kamel, A.S., Salama, H.A. & Tohamy, S. (2018). Preparation and infrared study of cellulose based amphiphilic materials. *Cellulose Chem. Technol*. **52**, 193–200.

Samarasekara, A.M.P.B., Kumara, S.P.D.A., Karunanayake L, Madhusanka, A.J S. & Amarasinghe, D.A.S. (2018). Study of thermal and mechanical properties of microcrystalline cellulose and nanocrystalline cellulose based thermoplastic. *Moratuwa Engineering Research Conference (MERCon), IEEE Proceedings*. 1-6.

Sanadi, A.R., Caulfield, D.F., Jacobson, R.E. & Rowell, R.M. (1995). Renewable agricultural fibers as reinforcing fillers in plastics: Mechanical properties of

kenaf fiber-polypropylene composites. *Ind. Eng. Chem. Res*. **34**, 1889–1896. doi: 10.1021/ie00044a041

Sanjay, M.R., Arpitha, G.R., Naik, L.L., Gopalakrisha, K. & Yogesha, B. (2016). Applications of natural fibers and its composites: An overview. *Sci. Res*. **7**, 108-114. doi: org/10.4236/nr.2016.73011

Satyamurthy, P. & Vigneshwaran, N. (2013). A novel process for synthesis of spherical nanocellulose by controlled hydrolysis of microcrystalline cellulose using anaerobic microbial consortium. *Enzym. Microbial. Technol*. **52**, 20-25. doi: org/10.1016/j.enzmictec.2012.09.002

Sawyer, L.C., Grubb, D.T. & Meyers, G.F. (2008). *Polymer Microscopy*. Heidelberg, Germany. Springer publisher. doi: 10.1007/978-0-387-72628-1

Saxena, M., Morchhale, R.K., Asokan, P. & Prasad, B.K. (2008). Plant Fiber — Industrial waste reinforced polymer composites as a potential wood substitute material. *J. Compos. Mater*. **42**, 367–384. doi:10.1177/0021998307087014

Schöne, J. Tondl, D. Lach, R., Rybnicek, J. & Grellmann, W. (2014). Analysis of PA 6 nanocomposites — indentation and creep behavior as a function of temperature and load level using different indentation techniques. POLIMERY. **10**, 722-728. dx.doi.org/10.14314/polimery.2014.722

Segal, L., Creely, J.J., Martin, A.E., Conrad, C.M. (1959). An Empirical method for estimating degree of crystallinity of native cellulose using the X-ray deffractometer. *Text. Res. J.* **29**, 786-794. doi: org/10.1177/004051755902901003

Sgarioto, M., Adhikari, R., Gunatillake, P.A., Moore, T., Malherbe, F., Nagel, M.D. & Patterson, J. (2014). Properties and in vitro evaluation of high modulus biodegradable polyurethanes for applications in cardiovascular stents. *J. Biomed. Mater.Res. B Appl. Biomater.***102B**, 1711-1719. doi:org/10.1002/jbm.b.33137

Shah, A.A., Hasan, F., Hameed, A. & Ahmed, S. (2008). Biological degradation of plastics; A comprehensive a review. *Biotechnol. Adv*. **26**, 246-265. doi: org/10.1016/j.biotechadv.2007.12.005

Shaheen, T.I. & Emam, H.E. (2018). Sono-chemical synthesis of cellulose nanocrystals from wood sawdust using Acid hydrolysis. Int. *J. Bio. Macromol*. **107**, 1599–1606. doi:10.1016/j.ijbiomac.2017.10.028

Sharma, S., Singh, I.& Virdi, J.S. (2003). Apotential Aspergillus species for biodegradation of polymeric materials. *Curr. Sci*. **84**, 1399-1402. doi.org/10.1007/s1135

Shi, B., Shlepr, M. & Palfery, D. (2011). Effect of blend composition and structure on biodegradation of starch/ ecoflex-filled polyethylene films. *J. Appl. Polym. Sci*. **120**, 1808-1816.

Singh, B. & Sharma, N. (2008). Mechanistic implications of plastic degradation, Polym. *Degrad. Stab*. **93**, 561–584. doi: org/10.1016/j.polymdegradstab.2007.11.008

Siotto, M., Zoia, L., Tosin, M. & Innocenti, F.D., Orlandi, M., Mezzanotte, V. (2013). Monitoring biodegradation of poly(butylenes sebacate) by gel permeation chromatography, ^{1}H-NMR and ^{31}P-NMR techniques. *J. Environ. Manage.* **116**, 27-35. doi: org/10.1016/j.jenvman.2012.11.043

Siro, I. & Plackett, D. (2010). Microfibrillated cellulose and new nanocomposite materials: a review. *Cellulose* **17**, 459-494. doi.org/10.1007/s10570-010-9405-y

Siyamak, S., Ibrahim, N. A., Abdolmohammadi, S., Yunus, W.M. Z. W. & Rahman, M.Z.AB. (2012a). Effect of fiber esterification on fundamental properties of oil palm empty fruit bunch fiber/poly(butylenes adipate-co-terephthalate) biocomposites. *Int. J. Mol. Sci.* **13**, 1327-1346.

Siyamak, S., IbrahimN.A., Abdolmohammadi, S., Yunus, W.M.Z.B.W. & Rahman, M.Z.A. (2012b). Enhancement of mechanical and thermal properties of oil palm empty bunch fiber poly(butylenes adipate-co-terephthalate)

biocomposites by matrix esterification using succinic anhydride. *Molecules*, **17**, 1969-1991.

Sjödin, A., Carlsson, H., Thuresson, K., Sjölin, S., Bergman, A. & Östman, C. (2001). Flame retardants in indoor air at an electronics recycling plant and at other work environments. *Environ. Sci. Technol*. **35,** 448-454. doi: 10.1021/es000077n

Sofla, M.R.K., Brown, R.J., Tsuzuki, T. & Rainey, T.J. (2016). A comparision of cellulose nanocrystals and cellulose nanofibres extracted from bagasse using acid and ball milling methods. *Adv. Nat. Sci: Nanosci, Nanotechnol*. **7,** 1-9. DOI: 10.1088/2043-6262/7/3/035004

Sonia, A. & Dasan, K.P. (2013). Cellulose microfibers (CMF)/poly(ethylene-co-vinyl acetate) (EVA) composites for food packaging applications: A study based on barrier and biodegradable behavior, *J. Food Eng.* **118,** 78–89. doi.org/10.1016/j.jfoodeng.2013.03.020

Spiridon, I., Darie, R.N. & Kangas, H. (2016). Influence of fiber modifications on PLA/fiber composites. Behavior to accelerated weathering. *Composites Part B*. **92**, 19-27. doi: 10.1016/j.compositesb.2016.02.032

Sreekumar, P.A., Joseph, K., Unnikrishnan, G. & Thomas, S. (2007). A comparative study on mechanical properties of sisal-leaf fibre-reinforced polyester composites prepared by resin transfer and compression moulding techniques. *Compos. Sci. Technol*. **67**, 453–461. doi: 10.1016/j.compscitech.2006.08.025

Stelte, W. & Sanadi, A.R. (2009). Preparation and characterization of cellulose nanofibers from two commercial hardwood and softwood. *Ind. Eng. Chem. Res*. **48**, 11211-11219. doi: 10.1021/ie9011672

Su, S.K. & Wu, C.S. (2011). Polyester biocomposites from recycled natural fibers: characterization and biodegradability. *J. Appl. Polym. Sci.* **119**, 1211-1219.

Tavares, L. B., Ito, N. M., Salvadori, M. C., dos Santos, D. J., & Rosa, D. S. (2018). PBAT/kraft lignin blend in flexible laminated food packaging:

Peeling resistance and thermal degradability. *Polym. Test.* **67**, 169–176. doi:10.1016/j.polymertesting.2018.03.004

Teamsinsungvon, A., Ruksakulpiwat, Y. & Jarukumjorn, K. (2010). *Properties of Biodegradable Poly(lactic acid)/Poly(butylene adipate-co-terephthalate)/Calcium Carbonate Composites, Advanced Materials Research* **123-125,** 193-196.

Teixeira, Ed.M., Correa, A.C., Manzoli, A., Leite, F.D.L., Oliveira, C.R.D. & Mattoso, L.H.C. (2010). Cellulose nanofibers from white and naturally colored cotton fibers, *Cellulose.* **17,** 595–606. doi.org/10.1007/s10570-010-9403-0

Tesfaye, M., Patwa, R., Dhar, P. & Katiyar, V. (2017). Nanosilk-grafted poly(lactic acid) films: Influence of cross-linking on rheology and thermal stability, *ACS Omega* **2**, 7071–7084. doi: 10.1021/acsomega.7b01005

Thomas, S. & Stephen, R. (2010). *Rubber Nanocomposites: Preparation, Properties, and Applications.* Heidelberg, Germany, *Springer publisher*.

Thomas, S., Chan, C.H., Pothen, L.A., Rajisha, K.R., & Maria, H. (2013) *Natural Rubber Materials: Volume 1: Blends and IPNs.* The Royal Society of Chemistry. Cambridge CB4 0WF, UK.

Thomas, S.P., Thomas, S., Abraham, R. & Bandyopadhyay, S. (2008). *Polystyrene/calcium phosphate nanocomposites: contact angle studies based on water and methylene iodide.* eXPRESS Polym. Lett. **2**, 528-538.

Trovatti, E., Fernandes, S.C.M., Rubatat, L., Perez, D.d.S., Freire, C.S.R., Silverstre, A.J.D. & Neto, C.P. (2012). *Pullulan-nanofibrillated cellulose composites films with improved thermal and mechanical properites. Compos. Sci. Technol.* **72**, 1556-1561.

Vinayak, D.L., Guna, V.K., Madhavi, D., Arpitha, M. & Reddy, N. (2017). Ricins communis plant residues as a source for natural cellulose fiber potentially exploitable in polymer composites. *Ind. Crops Prod.* **100**, 126-131. doi: org/10.1016/j.indcrop.2017.02.019

Voronova, M.I., Surov, O.V., Guseinov, S.S., Barannikov, V.P., & Zakharov, A.G. (2015). Thermal stability of polyvinyl alcohol/nanocrystalline cellulose composites. Carbohydr. Polym. **130**, 440–447. doi:10.1016/j.carbpol.2015.05.032

Wan, Y.Z., Luo, H., He, F., Liang, H., Huang, Y. & Li, X.L. (2009). Mechanical, moisture absorption, and biodegradation behaviours of bacterial cellulose fibre-reinforced starch biocomposites. *Compos. Sci. Technol*. **69**, 1212–1217. doi: 10.1016/j.compscitech.2009.02.024

Wang, H., Wei, D., Zheng, A. & Xiao, H. (2015). Soil burial biodegradation of antimicrobial biodegradable PBAT films. *Polym. Degrad. Stab*. **116**, 14-22. doi:10.1016/j.polymdegradstab.2015.03.007

Wang, K.H., Wu, T.M., Shih, Y.F. & Huang, C.M. (2008). Water bamboo husk reinforced poly(lactic acid) green composites. *Polym. Eng. Sci.* **48**, 1833-1839.

William, G.E., Ballerini, A. & Zhang, J. (2005). Polymer nanocomposites: synthetic and natural fillers a review. *Maderas: Clencia Technologia.* **7**, 159-178. doi: org/10.4067/S0718-221X2005000300002

Wu, C.S. (2012). Characterization of cellulose acetate-reinforced aliphatic-aromatic copolyester composites. *Carbohydr. Polym.* **87**, 1249-1256. doi: org/10.1016/j.carbpol.2011.09.009

Yan, F.Y., Krishniah, D., Rajin, M. & Bono, A. (2009). Cellulose extraction from Palm Kernel cake using liquid phase oxidation. *J. Eng. Sci. Technol*. **1,** 57-68.

Yang, J. & Ye, D. Y. (2012). Liquid crystal of nanocellulose whiskers grafted with acrylamide. *Chin. Chem. Lett.* **23**, 367-370. doi.org/10.1016/j.cclet.2011.12.014

Yu, T. & Li, Y. (2014). Influence of poly(butylenes adipate-co-terephthalate) on the properties of the biodegradable composites based on ramie/poly(lactic acid). *Composites: Part A*. **58,** 24-29. doi: org/10.1016/j.compositesa.2013.11.013

Zhang, J.F., He, A., Li, J.X., Jian, X.M. & Han, C.C. (2006). Studies on the controlled morphology and wettability of polystyrene surfaces by electrospinning or electrospraying. *Polymer*. **47**, 7095-7102.

Zhou, Y.M., Fu, S. Y., Zheng, L. M. & Zhan, H.Y. (2012). Effect of nanocellulose isolation techniques on the formation of reinforced poly(vinyl alcohol) nanocomposite films. *eXPRESS Polym. Lett.* **6**, 794-804. DOI: 10.3144/expresspolymlett.2012.85

APPENDICES

Awards

- IUPAC Fellowship-2017
- Carl Klason Student Award-2017
- PhD Fellowship -2017 Fellowship-2017
- INSA Fellowship -2017

Award ceremony of 25th POLYCHAR 2017, World Forum on Advances Materials 2017, Oct-12th

Carl Klason Student Award 2017

is awarded to

JYOTI GIRI

during

25th POLYCHAR 2017
World Forum on Advanced Materials 2017

held from October 9 – 13, 2017 at
Putra World Trade Centre, Kuala Lumpur

Organised by
INSTITUT KIMIA MALAYSIA

Under the auspices of
THE SCIENTIFIC COMMITTEE OF WORLD FORUM ON ADVANCED MATERIALS
INTERNATIONAL UNION OF PURE AND APPLIED CHEMISTRY

Dato' Dr Ong Eng Long
President
Institut Kimia Malaysia

Prof. Dr. Witold Brostow
President
POLYCHAR Scientific Committee

Dr. Sven Henning
Chairman
POLYCHAR Prize Committee

IUPAC FELLOWSHIP 2017

is awarded to

JYOTI GIRI

during

25th POLYCHAR 2017
World Forum on Advanced Materials 2017

held from October 9 – 13, 2017 at
Putra World Trade Centre, Kuala Lumpur

Organised by
INSTITUT KIMIA MALAYSIA

Under the auspices of
THE SCIENTIFIC COMMITTEE OF WORLD FORUM ON ADVANCED MATERIALS
INTERNATIONAL UNION OF PURE AND APPLIED CHEMISTRY

Dato' Dr Ong Eng Long
President
Institut Kimia Malaysia

Prof. Dr. Witold Brostow
President
POLYCHAR Scientific Committee

Dr. Sven Henning
Chairman
POLYCHAR Prize Committee

Conference and Workshop Participations

PolymerTech 2014, *Poster presentation*,**"Structure-Properties Correlations Studies in Biodegradable Composites Comprising Rice Husk and Microfibrillated Cellulose".** Merseburg, Germany**,** *25th - 27th june 2014.*

J.Giri , S.P. Khatiwada ,H.H. Le, H.-J. Radusch, R. Lach, W. Grellmann, A.K. Bledzki,

L.K. Shrestha, R. Adhikari

PSD-Nepal Scientific Writing and Publishing Workshop. *3rd -4th November 2014.*

KaSAM-2014, *Poster presentation* **"Influence of Microcrystalline Cellulose Extracted from Wheat Stalk on the Properties of Composites with Ecoflex".** Pokhara, Nepal. *7th -10th September 2014*

J. Giri, H. H. Le, H-J. Radusch, R. Lach, W. Grellmann, G.-H. Michler, R. Adhikari

ISEPD- 2015, *Poster presentation* **"Morphological and Mechanical Properties of Completely Biodegradable Composites of Rice Husk and Microfibrillated Cellulose",** Kathmandu, Nepal. *12th- 13th January 2015*

J. Giri, S. P. Khatiwada, H. H. Le, H.-J. Radusch, R. Lach, W. Grellmann, A. K. Bledzki, L. K. Shrestha, R. Adhikari

IWOSEE 2015, *Oral presentation* **"Biodegradable Copolyester Composites reinforced with Wheat Stalk Microcrystalline Cellulose".** Merseburg, Germany. *12th April, 2015*

J.Giri, H. H. Le, H.-J. Radusch, R. Lach, W. Grellmann, R. Adhikari

IUPAC-2015, *Poster presentation* **"Biodegradable Composites of Copolyester with Microfibrillated Cellulose from Wheat Stalk".** Busan Korea. *9th -14th August 2015*

J. Giri, H. H. Le, R. Lach, W. Grellmann, R. Adhikari

ISC- 2015, Oral presentation entitled **"Biodegradable Copolyester Composites with Wheat Stalk Microfibrillated Cellulose". Kathmandu, Nepal,** *8h- 9th December 2015*

J.Giri, H.H. Le, H.-J. Radusch, R. Lach, W. Grellmann, R. Adhikari

ICIDN- 2015, Oral presentation entitled **"Studies on Degradable Polyester Based Composites for Biomedical Application",** Kathmandu Nepal. *15h- 18th December 2015*

J.Giri, H.H. Le, H.-J. Radusch, R. Lach, W. Grellmann, R. Adhikari

IWOSEE 2015, *Oral presentation* **"Biodegradable Copolyester Composites reinforced with Wheat Stalk Microcrystalline Cellulose".** Pokhara Nepal, *12th April, 2015*

J.Giri, H.H. Le, H.-J. Radusch, R. Lach, W. Grellmann, R. Adhikari

16ACC, *Oral presentation* **"Reinforcement of Wheat Stalk Microcrystalline Cellulose in Biodegradable Copolyester Composites"** Dhaka, Bangladesh, *16th -19th March, 2016*

J. Giri, R. Adhikari, R. Lach, H. H. Le, W. Grellman, H.-J.Radusch

7th National Conference on Science and Technology, Oral presentation "**Completely**

Biodegradable Composites based on Copolyester". Kathmandu, Nepal, *29th -31st March, 2016*

J. Giri, R. Lach, H. H. Le, W. Grellmann, H.-J. Radusch, G. H. Michler, J. M. Saiter, S. Henning, R. Adhikari

2nd NSNMP-2016, *Oral presentation* "**Biodegradable Copolyester Composites Reinforced by Wheat Stalk Microcrystalline Cellulose".** Dhulikhel, Nepal, *1st June, 2016*

J. Giri, R. Lach, H. H. Le, W. Grellmann, H.-J. Radusch, G. H. Michler, J. M. Saiter, S. Henning, R. Adhikari

PolyCHAR 2017, *Poster presentation* **"Biodegradable Copolyester Composites reinforced with Wheat Stalk Microcrystalline Cellulose",** Kwalalampur, Malaysia, *7th - 12th October, 2017*

J.Giri , H.H. Le, H.-J. Radusch, R. Lach, W. Grellmann, R. Adhikari

PolyMerTech-2018, *Oral presentation* **"Wheat Stalk Microcellulose as a Bioresource to Fabricate Biodegradable Copolyester Composites". Merseburg, Germany,** *13th -15th June, 2017*

J. Giri, R. Adhikari, R. Lach, H. H. Le, W. Grellman, H.-J.Radusch

PolyMerTech2018, *Poster presentation* **"Thermal, Mechanical and Surface Properties of Wheat Stalk Nanocellulose-Filled Biodegradable Composites" Merseburg, Germany.** *13th -15th June, 2017*

J. Giri, S. Bhasney, R. Lach, V. Katiyaar, R. Adhikari

8th IUPAC Green Chemistry 2018, *Oral presentation* **"Thermal, Mechanical and Surface Properties of Wheat Stalk Nanocellulose-Filled Biodegradable Composites", Bangkok , Thialand,** *9th -14th September, 2018*

J. Giri, S. Bhasney, R. Lach, V. Katiyaar, R. Adhikari

47th IUPAC World Chemistry Congress, *Poster presentation* **"Degradation Behavior of Wheat Straw Based Micro- and Nanocellulose Fabricated Green Composites with Copolyester",** Paris, France, 7th-12th July, 2019

J. Giri, R. Lach, J. M. saiter, S. Henning, V. Katiyar, R. Adhikari

14. Problemseminar
Deformation und Bruchverhalten von Kunststoffen

polymertec 14
Internationale wissenschaftliche Tagung Polymerwerkstoffe in Merseburg

Teilnahmebescheinigung

Certificate of attendance

Hiermit wird bestätigt, dass
Here we confirm that

Mrs. Jyoti Giri

vom 25.06 bis 27.06.2014 an der Tagung polymertec^{14} / 14. Problemseminar „Deformation und Bruchverhalten von Kunststoffen“ in Merseburg teilgenommen hat.
attended the Conference polymertec^{14} as well as the 14th Seminar „Plastics deformation and fracture behavior” which took place in Merseburg, from 25th ´til 27th June 2014.

Die Tagung beinhaltete folgende Sektionen:
The Conference included the following sections:

- Polymerchemie & Analytik *(Polymer chemistry and polymer analytics)*
- Struktur & Morphologie *(Structure and morphology)*
- Polymerblends & Nanocomposites *(Polymer blends and nanocomposites)*
- Kautschuk & Gummi *(Natural and synthetic rubber)*
- Kunststoffverarbeitung *(Polymer processing)*
- Deformation & Bruchverhalten von Kunststoffen *(Plastics deformation and fracture behavior)*
- Kunststoffinnovationen & Anwendungen *(Plastics innovations and applications)*

IPW

Institut für Polymerwerkstoffe e.V.
An-Institut an der Hochschule Merseburg

Institut für Polymerwerkstoffe e.V.
An-Institut an der HS Merseburg
Dr.-Ing. Marcus Schoßig
Geusaer Str., Geb. Fo 134
06217 Merseburg

Dr. Marcus Schoßig

2nd International Conference on

INFECTIOUS DISEASES AND NANOMEDICINE – 2015
(ICIDN - 2015), DECEMBER 15 - 18, 2015

Certificate

It is herewith certified that

Prof. / Dr./ Mr./ Mrs. **Jyoti Giri, NEPAL**

participated/contributed a paper as keynote/invited/
oral lecture/poster
in
2nd International Conference on
Infectious Diseases and Nanomedicine – 2015
(ICIDN -2015)
held in Kathmandu, Nepal.

S. Thapa
Santosh Thapa
Co-convener

Dr. Rameshwar Adhikari
Convener

Supported by:

ESCMID EUROPEAN SOCIETY OF CLINICAL MICROBIOLOGY AND INFECTIOUS DISEASES

AMERICAN SOCIETY FOR MICROBIOLOGY

IUPAC-2015

48th IUPAC General Assembly August 7-14, 2015
45th IUPAC World Chemistry Congress August 9-14, 2015
Bexco, Busan, Korea

Certificate of Attendance

On Behalf of the Organizing Committee of the IUPAC-2015,
I hereby certify that

Jyoti Giri

has attended the 45th IUPAC World Chemistry Congress
held on August 9-14, 2015 at BEXCO, Busan, Korea.

Myung Soo Kim

Chairman, Organizing Committee
IUPAC-2015

IUPAC INTERNATIONAL UNION OF PURE AND APPLIED CHEMISTRY

KCS KOREAN CHEMICAL SOCIETY

Nepal Academy of Science and Technology

CERTIFICATE

Awarded to

Jyoti Giri

for active participation/paper presentation/~~poster presentation~~

in

THE 7th NATIONAL CONFERENCE ON SCIENCE AND TECHNOLOGY

SCIENCE, TECHNOLOGY AND INNOVATION FOR NEPAL'S GRADUATION TO DEVELOPING COUNTRY STATUS

March 29-31, 2016

Kathmandu, Nepal

Ramila Rani

Mrs. Ramila Shrestha Raut
Chief, Promotion Division

Dr. Buddhi Ratna Khadge
Secretary

Prof. Dr. Jiba Raj Pokharel
Vice-Chancellor

IUPAC
International Union of Pure and Applied Chemistry

INSTITUT KIMIA MALAYSIA

POLY CHAR

Certificate of Attendance

This is to certify that

JYOTI GIRI

has participated as a poster presenter in the

25TH POLYCHAR 2017
WORLD FORUM ON ADVANCED MATERIALS 2017

held on **OCTOBER 9 – 13, 2017 at**
PUTRA WORLD TRADE CENTRE, KUALA LUMPUR

Organised by

INSTITUT KIMIA MALAYSIA

Under the auspices of

THE SCIENTIFIC COMMITTEE OF WORLD FORUM ON ADVANCED MATERIALS
INTERNATIONAL UNION OF PURE AND APPLIED CHEMISTRY

Dato' Dr Ong Eng Long
President
Institut Kimia Malaysia

Jyoti GIRI

Kathmandu
Nepal

Paris, July 12th, 2019

CERTIFICATE OF ATTENDANCE

We are pleased to confirm the attendance of

Jyoti GIRI

50th General Assembly & 47th IUPAC World Chemistry Congress

5 - 12 July 2019 - Paris, France

HOPSCOTCH CONGRÈS

23/25 RUE NOTRE-DAME DES VICTOIRES CS 70228
75091 PARIS CEDEX, FRANCE
+33 1 41 34 20 00 - www.hopscotchcongres.com
Hopscotch Congrès – SAS au capital de 68 100 euros – RCS Nanterre B422 322 479

PUBLICATIONS

List of Publications

1. Jyoti Giri, Rameshwar Adhikari

   Structural and Thermal Characterization of different Types of Cellulosic Fibers

   BIBECHANA. 2019, ***16***, 177-186. (**Published**)

   DOI: https://doi.org/10.3126/bibechana.v16i0.21650

2. Jyoti Giri, Ralf Lach, Wolfgang Grellmann, Abu Bin Hasan Susan, Jean-Marc Saiter, Sven Henning, Vimal Katiyar, Rameshwar Adhikari.

   Compostable Composites of Wheat Stalk Micro and Nanocrystalline Cellulose and Poly(butylene adipate-co-terephthalate): Surface Properties and Degradation Behaviour. J.Appl. Polym. Sci. 2019, ***48149***, 1-10. (**Published**)

   DOI: 10.1002/app.48149

JOURNAL OF Applied Polymer SCIENCE

Compostable composites of wheat stalk micro- and nanocrystalline cellulose and poly(butylene adipate-*co*-terephthalate): Surface properties and degradation behavior

Jyoti Giri,[1,2,3] Ralf Lach,[4] Wolfgang Grellmann,[4] Md. Abu Bin Hasan Susan,[5] Jean-Marc Saiter,[6] Sven Henning,[7] Vimal Katiyar,[8] Rameshwar Adhikari[1,3,9]

[1]Central Department of Chemistry, Tribhuvan University, Kathmandu, Nepal
[2]Department of Chemistry, Tri-Chandra Campus, Tribhuvan University, Kathmandu, Nepal
[3]Nepal Polymer Institute (NPI), Kathmandu, Nepal
[4]Polymer Service GmbH Merseburg (PSM), Merseburg, Germany
[5]Department of Chemistry, Dhaka University, Dhaka, Bangladesh
[6]Université de Normandie Rouen Laboratoire SMS Faculté des Sciences and Onyx Developpement, Rouen, France
[7]Fraunhofer Institute for Microstructure of Materials and Systems (IMWS), Halle, Germany
[8]Department of Chemical Engineering, Indian Institute of Technology (IIT), Guwahati, India
[9]Research Centre of Applied Science and Technology (RECAST), Tribhuvan University, Kathmandu, Nepal
Correspondence to: R. Lach (E-mail: ralf.lach@psm.uni-halle.de) and R. Adhikari (E-mail: nepalpolymer@yahoo.com)

ABSTRACT: An agricultural waste, the wheat stalk, was used for the extraction of microcrystalline cellulose (MCC) and nanocrystalline cellulose (NCC) *via* a series of thermochemical and mechanical treatments. The MCC and NCC were then compounded with the biodegradable polymer, poly(butylene adipate-*co*-terephthalate), PBAT, by melt mixing. The properties of the composites were evaluated by soil composting, contact angle and water absorption measurements, scanning electron microscopy (SEM) and gel permeation chromatography (GPC). The cellulosic filler was found, as per SEM results, to uniformly disperse in the polymer matrix forming a quite homogeneous composite which visibly degraded completely within a few months under soil composting and showed high water absorption, these properties being enhanced with the filler content. Compared to the neat PBAT, the composites showed enhanced surface hydrophilicity thereby increasing the ability of degradation. In spite of seemingly remarkable change in mechanical stability of the polymers under soil burial for several months, relatively low lowering of the molecular weight was observed. © 2019 Wiley Periodicals, Inc. J. Appl. Polym. Sci. **2019**, *136*, 48149.

KEYWORDS: composting; electron microscopy; gel permeation chromatography; polymer composites; surface wetting

Received 24 January 2019; accepted 11 May 2019
DOI: 10.1002/app.48149

INTRODUCTION

Plastics have become a part of life in the modern civilization but have seemingly posed serious challenges (and in some cases tremendous threats) to the mankind.[1–3] In particular, nowadays, catastrophic deposition of fossil fuel-based commodity plastics (such as polyolefins, polyesters, polycarbonates, and foamed polystyrenes) on coastal areas find extensive discussion and these have even created unpleasant rumors.[4–6] The microplastics have created deep-rooted concerns pertaining to possible environmental hazards and threats to human health and wellbeing of aquatic and soil organisms. In fact, the classical plastics need careful attention in terms of their management and ecofriendly recycling.[7–9]

The petroleum-based plastics, being very rebellious in terms of degradation and combustion, can even cause more pollution in water and air.[10] Thus, searches for alternatives of such plastics are going on. Many researchers have proposed using biodegradable copolyesters,[11] which are easily attacked by microbes in the environment to disintegrate into smaller fragments by hydrolyzing their ester bonds.[12,13] In this context, several "biodegradable" and biobased plastics have been commercialized.[14–16] The composites of these materials with natural fibers are more environment-friendly and have good mechanical, thermal and other functional properties similar to the tough synthetic polymers.[17–20] Many studies have proved that the degradation

behavior of such polymers can be tuned preciously on mixing with biofillers of animals or plant origins such as chitosan, hydroxyapatite, microcrystalline cellulose (MCC), and nanocrystalline cellulose (NCC).[19,21,22]

Turning towards the renewable flora-based resource of the nature, either from agriculture or from the forest products, it can be observed that major part of the plant bodies are made up of macromolecular cellulosic materials. After end use of the products, a large part of the agricultural and forest residues becomes wastes. Thus, these waste parts of the plants can be one of the renewable resources to prepare MCC and NCC, which is in line with one of the major principles of the green chemistry signifying the conversion of waste to value added products.[11,20,23–27]

This article discusses the influence of biobased fibrous filler originating from agricultural wastes on the wetting properties, degradability and stability of the polymer composites based on commercially available, degradable aliphatic–aromatic copolyester. One of the timely and relevant questions at hand is whether or not the given degradable product is prone to produce persistent microplastics aggregates.

EXPERIMENTAL PART

Materials

Chemicals. The laboratory grade chemicals (such as NaOH, NaOCl, $NaHSO_3$, H_2SO_4, and absolute alcohol) were purchased from Qualigen Fisher Scientific, Mumbai and were used without further purification.

The Polymer Matrix. Completely biodegradable poly(butylene adipate-*co*-terephthalate), PBAT (Ecoflex FBX 7011, a commercial product of BASF SE, Ludwigshafen, Germany), was used as matrix. According to the manufacturer, it has density of 1.26 g/cm^3. The average molecular weight (M_w) and polydispersity index (D) of the polymer determined using polystyrene standard was found to be 93 800 g/mol and 2.1.

The Filler. The MCC and NCC were extracted from the agricultural waste, the wheat stalk (*Triticum aesativa*) straw, *via* a series of mechanical and chemical treatments using standard protocols.[10,28–30] Briefly, the wheat stalks were chopped into small pieces and ground to powder to particle diameter < 200 μm. The wheat stalk flour was then treated with 5% NaOH solution (solid to liquid ratio 1:50 for 4 h at 60 °C to remove lignin and hemicelluloses).[28] The powder was washed thoroughly with deionized water and bleached with 4% NaOCl solution for 1 h at 60 °C. Finally, the bleached powder was treated with 10 and 64% concentrated sulfuric acid, respectively for microfibrillation and nanofibrillation for an hour.

The MCC and NCC formed were washed properly with deionized water to neutral pH; finally with ethanol and dried in vacuum oven at 80 °C for 8 h. NCC was separated from the acid solution by centrifuging and washed with deionized water to neutral pH and dried in the lyophilizer using standard protocols.

Composites Preparation

The required amount of polymer and MCC or NCC was melt-mixed using an internal mixture (Brabender Plasti-Corder PL-2100) at 120 °C for 15 min at the screw rotation speed of 70 rpm. The mixtures were then compression-molded to approximately 1 mm thick plaques using molding apparatus (COLLIN P200P/M) at 160 °C using 100 MPa pressure for 4 min followed by water cooling.

For the NCC composites, the strips, 1 mm thick and 5 mm wide, were prepared using twin-screw extruder mixing the constituents at the speed of 100 rpm for 7 min. The samples prepared in this way are listed in Table I.

Characterization Techniques

Scanning Electron Microscopy (SEM). Morphology of the samples was observed by SEM (JEOL JSM 6300 and Zeiss Gemin FESEM). The cryo-fractured surfaces of each specimen prepared by using liquid nitrogen were sputter-coated with about 5 nm thin gold film prior to Joel SEM imaging.

Fourier Transform Infrared (FTIR) Spectroscopy. The FTIR spectra of the samples were recorded by FTIR spectrometer (Perkin Elmer FTIR 2000) in attenuated total reflectance (ATR) mode within the wavenumber range of 4000 to 700 cm^{-1} with resolution of 20 cm^{-1} and 4 scans per sample.

Contact Angle Measurements. The surface contact angles were measured on the sample surfaces at room temperature using drop shape analyzer (DSA25, KRÜSS GmbH, Germany) with ~4 μL drop volume of Millipore water at 23 °C by sessile drop method.[31]

Table I. List of Polymer Composites Studied in this Work with their Name Codes

Sample code	PBAT weight fraction	MCC weight fraction	Sample code	PBAT weight fraction	MCC weight fraction
PBAT	100	0	PBAT	100	0
M-05	100	5	M-01	100	1
M-10	100	10	M-02	100	2
M-20	100	20	M-03	100	3
M-40	100	40	M-05	100	4
M-60	100	60	M-10	100	5

M-X = composites with the MCC; and N-X = composites with the NCC; the number followed by hyphen (–) denote the weight fraction of the filler per 100 g parts by the weight of PBAT.

Water Absorption Test. The water absorption was carried out in an environmental chamber VCL 7018 from Vötsch Industrietechnik GmbH, Germany using 2.5 cm × 2.5 cm size samples at 23 °C for a week. The water content was monitored gravimetrically[32]:

$$\text{Water absorbed by the composites } (\%) = \frac{w_f - w_i}{w_i} \times 100\ \%, \quad (1)$$

where w_i and w_f denote the initial and final weight of the specimen at hand.

Soil Compositing Experiments. Soil composting degradation tests were performed for the PBAT/MCC composites using 8 cm × 8 cm specimens. The composites were buried flat 40 cm down into the soil at different places, at least 15 cm apart from each place. After the burial, samples were watered and legumes were planted on the top of the soil. Water was sprinkled two times a day (morning and evening) to keep the soil moist.[22] Surface morphology of the samples was observed by digital camera before and after composting while detailed morphological studies were carried out by SEM.

Gel Permeation Chromatography (GPC). GPC analysis was carried out using Shimadzu LC Solution Chromatograph with refractive index detector (RID-10A), at 1 mL/min eluent flow rate and 40 μL sample injection volume. In a typical experiment (40 mg) of specimens were dissolved in 20 mL of HPLC grade chloroform for 2 days and filtered using 0.25 μm membrane filters (HPLC—high performance liquid chromatography). The instrument was calibrated with polystyrene (PS) standards.[33]

RESULTS AND DISCUSSION

Structural Characterization

Figure 1 presents the typical morphological illustration of one of the composites on the basis of SEM analysis. The lower and higher magnification SEM micrographs depicting the internal morphology of the composite comprising 40 weight fraction MCC (*i.e.*, the sample M-40) is shown in Figure 1. The weight fractions of the constituents for morphology comparison is chosen in such a way that the filler content is maximum for insuring the filler still acting as dispersed phase.

The micrograph in the lower magnification [Figure 1(a)] shows that there are regions with relatively smoother as well as rougher textures. The filler particles are indicated by white arrows so that they can be easily distinguished in the micrographs. Nevertheless, at the first glance, it can be observed that the composite is quite homogeneous mixture of the polymer and the MCC. The average thickness of the MCC fibers is 5 μm while the average length is about 100 μm.

A closer look at the higher magnification of SEM micrograph [see Figure 1(b)] shows that there is no strong chemical interaction between the polymer matrix and filler in agreement with then FTIR results. In addition, the presence of small gaps at the MCC/PBAT interfacial region also supports this notion.

These results are in consistence with the conclusions drawn in similar works reported in the literature including blends and composites with chitosan,[22] starch,[34] clay,[35] and other systems comprising polylactides and other degradable systems.[36–39]

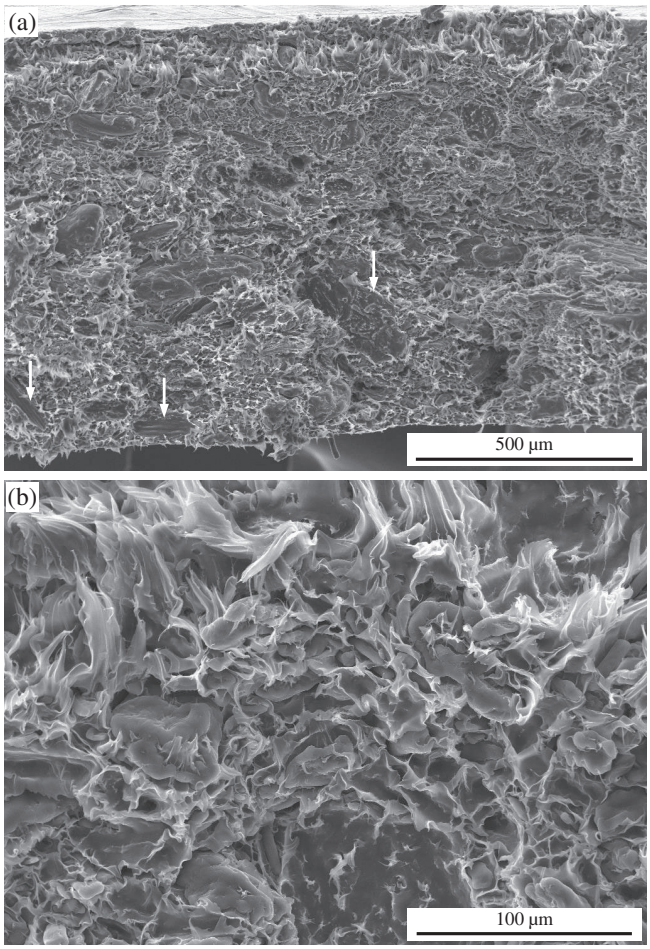

Figure 1. SEM micrographs of cryo-fractured surface of sample comprising 40 parts by weight of microcrystalline cellulose (MCC) (M-40) showing homogeneous dispersion of the MCC along the specimen cross-section; lower (a) and higher (b) magnifications.

The microscopic results also provide important clues on the dispersion and possible segregation of any of the components in a composite material.[37–41] The closer look at the low-resolution SEM micrograph of the composite in Figure 1(a) towards any of the edges of the specimen shows primarily the surface coverage by the PBAT phase as there is no clear sign of MCC particles (shown by white arrows) present at the surface.

For comparison, in Figure 2, the morphology of a nanocomposite of the PBAT comprising five weight fraction of the NCC (the sample N-5), extracted from the same source as the MCC, is presented. Also here, lower and higher magnifications of the SEM images are presented. Indeed, the nanofiller content that brings the significant effect of large surface areas on the properties of the nanocomposites lies in the range of 1–5 wt%.[42–44] Thus, it makes sense to present the results comprising lower amount of the nanofiller.

As in the previous case with the MCC, the dispersion of the NCC in the polymer matrix is quite uniform, with no noticeable tendency of agglomeration of the filler into the polymer matrix. The agglomeration tendency of the nanofiller into the polymer is a sign of the incompatibility of the filler with the adhering

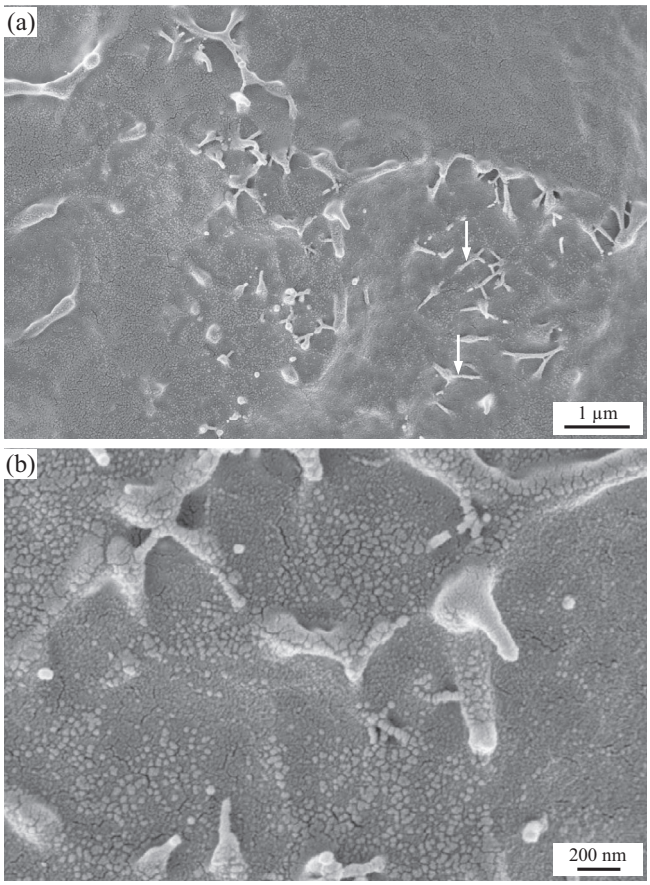

Figure 2. SEM micrographs of sample comprising five parts by weight of nanocrystalline cellulose NCC (N-5); lower (a) and higher (b) magnifications.

matrix.[45] The micrographs presented in Figure 2 depict a reasonable PBAT/NCC compatibility, which is also supported by the presence of cylindrical shaped fillers with thickness in the range of 40–80 nm.

The cryo-fractured surface of the sample under the SEM looks quite smooth due to the homogeneous dispersion of NCC in the PBAT matrix as well as good compatibility of NCC with PBAT. On measuring the thickness of individual nanocrystals and corresponding microcrystals presented in the SEM images, the average number of the nanocrystals per microcrystal bundle can be estimated as 100. Thus, it can be concluded that the nanofibrillation brings in case of cellulosic materials an increase in the surface area by at least 100 times. Therefore, the nanocomposites can be considered to be about 100 times more effective than the conventional counterparts in terms of several physical properties such as water absorption and ease of degradability.

Spectroscopic Characterization

Figure 3 shows absorption spectra of the M-5 composites which are exactly similar in pattern as of the PBAT. The PBAT, M-5 and N-5 all show absorption peaks at 2959 to 2845 cm^{-1} (corresponding to C—H stretching),[46,47] the intense peak at 1711 cm^{-1} (representing C═O stretching) and another intense

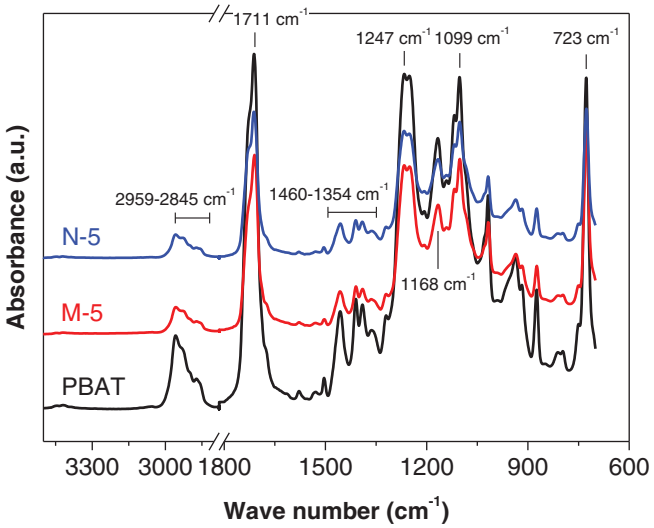

Figure 3. FTIR absorption spectra of the PBAT compared to that of sample comprising five parts by weight of microcrystalline cellulose (M-5) and sample comprising five parts by weight of nanocrystalline cellulose (N-5) composites. [Color figure can be viewed at wileyonlinelibrary.com]

peak at 1247 cm^{-1} (corresponding to C—O stretching of carbonyl group).[49,50] The small peaks at 1460–1354 cm^{-1}[48] gives absorption for vibrational stretching of C—H bond in CH_3 group of the PBAT. The peak at 1099 cm^{-1} indicates the presence of C—O—C stretching vibration of ester bond of the PBAT. Similarly, the peak centered at 723 cm^{-1} represents the aromatic ring present in the PBAT.[51]

In contrast, there are no visible peaks corresponding to MCC and NCC surface. The presence of all those peaks corresponding to the PBAT in both the composites indicates the dominance of PBAT towards the surface of the composite films. This could be due to the lower concentration of MCC and NCC in the composites and no specific chemical bond formed during compounding of MCC and NCC with PBAT, although there is quite homogeneous mixing.

The spectroscopic data are very well consistent with the microscopic results which also showed no segregation of the fibers towards the surface [compare with Figure 1(a)]. These are also in agreement with literatures.[52] The FTIR spectra further illustrate that in spite of good compatibility between MCC as well as NCC with the PBAT, there is no bonding of chemical nature, also supporting the notion of microscopic results (see Figure 1).

Surface Contact Angle Measurements

The surface property of the composites, particularly the hydrophilicity, also correlates with their susceptibility towards degradation. The nature of the surface determines how the material responds with highly polar substances such as water. During contact angle measurements, generally, the water droplets form the angles with interacting surfaces whose dimension depends upon hydrophilicity or hydrophobicity of the substrate. Higher contact angle represents hydrophobicity whereas lower contact angle represents hydrophilicity.[53,54]

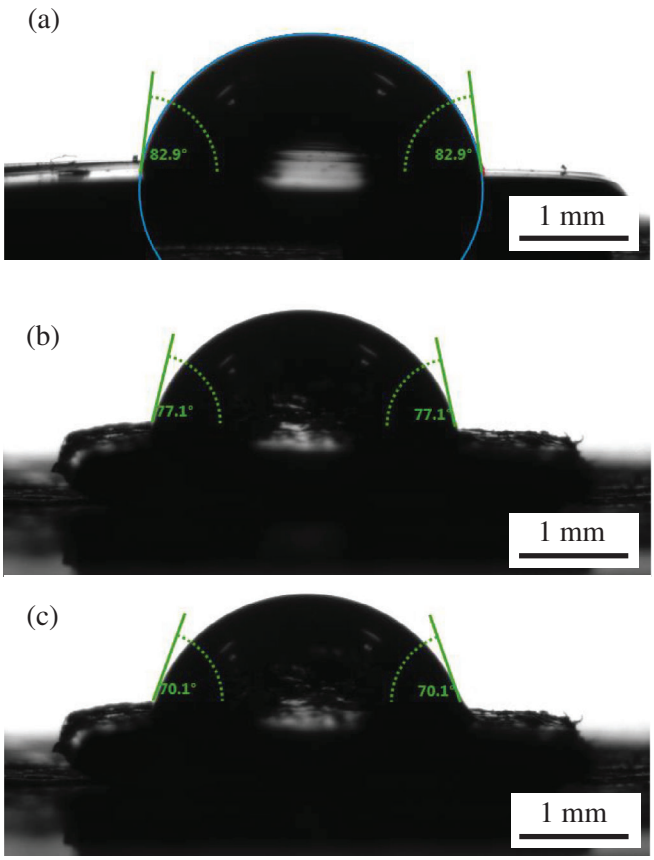

Figure 4. Photographs showing spontaneous contact angles of water droplets on the surfaces of (a) pure PBAT, (b) composite comprising five parts by weight of microcrystalline cellulose (M-5), and (c) composite comprising five parts by weight of nanocrystalline cellulose (N-5). [Color figure can be viewed at wileyonlinelibrary.com]

Figure 4 shows spontaneous contact angles formed by water droplets on the surfaces of pure PBAT and two different composites (M-5 and N-5). At the first glance, the contact angle on the PBAT surface looks slightly larger (implying slightly higher hydrophobicity) than on that of the composites. Indeed, the contact angles θ measured for the surfaces of PBAT, M-5, and N-5 composites are 83.3°, 77.1°, and 70.1°. The decreased hydrophobicity of the composites surfaces compared to the pure PBAT can be attributed to the presence of the hydrophilic cellulosic fractions.[55] The fact, that the spontaneous contact angles of both the composites M-5 and N-5 are not similar, further illustrates that the hydrophobicity of the specimens primarily depends not only on the chemical nature but also on the dimensional nature (micro- or nanoscale) of the biofiller which means that we observe scale effect. The similar scale effect is also observed for M-10 (θ = 71.1°) and N-10 (θ = 68.8°), respectively (see Figure 5). The results imply that the lower the particle size of the hydrophilic fillers the higher would be the ease of filler dispersion in composites and thus higher would be the interaction with water, the result is consistent with literature work.[54]

The results from surface contact angle measurement, however, suggest that there is some segregation of the cellulose towards the sample surface that attracts water onto it. It should be recalled that no clearly visible evidence of surface segregation of the filler was observed in the electron micrographs. It has to be kept in mind that the electron microscopic data provide quite local structural details of the materials, as a matter of fact, that do not necessarily correlate with the macroscopic properties with high precision.[41]

To analyze the wetting behavior of the samples in more details, the contact angles formed by the composites were investigated at different intervals of time. The results are summarized in Figure 5 with contact angles presenting variation of time with residence of the water drops onto the samples surface.

It can be further observed that the contact angle is decreasing with progress of time and increase in NCC contents for PBAT/NCC composite, indicating enhancing hydrophilic character. For instance, N-10 composite has the contact angle value of 77.1° which decreases to 68.8° after 60 s of water–substrate interaction.

Figures 4 and 5 both show lower contact angle values for the composites containing the NCC particles. In other words, lover the particles size lover will be the contact angle values. These observations manifest the increasing hydrophilic character in nanocomposites in comparison to the microcomposites due to the wider homogeneous dispersion of NCC in the PBAT matrix. NCC being smaller in size and dispersion is 100 times more than that of MCC as indicated by the morphological explanation. Similar types of results were reported in literature where the hydrophilic nanocellulose in the composites interacts with water showing lower contact angle value.[54] Other hydrophilic nanoparticles such as calcium phosphate in polystyrene also increase hydrophilicity[56] whereas hydrophobic glass fiber in epoxy resin showed decrease in hydrophilic character of the composite,[57] which indicate that the nature of filler in composite changes wettability of the composite. This directly proves that MCC and NCC being hydrophilic in nature increases hydrophilicity in their composites with PBAT. Moreover wider dispersion of NCC in PBAT matrix further increases hydrophilic character.

In conclusion, the wettability behavior can be correlated with the degradation susceptibility of the composites at hand, the nanocomposites being more susceptible to water absorption and thereby providing higher ease of degradation under soil burial conditions (to be discussed later in another section). Thus, in order to gain additional insight into, the water absorption behavior of the composites materials were studied in more details using environmental chamber using the composites with MCC.

Water Absorption Behavior

As already mentioned in earlier section, the water absorption property of the composites can be regarded as an important signature for their degradability. Figure 6 shows the percentage water uptake capacity of different PBAT/MCC composites as a function of MCC content at 23 °C. It can be observed that the pure PBAT absorbs about 1 wt% of water with respect to total weight of the polymer after 24 h. This practically insignificant amount of water absorption can be attributed to the partial polarity in the C=O bond present in the PBAT.[58] This notion is also

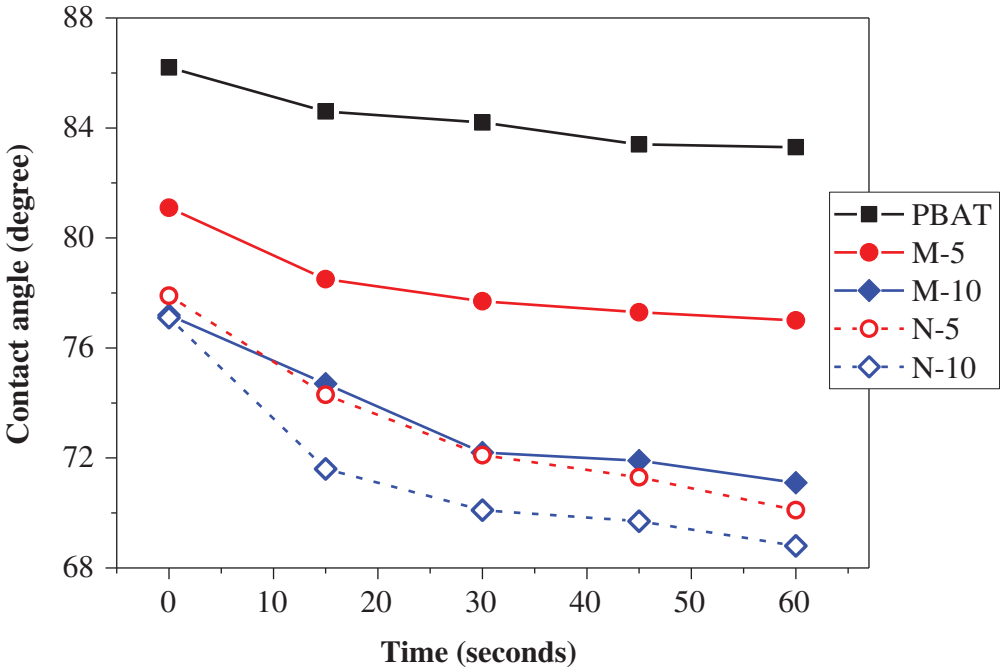

Figure 5. Contact angles of water droplets on different samples surfaces after various time intervals. [Color figure can be viewed at wileyonlinelibrary.com]

supported by the relatively low contact angle of the pure PBAT (see Figure 5) compared to purely hydrophobic polymers such as polypropylene PP (θ = 170°) and polystyrene PS (θ = 140° – 150°).[59,60]

Figures 6 and 7 depict the amount of water uptake as a function of the time of treatment of the samples inside the environmental chamber recorded up to 7–8 days for the composites with different amount of MCC and NCC, respectively. The nature of the shape of the curves is found to be identical for both MCC and NCC composites independent of the amount of the filler content. A steady-state plateau is reached for each sample after about 6 days.

The composite M-10 absorbed quite little amount of water (2% of its dry weight after 6 days) whereas pure PBAT absorbed even smaller amount of water (only 1% of its dry weight). The water absorption was found to be further increase with the increase of the exposure time and content of MCC. For instance, the sample M-60 saturates with water, about 12% of the sample weight on exposure to water vapor in the environmental chamber.[61]

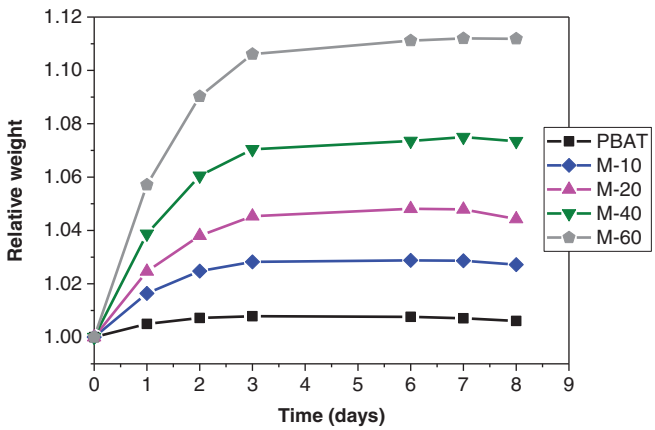

Figure 6. Variation of the water uptake amount by the PBAT-based composites comprising different amounts of microcrystalline cellulose (MCC). [Color figure can be viewed at wileyonlinelibrary.com]

Similar phenomena were seen in PBAT/NCC composites at laboratory at 23 °C for water uptake behavior with increasing concentration of NCC and with the function of time (see Figure 7). The comparison of Figures 6 and 7 shows that the amount of water absorbed is independent of particle size as N-10 and M-10 absorb practically equal amount of water.

The increasing trend of water absorption phenomena shown in Figures 6 and 7 can be correlated to state the increasing concentration of MCC and NCC enhances water-holding capacity in the composites, respectively.[31] The notion that the water absorption occurs due to the increasing concentration of MCC and NCC in PBAT matrix is supported by literature.[61–65] Biomaterial chitosan also increases water absorption in PBAT/chitosan composite with its increasing concentration.[62] polylactide (PLA)/NCC absorbs higher amount of water compared to PLA/MCC.[63] Moreover, higher water interaction is observed for higher content of NCC in PLA.[64]

Degradation under Soil Burial Conditions

Morphological studies of the samples subjected to degradation under soil burial conditions were carried out using optical and electron microscopy which offer reliable information on the physical state of the composites under various stress conditions. Different stages of the surface morphological features of the samples subjected to different periods of soil burial were studied. The results are presented in Figures 8 and 9.

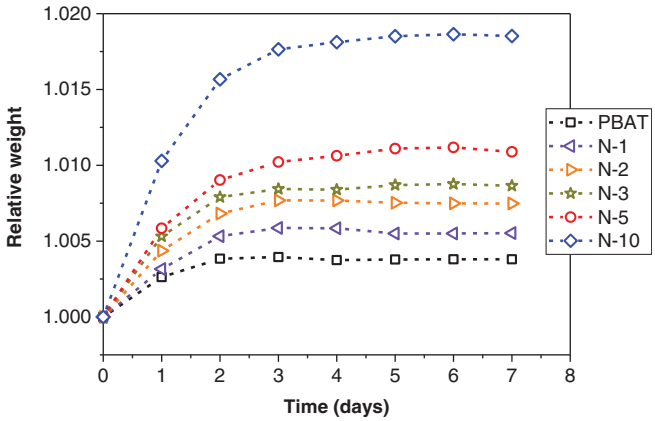

Figure 7. Variation of the water uptake amount by the PBAT-based composites comprising different amounts of nanocrystalline cellulose (NCC). [Color figure can be viewed at wileyonlinelibrary.com]

The photographs in Figure 8 shows that compared to the highly ductile nature of the PBAT, on soil composting, both the PBAT as well as its composites became quite brittle. The surface of the composites was found to be attacked by the microbes with some noticeable residual microbial pigments and the fungal growth on the sample surfaces. After 4 months of composting, the samples turned very brittle, the fragility of the specimen being more pronounced for the composites having higher amount of the MCC in the composites, also in consistence with the previous works.[22]

Among the results presented in Figure 8, morphological features of the composite M-20 were studied in detail with electron microscopy. Figure 9 shows fracture surface morphology of the sample M-20 after 2 and 4 months of soil composting.

In the beginning of the degradation [Figure 9(a,b)], the void-like structures of various sizes appear in the samples, which might have been formed by consumption of the filler particles as nutrients by the microbes. With increase in the soil burial period [Figure 9(a,b)], the amount of the fillers decrease which completely vanish after 4 months of soil burial [see Figure 9(c,d)]. At the same time, the PBAT matrix gets teared in random way further implying that the cellulosic filler augments the degradation of the PBAT.[33,66,67]

The samples became mechanically unstable and brittle upon soil burial for 4 months. Thus, even the sample collection after more than 4 months of degradation was not possible.

The variation of the molecular properties of the PBAT in neat form and in the form of related composites materials was investigated by gel permeation chromatography (GPC) using PS standard. The results are summarized in Table II.

GPC delivers quite reliably the comparative data for molecular size and their polydispersity index (D) (as denoted by the M_w/M_n values, where M_w and M_n stand for weight and number average molecular weights, respectively) of the polymer. For the sake of simplicity in comparison, we limit our discussion on the value of M_w.

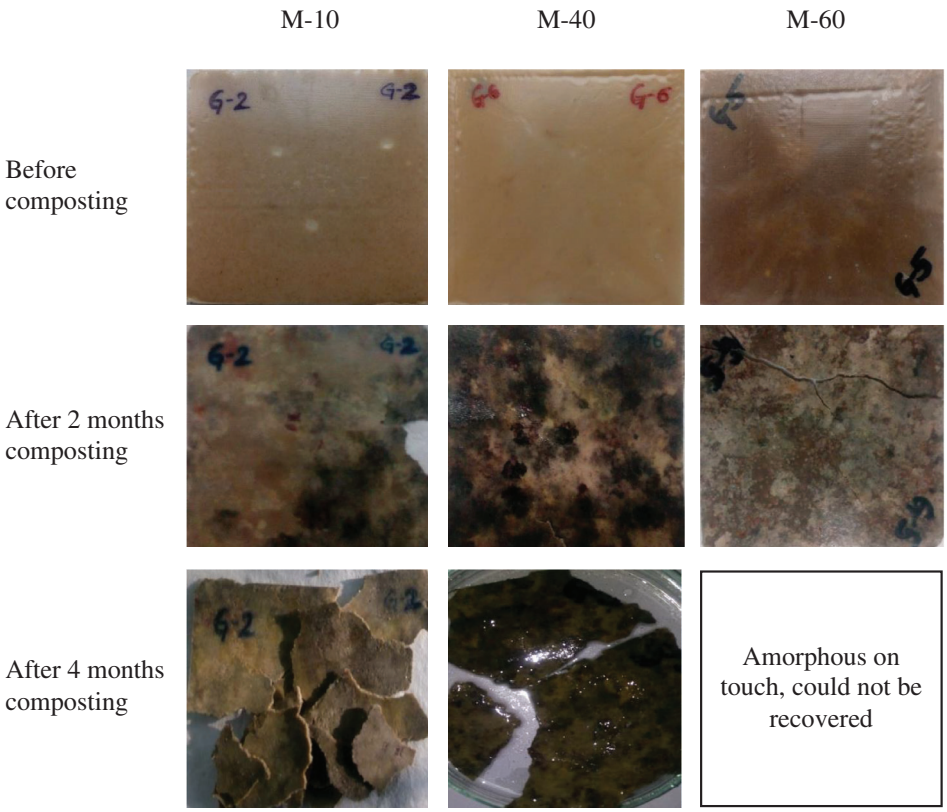

Figure 8. Photographs of different PBAT/MCC composites subjected to soil burial for different periods of time as indicated. [Color figure can be viewed at wileyonlinelibrary.com]

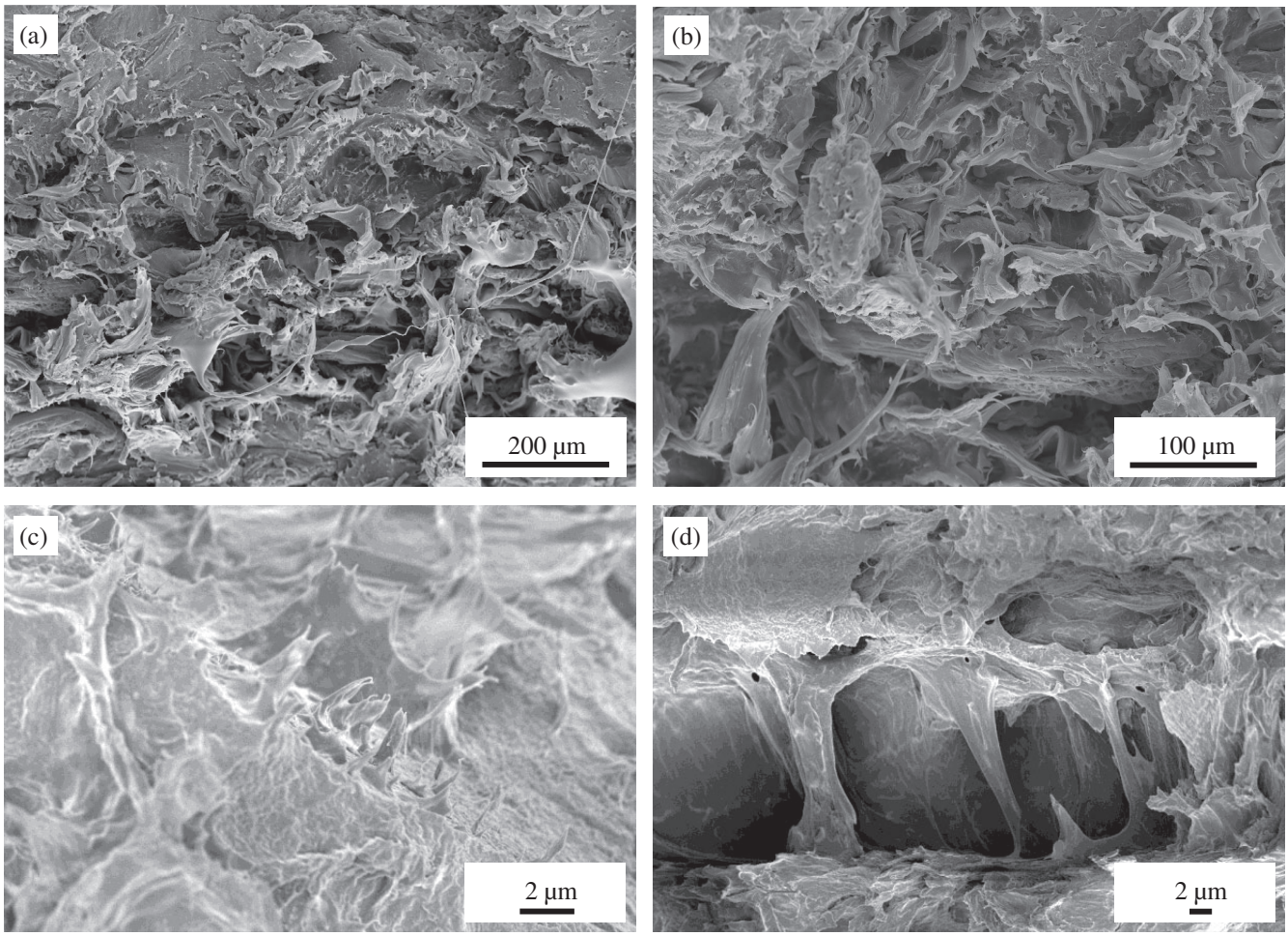

Figure 9. SEM micrographs of different lower (a, c) and higher (b, d) magnifications showing the fracture surface morphology of M-20 after 2 (a, b) and 4 (c, d) months of soil composting.

Table II. Molecular Weight Variation of PBAT in Pure Form and in Different Composites with MCC at Different Interval of Soil Burial Tests

	Nondegraded		2 months[a]		4 months[a]	
Sample code	M_w (kg/mol)	D	M_w (kg/mol)	D	M_w (kg/mol)	D
PBAT	48.62	2.01	[b]	[b]	21.60	2.04
M-20	37.27	1.90	32.61	2.03	23.32	2.66
M-40	[b]	[b]	[b]	[b]	18.64	2.36

[a] Soil burial period for composting experiment.
[b] Not measured.

The PBAT shows a complex chromatogram (details not presented here) with several peaks implying a wide distribution of molecular weights and distributions. We concentrate on the major peak values in this article.

From Table II, it is apparent that, under soil burial conditions, the M_w values of the pure PBAT decreases from 48.62 kg/mol to 21.60 kg/mol in 4 months. The value of D remains, however, constant. In case of M-20 composite, the M_w value for PBAT is smaller as compared to neat PBAT implying the processing-induced molecular weight degradation. Under soil burial condition, the M_w value decreases in the similar manner as the pure PBAT (from 37.27 kg/mol to 23.32 kg/mol in 4 months). Thus, the M_w value variation for the composite M-40 is more drastic as the apparent M_w value for PBAT in this case after 4 months is 18.64 kg/mol.

The results imply that cellulosic filler enhances the degradability of the polymer which is consistent also with the results from the microscopic studies; the higher amount of filler being more favorable for the molecular weight reduction. Similar type of molecular weight lowering was observed on soil composting of poly(butylene sebacate).[68]

It can be concluded that the PBAT shows significant ease of degradation in molecular weights under soil burial conditions which is further enhanced by the presence of the cellulosic filler. However, it should be stressed that the polymer chains are not completely degraded but are rather turned into smaller fragments that may be present for longer times as microscopic particles in the soil forming a sort of microplastics aggregates. The PBAT might be prone to further microbial degradation but based on the current results the duration of the PBAT in the soil and even in water flowing through the soil, as microscopic particles cannot be ascertained.

CONCLUSIONS

Micro- and nanocrystalline celluloses extracted from wheat stalk were compounded with biodegradable aliphatic–aromatic copolyester and their structural and degradation behavior was studied using various analytical techniques. The results can be summarized as follows:

1. The microscopic results revealed quite uniform mixture of the composites components. The biofiller was found to occasionally distribute towards the composite surfaces. The spectroscopic results attested the sparse distribution of the filler towards the surface.
2. Nanofiller was found to be, as expected, better reinforcing filler which also contributed more effectively to increase the hydrophilic character of the composites surfaces thereby enhancing the enhanced degradation of the composites.
3. The degradability of the composites was observed to increase with filler content on one hand, and with the period of soil burial experiment on the other.
4. The GPC results confirmed the degradation of molecular weight of the polymer under soil burial conditions while the macromolecular chains were not completely destroyed.

ACKNOWLEDGMENTS

J.G. sincerely acknowledges the Indian National Science Academy (INSA) and Nepal Academy of Science and Technology (NAST) for providing the fellowship to visit IIT Guwahati and for providing PhD research grants. She further thanks German Research Foundation (DFG) for offering financial supports for research stays in Germany.

REFERENCES

1. Panaitescu, D. M.; Frone, A. N.; Ghiurea, M.; Spataru, C. I.; Radovici, C.; Iorga, M. D. Properties of polymer composites with cellulose microfibrils. In Advances in Composite Materials: Ecodesign and Analysis; Attaf, B., Ed., IntechOpen, **2011**, Chapter 5. p. 103-22.
2. Verma, R.; Vinoda, K. S.; Papireddy, M.; Gowda, A. N. S. Toxic pollutants from plastic waste—a review, in: "International Conference on Solid Waste Management (5IconSWM 2015)", Proc. *Proc. Environ. Sci.* **2016**, *35*, 701-8.
3. Rist, S.; Almroth, B. C.; Hartmann, N. B.; Karlsson, T. M. A critical perspective on early communications concerning human health aspects of microplastics. *Sci. Total Environ.* **2018**, *626*, 720-6.
4. Hollman, P. C. H.; Bouwrneester, H.; Peters, R. J. B. Microplastics in the Aquatic Food Chain, Sources Measurement, Occurrence and Potential Health Risk, RIKILT Wageningen UR (University & Research Centre), RIKIT Report 2013.003, Wageningen, **2013**.
5. Barboza, L. G. A.; Vethaak, A. D.; Lavorante, R. B. O.; Lundebye, A. K.; Guilhermino, L. Marine microplastic debris: An emerging issue for food security, food safety and human health. *Mar. Pollut. Bull.* **2018**, *133*, 336-48.
6. Murtaza, G.; Habib, R.; Nawaz, R.; Javed, T.; Sardar, K.; Rasool, F.; Shahzad, M.; Rasool, A. A review study of waste-plastic and its deadly effects on eco-system. *Imp. J. Interdiscip. Res.* **2016**, *2*, 1330-9.
7. Hopewell, J.; Dvorak, R.; Kosior, E. Plastics recycling: Challenges and opportunities. *Philos. Trans. R. Soc. Lond. B Biol. Sci.* **2009**, *364*, 2115-26.
8. Trevail, A. M.; Kühn, S.; Gabrielsen, G. W. The State of Marine Microplastic Pollution in the Arctic, Kortrapport/-Brief Report No. 033, Norsk Polarinstitutt, FRAM Center, Tromsø, **2015**.
9. Cialdini, R. B.; Reno, R. R.; Kallgren, C. A. A focus theory of normative conduct: Recycling the concept of norms to reduce littering in public places. *J. Pers. Soc. Psychol.* **1990**, *58*, 1015-26.
10. Frone, A. N.; Panaitescu, D. M.; Donescu, D. Some aspects concerning the isolation of cellulose micro- and nanofibers. *UPB Sci. Bull. B: Chem. Mater. Sci.* **2011**, *73*, 133-52.
11. Siyamak, S.; Ibrahim, N. A.; Abdolmohammadi, S.; Md, W.; Yunus, Z. W.; Rahman, M. Z. A. B. Enhancement of mechanical and thermal properties of oil palm empty fruit bunch fiber poly(butylene adipate-co-terephthalate) biocomposites by matrix esterification using succinic anhydride. *Molecules*. **2012**, *17*, 1969-91.
12. Leja, K.; Lewandowicz, G. Polymer biodegradation and biodegradable polymers – A review. *Polish J. Environ. Stud.* **2010**, *19*, 255-66.
13. Yamamoto, M.; Witt, U.; Skupin, D. I. G.; Beimborn, D.; Müller, R. J. Biodegradable aliphatic–aromatic polyesters: "Ecoflex®". In Biopolymers, Vol. 4: Polyesters III: Applications and Commercial Products; Doi, Y.; Steinbüchel, A., Eds., Wiley-VCH: Weinheim, **2004**. p. 299-305.
14. Armentano, I.; Dottori, M.; Fortunati, E.; Mattioli, S.; Kenny, J. M. Biodegradable polymer matrix nanocomposites for tissue engineering: A review. *Polym. Degrad. Stab.* **2010**, *95*, 2126-46.
15. Armani, D. K.; Liu, C. Microfabrication technology for polycaprolactone, a biodegradable polymer. *J. Micromech. Microeng.* **2000**, *10*, 80-4.
16. Woodruff, M. A.; Hutmacher, D. W. The return of a forgotten polymer – Polycaprolactone in the 21st century. *Prog. Polym. Sci.* **2010**, *35*, 1217-56.
17. Vinayaka, D. L.; Guna, V. K.; Madhavi, D.; Arpitha, M.; Reddy, N. Ricinus communis plant residues as a source for natural cellulose fibers potentially exploitable in polymer composites. *Ind. Crops Prod.* **2017**, *100*, 126-31.

18. Graupner, N.; Ziegmann, G.; Wilde, F.; Beckmann, F.; Müssig, J. Prodedural influences on compression and injection moulded cellulose fibre-reinforced polylactide (PLA) composites: Influence of fibre loading, fibre length, fibre orientation and voids. *Compos. A: Appl. Sci. Manuf.* **2016**, *81*, 158-71.
19. Sapkota, J.; Jorfi, M.; Weder, C.; Foster, E. J. Reinforcing poly(ethylene) with cellulose nanocrystals. *Macromol. Rapid Commun.* **2014**, *35*, 1747-53.
20. Mandal, A.; Chakrabarty, D. Studies on the mechanical, thermal, morphologhical and barrier properties of nanocomposites based on poly(vinyl alcohol) and nanocellulose from sugarcane bagasse. *J. Ind. Eng. Chem.* **2014**, *20*, 462-73.
21. Fernandes, E. M.; Pires, R. A.; Mano, J. F.; Reis, R. L. Bionanocomposites from lignocellulosic resources: Properties, applications and future trends for their use in the biomedical field. *Prog. Polym. Sci.* **2013**, *38*, 1415-41.
22. Pokhrel, S.; Lach, R.; Le, H. H.; Wutzler, A.; Grellmann, W.; Radusch, H. J.; Dhakal, R. P.; Esposito, A.; Henning, S.; Yadav, P. N.; Saiter, J. M.; Heinrich, G.; Adhikari, R. Fabrication and characterization of completely biodegradable copolyester–chitosan blends: Spectroscopic and thermal characterization. *Macromol. Symp.* **2016**, *366*, 23-34.
23. Park, H. Y.; Kim, S. S.; Kim, S. G.; Seo, K. H. Modification of physical properties of PBAT by using TPS. *Int. Proc. Chem. Biol. Environ. Eng.* **2012**, *46*, 67.
24. Siyamak, S.; Ibrahim, N. A.; Abdolmohammadi, S.; Md, W.; Yunus, Z. W.; Rahman, M. Z. A. B. Effect of fiber esterification on fundamental properties of oil palm empty fruit bunch fiber/poly(butylenes adipate-co-terephthalate) biocomposites. *Int. J. Mol. Sci.* **2012**, *13*, 1327-46.
25. Cherian, B. M.; Leão, A. L.; de Souza, S. F.; Costa, L. M. M.; de Olyveira, G. M.; Kottaisamy, M.; Nagarajan, E. R.; Thomas, S. Cellulose nanocomposites with nanofibers isolated from pineapple leaf fibers for medical applications. *Carbohydr. Polym.* **2011**, *86*, 1790-8.
26. Siró, I.; Plackett, D. Microfibrillated cellulose and new nanocomposite materials: A review. *Cellulose*. **2010**, *17*, 459-94.
27. Mariño, M.; da Silva, L. L.; Durán, N.; Tasic, L. Enhanced materials from nature: Nanocellulose from citrus waste. *Molecules*. **2015**, *20*, 5908-23.
28. Das, M.; Chakraborty, D. Effect of alkalization and fiber loading on the mechanical properties of bamboo fiber composites, part 1: Polyester resin matrix. *J. Appl. Polym. Sci.* **2009**, *112*, 489-95.
29. Rajan, K. R.; Veena, N. R.; Maria, H. J.; Rajan, R.; Skrifvars, M.; Joseph, K. Extraction of bamboo microfibrils and development of biocomposites based on polyhydroxybutyrate and bamboo microfibrils. *J. Compos. Mater.* **2010**, *45*, 1325-9.
30. Liu, D. Y.; Yuan, X. W.; Bhattacharyya, D.; Easteal, A. J. Characterisation of solution cast cellulose nanofibre-reinforced poly(lactic acid). *eXPRESS Polym. Lett.* **2010**, *4*, 26-31.
31. Pal, A. K.; Katiyar, V. Thermal degradation behavior of nanoamphiphilic chitosan dispersed poly(lactic acid) bionanocomposite films. *Int. J. Biol. Macromol.* **2017**, *95*, 1267-97.
32. Wang, H.; Wei, D.; Zheng, A.; Xiao, H. Soil burial biodegradation of antimicrobial biodegradable PBAT films. *Polym. Degrad. Stab.* **2015**, *116*, 14-22.
33. Tesfaye, M.; Patwa, R.; Dhar, P.; Katiyar, V. Nanosilk-grafted poly(lactic acid) films: Influence of cross-linking on rheology and thermal stability. *ACS Omega*. **2017**, *2*, 7071-84.
34. Nayak, S. K. Biodegradable PBAT/starch nanocomposites. *Polym. Plast. Technol. Eng.* **2010**, *49*, 1406-18.
35. Fukushima, K.; Rasyida, A.; Yang, M. C. Characterization, degradation and biocompatibility of PBAT-based nanocomposites. *Appl. Clay Sci.* **2013**, *81–82*, 291-8.
36. George, M.; Shen, W. Z.; Montemagno, C. Development and property evaluation of poly (lactic) acid and cellulose nanocrystals-based films with either silver or peptide antimicrobial agents: Morphological, permeability, thermal and mechanical characterization. *IOSR J. Polym. Text. Eng.* **2016**, *3*, 33-43.
37. Shi, Q. F.; Zhou, C. J.; Yue, Y. Y.; Guo, W. H.; Wu, Y. Q.; Wu, Q. L. Mechanical properties and in vitro degradation of electrospun bio-nanocomposite mats from PLA and cellulose nanocrystals. *Carbohydr. Polym.* **2012**, *90*, 301-8.
38. Zehetmeyer, G.; Meira, S. M. M.; Scheibel, J. M.; de Oliveira, R. V. B.; Brandelli, A.; Soares, R. M. D. Influence of melt processing on biodegradable nisin–PBAT films intended for active food packaging applications. *J. Appl. Polym. Sci.* **2016**, *133*, 43212.
39. Carbonell-Verdu, A.; Ferri, J. M.; Dominici, F.; Boronat, T.; Sanchez-Nacher, L.; Balart, R.; Torre, L. Manufacturing and compatibilization of PLA/PBAT binary blends by cottonseed oil-based derivatives. *eXPRESS Polym. Lett.* **2018**, *12*, 808-23.
40. Kausch, H. H.; Michler, G. H. Effect of nanoparticle size and size-distribution on mechanical behavior of filled amorphous thermoplastic polymers. *J. Appl. Polym. Sci.* **2007**, *105*, 2577-87.
41. Michler, G. H.; Baltá-Calleja, F. J. Nano- and Micromechanics of Polymers: Structure Modification and Improvement of Properties; Carl Hanser Verlag: Munich, **2012**.
42. Cho, J.; Joshi, M. S.; Sun, C. T. Effect of inclusion size on mechanical properties of polymeric composites with micro and nano particles. *Compos. Sci. Technol.* **2006**, *66*, 1941-52.
43. Yang, Y.; Lan, J.; Li, X. C. Study on bulk aluminum matrix nano-composite fabricated by ultrasonic dispersion of nano-sized SiC particles in molten aluminum alloy. *Mater. Sci. Eng. A*. **2004**, *380*, 378-83.
44. Paul, D. R.; Robeson, L. M. Polymer nanotechnology: Nanocomposites. *Polymer*. **2008**, *49*, 3187-204.
45. Brinchi, L.; Cotana, F.; Fortunati, E.; Kenny, J. M. Production of nanocrystalline cellulose from lignocellulosic biomass: Technology and applications. *Carbohydr. Polym.* **2013**, *94*, 154-69.
46. Pei, A.; Zhou, Q.; Berglund, L. A. Functionalized cellulose nanocrystals as biobased nucleation agents in poly(L-lactide)

(PLLA) – Crystallization and mechanical property effects. *Compos. Sci. Technol.* **2010**, *70*, 815-21.

47. Satyamurthy, P.; Jain, P.; Balasubramanya, R. H.; Vigneshwaran, N. Preparation and characterization of cellulose nanowhiskers from cotton fibres by controlled microbial hydrolysis. *Carbohydr. Polym.* **2011**, *83*, 122-9.
48. Al-Itry, R.; Lamnawar, K.; Maazouz, A. Improvement of thermal stability, rheological and mechanical properties of PLA, PBAT and their blends by reactive extrusion with functionalized epoxy. *Polym. Degrad. Stab.* **2012**, *97*, 1898-914.
49. Kumar, M.; Mohanty, S.; Nayak, S. K.; Parvaiz, M. R. Effect of glycidyl methacrylate (GMA) on the thermal, mechanical and morphological property of biodegradable PLA/PBAT blend and its nanocomposites. *Bioresour. Technol.* **2010**, *101*, 8406-15.
50. Spoljaric, S.; Genovese, A.; Shanks, R. A. Polypropylene–microcrystalline cellulose composites with enhanced compatibility and properties. *Compos. A: Appl. Sci. Manuf.* **2009**, *40*, 791-9.
51. Weng, Y. X.; Jin, Y. J.; Meng, Q. Y.; Wang, L.; Zhang, M.; Wang, Y. Z. Material behavior biodegradation behavior of poly(butylene adipate-co-terephthalate) (PBAT), poly(lactic acid) (PLA) and their blend under soil conditions. *Polym. Test.* **2013**, *32*, 918-26.
52. Adhikari, R.; Bhandari, N. L.; Causin, V.; Le, H. H.; Radusch, H. J.; Michler, G. H.; Saiter, J. M. Study of morphology, mechanical properties, and thermal behavior of green aliphatic–aromatic copolyester/bamboo flour composites. *Polym. Eng. Sci.* **2012**, *52*, 2296-303.
53. Wang, X.; Cui, X. X.; Zhang, L. P. Preparation and characterization of lignin-containing nanofibrillar cellulose. *Proc. Environ. Sci.* **2012**, *16*, 125-30.
54. Pereda, M.; Amica, G.; Rácz, I.; Marcovich, N. E. Structure and properties of nanocellulose films based on sodium caseinate and nanocellulose fibers. *J. Food Eng.* **2011**, *103*, 76-83.
55. Dai, X. Y.; Xiong, Z.; Na, H. N.; Zhu, J. How does epoxidized soybean oil improve the toughness of microcrystalline cellulose filled polylactide acid composites? *Compos. Sci. Technol.* **2014**, *90*, 9-15.
56. Thomas, S. P.; Thomas, S.; Abraham, R.; Bandyopadhyay, S. Polystyrene/calcium phosphate nanocomposites: Contact angle studies based on water and methylene iodide. *eXPRESS Polym. Lett.* **2008**, *2*, 528-38.
57. Hameed, N.; Thomas, S. P.; Abraham, R.; Thomas, S. Morphology and contact angle studies of poly(styrene-co-acrylonitrile)-modified epoxy resin blends and their glass fibre-reinforced composites. *eXPRESS Polym. Lett.* **2007**, *1*, 345-55.
58. Morokuma, K. Molecular orbital studies of hydrogen bonds, III. C=O···H–O hydrogen bond in $H_2CO\cdots H_2O$ and $H_2CO\cdots 2H_2O$. *J. Chem. Phys.* **1971**, *55*, 1236-44.
59. Liu, M.; Jia, Z.; Liu, F.; Jia, D.; Guo, B. Tailoring the wettability of polypropylene surfaces with halloysite nanotubes. *J. Colloid Interface Sci.* **2010**, *350*, 186-93.
60. Zhang, J. F.; He, A.; Li, J. X.; Xu, J.; Han, C. C. Studies on the controlled morphology and wettability of polystyrene surfaces by electrospinning or electrospraying. *Polymer.* **2006**, *47*, 7095-102.
61. Wu, C. S. Characterization of cellulose acetate-reinforced aliphatic–aromatic copolyester composites. *Carbohydr. Polym.* **2012**, *87*, 1249-56.
62. Pokhrel, S. Chitosan-based Polymer Blends: Preparation, Mechanical Properties and Biodegradability. Ph.D. Thesis, Tribhuvan University, Central Department of Chemistry, Institute of Science and Technology, Kathmandu, **2016**.
63. Samarasekara, A. M. P. B.; Kumara, S. P. D. A.; Madhusanka, A. J. S.; Amarasinghe, D. A. S.; Karunanayake, L. Study of thermal and mechanical properties of microcrystalline cellulose and nanocrystalline cellulose based thermoplastic, In 2018 Moratuwa Engineering Research Conference (MERCon), IEEE Proceedings, 2018, p 465.
64. Liu, J.; Zhuo, Y. G.; Du, S. Z.; Li, Q. S. Preparation and characterization of PLA/NCC nanofibers. *Integr. Ferroelectr.* **2017**, *179*, 31-7.
65. Kramer, F.; Klemm, D.; Schumann, D.; Heßler, N.; Wesarg, F.; Fried, W.; Stadermann, D. Nanocellulose polymer composites as innovative pool for (bio)material development. *Macromol. Symp.* **2006**, *244*, 136-48.
66. Singh, B.; Sharma, N. Mechanistic implications of plastic degradation. *Polym. Degrad. Stab.* **2008**, *93*, 561-84.
67. Liu, Y.; Li, Y.; Chen, H. M.; Yang, G.; Zheng, X. T.; Zhou, S. B. Water-induced shape-memory poly(d,l-lactide)/microcrystalline cellulose composites. *Carbohydr. Polym.* **2014**, *104*, 101-8.
68. Siotto, M.; Zoia, L.; Tosin, M.; Innocenti, F. D.; Orlandi, M.; Mezzanotte, V. Monitoring biodegradation of poly(butylenes sebacate) by gel permeation chromatography, ^{1}H-NMR and ^{31}P-NMR techniques. *J. Environ. Manage.* **2013**, *116*, 27-35.

BIBECHANA
A Multidisciplinary Journal of Science, Technology and Mathematics
ISSN 2091-0762 (Print), 2382-5340 (0nline)
Journal homepage: http://nepjol.info/index.php/BIBECHANA
Publisher: Research Council of Science and Technology, Biratnagar, Nepal

Structural and thermal characterization of different types of cellulosic fibers

Jyoti Giri [1,2,3], Ralf Lach [4], Janak Sapkota [5], Md. Abu Bin Hasan Susan [6], Jean-Marc Saiter [7], Sven Henning [8], Vimal Katiyar [9], Rameshwar Adhikari [1,3,10]

[1]Central Department of Chemistry, Tribhuvan University, Kathmandu, Nepal
[2]Department of Chemistry, Tri-Chandra Campus, Tribhuvan University, Kathmandu, Nepal
[3]Nepal Polymer Institute (NPI),P. O. Box 24411, Kathmandu, Nepal
[4]Polymer Service GmbH Merseburg (PSM), Merseburg, Germany
[5]Institute of Polymer Processing, Department of Polymer Engineering and Science, Montanuniversitaet Leoben, Otto-Glockel-Strasse 2, 800 Leoben, Austria
[6]Department of Chemistry, Dhaka University, Dhaka, Bangladesh
[7]Université de Normandie Rouen Laboratoire SMS Faculté des Sciences and Onyx Developpment, Groupe-Nutriset, Rouen, France
[8]Fraunhofer Institute for Microstructure of Materials and Systems (IMWS), Halle/S, Germany
[9]Department of Chemical Engineering, Indian Institute of Technology (IIT), Guwahati, India
[10]Research Centre of Applied Science and Technology (RECAST), Tribhuvan University,Kathmandu, Nepal
[*]Email: nepalpolymer@yahoo.com

Article history: Accepted 14 November, 2018
DOI: http://dx.doi.org/10.3126/bibechana.v16i0.21650

Abstract

Micro- and nanocrystalline cellulose were extracted from wheat stalk (WS) using different thermomechanical and chemical treatments and characterized by spectroscopic, microscopic and diffraction techniques. The virgin WS fibers were found to be structurally quite similar to the commercial microcrystalline cellulose (MCC). Similar to the commercial one, the MCC extracted from the WS possessed intense infrared (IR) peaks whereas those peaks became more broader in the nanocrystalline cellulose (NCC) of the same origin, which can be attributed to possible breakdown of inter- and intramolecular H-bonding due to strong acid treatment of the MCC. Microscopic results revealed characteristic textures of the MCC and the NCC, the MCC being irregular bundles of the primary crystals bound together with the amorphous phase. The latter was found to disintegrate upon acid hydrolysis giving rise to the rod-shaped nanocrystals having much larger surface area and thus possessing more intense hydrophilic character. The MCC was found to be more stable than the NCC which can be attributed to the presence of protective and binding coating provided by the amorphous cellulosic matter.

Keywords: Natural fibers, Morphology, Electron microscopy, FTIR spectroscopy, Cellulose.

1. Introduction

Polymers and fibers from renewable resources as well as their combinations in different forms have become attractive alternatives to conventional plastics, blends and composites for different practical applications [1, 2]. Cellulose is one of the most abundant renewable natural resources. With the advancement in nanotechnology, the interests of polymer scientists have been attracted by micro- and nanocellulose of microbial as well as plants origin [1, 2]. Among the natural fibers, cellulosics of various types and dimensionalities have special position in technical applications such as biodegradable tissue scaffolds, drug delivery vehicles and implantable biomaterials, aerospace engineering, functional devices and electronics.

The applications of such materials include not only in paints, inks, cosmetics, and coatings but also in textiles, flexible electronics, packaging materials, and optical appliances [3–6]. Nanocellulose composites have high mechanical properties and are non-toxic in nature and hence can be used in wide application areas.

It has been recognized that the natural fibers are being progressively introduced in nanocomposite materials sectors as reinforcing agents for the fabrication of lightweight materials. These fibers not only enhance the mechanical and thermal properties but can also induce ease of degradation in the composites with other polymers [7–9]. Biodegradation can also be observed based on the water absorption capacity of the composites, which is one of the criteria required to be easily attacked by microbes [8, 9].

In view of the potential opportunities of developing nanocellulose based enterprises based on agricultural wastes, a review on the extraction of micro- and nanocellulose was published a few years ago [10]. The objective of this paper is to discuss the structural and thermal properties of the micro- and nanocellulose materials that can be used for the fabrication of the degradable composite materials targeted for packaging applications.

2. Experimental

2.1 Chemicals and sample preparation

Chemicals such as absolute alcohol, NaOH, NaOCl, NaHSO3, and conc. H2SO4 used in this work were purchased from Qualigen Fisher Scientific, Mumbai, India and were used without further purification.

Dry straw of the wheat (Triticum aestivum) was collected from Kathmandu and chopped into about 1 mm long fragments and then powdered properly with the help of a laboratory grinder. The wheat stalk (WS) powder was turned into micro crystalline cellulose (MCC) and nanocrystalline cellulose (NCC) using the procedures explained elsewhere [10].

2.2 Characterization methods

Fourier Transform Infrared (FTIR) Spectroscopy was performed on Perkin Elmer FTIR2000) in attenuated total reflectance (ATR) mode within the wavenumber range of 4000 to 700 cm–1 with resolution of 20 cm–1 in the ATR mode.

Scanning Electron Microscope (SEM, JOEL 6300) and Field Emission Scanning Electron Microscope (FESEM; Zeiss Gemin FESEM) were used to visualize the morphology of the fibers. The specimen surface was coated with a thin film of gold for SEM investigations. Additionally, Transmission Electron Microscope (FETEM, JOEL, JEM-2100F) was used to study the crystalline structure of the

fibers. The specimens were prepared by dropping dilute solution of NCC powder in deionized water onto carbon coated copper grid followed by oven drying at 40 °C for 24 h.

Thermogravimetric Analysis (TGA) of the samples was carried out using Mettler-Toledo, TGA/SDTA 851 equipment, under the inert atmosphere of dry nitrogen from 30 °C to 600 °C with the heating rate of 20° C/min.

X-Ray Diffraction (XRD) was performed on X-ray diffractometer (Rigaku, TTRAX III 18KW and Bruker, Germany) running on the Cu-Kα radiation (λ = 1.5406 Å) at a scan rate of 0.05° per 0.5 s for 2Θ range 5–50°.

3. Results and Discussion

3.1 Spectroscopic characterization

Fig. 1(a) presents the FTIR spectra of commercial MCC (named as MCC-com, HM400X) and the wheat stalk powder. The FTIR spectra are similar; only a few peaks of the MCC are found to be sharper and distinct. Both the spectra have broad absorption bands between 3600 cm–1 to 3000 cm–1 representing the O-H stretching vibration and the strong intra- and intermolecular hydrogen bonds present in cellulose [11–14]. The FTIR peak located at 1593 cm–1 represents the small bending vibration of OH bond. The axial C-H stretching of cellulose can be seen at 2894 cm–1 which is more intense and sharper in MCC-com than in the WS. The C–H stretching and CH2 wagging vibrations of cellulose are signature by correlated by the peaks located at 1369 cm–1 and 1315 cm–1, respectively [11]. Likewise, the characteristic anti-symmetric bridge stretching of C–O and C–O–C pyranose ring vibration of cellulose is represented by the peak located at 1157 cm–1 [11]. Similar type of C–O stretching and C–O–C glycosidic bond stretching are attested by strong band at 1023 cm–1 [15, 16].

The absorption peak at 890 cm–1 represents the typical structure of cellulose showing C–O–C stretching vibration for β, 1,4-glycosidic linkages [13, 17]. In WS fibers, a few peaks (such as around 1300 cm–1) are quite different than commercial MCC (MCC-com), such as phenolic C–O stretching which the signatures of presence of lignin and similar natural polymers in the neat WS. WS fibers further bear quite sharp peak corresponding to aromatic rings centered at 1604 cm–1 for lignin in comparison to MCC-com [18, 19].

Fig. 1(b) compares the FTIR spectra of MCC with that of NCC obtained from the WS fibers. The MCC and NCC both have almost identical FTIR spectra as also reported by Satyamurthy and Vigneshwaran in cotton fibers [20]. The FTIR peaks of the NCC are weaker and less intense than the MCC, due to the reduction in crystallinity value and breakdown of numerous and intra- and intermolecular H-bonding between in the former [13, 19]. The prominent cellulose peaks appear more intense in the MCC as compared to the WS due to the exposure of the MCC crystallites resulting from the dissolution of lignin binder and hemicellulose during chemical treatments. Few more cellulosic peaks are observed, in the MCC and NCC, such as at 1642 cm–1 representing carbonyl C=O stretching of a saturated hydrocarbon [21].

It can be summarized that similar to the commercial one, the MCC extracted from the WS possessed intense peaks centered at 3329 cm–1, whereas these peaks became broad and diffuse in the NCC of the same origin, which can be attributed to possible breakdown of inter- and intramolecular H-bonding due to strong acid treatment.

3.2 Morphological characterization

The microscopic techniques provide direct evidence of morphological details of the materials at different length scales. The electron micrographs give fiber surface morphology, including their size and dimensionality as well as their overall surface texture.

The scanning electron micrograph of the MCC derived from the WS fiber is shown in Fig. 2 (a). The MCC fibers are semi-crystalline in nature with length of approximately 25 μm and width of 5 μm. In nature, the MCC has amorphous cellulose residing in between the micro-crystallites to form a long cylindrical structure with aspect ratio of approximately 5:1. The higher magnification SEM image in Fig. 2 (b) shows that the MCC bundles are made up of fine nanofibrillar texture. The dissolution of amorphous region of the WS fibers by different chemicals such as NaOH, NaOCl and H2SO4 can be attributed to the development of this texture.

The results reported on commercial MCC in an earlier work were also quite similar with respect to fibrillation and surface texture evolution, as well as shape and size of the MCC crystals [22-27].

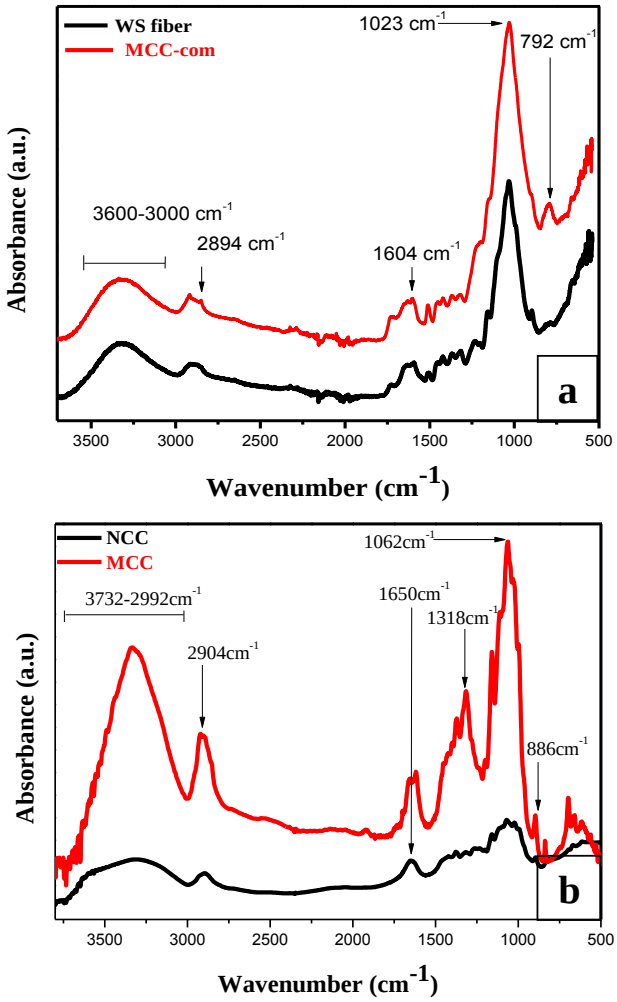

Fig. 1: FTIR spectra of different forms of natural fibers studied in this work: (a) pure wheat stalk (WS) powder compared to commercial MCC, and (b) the MCC and the NCC extracted from the WS powder.

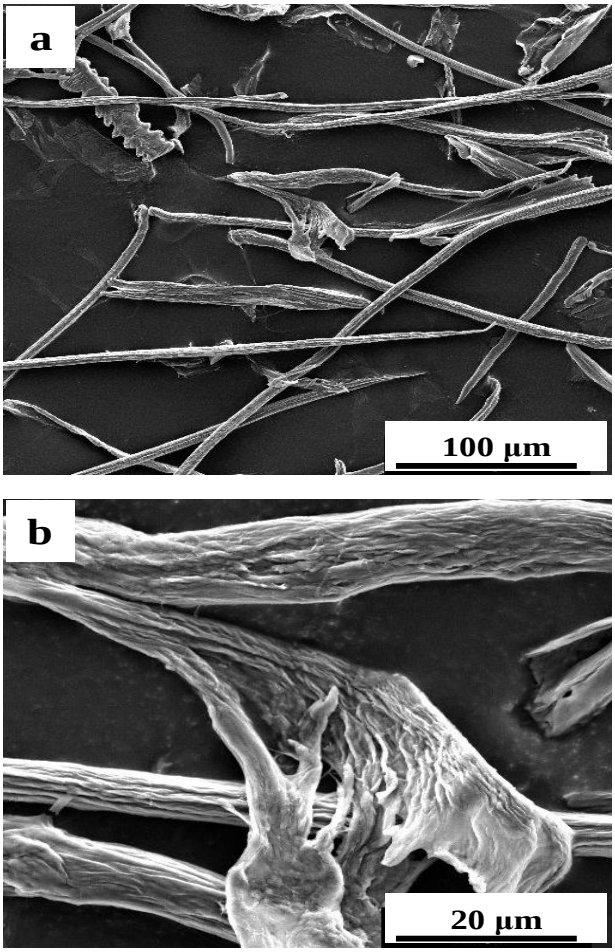

Fig. 2: Lower (top) and higher (bottom) magnifications of the SEM images of the MCC extracted from WS.

FESEM technique is very useful for morphological studies of MCC and NCC under almost environmental condition. In this work, NCC powder was observed by FESEM, Fig. 3.

The synthesized bulk NCC powder in the dry form seems to have course, porous surface with large agglomeration. Only few NCC crystallites are projecting outside from the agglomerate, Fig. 3 (a). The shape of the NCC is more distinct in Fig. 3 (b), showing its rod shaped texture. The largest NCC aggregates observed has the dimension approximately 1 μm long and 80 nm width, whereas the smallest one is about 200 nm long and 50 nm wide. These results are consistent with that reported in the literature [29–33].

The transmission electron micrographs presented in Fig. 4 (a) manifest that NCC fibers are in a bundle before nano-fibrillation out of the MCC, which are then exposed out on acid hydrolysis followed by the dissolution of amorphous region present between the nano-fibrils. These NCC get dispersed as rod-like crystals as shown in Fig. 4 (b). These crystals, being very hydrophilic in nature due to the presence of free –OH groups on their surfaces, can easily absorb water droplets or moisture, as demonstrated by cellular structures on the NCC crystals surfaces. The dimension of NCC from WS produced in this work is found to be approximately, 50 nm wide and 300 nm long. The results, in general, agree with the literature works [31–33].

From the microscopic results, it can be concluded that the MCC and NCC obtained from the WS fibers possess characteristic textures, the MCC being irregular bundles of the primary crystals bound together by the amorphous phase. The latter disintegrates upon acid hydrolysis giving rise to sharp rod-shaped nanocrystals which have much larger surface areas and thus possess strongly hydrophilic character.

The MCC and NCC fibers were studied also using XRD whereby the diffractograms were utilized to calculate the degree of crystallinity and d-spacing of the crystallites. In the first glance, the MCC spectrum shows a clear amorphous halo and a crystalline structure which the NCC spectrum has practically no amorphous halo showing the lack of amorphous phase. The NCC have quasi no amorphous halo showing the lack of amorphous phase.

The diffraction patterns of the MCC are shown in Fig. 5 (a). The XRD plot of the MCC shows two feeble 2Θ peaks in between 12 – 17° as well as two sharp peaks at 20.04° and 22.02° which have been assigned to the cellulose I [15, 35–38]. The high intensity of the peaks at 2Θ positions further indicates the highly crystalline nature of the cellulosic fibers.

The degree of crystallinity (χc) values for the NCC (50 %) was found to be much higher than for the MCC (31 %) which has been attributed as the result of strong acid hydrolysis induced dissolution of the amorphous zone embedding the crystalline fibrils [39, 40].

3.3 Thermal behavior

The plot in Fig. 6 illustrates of thermogravimetric analysis of MCC and NCC. Both show two-step degradation. The MCC shows initial weight loss up to 7 % at around 120 °C which corresponds to the removal of water and other volatile substances. The MCC itself starts to degrade at 225 °C, the major degradation occurs at Tmax of 373 °C, which can be observed from the accompanying differential curve.

The complete thermal degradation occurred at around 400 °C with the char yield of 1.33 % at 600 °C which is consistent with the values reported for the cellulosic materials of different origins [17]. The char yield limits the production of combustible gases and can even decrease the exothermic pyrolytic reaction inhibiting the thermal conductivity of the burning materials.

Similarly, NCC also losses its weight by 10 % due to removal of water and volatiles at around 120 °C while its degradation starts at 231 °C followed by the major degradation occurring at Tmax of 300 °C. The complete degradation of the NCC occurs at 408 °C leaving the residual mass of 22.16 % in the form of char after combustion at 600 °C. Thus, on comparing thermal behavior, on can observe that the MCC is found to be more thermally stable than the NCC.

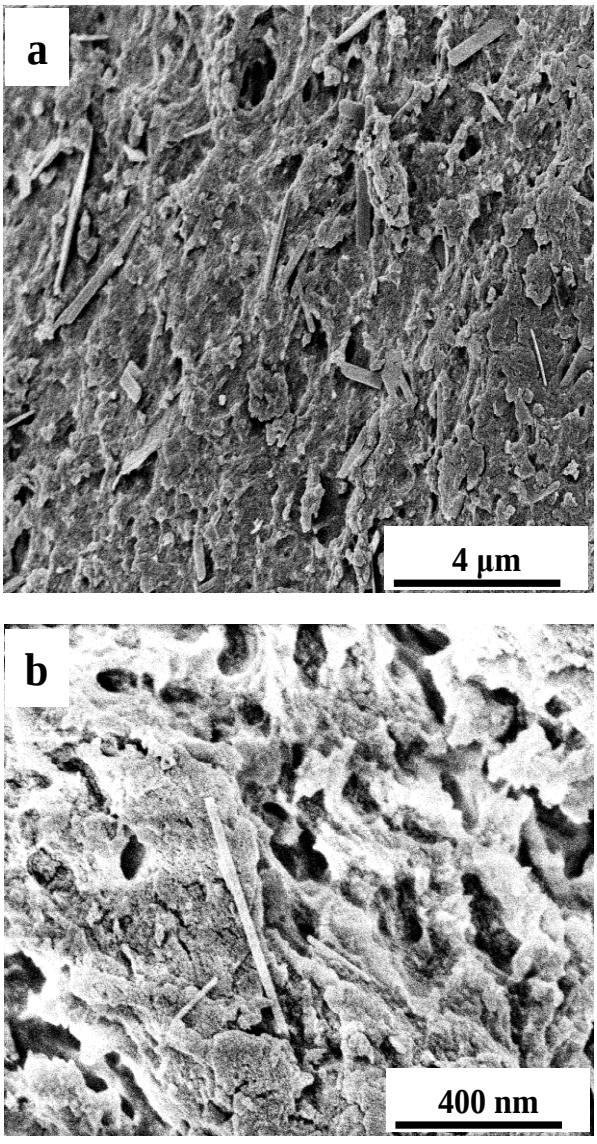

Fig. 3: Lower (a) and higher (b) magnifications of FESEM images showing nano-sized cellulose particles extracted from WS.

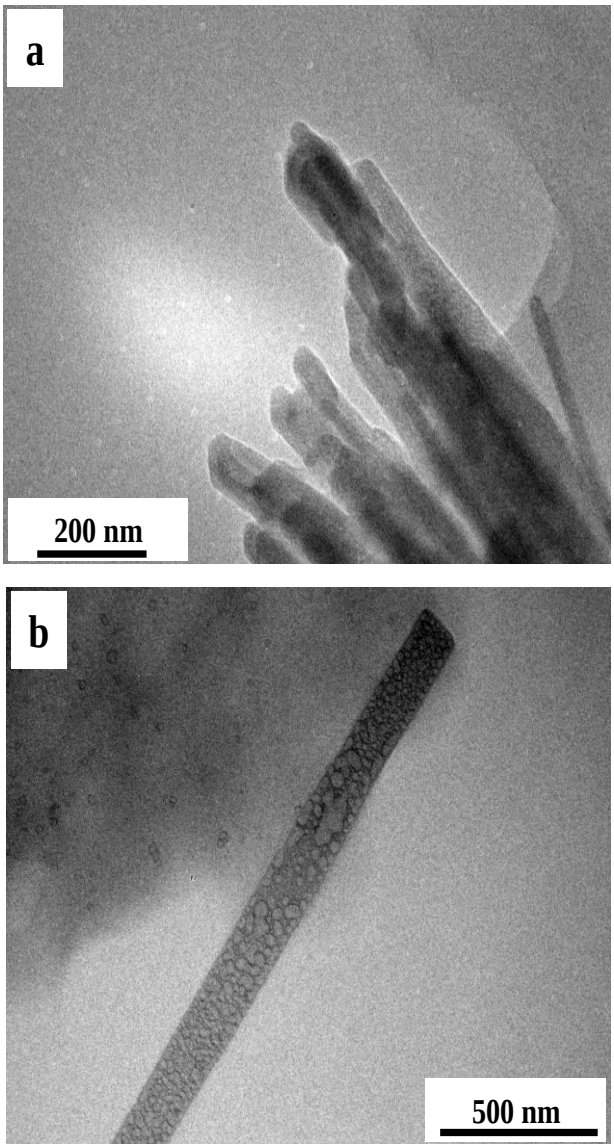

Fig. 4: TEM images of NCC extracted from MCC; (a) bundle showing NCC fibers in MCC, and (b) a single NCC crystallite dispersed from MCC.

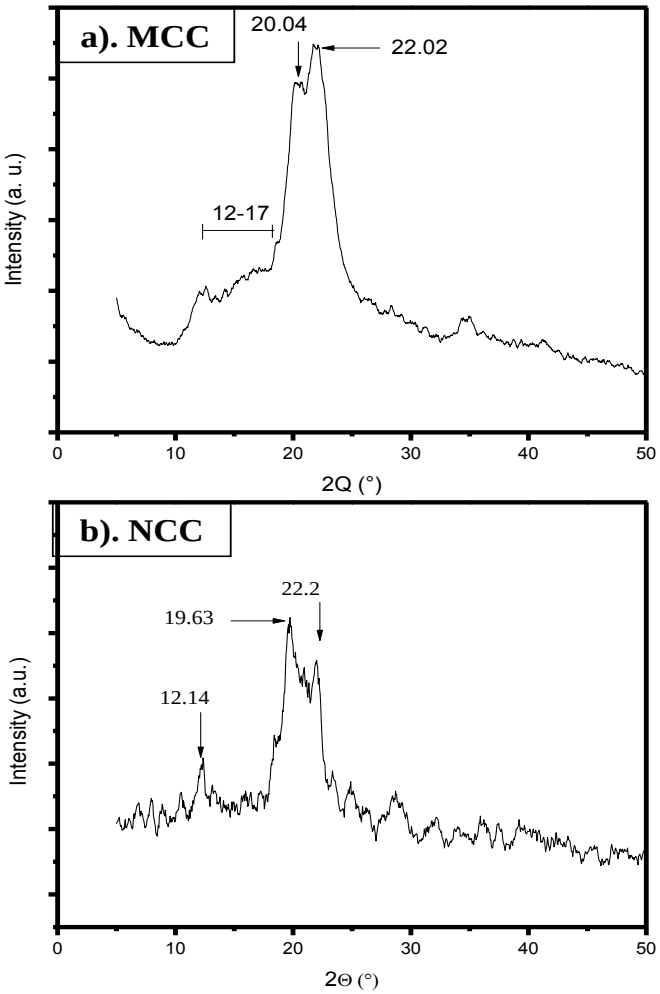

Fig. 5: XRD patterns of MCC and NCC extracted from WS fibers.

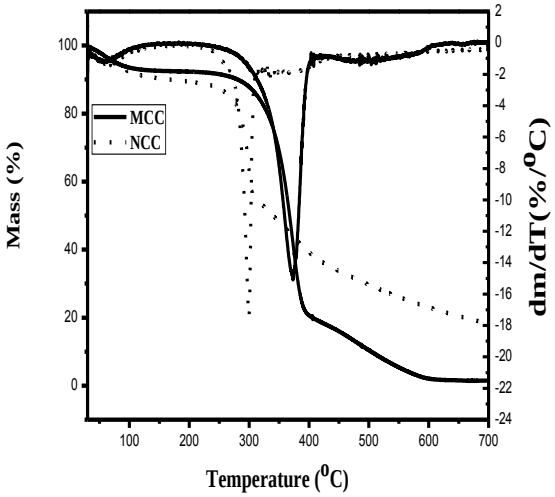

Fig. 6: TGA thermograms of MCC and NCC extracted from WS.

4. Conclusions

Micro- and nanocrystalline cellulose was extracted from wheat stalk using different thermomechanical and chemical treatments and characterized by spectroscopic, microscopic and diffraction techniques. The results presented in this paper can be concluded as follows:

(a) The spectroscopic analyses conclude that the virgin WS fibers are structurally quite similar to the commercial MCC. Similar to the commercial one, the MCC extracted from the WS possessed intense peaks centered at 3329 cm^{-1}, whereas these peak became broad and diffuse in the NCC of the same origin, which can be attributed to possible breakdown of inter- and intramolecular H-bonding due to strong acid treatment.

(b) From the microscopic evidences obtained from SEM and TEM, it is concluded that the MCC and NCC obtained from WS fibers are characterized by definite textures, the MCC being irregular bundles of the primary crystals bound together with the amorphous phase. The latter disintegrates upon acid hydrolysis to give rise to the rod-shaped sharp nanocrystals which have much larger surface area and thus intense hydrophilic character.

(c) The XRD results revealed that the natural fibers extracted from the WS predominantly contained Cellulose I form of the crystals whereby the nanofibrillation increased the degree of crystallinity by about two folds.

(d) The MCC and NCC thus prepared were found to be generally thermally stable while the NCC was found to be slightly less stable. The thermal stability of the MCC can be attributed to the security coating provided by the amorphous part of the cellulose which gets eliminated due to treatment with the strong acids.

Acknowledgements

JG thanks Nepal Academy of Science and Technology (NAST) for providing PhD research Fellowship and further acknowledges the Indian National Science Academy (INSA) for providing the fellowship for a research stay at Indian Institute of Technology Guwahati (IITG), India.

References

[1] A. Dufresne, Nanocellulose: From Nature to High Performance Tailored Materials, Walter de Gruyter GmbH & Co KG, Munich, Germany, 2017. ISBN 978-3-11-048041-2.

[2] S. Kalia, Lignocellulosic Composite Materials, Springer Series on Polymer and Composite Materials, Springer, Berlin, Germany, 2018. doi.org/10.1007/978-3-319-68696-7_5.

[3] T. T. Teeri, H. Brumer, G. Daniel, P. Gatenholm, Biomimetic engineering of cellulose-based materials. Trends. Biotech. 25 (2007) 299–306. doi.org/10.1016/j.tibtech.2007.05.002

[4] J. X. Sun, X. F. Sun, H. Zhao, R. C. Sun, Isolation and characterization of cellulose from sugarcane bagasse. Polym. Degrad. Stab. 84 (2004) 331–339. doi.org/10.1016/j.polymdegradstab.2004.02.008.

[5] D. Klemm, B. Philipp, T. Heinze, U. Heinze, W. Wagenknecht, Comprehensive Cellulose Chemistry, Functionalization of Cellulose, Volume II, WILEY-VCH Verlag, Weinheim, Germany, 1998. doi.org/10.1002/3527601937

[6] I. Siro, D. Plackett, Microfibrillated cellulose and new nanocomposite materials: a review, Cellulose. 17 (2010) 459–494. doi.org/10.1007/s10570-010-9405-y.

[7] A. Eldho, P. A. Elbi, B. Deepa, P. Jyotishkumar, L. A. Pothen, S. S. Narine, S. Thomas, X-ray diffraction and biodegradation analysis of green composites of natural rubber/nanocellulose, Polym. Degrad. Stab. 97 (2012) 2378–2387. doi.org/10.1016/j.polymdegradstab.2012.07.028.

[8] D. Bander, J. Sapkota, S. Josset, C. Weder, P. Tingaut, X. Gao, E. J. Foster, T. Zimmermann, Influence of mechanical treatments on the properties of cellulose nanofibers isolated from microcrystalline cellulose, React. Funct. Polym. 85 (2014) 134–141. doi.org/10.1016/j.reactfunctpolym.2014.09.009.

[9] N. L. Bhandari, W. Mormann, G.H. Michler, R. Adhikari, Functionalisation of bamboo and sisal fibres cellulose in ionic liquids, Mater. Res. Innovat. 17 (2013) 250–256. doi.org/10.1179/1433075X12Y.0000000068.

[10] J. Giri, R. Adhikari, A brief review on extraction of nanocellulose and its application, BIBECHANA 9 (2013) 81–87. doi.org/10.3126/bibechana.v9i0.7179.

[11] R. Gemci, Examining the effects of mercerization process applied under different conditions to imensional stability, Scientific Research and Essays 5 (2010) 560–571.

[12] N.A. Ibrahim, Effect of fiber treatment on the mechanical properties of kenaf fiber-ecoflex composites, J. Reinf. Plast. Comp. 29 (2010) 2192–2198. doi.org/10.1177/0731684409347592.

[13] P. Manimaran, P. Senthamaraikanna, M. R. Sanjay, M. K. Marichelvam, M. Jawaid, Study on characterization of *Furcraea foetida* new natural fiber as composite reinforcement for lightweight applications, Carbohydr. Polym. 181 (2018) 650–658. doi.org/10.1016/j.carbpol.2017.11.099.

[14] J.H. Pang, X. Liu, M. Wu, Y.Y. Wu, X.M. Zhang, R.C. Sun, Fabrication and characterization of regenerated cellulose films using different liquids, J. Spectr. (2014) Article ID 214057 (8 pages). .doi.org/10.1155/2014/214057.

[15] M.B. Guerrero, L.A.P. Maqueda, R. Artiaga, P.E.S. Jiménez, J.P. Cosp, Structural and chemical characteristics of sisal fiber and its components: effect of washing and grinding, J. Nat. Fib. 14 (2016) 26–39. doi.org/10.1080/15440478.2015.1137529.

[16] M.E. Sakhawy, S. Kamel, A. Salama, H.A. S. Tohamy, Preparation and infrared study of cellulose based amphiphilic materials. Cellulose Chem. Technol. 52 (2018) 193–200.

[17] C.S. Wu, Characterization of cellulose acetate-reinforced aliphatic- aromatic copolyester composites, Carbohydr. Polym. 87 (2012) 1249–1256. doi.org/10.1016/j.carbpol.2011.09.009.

[18] J.G. Gwon, S.Y. Lee, G.H. Doh, J.H. Kim, Characterization of chemically modified wood fibers using FTIR spectroscopy for biocomposites, J. Appl. Polym. Sci. 116 (2010) 3212–3219. doi.org/10.1002/app.31746.

[19] M. Pan, X. Zhou, M. Chen, Cellulose nanowhiskers isolation and properties from acid hydrolysis combined with high pressure homogenization, BioResources. 8 (2013) 933–943.

[20] P. Satyamurthy, N. Vigneshwaran, A novel process for synthesis of spherical nanocellulose by controlled hydrolysis of microcrystalline cellulose using anaerobic microbial consortium, Enzyme Microb. Technol. 52 (2013) 20–25. doi.org/10.1016/j.enzmictec.2012.09.002

[21] N. A. Rosli, I. Ahmad, I. Abdullah, Isolation and characterization of cellulose nanocrystals from Agave angustifolia fibre, Bioresources 8 (2013) 1893-1908.

[22] D. M. Panaitescu, A. N. Frone, M. Ghiurea, C. I. Spataru, C. Radovici, M. D. Iorga, 'Properties of polymer composites with cellulose microfibrils', In: Brahim Attaf (Ed.), Advances in Composites Materials-Ecodesign and Analysis, Intechopen, Chapter 5, pp. 103–122, 2011. ISBN: 978-953-307-150-3.

[23] K.P. Rajan, N. R. Veena, Hanna J. Maria, R. Rajan, M. Skrifvars, K. Joseph, Extraction of bamboo microfibrils and development of biocomposites based on polyhydroxybutyrate and bamboo microfibrils, J. Compos. Mater. 45 (2010) 1325–1329. doi.org/10.1177/0021998310381543.

[24] R. Krishnaprasad, N. R. Veena, Hanna J. Maria, R. Rajan, M. Skrifvars, K. Joseph, Mechanical and thermal properties of bamboo microfibril reinforced polyhydroxybutyrate biocomposites, J. Polym. Env. 17 (2009) 109–114. doi.org/10.1007/s10924-009-0127-x.

[25] M. Das, D. Chakraborty, The effect of alkalization and fiber loading on the mechanical properties of bamboo fiber composites, part1:-polyester resin matrix. J. Appl. Polym. Sci. 112 (2009) 489–495. doi.org/10.1002/app.29342.

[26] E. M. Cadena Chamoro, J. M. Velez, J. F. Santa, V. Otalvaro G., Natural fibers from plantain pseudostem (Musa Paradisiaca) for use in fiber-reinforced composites, J. Nat. Fib. 14 (2017) 678–690. doi.org/10.1080/15440478.2016.1266295.

[27] D. L. Vinayak, V. Guna, D. Madhavi, M. Arpitha, N. Reddy, Ricins communis plant residues as a source for natural cellulose fiber potentially exploitable in polymer composites. Ind. Crops Prod. 100 (2017) 126–131. doi.org/10.1016/j.indcrop.2017.02.019.

[28] G. C. Carrasco, A. Miettinen, C. Hendriks, E. Gamstedt, M. Kataja, J. Cuppoletti, Structural characterization of Kraft pulp fibres and their nanofibrillated materials for biodegradable composite applications, in J. Cuppoletti (Ed.), 'Nanocomposites and Polymers with Analytical Methods', Chapter 10, pp. 243–260, Intechopen 2011. doi.org/10.5772/21580.

[29] W. Gauitua, A. Ballerini, J. Zhang, Polymer nanocomposites: synthetic and natural fillers a review. Maderas Clencia y Technologia 7 (2005) 159–178. doi.org/10.4067/S0718-221X2005000300002.

[30] F. Kramer, D. Klemm, D. Schumann, N. Heßler, F. Wesarg, W. Fried, D. Stadermann, Nanocellulose polymer composites as innovative pool for (bio)material development, Macromol. Symp. 244 (2006) 136–148. doi.org/10.1002/masy.200651213.

[31] D. Y. Liu, X. W. Yuan, D. Bhattacharyya, A. J. Easteal, Characterisation of solution cast cellulose nanofibre-reinforced poly(lactic acid), eXPRESS Polym. Lett. 4 (2010) 26–31. doi.org/10.3144/expresspolymlett.2010.5.

[32] M. J. Cho, B. D. Park, Tensile and properties of nanocellulose-reinforced poly(vinyl alcohol) nanocomposites, J. Ind. Eng. Chem. 17 (2011) 36–40. doi.org/10.1016/j.jiec.2010.10.006.

[33] S. Mueller, C. Weder, E. J. Foster, Isolation of cellulose nanocrystals from pseudostems of banana plants, RSC Adv. 4 (2014) 907–915. doi.org/10.1039/C3RA46390G.

[34] J. Li, X. Wei, Q. Wang, J. Chen, G. Chang, L. Kong, J. Su, Y. Liu. Homogeneous isolation of nanocellulose from sugarcane bagasse by high pressure homogenization, Carbohydr. Polym. 90 (2012) 1609–1613. doi.org/10.1016/j.carbpol.2012.07.038.

[35] A. Sonia, K.P. Dasan, Cellulose microfibers (CMF)/poly(ethylene-co-vinyl acetate) (EVA) composites for food packaging applications: A study based on barrier and biodegradable behavior, J. Food Eng. 118 (2013) 78–89. doi.org/10.1016/j.jfoodeng.2013.03.020.

[36] E. D. M. Teixeira, A. C. Correa, A. Manzoli, F. D. L. Leite, C. R. D. Oliveira, L. H. C. Mattoso, Cellulose nanofibers from white and naturally colored cotton fibers, Cellulose. 17(2010) 595–606. doi.org/10.1007/s10570-010-9403-0

[37] M. Adsul, S. K. Soni, S. K. Bhargava, V. Bansal, Facile approach for the dispersion of regenerated cellulose in aqueous system in the form of nanoparticles, Biomacromolecules 13 (2012) 2890–2895. doi.org/10.1021/bm3009022.

[38] A. Mandal, D. Chakrabarty, Isolation of nanocellulose from waste sugarcane bagasse (SCB) and its characterization, Carbohydr. Polym. 86 (2011) 1291–1299. doi.org/10.1016/j.carbpol.2011.06.030.

[39] B. M. Cherian, A. L. Leao, S. Ferreira, D. Souza, S. Thomas, L. A. Pothan, M. Kottaisamy, Isolation of nanocellulose from pineapple leaf fibres by steam explosion, Carbohydr. Polym. 81 (2010) 720–725. doi.org/10.1016/j.carbpol.2010.03.046.

[40] D. Dai, M. Fan, Characteristic and performance of elementary hemp fibre, Mat. Sci. Appl. 1 (2010) 336–342. doi.org/10.4236/msa.2010.16049.

BIBECHANA

A Multidisciplinary Journal of Science, Technology and Mathematics

ISSN 2091-0762 (online)

Journal homepage: http://nepjol.info/index.php/BIBECHANA

A Brief review on extraction of nanocellulose and its application

Jyoti Giri [1], Rameshwar Adhikari [2,*]

[1] Department of Chemistry, Tri-Chandra Campus, Tribhuvan University, Kathmandu, Nepal

[2] Central Department of Chemistry, Tribhuvan University, Kirtipur, Kathmandu, Nepal

* Corresponding author: E mail: nepalpolymer@yahoo.com

Article history: Received 22 October, 2012; Accepted 7 November, 2012

Abstract

Cellulose is one of the most abundant renewable natural resources. With the advent of nanotechnology, the interests of cellulose scientists have diverted towards the extraction of nanocellulose from various plant sources and utilize them in technical applications. The reason behind the rapid progress in the nanocellulose chemistry and engineering lies in the promising properties of the nanocellulose and the products thereof. In fact, nanocelluloses combine the important properties of cellulose with amazing features of nanoscale materials. With the perspective of potential of cellulosic materials production in Nepal basically from agricultural wastes and uses in several applications such as in the preparation of biomaterials, this paper reviews the current knowledge in research and development of nanocelluloses in particular for biomedical applications. After the introduction to the chemical constitution and microfibrillar arrangement of nanocellulose in the cellulose bundles together with other constituents, the ways of preparation of nanocellulose and its functionalization approaches will be discussed. Finally, the application of nanocellulose for preparing biomaterials scaffolds will be introduced

Keywords: Nanocellulose; tissue engineering; functionalization; biopolymer

1. Introduction

Cellulose is main lignocellulosic component of cell wall in plants along with hemicellulose, lignin, pectin, wax and constitutes 25 -50% of the plants [1]. Cellulose can be replenished by photosynthesis and its estimated biosynthesis is 10^{11} tons per year [2]. The simple molecular structure of cellulose is given in Fig. 1.

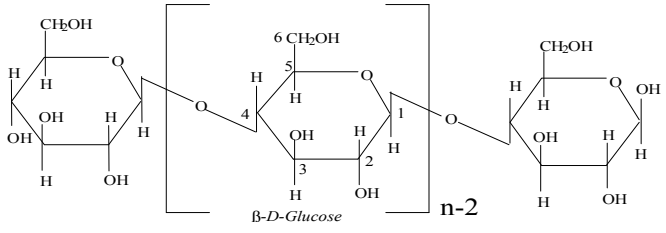

Fig. 1: Structure of cellulose macromolecule.

Cellulose is linear polymer of β-anhydroglucopyranoside with 1, 4 β-glycosidic linkage. The structure is supported by the free secondary OH groups at C-2, C-3 position and primary OH group at C-6 position [1,3,4]. Its general molecular formula is $(C_6H_{10}O_5)_n$ and density is 1.50 g/cm^3. About several hundred to10 millions of glucose units condense to form a straight chain of a polysaccharide unit in the term of cellulose nanofiber. The free OH groups in one polysaccharide thread have higher possibilities to form hydrogen bonds with another thread. Therefore a number of nanofibers bind through intermolecular hydrogen-bonding with each other to form microfibers and then to microscopic cellulose fibers. The cellulose macromolecule assembled in semicrystalline filament is expressed in term of microfibers and nanofibers. The OH groups are also the active sites for the chemical modifications [5].

Hemicellulose is amorphous polysaccharide which is a mixture of carbohydrates comprising 3- 6 membered units [1,6]. Lignin is complex dendridic network of phenyl propene which acts as binder in cellulose fiber to give the exact morphology for plant cell wall [1,6]. Similarly pectin is heteropolysaccharide of 1-4 linked galacturonic acid with methyl esters of different sugar units [1,6]. Wax has various composition of esters obtained from fatty acids and long chain alcohols. e.g. rice bran wax, soy wax etc. [2,6].

Cellulose occurs in 4 major polymorphic forms: cellulose I, II, III and IV. Cellulose fibrils are either man-made (regenerated also called fibers) or natural. Cellulose with these two origins has predominantly structures I and II[2]. In cellulose I crystal structure has parallel unit cell whereas in cellulose II unit cells of crystals are antiparallel[2]. Cellulose III is obtained on treating cellulose I and II with ammonia. Likewise cellulose IV can be prepared by heating cellulose III [7]. Although native Cellulose has I structure, it can be converted into other forms by different treatments. Cellulose fibrils are partly crystalline with cellulose I_α and I_β. Cellulose I_α has a single chain triclinic structure and I_β has two chain monoclinic structures[2]. These special arrangements provide the cellulose nanofibers with remarkably interesting mechanical properties [8].

Lignin, hemicellulose and wax matrix bind the cellulose fibers in plant cell wall. In a single fiber, a number of threads like microfibrils are bound together which are called microfibers. Their size varies from 10 to 40 μm in diameter depending upon the types of plants; see Table 1 [9].

Table 1: Average fiber dimensions of some cellulose raw materials [9].

Cellulose material	Fiber length (μm)	Fiber width (μm)
Spruce	3400	31
Pine	3100	25
Beech	1200	21
Eucalypt	850	20
Bamboo	2700	14
Cotton linters	9000	19
Wheat straw	1410	15
Baggage	1700	20

Each microfiber is a bundle of individual nanosize thread, called as nanofiber or nanofibril which consists of a number of filamental cellulose chain passing through numerous crystallites in thread like fashion. The elementary nanofibril has diameter of 3-15 nm and length with an average aspect ratio of 20-200 [10]. These nanofibrils contain ordered nanocrystallites and disordered amorphous domains placed in definite intervals [11].

Cellulose fibers being most abundant, constantly replenished in nature by photosynthesis [2,12] and being stronger than steel, glass fiber etc, has attracted new trends of development in material science [13,14].

High mechanical strength, stiffness, large surface area and biodegradability are the properties often referred to nanocellulose which make it as tempting raw material for new biobased composites. Around 1990, their strong hydrophilic nature, resistant to many chemicals, safety to life, reproducibility and recyclability, brought nanocellulose in many intense applications compared to cellulose and microcellulose [15]. Additionally the recent advances in nanocellulose supports medical fields in different aspect as implant materials (artificial organs), biodegradable tissue scaffolds, drug delivery vehicles, etc. Further nanofiber composites are used for making flexible circuits, solar panels and other electronics devices. Many more applications in paints, pigment, inks, screens, coatings, packaging materials, optical appliances, cosmetics etc. also make use of cellulosic materials [15,16].

The aim of this paper is to review the extraction methods of nanocellulose from renewable natural resources and give an overview of various applications as novel biomaterials.

2. Extraction Micro- and Nanocellulose

With the beginning of civilization cellulose is being used for many purpose; such as for making clothes, ropes, housing materials and paper from fiber. Time passed by and new ideas with novel developments started. In late 1970s, Turbak, Snyder and Samberg introduced the new material microfibrillated (MFC) and nanofibrillated cellulose (NFC) [17]. Cotton [11,12], ramie [11], jute [11,18], bamboo [19,22], sisal [9], rice [19], starch [21] etc have been used to extract nanocellulose.

There are various procedures for the preparation of micro and nanofibrillated cellulose. Deshpande & co-workers had extracted microfibrillated cellulose by compression and roller mechanical techniques and blended with polyesters to prepare high strength composite materials [19]. Rajan & co-workers microfibrillated bamboo fibers by chemical treatment with NaOCl / NaOH and acetic acid in an autoclave which were then compounded with polyhydroxybutyrate (PHB) matrix [22]. Similarly, Okubo, Fujii & Yamashita extracted microfibers by steam explosion process and developed composites with polylactic acid (PLA) matrix, whose bending, fracture properties were improved [18].

In nature even the waste materials could be of high value as they could be one of the sources for raw material to isolate micro-nanocellulose. Sun & co-workes and Mandal & co-workers isolated cellulose microfibers from the waste sugarcane dewaxed bagasse by chemical treatments followed by ultasonication process and oxidation with hydrogen peroxide (H_2O_2) and sodium hydroxide (NaOH) [2,12].

Liu, Yuan & Bhattacharyya extracted suspension of nanocellulose fiber from flax yarns. Mercerized flax yarns on acid treatment and neutralization with alkali yielded nanocellulose. The PLA composites with these nanofibers showed significant increase in tensile strength and modulus whereas elongation at break was decreased with fiber content [23]. Cherian & co-workers used pineapple leaf fiber (PALF) to extract nanocellulose by chemical as well as mechanical process. Fibers on delignification, bleaching and steam explosion gives nanocellulose width in the range of 5-60 nm [24]. Kukle & co-workers optimized the percentage of NaOH, temperature, time and pressure for nanoscaled disintegration of hemp fibers after steam explosion to isolate the nanocellulose [8]. Likewise, Luduena and co-workers obtained nanocellulose from rice husk by chemical process [25].

In the survey it is found that there are many different methods for the extraction / preparations of cellulose, cellulose micro and nanofibrils which can be summarized as chemical and mechanical processes [13].

3. Chemical process

The chemical process comprises the treatment of raw cellulosic mass with required amount of alkali for delignification, organosolvation (with acetic acid, aqueous methanol or ethanol), and acid treatment

for the hydrolysis. Chemical process also involves oxidation with oxidizing agent hydrogen peroxide (H_2O_2), sodium hypochlorite (NaOCl) for bleaching the coloured materials.

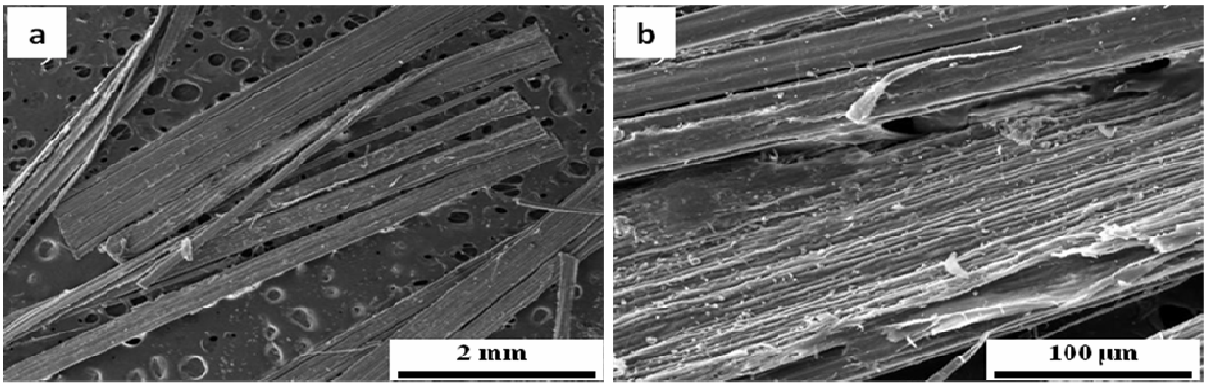

Fig. 2: SEM images of chemical treated hemp fiber: [a] Washed, [b] delignified [10].

4. Mechanical process

Mechanical process can be carried out in different ways: roller mechanical technique, compression mechanical technique, cryocrushing, sonication, homogenization and wet cooking process (steam explosion).

4.1 Compression (CMT) and roller mechanical (RMT) techniques

In CMT delignified fibers of cellulosic materials are placed in a bed of stripes placed between the two plates and subjected to a constant load of 10 tons for 10 seconds. In contrast, RMT delignified stripes are forced between the two rollers, one of which is fixed while the other is rotating [3].

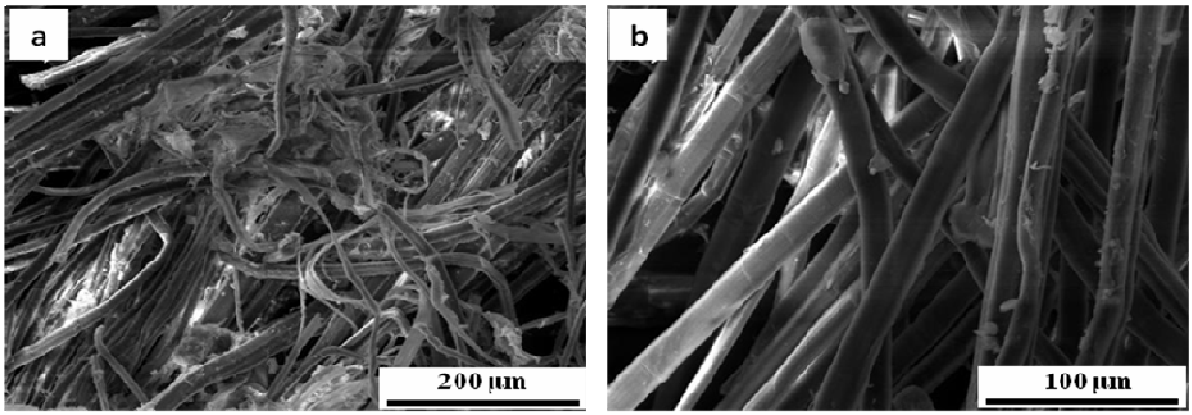

Fig. 3: SEM images of mechanical and chemical treated delignified hemp fiber for micro, nanofibrillation: [a] steam exploded, [b] acid hydrolysed steam exploded fibers [8].

4.2 Homogenization

In this process fibers (either crude one or delignified ones) are passed through a valve at high pressure and exposed to a pressure drop to atmospheric condition when the valve is released resulting in high shear force on the fiber surface [3,21].

4.3 Cryocrushing

The fibers are first frozen in liquid nitrogen. The embrittled glassy fibers are then subjected to high speed crushing. The high shear and impact forces acting on the fibers turn them to powder comprising microfibrils. The cryocrushed fibers may then be dispersed uniformly into water suspension using a disintegrator [21].

4.4 Steam explosion

It is a thermomechanical process to breakdown the structural components of cellulose. The process is accompanied with heat carried by steam. Steam at high pressure penetrates the lignocellulosic biomass through diffusion. The sudden release of pressure generates shear force which hydrolyze the glycosidic bond and hydrogen bonds between the glucose chains, leading to the formation of nanofibers [24].

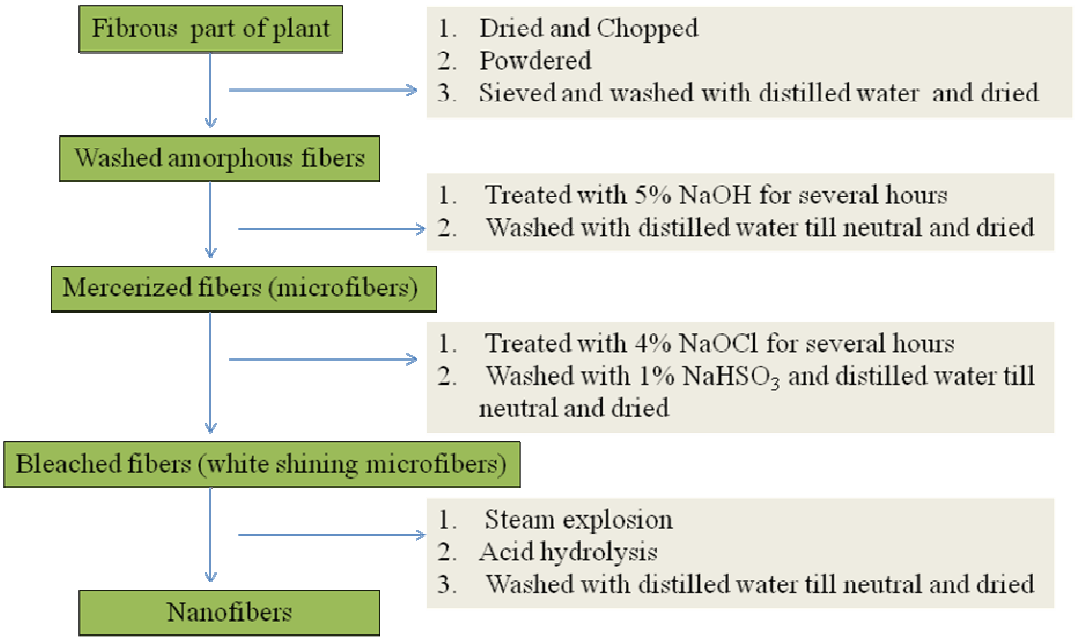

Fig. 4: Scheme for nanofibers extraction from lignocellulosic materials using chemical and mechanical treatments.

It is convenient method and common practice both chemical and mechanical processes to prepare nanocellulose from lignocellulosic materials. The unified chemical /mechanical scheme is presented in Fig. 4.

5. Applications

The nanofibers obtained have several potential applications in the field of electronics, used to prepare flexible circuits, flexible solar panels, optical applications, etc [5]. For instance, the acetate functional derivatives of sisal cellulose have been found to be applicable in textile (clothing and fabric), high absorbency products (diapers, cigarette- filters and other filters), thermoplastic products (films and plastic instruments), nourishing (food packaging), cosmetics and pharmaceuticals (extended capsule, tablet release agents and encapsulating agents), medicinal (hypoallergenic surgical products) and others [16].

Cellulose nanocrystals with defined dimension formulate the cellulose based nano composites for different coating applications and in packaging materials. Cellulose bears high capacity to hold water, and therefore has higher compatibility with human body. Thus nanocellulose can be used to fabricate tissue scaffolds and implants, wound dressing, biocompatible coatings and drug release formulations.

6. Concluding Remarks

Nanocellulose is an interesting material with amazing properties and can be applied for many useful purposes such as in textile industries, nanomedicine, food packaging, cosmetics and pharmacy. Other potential applications are use as polymer nanocomposites in combination with other polymers, hydrogels and technical materials. The research works envisioned in our laboratory are focusing on the extraction, chemical modification and applications of nanocellulose especially in the preparation of composite materials, biomedical and tissue engineering devices with the aid of electrospinning. In the frame of a University Grants Commission (UGC) supported project, we are working to develop standard protocols to extract the nanocellulose from some agricultural wastes and prepare useful devices for biomedical applications.

Acknowledgements

The authors would like to thank the University Grants Commission (UGC), Nepal for providing us with the Faculty Research Grant 2068/2069 (Project: Extraction of Micro- and Nanofibers from Renewable Resources to Develop Completely Biodegradable Plastics Composites).

References

[1] T.T. Teeri , H. Brumer-III, G. Daniel and P. Gatenholm Trends in Biotechnology, 25 (2007) 299-306.
[2] J.X. Sun, X.F. Sun, H. Zhao and R.C. Sun, Polymer Degradation Stability, 84 (2004) 331-339.
[3] Stelte W. and Sanadi A.R., Preparation and Characterization of Cellulose Nanofibers from Two Commercial Hardwood and Softwood Pulps, Industrial Engineering and Chemical Research, 48 (2009) 11211-11219.
[4] J.Yang and D.Y. Ye, Chinese Chemical Letters, 23 (2012) 367-370.
[5] D. Klemm, B. Philipp, T. Heinze, U. Heinze and W. Wagenknecht, Comprehensive Cellulose Chemistry, Functionalization of Cellulose, Volume II, WILEY-VCH Verlag GmbH,Weinheim (1998).
[6] S.J. Eichhorn, C.A. Baillie, N. Zafeiropoulos, L.Y. Mwailambo, M.P. Ansell, A. Dufresne, K.M. Entwistle, P.J. Herrere-Franco, G.C. Escamilla, L. Groom, M. Hughes, C. Hill, T.G. Rials and P.M. Wild, Journal of Materials Science, 36 (2001) 2107-2131.
[7] S. Park, J.O. Baker, M. E. Himmel, P.A. Parilla and D. K. Johnson, Biotechnology for Biofuels, 3(2010)10.
[8] S. Kukle, J. Gravitis, A. Putnina and A. Stikute. Proceedings of 8th International Scientific and Practical Conference., 1 (2011) 230-237.
[9] D. Klemm, B. Philipp, T. Heinze, U. Heinze and W. Wagenknecht, Comprehensive Cellulose Chemistry, Fundamentals and Analytical Methods, Volume I, WILEY-VCH Verlag GmbH,Weinheim (1998).
[10] W.J. Orts, J. Shey, S.H. Imam, G.M. Glenn, M.E. Guttman and J.F. Revol, Journal of Polymers and Environment, 13 (2005) 301-306.
[11] M. Ioelovich, BioResources, 3 (2008) 1403-1418.
[12] A. Mandal and D. Chakrabarty, Carbohydrate Polymers, 86 (2011) 1291-1299.
[13] F.Y. Yan, D. Krishniah, M. Rajin, and A. Bono, Journal of Engineering Science and Technology, 4 (2009) 57-68.
[14] D.M. Panaitescu, A.N. Frone, M. Ghiurea, C.I. Spataru, C. Radovici and M. D. Iorga, Properties of Polymer Composites with Cellulose Microfibrils, In: Advances in Composite Materials- Ecodesign and Analysis, Brahim Attaf (Ed.), InTake Open Access Book (2011).
[15] Y.H. Han, S.O. Han, D. Cho and H. Kim-II, Macromolecular Research, 16 (2008) 253-260.
[16] M.P.D. Paula, T.M. Lacerda and E. Frollini, eXPRESS Polymer Letters, 2 (2008) 423-428.

[17] A.F. Turbak, F.W. Snyder and K.R. Sandberg, Journal of applied Polymer Science, Applied Polymer Symposia, 37 (1983) 815-827.
[18] K. Okubo, T. Fujii and N. Yamashita, JSME International Journal, 48 (2005) 199-204.
[19] A.P. Deshpande, M.B. Rao and C. L. Rao, Journal of Applied Polymer Science., 76 (2000) 83-92.
[20] K.P. Rajan, N.R. Veena, H.J. Maria, R. Rajan, M. Skrifvars and K. Joseph, Journal of Polymers and Environment, 17 (2009) 109-114.
[21] I. Siro and D. Plackett, Cellulose., 17 (2010) 459-494.
[22] K.P. Rajan, N.R. Veena, H.J. Maria, R. Rajan, Journal of Composite Materials, 45 (2010) 1325-1329.
[23] D.Y. Liu, X.W. Yuan, D. Bhattacharyya and A.J. Easteal, eXPRESS Polymer Letters, 4 (2010) 26-31.
[24] B.M. Cherian, A.L. Leao, S.F. De-Souza, S. Thomas, L.A. Pothan and M. Kottaisamy, Carbohydrate Polymers, 81 (2010) 720-725.
[25] L. Luduena, D. Fasce, V.A. Alvarez and P. M. Stefani, BioResoources, 6 (2011) 1440-1453.

Nanocellulose: Nobel material

Jyoti Giri
Tri-Chandra Multiple Campus, Tribhuvan University, *E-mail; girijys@yahoo.com*

1. Introduction

Advanced technology is mostly focused on nanomaterials for its smart applications. Cellulose was introduced by Anseylm Payen in 1986. Cellulose is polymer of β-D glucopyranoside. A bundle of cellulose has semicrystalline structure with amorphous and crystalline part. The dissolution of amorphous part can generate nanocellulose. Nowadays nanodimension bearing celluloses are in practice for many fields for new approaches. Usually cellulose are simply a food material for organisms but the reduction in particle size in nanometric level increases its activity in numerous fields such as medical for drug delivery, tissue implants, bandage, ultra filtration, composites for vehicles , papers, fibers and many more. As Cellulose is a non-toxic and biofriendly material aids its application in all sensitive areas.

2. Preparation of Nanocellulose

Nanocellulose can be prepared by different mechanical, thermal, chemical and bacterial treatments of cellulose fiber.

Mechanical process involves ultra grinding of cellulose fibers by applying mechanical shear force between the microfibrillated cellulose and breaking the amorphous zone with the specified grinder.

Steam explosion is the thermal process where steam energy provides shear force between microfibrils to detach lignin binder and amorphous cellulose.

Chemical process involves series of chemical treatments to reduce the particle size. Mercerization (treatment with NaOH) removes lignin and hemicellulose, bleaching (treatments with NaClO or $NaClO_3$) whitens, and 60 % Conc. H_2SO_4 treatment nanofibrillates the cellulose fiber. Nanofribrillated cellulose can be washed and separated by dialysis membrane with the specific pore size. Nanocellulose prepared can be dried in lyophilizer.

Bacterial process is the culture of suitable bacteria with specific genera and species which produce nanocellulose with specific dimension e.g. acetobacter xylinum. It is mostly used in biomedical application for drug delivery, medical devices, tissues implants and many more.

3. Preparation of composites

Composites of the nanocellulose can be prepared by homogeneous mixing of polymers with suitable compatibility and mode of application. The mixing process can be carried out by various methods such as solution casting, melt mixing, injection moulding or situ generation of polymer matrix.

4. Characterization of Nanocellulose and composites

Nobel materials should have advanced property for its nobel application which can be studied by various methods of analysis; Morphological characterization, Mechanical stability, Thermal stability.

4.1 Morphology of Nanocellulose

Surface or morphological characterization can be done by Scanning Electron Microscopy (SEM), Optical Microscopy (OM) or Transmission Electron Microscopy (TEM). Although all the techniques are different but they all give information about the particle size, dispersion and interaction of nanofiller with the polymer matrix. Baterial nanoellulose shown in above Fig. 1 have tiny threads of nanoellulose networks forming sheets for numerous applicable sites.

4.2 Mechanical and Thermal stability

The increase in load bearing or mechanical strength of the composites is one of the major reinforcement one would like to see and can be evaluated by tensile test, fracture analysis, compression test, Dynamic Mechanical Analysis (DMA) and Martens Hardness (HM). Similarly thermal properties are measured by Thermogravimetric Analysis (TGA) and Diffrential Scanning Calorimetry (DSC). Loading of nanocellulose

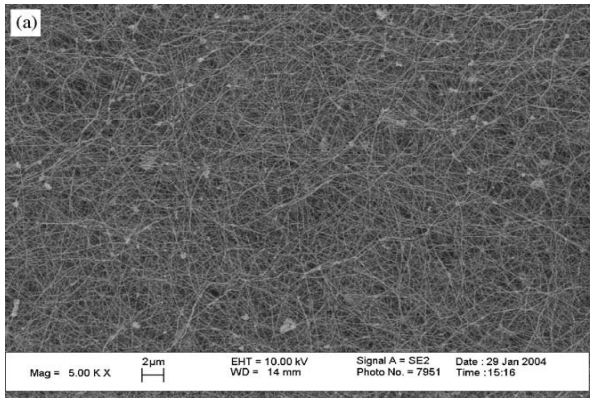

Figure 1: Scanning electron micrograph (SEM) image of bacterial cellulose

in polymer matrix can reinforce mechanical strength in composites but at the same time degrades the thermal stability. Glass transition temperature, temperature of melting, enthalpy of melting and enthalpy of crystallization are affected by nanocellulose loaded in composites

5. Applications

Nowadays natural fiber reinforced polymer composites are used in many sectors due to its easy processibility, biodegradability, renewable, neutral to the CO_2 emission, low cost and abundant resources in nature even from the wastes of cultivated plants. Direct contact of many nano-sized particles usually gives hazardous effects to humans but nanocellulose is non toxic. The fabricated nanofiber can form composites with all types of polymer. Acetyl, silyl derivatives of nanocellulose into polymer nanocomposites are used to prepare very high quality of textile (clothing and fabric), high absorbency products (diapers, cigarette- filters etc., thermoplastic products (films and molded parts), nourishing, food packaging, cosmetics and pharmaceuticals (extended capsule, tablet release agent and encapsulating agent), medicinal (hypoallergenic surgical products) and others.

Nanocellulose even finds its applications in electronics sector to prepare flexible circuits, flexible solar panels, optical applications etc.

Cellulose nanocrystals with defined dimension formulate the cellulose based nanocomposites for different coating applications and packaging materials. As cellulose bear high capacity to hold water, it has higher compatibility with human body, including tissue scaffolds and implants, wound dressing, biocompatible coating and drug release formulations, etc.,

6. Conclusion

Nanocellulose is one of the best alms of the nature which helps to fullfill all the need of the mankind such as food, shelter, clothing, medical appliances and numerous advancements. At the same time they are regenerative in nature. Their intoxic behavior and easy processibility makes them one of the noble and smart materials of this 21st century.

7. Acknowledgement

My sincere acknowldgement goes to Professor Rameshwar Adhikari for encouraging me to work on nanocellulose in my Ph.D. research.

8. References

1 S.J. Eichhorn, C.A. Baillie, N. Zafeiropoulos, L.Y. Mwailambo, M.P. Ansell, A. Dufresne, K.M.Entwistle, P.J. Herrere-Franco, G.C. Escamilla, L.Groom, M. Hughes, C. Hill, T.G. Rials, P.M. Wild. Review- Current international research into cellulosic fibres and composites. Journal of Materials Science 36(2001) 2107-2131

2 Leandro Luduena, Diana Fasce, Vera.A. Alvarez, and Pablo M. Stefani. Nanocellulose From Rice Husk Following Alkaline Treatment to Remove Silica. BioResources 6(2), 1440-1453(2011)

3 D.Y,Liu, X.W. Yuan, D. Bhattacharyya, A.J.Easteal. Characterization of Solution Cast Cellulose Nanofibre-Reinforced Poly(Lactic Acid). eXPRESS Polymer Letters Vol.4, No. 1(2010) 26-31

4 Istvan Siro, David Plackett. Microfibrillated celuulose and new nanocomposite materials: a review. Springer Science +Business Media B.V.Cellulose (2010) 17:459-494